



Strathclyde Institute of Pharmacy and Biomedical Sciences

PhD thesis

**Synthesis and evaluation of novel non-viral gene delivery systems
for prostate cancer targeting**

BY

Najla A. Altwaijry

A thesis presented in fulfilment of the requirements for the degree of

Doctor of Philosophy

2018

This thesis is the result of the author's original research. It has been composed by the author and has not been previously submitted for examination which has led to the award of a degree.

The copyright of this thesis belongs to the author under the terms of the United Kingdom Copyright Act as qualified by University of Strathclyde Regulation 3.50. Due acknowledgment must always be made to the use of any material contained in, or derived from, this thesis.

Signed:

Date:

Acknowledgements

First and foremost, I would like to thank my God for giving me the strength, ability and opportunity to undertake this path and to persevere until completion.

It gives me great pleasure to express here my sincere gratitude to my advisor Dr. Christine Dufés for her continuous patience and support during my years of study. Your guidance has helped me in more ways than one throughout the research and writing of this thesis. I still cannot imagine a better advisor and mentor for my Ph.D study.

I also would like to express my appreciation to the Government of Saudi Arabia, as represented by Princess Nourah bint Abdulrahman University and the Saudi Cultural Bureau in London, for funding this project.

Bringing this thesis to a successful completion would not have been possible without the contribution of several individuals to whom I would like to take this opportunity to express my sense of gratitude. Special thanks to Dr. John Parkinson for his kind assistance with NMR. Thanks also to the technical staff at pure and applied chemistry, Mr Craig Irving and Ms Patricia Keating, for their help with NMR and mass spectroscopy. Many thanks also to Mrs Monika Warzecha for her help with atomic force microscopy images. Special thanks to my colleague, Dr. Sukrut Somani, for his kind advice and help throughout my years of study, not to mention all my colleagues at Lab 224: Partha, Joan, Intouch, Jamal and Jitkasem.

Lastly, words cannot express my heartfelt appreciation to my family. To my mother, I can never be grateful enough for your unconditional love, support and endless prayers. My precious son Abdullah, thank you for being such a wonderful boy, you've brought lights and colours into my life. Special thanks to all my brothers and sisters for your encouragement and support.

This thesis is dedicated to my beloved late father, whose faith in me was, is and always will be the reason behind my success in life.

Contents

Chapter 1 : Introduction	1
1.1. Prostate cancer	2
1.1.1. Prostate anatomy and histology	2
1.1.2. Prostate cancer epidemiology	5
1.1.3. Types of prostate cancer	5
1.1.4. Pathophysiology of the disease	8
1.1.5. Screening.....	10
1.1.6. Diagnosis.....	10
1.1.7. Treatments.....	14
1.2. Gene therapy	18
1.2.1. History of gene therapy.....	18
1.2.2. Cancer gene therapy.....	20
1.2.3. Gene delivery	26
1.3. Cancer targeting	36
1.3.1. Passive targeting	36
1.3.2. Active targeting.....	37
1.4. Delivery barriers	39
1.4.1. Systemic barriers.....	39
1.4.2. Cellular barriers	40
1.5. Aim and objectives	43
Chapter 2 : Synthesis and characterisation of lactoferrin- and peptide- bearing polypropyleneimine dendrimers.....	44
2.1. Introduction.....	45
2.1.1. Prostate cancer targeting ligands	46
2.1.2. Structural elucidation	52
2.1.3. DNA complexation study	54

2.1.4. Photon correlation spectroscopy	56
2.1.5. Atomic force microscopy.....	60
2.1.6. Aim and objectives	61
2.2. Materials and methods	62
2.2.1. Materials	62
2.2.2. Methods.....	64
2.3. Results.....	74
2.3.1. Conjugation of lactoferrin and Peptide2 to DAB dendrimer	74
2.3.2. Characterization of lactoferrin- and peptide- bearing DAB dendriplexes	96
2.4. Discussion	114
Chapter 3 : <i>In vitro</i> evaluation of lactoferrin- and peptide - bearing DAB dendrimers	129
3.1. Introduction.....	130
3.1.1. Transfection assay.....	131
3.1.2. Confocal microscopy	132
3.1.3. Anti-proliferation assay	133
3.1.4. Fluorescence activated cell sorting (FACS)	134
3.1.5. Cellular uptake mechanism.....	135
3.1.6. Aims and objectives	139
3.2. Materials and methods	140
3.2.1. Materials	140
3.2.2. Methods.....	142
3.3. Results.....	150
3.3.1. Transfection assay.....	150
3.3.2. Cellular uptake	162
3.3.3. Mechanism of cellular uptake	176
3.3.4. Peptide2 binding affinity assay	185
3.3.5. Enzyme-linked immunosorbent assay	189

3.3.6. Tetrazolium reduction assay (MTT)	191
3.4. Discussion	205
Chapter 4 : <i>In vivo</i> evaluation of lactoferrin-bearing polypropylenimine dendriplex ..	224
4.1. Introduction.....	225
4.1.1. Animal models	227
4.1.2. Bioluminescence imaging.....	229
4.2 Materials and methods	232
4.2.1 Materials	232
4.2.2. Methods.....	233
4.2.3. Statistical analysis	234
4.3. Results.....	235
4.3.1. Therapeutic efficacy.....	235
4.3.2. Bioluminescence imaging.....	241
4.4. Discussion	243
Chapter 5 : General Discussion	248
Chapter 6 : Conclusion and future plans.....	262
6.1. Conclusion	263
6.2. Future work.....	266
References.....	269
Appendix I: List of Publications.....	294
Appendix II : Conference Abstracts	295

Table of Figures

Figure 1-1 Representation of a normal prostate, showing its size and location under the bladder and behind the rectum (adapted from Bagnall, 2014).....	4
Figure 1-2 Normal anatomy of the prostate, divided into zones according to McNeal (adapted from Bagnall, 2014).....	4
Figure 1-3 Anatomical differences between normal and cancerous prostate tissue: A) normal shape of the basal and luminal cells in the prostate; B) tissue morphological changes in prostate cancer (adapted from Ramon and Denis, 2007).....	10
Figure 1-4 Modified Gleason grading system with five histological stages, where Grade 5 is the most advanced stage (Adapted from Shah and Zhou, 2012).	14
Figure 1-5 Chemical structure for the most common cationic polymers used in gene delivery (adapted from Taira <i>et al.</i> , 2005)	31
Figure 1-6 Different methods used in dendrimer preparation A) divergent synthesis method, which initiated upward and B) convergent method which started backward (adapted from Klajnert and Bryszewska, 2001)	32
Figure 1-7 Synthesis of PAMAM dendrimer and chemical structure of its different generations (adapted from Dufès <i>et al.</i> , 2005).	34
Figure 1-8 Synthesis of DAB dendrimer (adapted from Dufès <i>et al.</i> , 2005).	34
Figure 1-9 Active tumour cell targeting (by receptor-mediated endocytosis) (adapted from Wagner <i>et al.</i> , 1994).....	39
Figure 2-1 General structure of prostate specific membrane antigen divided into external, transmembrane and internal parts (adapted from Chang, 2004).....	48
Figure 2-2 Integrins receptors family (Adapted from Barczyk <i>et al.</i> , 2010)	50
Figure 2-3 Zeta potential of charged particles (adapted from Shimko <i>et al.</i> , 2012).....	59
Figure 2-4 Protein modification reaction steps with Traut's reagent (2-Iminothiolane) to carry free sulfhydryl group (Adapted from Hermanson, 2013)	66
Figure 2-5 NMR spectra of DAB (A) and DAB-cross-linker (B: ¹ H-NMR, C: C-NMR).....	76
Figure 2-6 Peaks integration in the spectrum of DAB-GMBS molecule	78
Figure 2-7 Mass spectroscopy spectrum of DAB-GMBS using two (A) and six-molar excess (B) of GMBS over DAB.	79
Figure 2-8 MALDI-TOF spectrum of DAB-GMBS showing one to two GMBS molecules linked to each dendrimer molecule.	80

Figure 2-9 ¹ H-NMR spectra of A) Lactoferrin protein and B) DAB-Lf, where (l, m, and n) are lactoferrin residues.....	82
Figure 2-10 Conjugation reaction steps of DAB-Lf	83
Figure 2-11 MALDI-TOF mass spectroscopy of the dendriplex DAB-Lf (A) and lactoferrin alone (B) as standard sample.	84
Figure 2-12 ¹ H-NMR spectra of Peptide2 (A) and DAB-Peptide2 (B)	87
Figure 2-13 NOESY NMR spectrum of DAB-Peptide2.....	88
Figure 2-14 DOSY spectra of Peptide2 (A), DAB-Peptide2 (B), and DAB-PEG2k-Peptide2 (C) using 90% H ₂ O and 10% D ₂ O as solvent.	89
Figure 2-15 MALDI-TOF spectrum of DAB-Peptide2	90
Figure 2-16 Diagram shows the final synthesis step of DAB-PEG2k-Peptide2 and ¹ H-NMR spectrum of DAB-PEG2k-Peptide2 dendrimer	91
Figure 2-17 DAB-PEG3.5-Peptide2 ¹ H-NMR spectrum and structure	92
Figure 2-18 ¹ H-NMR spectrum of DAB-PEG2k-PEG3.5k-Peptide2.....	93
Figure 2-19 ¹ H-NMR spectra of Peptide4 (A) and DAB-Peptide4 (B)	94
Figure 2-20 ¹ H-NMR spectra of DAB-PEG2k-Peptide4.....	95
Figure 2-21 DNA condensation to DAB-Lf at various DAB-Lf: DNA weight ratios (n=4).97	97
Figure 2-22 DNA condensation to Lactoferrin at various Lf: DNA weight ratios (n=4)	97
Figure 2-23 DNA condensation to DAB-Pep2 (A) and DAB-PEG2k-Pep2 (B) dendriplexes at various dendrimer: DNA weight ratios (n=4).....	98
Figure 2-24 DNA condensation to DAB-PEG2k-Peptide4 dendriplex at various dendrimer: DNA weight ratios (n=4)	99
Figure 2-25 Gel retardation assay of DAB-Lf dendriplexes at various dendrimer: DNA weight ratios (20:1, 10:1, 5:1, 2:1, 1:1, 0.5:1) and DNA only as control.	100
Figure 2-26 Gel retardation assay of DAB-PEG2k-Peptide2 dendriplexes at various dendrimer: DNA weight ratios (20:1, 10:1, 5:1, 2:1, 1:1, 0.5:1) and DNA only as control. .	101
Figure 2-27 Gel retardation assay of DAB-PEG2k-Peptide4 dendriplexes at various dendrimer: DNA weight ratios (20:1, 10:1, 5:1, 2:1, 1:1, 0.5:1) and DNA only as control. .	102
Figure 2-28 Average size (A) and zeta potential (B) of DAB-Lf dendriplexes at various dendrimer: DNA weight ratios (n=9).....	104
Figure 2-29 Average size (A) and zeta potential (B) of DAB-Peptide2 dendriplexes at various dendrimer: DNA ratios (n=9)	106
Figure 2-30 Average size (A) and zeta potential (B) of DAB-PEG2k-Peptide2 dendriplexes at various dendrimer: DNA ratios (n=9).....	108

Figure 2-31 Average size (A) and zeta potential (B) of DAB-PEG2k-Peptide4 dendriplexes at various dendrimer: DNA ratios (n=9).....	110
Figure 2-32 AFM force image of DAB-Lf dendriplex (weight ratio 5:1). Images size A) 7 μ m and B) 3 μ m.	111
Figure 2-33 AFM force image of DAB-PEG2k-Peptide2 dendriplex (weight ratio 20:1). Images size A) 10 μ m and B) 3 μ m.....	112
Figure 2-34 AFM force image of DAB-PEG2k-Peptide4 dendriplex (weight ratio 20:1). Images size A) 10 μ m and B) 3 μ m.....	113
Figure 3-1 Hydrolysis reaction of o-nitrophenyl- β -D-galactopyranoside (adapted from Miller, 1972).	132
Figure 3-2 Confocal microscopy basic setup (adapted from Semwogerere and Weeks, 2005)	133
Figure 3-3 Reduction reaction of 3-(4,5-dimethylthiazol-2-yl)-2,5-diphenyltetrazolium bromide (MTT) to form the lipophilic compound formazan.	134
Figure 3-4 Clathrin-mediated endocytosis pathway (adapted from Grant and Sato, 2006).	137
Figure 3-5 Common mechanisms of cellular uptake (adapted from Panariti <i>et al.</i> , 2012)... ..	138
Figure 3-6 Transfection efficiency of DAB-Lf dendriplex in PC-3 (A), DU145 (B) and LNCaP cells (C). Results were expressed as the mean \pm SEM of three replicates (n=15). The data were analysed by one-way ANOVA, repeated measurements; *: $P \leq 0.05$ versus the positive control DAB.	151
Figure 3-7 Transfection efficiency of DAB-Peptide2 dendriplex in PC-3 (A), DU145 (B) and LNCaP cells (C). Results were expressed as the mean \pm SEM of three replicates (n=15). The data were analysed by one-way ANOVA, repeated measurements; *: $P \leq 0.05$ versus the positive control DAB.	153
Figure 3-8 Transfection efficiency of DAB-PEG2k-Peptide2 dendriplex in PC-3 (A), DU145 (B) and LNCaP cells (C). Results were expressed as the mean \pm SEM of three replicates (n=15). The data were analysed by one-way ANOVA, repeated measurements; *: $P \leq 0.05$ versus the positive control DAB-PEG.	155
Figure 3-9 Transfection efficiency of DAB-PEG3.5k-Peptide2 dendriplex in PC-3 (A), DU145 (B) and LNCaP cells (C). Results were expressed as the mean \pm SEM of three replicates (n=15). The data were analysed by one-way ANOVA, repeated measurements; *: $P \leq 0.05$ versus the positive control DAB-PEG.	157
Figure 3-10 Transfection efficiency of DAB-PEG2k-PEG3.5k-Peptide2 dendriplex in PC-3 (A), DU145 (B) and LNCaP cells (C). Results were expressed as the mean \pm SEM of three	

replicates (n=15). The data were analysed by one-way ANOVA, repeated measurements; *: $P \leq 0.05$ versus the positive control DAB-PEG.	159
Figure 3-11 Transfection efficiency of DAB-PEG2k-Peptide4 dendriplex in PC-3 (A), DU145 (B) and LNCaP cells (C). Results were expressed as the mean \pm SEM of three replicates (n=15). The data were analysed by one-way ANOVA, repeated measurements; *: $P \leq 0.05$ versus the positive control DAB-PEG.	161
Figure 3-12 Confocal microscopy images for the cellular uptake of fluorescein-labelled DNA at a concentration of 2.5 $\mu\text{g}/\text{well}$, complexed with DAB-Lf, DAB or uncomplexed, after incubation for 24 hours with PC-3, DU145 and LNCaP cells.....	163
Figure 3-13 Confocal microscopy images for the cellular uptake of fluorescein-labelled DNA at a concentration of 2.5 $\mu\text{g}/\text{well}$, complexed with DAB-Peptide2, DAB or uncomplexed, after incubation for 24 hours with PC-3 and DU145 cells.....	165
Figure 3-14 Confocal microscopy images for the cellular uptake of fluorescein-labelled DNA at a concentration of 2.5 $\mu\text{g}/\text{well}$, complexed with DAB-PEG2k-Peptide2, DAB-PEG or uncomplexed DNA, after incubation for 24 hours with PC-3, DU145 and LNCaP cells.....	166
Figure 3-15 Flow cytometry histograms showing fluorescence emission intensity as a quantitative measurement of the cellular uptake of fluorescein-labelled DNA complexed with DAB-Lf and DAB in A) PC-3, B) DU145 and C) LNCaP prostate cancer cell lines.	169
Figure 3-16 Fluorescence emission intensity as a quantitative measurement of the cellular uptake of fluorescein-labelled DNA complexed with various carriers in various prostate cancer cell lines (PC-3, DU145 and LNCaP) (n=3). *: $P \leq 0.05$ versus the highest cellular uptake.	170
Figure 3-17 Flow cytometry histograms showing fluorescence emission intensity as a quantitative measurement of the cellular uptake of fluorescein-labelled DNA complexed with DAB-Peptide2 and DAB in A) PC-3, B) DU145 and C) LNCaP prostate cancer cell lines.	171
Figure 3-18 Fluorescence emission intensity as a quantitative measurement of the cellular uptake of fluorescein-labelled DNA complexed with DAB-Peptide2, DAB, or uncomplexed in PC-3 (A), DU145 (B) and LNCaP (C) cell lines (n=3). *: $P \leq 0.05$ versus the highest cellular uptake.....	172
Figure 3-19 Flow cytometry histograms showing fluorescence emission intensity as a quantitative measurement of the cellular uptake of fluorescein-labelled DNA complexed with DAB-PEG2k-Peptide2 or DAB-PEG in PC-3, DU145 and LNCaP prostate cancer cell lines. The P2 gating area show the percentage of cells that took up each specific treatment in a total of 10000 events.	174

Figure 3-20 Fluorescence emission intensity as a quantitative measurement of the cellular uptake of fluorescein-labelled DNA complexed with DAB-PEG2k-Peptide2, DAB-PEG, or uncomplexed in PC-3 (A), DU145 (B) and LNCaP (C) (n=3). *: $P \leq 0.05$ versus the highest cellular uptake. 175

Figure 3-21 Flow cytometry quantification of the cellular uptake of fluorescein-labelled DNA complexed to DAB-Lf dendrimer in PC-3 (A), DU145 (B) and LNCaP (C) prostate cancer cell lines after pre-treating them with different uptake inhibitors: free lactoferrin (Lf), phenylarsine oxide (Ph.O), filipin (Fil), colchicine (Col) and poly-L-lysine (PLL) (n = 3), *: $P \leq 0.05$ compared with DAB-Lf dendriplex without pre-treatment. 178

Figure 3-22 Flow cytometry quantification of the cellular uptake of fluorescein-labelled DNA complexed to DAB-Lf dendrimer in PC-3 (A) and DU145 (B) cells after pre-treating them with phenylarsine oxide (Ph.O) 20 μ M, and filipin (Fil) 10 μ g/ml (n = 3), *: $P \leq 0.05$ compared with DAB-Lf dendriplex without pre-treatment. 179

Figure 3-23 Confocal microscopy imaging of A) PC-3, B) DU145 and C) LNCaP cellular uptake of fluorescein-labeled DNA (2.5 μ g/well) complexed with DAB-Lf, after pre-treatment with various cellular uptake inhibitors: poly-L-lysine (PLL), phenylarsine oxide (Ph.O), filipin (Fil), colchicine (Col) and free lactoferrin (Lf) (B). Blue: nuclei stained with DAPI (excitation: 365 nm, emission bandwidth: 435–485 nm), green: fluorescein-labeled DNA (excitation: 470 nm, emission bandwidth: 515–555 nm), red: Alexa Fluor[®]647 probe (excitation: 633 nm laser line, bandwidth: 650-690 nm) (Bar: 10 μ m). 180

Figure 3-24 Flow cytometry quantification of the cellular uptake of fluorescein-labelled DNA complexed to DAB-PEG2k-Peptide2 dendrimer in prostate cell lines PC-3 (A), DU145 (B) and LNCaP (C) after pretreatment with uptake inhibitors: free Peptide2 (Pep2), phenylarsine oxide (Ph.O), filipin (Fil), colchicine (Col) and poly-L-lysine (PLL) (n = 3), *: $p < 0.05$ compared with untreated DAB-PEG2k-Pep2 dendriplex. 184

Figure 3-25 MALDI-TOF spectrum of Peptide2 -FITC 185

Figure 3-26 Cellular uptake intensity of Peptide2 labelled with FITC in PC-3 (black), DU145 (grey) and LNCaP (white) cell lines (n=3) *: $P \leq 0.05$ compared with the fluorescence intensity of the highest binding at the same concentration. 187

Figure 3-27 Cellular uptake intensity histograms of Peptide2 labelled with FITC in PC-3, DU145 and LNCaP cell lines. The P2 gate represents the percentage of cells with positive FITC-Pep2 binding. 188

Figure 3-28 DAB-PEG2k-Peptide2 dendriplex-mediated transfection of TNF α after different treatment periods in A) PC-3, B) DU145 and C) LNCaP cell lines, using ELISA as detection method.....	190
Figure 3-29 Anti-proliferative effect of DAB-Lf: DNA, DAB:DNA, DNA, DAB-Lf and DAB in PC-3 cell line at different concentrations (0.05 to 200 μ g/ml), using various therapeutic DNA encoding A) TNF, B) TRAIL, C) IL-12. (Dark grey: DAB-Lf: DNA, grey: DAB: DNA, black: DAB-Lf only, striped white: DAB only, white: DNA only)	193
Figure 3-30 Anti-proliferative effect of DAB-Lf: DNA, DAB:DNA, DNA, DAB-Lf and DAB in DU145 cell line at different concentrations (0.05 to 200 μ g/ml), using various therapeutic DNA encoding A) TNF, B) TRAIL, C) IL-12. (Dark grey: DAB-Lf: DNA, grey: DAB: DNA, black: DAB-Lf only, striped white: DAB only, white: DNA only)	194
Figure 3-31 Anti-proliferative effect of DAB-Lf: DNA, DAB: DNA, DNA, DAB-Lf and DAB in LNCaP cell line at different concentrations (0.05 to 200 μ g/ml), using various therapeutic DNA encoding A) TNF, B) TRAIL, C) IL-12. (Dark grey: DAB-Lf: DNA, grey: DAB: DNA, black: DAB-Lf only, striped white: DAB only, white: DNA only)	195
Figure 3-32 Anti-proliferative effect of DAB-Peptide2: DNA (dark grey), and DAB-Peptide2 (white) in DU145 cell line at different concentrations (200 to 0.05 μ g/ml), using therapeutic DNA encoding TNF α	197
Figure 3-33 Anti-proliferative effect of DAB-PEG2k-Peptide2: DNA, DAB-PEG: DNA, DAB-PEG2k-Peptide2 only, and DNA in PC-3 cell lines at different concentrations (0.026 to 100 μ g/ml), using various therapeutic DNAs encoding A) TNF and B) TRAIL. (Dark grey: DAB-PEG2k-Pep2: DNA, grey: DAB-PEG: DNA, black: DAB-PEG2k-Pep2 only and white: DNA only).	199
Figure 3-34 Anti-proliferative effect of DAB-PEG2k-Peptide2: DNA, DAB-PEG: DNA, DAB-PEG2k-Peptide2 only, and DNA in DU145 cell lines at different concentrations (0.026 to 100 μ g/ml), using various therapeutic DNAs encoding A) TNF and B) TRAIL. (Dark grey: DAB-PEG2k-Pep2: DNA, grey: DAB-PEG: DNA, black: DAB-PEG2k-Pep2 only and white: DNA only).	201
Figure 3-35 Anti-proliferative effect of DAB-PEG2k-Peptide2: DNA, DAB-PEG: DNA, DAB-PEG2k-Peptide2 only, and DNA in LNCaP cell lines at different concentrations (0.026 to 100 μ g/ml), using various therapeutic DNAs encoding A) TNF and B) TRAIL. (Dark grey: DAB-PEG2k-Pep2: DNA, grey: DAB-PEG: DNA, black: DAB-PEG2k-Pep2 only and white: DNA only).	203

Figure 4-1 Bioluminescent imaging instrumentation (adapted from Behrooz <i>et al.</i> , 2013)	231
Figure 4-2 (A) Tumour growth studies in PC-3 xenograft tumour model after intravenous injection of lactoferrin-bearing DAB dendrimer complexed with DNA encoding TNF α (green), TRAIL (red), IL-12 (blue), or DAB-Lf only (brown), uncomplexed DNA encoding TNF α (pale green), TRAIL (orange), and IL-12 (cyan) (DNA dose 50 μ g/ml), and an untreated group (black). (B) Percentage change in animal body weight during treatment period (colour code as A). (C) Overall tumour response to treatments at the end of the study. (D) Time to disease progression where animals were removed from the study once their tumour reached 10 mm diameter.....	239
Figure 4-3 (A) Tumour growth studies in DU145 xenograft tumour model after intravenous injection of lactoferrin-bearing DAB dendrimer complexed with DNA encoding TNF α (green), TRAIL (red), IL-12 (blue), or DAB-Lf only (brown), uncomplexed DNA encoding TNF α (pale green), TRAIL (orange) and IL-12 (cyan) (pale blue) (DNA dose 50 μ g/ml), and an untreated group (black). (B) Percentage change in animal body weight during treatment period (colour code as A). (C) Overall tumour response to treatments at the end of the study. (D) Time to disease progression where animals were removed from the study once their tumour reached 10 mm diameter.	240
Figure 4-4 Bioluminescence imaging of the tumours after treatment with lactoferrin-bearing DAB dendriplex complexed with DNA encoding TNF α (cplx DL-TNF), TRAIL (cplx DL-TRAIL) and IL-12 (cplx DL-IL12) in a PC-3M-Luc-C6 tumour model.....	242

Tables

Table 1-1 Gleason grading system patterns (adapted from Shah and Zhou, 2012).	14
Table 2-1 List of materials used in chapter 2.	62
Table 2-2 List of the peptides proposed for use as targeting ligands	68
Table 2-3 Chemical compositions of Peptide2- bearing DAB dendrimer formulations.....	70
Table 2-4 DAB-GMBS characterisation using 2D-NMR (COSY, HMBC and HSQC)	75
Table 2-5 LC/MS spectra analysis for DAB-GMBS at Figure 2-7.....	79
Table 2-6 MALDI-TOF spectrum analysis of DAB-GMBS	80
Table 2-7 List of Peptide2 characteristic peaks in the ¹ H-NMR spectrum of DAB-Peptide2	86
Table 2-8 Diffusion coefficient of Peptide2, DAB-Pep2 and DAB-PEG2k-Pep2	89
Table 2-9 List of Peptide4 characteristic peaks in the ¹ H-NMR spectrum of DAB-Peptide4 and DAB-PEG2k-Peptide4.....	95
Table 2-10 Size and zeta characterisation for the different PEGylated forms of Peptide2- bearing DAB dendrimers	109
Table 3-1 List of materials used in chapter 3.	140
Table 3-2 Anti-proliferative activity of DAB-Lf and DAB complexed with various therapeutic DNA (TNF α , TRAIL or IL-12) and the cytotoxic effect of the dendrimers on PC-3, DU145 and LNCaP prostate cancer cell lines.	196
Table 3-3 Anti-proliferative activity of DAB-PEG2k-Pep2 and DAB-PEG complexed with various therapeutic DNA (TNF α or TRAIL) and the cytotoxic effect of DAB-PEG2k-Pep2 dendrimer on PC-3, DU145 and LNCaP prostate cancer cell lines.	204
Table 4-1 List of materials used in chapter 4.	232

List of abbreviations

BLI	Bioluminescence imaging
BSA	Bovine serum albumin
Col	Colchicine
D ₂ O	Deuterated water
DAB	Diaminobutyric polypropylenimine dendrimer
DAB-Am16	Diaminobutyric polypropylenimine hexadecaamine
DAB-Lf	Lactoferrin-bearing generation 3-diaminobutyric polypropylenimine dendrimer
DAB-PEG2k-Pep2	Peptide2-bearing PEGylated generation 3-diaminobutyric polypropylenimine dendrimer
DAB-PEG2k-Pep4	Peptide4-bearing PEGylated generation 3-diaminobutyric polypropylenimine dendrimer
DAB-Pep2	Peptide2-bearing generation 3-diaminobutyric polypropylenimine dendrimer
DAPI	4', 6-diamidino-2-phenylindole
DMSO	Dimethyl sulfoxide
DNA	Deoxyribonucleic acid
dsDNA	Double stranded deoxyribonucleic acid
ECM	Extracellular matrix
EDTA	Ethylenediaminetetraacetic acid,
EPR	Enhanced permeability and retention
ESI	Electron spray ionization
FACS	Fluorescence-Activated Cell Sorting
FBS	Fetal Bovine Serum
FDA	Food and Drug Administration
Fil	Filipin complex from <i>Streptomyces filipinesis</i>
GMBS	N- γ -maleimidobutyryl-oxysuccinimide ester

HEPES	N-2-hydroxyethylpiperazine-N-2-ethane sulfonic acid
HMBC	Heteronuclear multiple-bond correlation spectroscopy
HSQC	Heteronuclear single quantum correlation spectroscopy
IC ₅₀	Growth inhibitory concentration
IFN	Interferon
IL	Interleukin
IR	Infrared radiation
IV	Intravenous injection
LC-MS	Liquid chromatography- mass spectroscopy
Lf	Lactoferrin
LNCaP	Prostate adenocarcinoma cell line
MALDI-TOF	Matrix-assisted laser desorption/ionization-time of flight
MWCO	Molecular weight cut-off
MEM	Minimum essential media
MRI	Magnetic resonance imaging
MS	Mass spectroscopy
NMR	Nuclear magnetic resonance
NOE	Nuclear Overhauser effect
NPs	Nanoparticles
ONP	O-nitrophenol
ONPG	O-nitrophenyl- β -D-galactosidase
PAMAM	Polyamidoamine dendrimer
PBS	Phosphate buffered saline
pCMV β -Gal	Plasmid DNA encoding β -galactosidase
pORF9- mTNF α	Plasmid encoding TNF α
pORF- mTRAIL	Plasmid encoding TRAIL
pORF- mIL-12	Plasmid encoding IL-12

PEG	Polyethylene glycol
PEI	Polyethyleneimine
Pep2	Peptide2 (CWQPDTAHHWATL)
Pep4	Peptide4 (CPRPRGDNPLTCGGKKK)
Ph.O	Phenylarsine Oxide
PLB	Passive lysis buffer
PLL	Poly-L-lysine
PPI	Polypropylenimine
PSA	Prostate specific antigen
PSMA	Prostate specific membrane antigen
RNase	Ribonuclease
RPMI	Roswell Park Memorial Institute medium
SDS	Sodium dodecyl sulphate
SEM	Standard error of the mean
SEM	Scanning electron microscope
TEM	Transmission electron microscopy
Tf	Transferrin
TfR	Transferrin Receptor
TMS	Tetramethylsilane
TNF α	Tumour necrosis factor alpha
TRAIL	Tumour necrosis factor-related apoptosis-inducing ligand

Summary

Prostate cancer is the second most widespread cancer in men worldwide. Treatment choices are limited to prostatectomy, hormonal and radiotherapy that commonly have deleterious side effects and vary in their efficacy, depending on the stage of the disease.

Among novel experimental strategies, gene therapy holds great promise for the treatment of cancer, but its use is currently limited by the lack of delivery systems able to selectively deliver the therapeutic genes to the tumours after intravenous administration without major drawbacks.

Given that lactoferrin receptors, prostate specific membrane antigen (PSMA) and integrins are overexpressed on prostate cancer cells, the purpose of this study is to determine whether lactoferrin, Peptide2 (CWQPDTAHHWATL) and Peptide4 (CPRPRGDNPPPLTCGGKKK) bearing diaminobutyric polypropylenimine (DAB) based dendriplexes would improve the targeting of therapeutic genes *in vitro* and *in vivo*.

The chemical and physical characteristics of the synthesised dendrimers were first determined, followed by various *in vitro* experiments, to assess the improvement in the transfection and cellular uptake of the modified dendriplexes in PC-3, DU145 and LNCaP prostate cancer cell lines. Finally, *in vivo* studies were carried out using BALB/c nude mice to investigate the anti-cancer effects of the Lf-bearing dendriplexes encoding TNF α , TRAIL, or IL-12.

DAB-Lf significantly increased the cellular uptake of the DNA in all prostate cancer cells. The highest DNA uptake, observed in PC-3 cells, was double than that observed in cells treated with non-targeted dendriplex. The anti-proliferative efficacy of DAB-Lf dendriplex encoding TNF α , TRAIL, or IL-12 was significantly improved compared with unmodified DAB dendriplex. *In vivo*, intravenous injections of DAB-Lf dendrimer complexed with plasmid

DNA encoding TNF α and TRAIL have resulted in complete regression in 70% and 40% of tumours respectively at the end of the experiment in tumour-bearing mice.

DAB-PEG2k-Pep2 significantly improved the cellular uptake in LNCaP and DU145 cells, but not in PC-3 cells compared with the non-targeted dendriplex. The therapeutic DNA encoding TNF α was successfully transfected after complexation with DAB-PEG2k-Pep2 in all three cell lines, with significant variance in the cytokine concentration between cell lines. The IC₅₀ of DAB-PEG2k-Pep2 dendriplex encoding TNF α was significantly improved compared with untargeted DAB-PEG dendriplex in LNCaP cells.

In conclusion, DAB-Lf is a promising DNA carrier for targeting prostate cancer. This study is one of few showing significant tumour regression after intravenous administration of gene therapy using non-viral vectors as a single therapy approach. Peptide2 was also found to be an effective ligand for PSMA, however more improvement in the formulation is still required to obtain an enhanced therapeutic effect.

Chapter 1 : Introduction

1.1. Prostate cancer

1.1.1. Prostate anatomy and histology

The prostate is a gland in the male reproductive system, located below the bladder and in front of the rectum, with its base at the bladder neck and its apex at the genital diaphragm. A capsule of smooth muscles and fibres encapsulates the prostate and separates it from the rectum (Figure 1-1) (Hammerich *et al.*, 2009; Rocers, 2011). The gland is linked with the seminal vesicles and vas deferens through the ejaculatory ducts that meet at the centre of the prostate and combine with the urethra as it passes through it (Hammerich *et al.*, 2009). It is composed of 70% glandular tissues and 30% fibromuscular tissues (Muruve, 2013). The glandular part contains fifty secretory glands and ducts, whose main function is the secretion of a fluid which constitutes around 30% of the total semen volume. This fluid liquefies the sperm and protects it by creating an environment that allows it to survive for a period of time. The fibromuscular tissue is composed of smooth muscle and connective tissue to provide the prostate with the required strength to expel the fluids during ejaculation (Rocers, 2011).

In 1968, McNeal established the most commonly used anatomical division of prostate into three zones (Figure 1-2) (McNeal, 1968; Selman, 2011):

- The peripheral zone, which includes the posterior and lateral sides of the prostate, containing most (70%) of the glandular tissue (Muruve, 2013). Most of the prostate disorders such as chronic prostatitis, post-inflammatory atrophy, and cancer, arise in the peripheral zone, (Hammerich *et al.*, 2009).
- The central zone, which consists of around 25% of the prostate tissue and surrounds the ejaculatory ducts.
- The transition zone, which surrounds the part of the urethra that passes through the prostate. It is consisting of three lobes, two lateral and one central. Benign prostatic

hyperplasia usually develops at this site, leading in some cases to obstruction of the urethra (Muruve, 2013).

Histologically, the prostate is composed of two types of cells, basal and luminal cells. The basal cells are smaller in size and arranged linearly to form a layer, acting as a barrier and creating a support for the luminal cells (Wang *et al.*, 2007). Mostly, basal cells display growth factor receptors to couple with different forms of growth factors that are essential for cellular proliferation (Reynolds and Kyrianou, 2006). Androgen receptors are also expressed in a few basal cells, considered to be stem cells for their ability to differentiate to luminal (secretory) or neuroendocrine cells (Ramon and Denis, 2007; Wang *et al.*, 2007). In addition, luminal columnar cells form a layer that is located just above the basal cell layer. They are responsible for the synthesis of seminal fluid, which requires androgen hormones, thus explaining the high expression of androgen receptors in their cell membrane (Figure 1-3) (Wang *et al.*, 2007; Hammerich *et al.*, 2009).

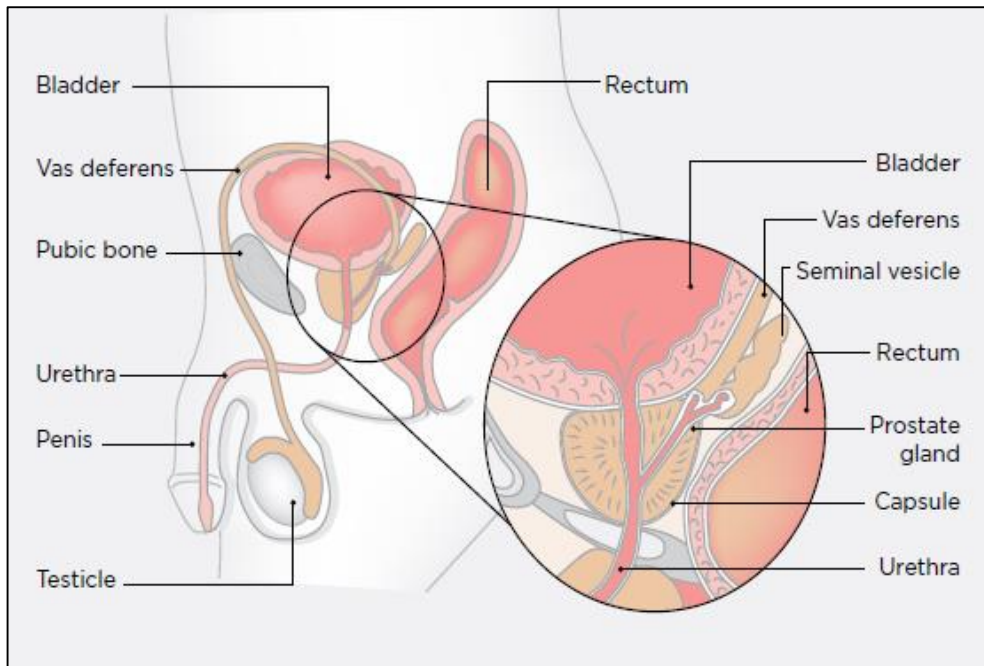


Figure 1-1 Representation of a normal prostate, showing its size and location under the bladder and behind the rectum (adapted from Bagnall, 2014).

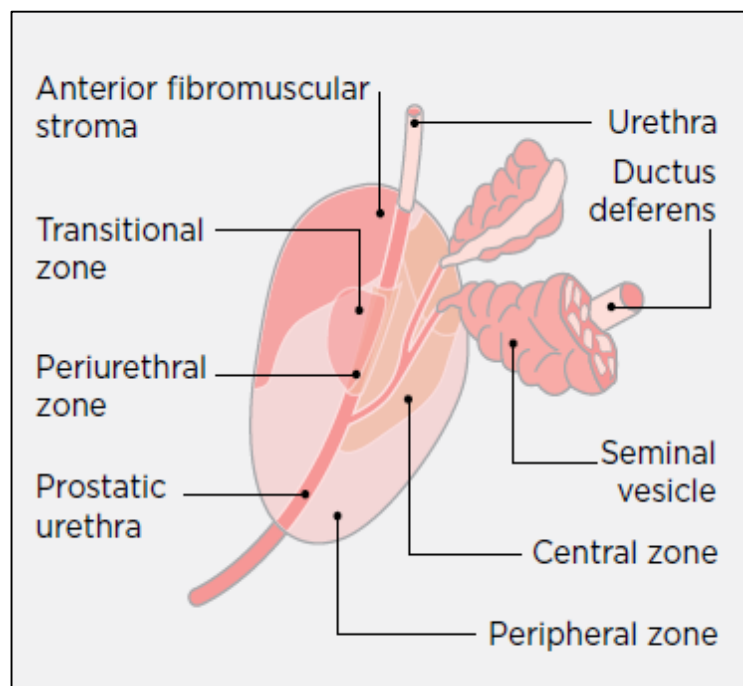


Figure 1-2 Normal anatomy of the prostate, divided into zones according to McNeal (adapted from Bagnall, 2014).

1.1.2. Prostate cancer epidemiology

Prostate cancer is one of the most leading causes of death in men worldwide. It is found to be the fourth most widespread cancer in the world, the second most common cancer in men, and the first in Europe and North America (GLOBALCAN, 2012; Brawley, 2013). According to the World Health Organisation, prostate cancer is estimated to cause 1.1 million new diagnosed cases and 307,000 deaths annually worldwide (GLOBOCAN, 2012).

In the UK, prostate cancer is the most commonly diagnosed cancer in men, with approximately 25% of the total cancer cases and 10,000 deaths annually (Philippou *et al.*, 2014; Cancer Research UK, 2015).

A continuous rise in the prostate cancer incidence rate has been recorded with a three-fold increase in Europe between 1975 and 2011 (Cancer Research UK, 2015). Around 190,000 new cases arise each year with 80,000 deaths occurring annually from prostate cancer (Damber and Aus, 2008). These statistics show prostate cancer as growing health problem, demonstrating the insufficiency of the currently available diagnostic and therapeutic approaches.

1.1.3. Types of prostate cancer

1.1.3.1. Prostatic adenocarcinoma

Adenocarcinoma is the most common type of prostate cancer, accounting for more than 90% of cases. It is a malignant glandular neoplasm that affects the epithelial tissues, including the secretory and luminal cells. The tumours are usually initiated in the peripheral zone, then spread locally around the prostate capsule from the seminal vesicles, the neck of the bladder and the rectum (Wagner, 2016). Immunohistochemical markers such as prostate specific antigen (PSA), prostatic acid phosphatase (PAP), and alpha-methylacyl coenzyme A (CoA)-reductase (AMACR) are usually expressed during the progression of adenocarcinoma. The high expression of these markers could be used as a diagnostic tool for prostate cancer (Baig

et al., 2015). The progression of the adenocarcinoma leads to the development of metastatic stages of the disease, as well as hormone refractory prostate cancer (Ramon and Denis, 2007).

1.1.3.1.1. Metastasis

Prostate cancer tends to metastasise into different organs, spreading from the pelvis to the lymph nodes, bones, adrenal glands, liver, lung and brain (Wagner, 2016). Cancer metastasis arises due to several changes in the primary cancer cell and tumour surrounding environment. The genetic instability in cancer cells can cause some cellular heterogeneity and DNA mutation that assist in cellular metastasis such as the loss of KAI1 (11p11.2) gene in prostate cancer cells (Gupta and Massagué, 2006). Furthermore, the stressed environment that is developed during the localized tumour growth such as the complexed extracellular matrix components, the low oxygen environment (hypoxia), and the limited nutrients supply, all cause cancer cells to evolve to a more invasive and aggressive form of cells.

The pattern of organ metastasis is not a random process; cancer cells tend to invade organs that are compatible with their primary cell growth in a predictable manner. Blood flow is believed to have an impact on selecting the site of metastasis. Cellular genetic mutations as well as the extra cellular matrix binding are also affecting the metastasis pattern (Kakhki *et al.*, 2013). However, there is no clear understanding on how the cells maintain this process. For example, in case of prostate cancer bone metastasis, the adhesion molecules that most commonly correlated with bone marrow metastasis are cadherin, stromal cell- derived factor 1 (SDF-1/CXCL12), and integrin $\alpha 2\beta 1$ (Ziaee *et al.*, 2015). In addition, tumours tend to metastasise in regions with specific anatomical criteria. In case of prostate cancer, the active red bone marrow was found to be the favourable place for cancer cells to develop metastasised tumours in bone due to the lateral site and the available vascular spaces in the bone marrow, which allows cancer cells to freely penetrate inside these spaces (Kakhki *et al.*, 2013).

1.1.3.1.2. Hormone refractory prostate cancer

A major treatment for metastasised prostate cancer is androgen deprivation therapy, which is based on the use of medications or procedures to prevent the release of testosterone and dihydrotestosterone to reduce the growth of this androgen-dependant tumours. Hormone refractory showed a therapeutic response for around 18 to 24 months before developing resistance to this therapy. Each year in the USA, around 25,000 prostate cancer cases develop resistance to hormone therapy, stimulating the growth of androgen-independent prostate cancer (AIPC) or hormone refractory prostate cancer (HRPC), where the cancer continues to grow despite hormonal treatment (Garnick, 2016). The mechanism by which HRPC is generated is not clear yet; it is thought that cells would change the androgen receptors (AR) activation pathway by receptors mutation or change the receptor activation pathway. For example, the activation function domain AF-1 in AR receptors can be activated even in the absence of androgen hormones which is believed to be responsible for AR activation in hormone refractory (Girling *et al.*, 2007).

The first sign of HRPC is a rise in PSA, which has been reduced during treatment, while bone and soft tissue metastasis are further indications of hormone resistance and thus of treatment failure (Ramon and Denis, 2007). Chemotherapy is the common option in treating HRPC; it would lead to improve the survival for up to ten months (Di Lorenzo *et al.*, 2007).

1.1.3.2. Other types of prostate cancer

There are other rare types of prostate cancers such as small cell carcinoma, squamous cell carcinoma and prostatic sarcoma that count around 1.5 to 2% of all prostate cancer cases in total. These rare types are very aggressive forms of prostate cancer (Tavora, 2013; Wagner, 2014). The diagnosis of these cancers is very complicated, since serum PSA levels are usually in the normal range, which is the main factor contributing to delayed diagnosis (Malik *et al.*, 2011). Common treatment options such as hormone therapy, radiation therapy and

prostatectomy are usually not applicable to these types of cancer. However, in some cases good control of the disease and improved survival time have been achieved by a combination of radiotherapy and chemotherapy (Munoz *et al.*, 2007).

1.1.4. Pathophysiology of the disease

The pathophysiology of prostate cancer can be histologically divided into three main levels based on tissue mutations. Morphological changes in prostate tissue start gradually and may take decades to evolve into cancer. In a normal prostate, the basal and luminal (secretory) cells are arranged in two layers in the gland, supported by the basal membrane (Figure 1-3, A). The histological changes start with the proliferative inflammatory atrophy (PIA), which appears as a dilation of the glands with notable change in the secretory cells. At this stage, prostate tissues undergo cell atrophy with signs of chronic inflammation (Woenckhaus and Fenic, 2008; Shah and Zhou, 2012). PIA mutation in the tissue is not categorized as cancer, although there is strong evidence that it could be considered as a precursor lesion to prostatic intraepithelial neoplasia (PIN) and then prostatic carcinoma (Ramon and Denis, 2007; Woenckhaus and Fenic, 2008).

The second progressive level of the histophysiology of prostate cancer is the PIN which is considered a precursor for prostate cancer and can be divided into two grades: low- and high-grade PIN. An enlargement in the nucleus of the secretory cells and a decrease in the number of stem cells with no changes in the basal membrane are the main histological mutations in the low-grade PIN. The morphological transformation progresses gradually until it reaches high-grade PIN, where the secretory cells are atrophied. Tissue malformation can be easily distinguished at this stage by a biopsy test (Ramon and Denis, 2007). The basal membrane starts to break down, which causes the basal cells to lose their cell-to-cell arrangement as well as increasing the invasion tendency to the prostate glandular tissue (Brawer, 2005; Ramon and Denis, 2007) (Figure 1-3, B). Some genetic changes also occur in high-grade PIN, such as

gaining chromosomes 7q31, 8q and Xq, and losing 8p, 10q, 13q and 16q, which are considered genetic precursors of prostate cancer (Nelson *et al*, 2003). However, in some cancer cases, the disease progresses from normal epithelium to cancerous tissue without passing through the intermediate stages of PIA and PIN (Ramon and Denis, 2007).

The development of high-grade PIN to cancerous tissue is strongly correlated with the genetic changes in the cancer cells that affect the normal balance in the adhesion molecules, leading to more degradation in the cell membrane with the loss of cell-to-cell adhesion. Cancerous tissues undergo abnormal expression of N-cadherin (gene at chromosome 18q11.2) and loss of E-cadherin (gene at chromosome 16q21/22), which is normally found in prostate cells. This change in cadherin level creates a stromal invasion of the tissue, which is the main criterion of cancerous tissue and can be defined as the invasive growth of cancer cells beyond the disrupted basal membrane. In addition, the continuous release of N-cadherin in cancer cells increases the metastatic ability which is the migration of some cancer cells to the surrounding organs such as the rectum and the bone (Ramon and Denis, 2007).

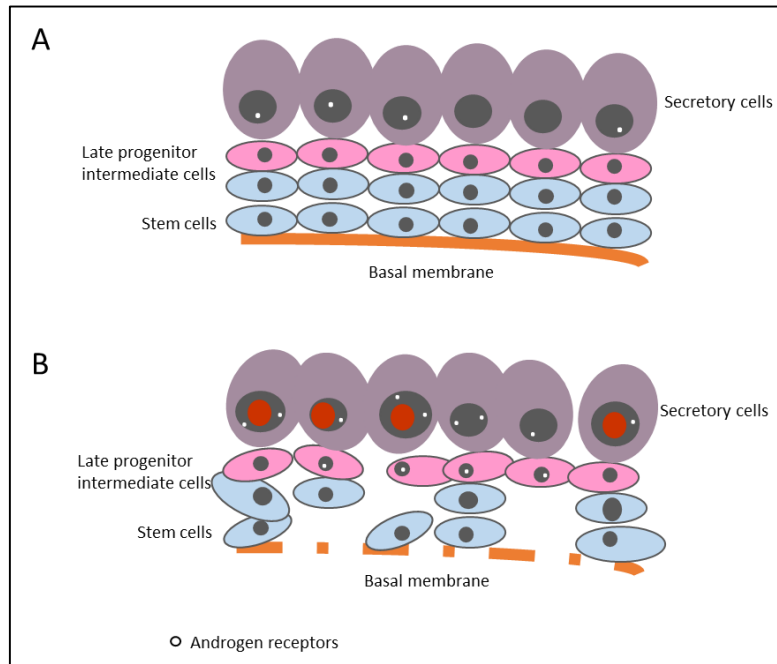


Figure 1-3 Anatomical differences between normal and cancerous prostate tissue: A) normal shape of the basal and luminal cells in the prostate; B) tissue morphological changes in prostate cancer (adapted from Ramon and Denis, 2007)

1.1.5. Screening

Prostate cancer screening is usually performed by blood testing for prostate specific antigen (PSA), since a high serum level indicates prostate disorders such as prostatitis, benign prostatic hyperplasia, or malignant tumours. Some countries have a prostate screening policy, which in the USA is applied to any man above 50 years old, or above 40 years for African-American men or men with previously affected first-degree relatives. Other countries have no defined rules for prostate cancer screening, since there is no strong evidence supporting the hypothesis that early detection actually reduces the mortality rate of the disease (Ramon and Denis, 2007).

1.1.6. Diagnosis

Unfortunately, most prostate cancer patients are rarely seeking diagnosis due to their limited prostate cancer symptoms. However, there are some signs and symptoms that should draw the patient's attention to the need for screening, such as haematuria, haemospermia and difficulty in urination due to prostatitis, which are signs of localized prostate cancer. Other symptoms

which may arise at later stages of the disease include bone pain and rectal obstruction (Philippou *et al.*, 2014).

A PSA blood test and digital rectal examination (DRE) are the primary diagnostic procedures that should be performed. Depending on their results, additional tests such as transrectal ultrasound and biopsy may be done.

1.1.6.1. Prostate specific antigen

Prostate specific antigen (PSA) is a human glycoprotein serine protease that is secreted specifically from the prostate epithelium. PSA is released in the semen of normal healthy males to assist the prostate function in lysis of the seminal coagulum. It is also found to be released in blood serum in its free or protein complexed forms (Stephen, 2012; Philippou *et al.*, 2014). PSA was first approved as a biomarker for prostate cancer in the 1990s. The diagnostic test, based on measuring the PSA level in blood serum, was developed for two reasons. First, most prostate cancer patients have been found to have an elevated PSA level which is linked to the high production of PSA in prostate cancer tissues (Stephen, 2012; Philippou *et al.*, 2014). In addition, the morphological mutations in the cancerous prostate glands increase the PSA serum level by the uncontrolled flow of PSA to the surrounding capillaries, which occurs due to the laceration of the tissue barriers between the cancerous glands and the capillary tubes. Secondly, any abnormality in the PSA serum level will particularly indicate prostate gland dysfunction, since its production is found to be very specific to prostate tissues. In normal base, the PSA serum level is around 2 ng/ml with an alerting abnormal level of 4 ng/ml and above (Philippou *et al.*, 2014).

Although the PSA test is sensitive for the antigen level in blood, its serum elevation is not very specific for cancer alone, i.e. a high serum level of PSA is considered a sign of various prostatic disorders, either benign or cancerous, such as prostatitis, benign prostatic hypertrophy and prostate cancer. This is considered the main drawback in using PSA as a diagnostic test and

explains the use of the digital rectal examination (DRE) test with it in most diagnostic guidelines (Stephen, 2012). For example, at PSA concentrations above 4 ng/ml, only 30% of cases develop a positive diagnosis of prostate cancer. The positive prediction rate increases to 42-64% if PSA is higher than 10 ng/ml (Philippou *et al.*, 2014). Unfortunately, some prostate cancer cases (6.6%) express very low PSA levels (0.5ng/ml) (Artibani, 2012).

1.1.6.2. Digital rectal examination

Digital rectal examination (DRE) is a physical examination of the rectum for any abnormality in the prostate. It is usually performed in parallel with the PSA serum test, since DRE can lead to a positive diagnosis even if the PSA level is normal. For instance, 30% of screened patients with a PSA level of 2.5 ng/ml are found during DRE to have abnormalities in the rectum, requiring more specific investigation by taking a prostate biopsy to confirm the positive diagnosis (Ramon and Denis, 2007).

1.1.6.3. Transrectal ultrasound

Transrectal ultrasound (TRUS) is a diagnostic test where a special endoscope is inserted into the patient's rectum to take ultrasound images, allowing the detection of abnormalities in the prostate such as size enlargement and tissue mutations. This imaging technique is usually used following the PSA test if its serum level was abnormally high to confirm the positive diagnosis (Philippou *et al.*, 2014). It is usually performed in parallel with a biopsy to help in guiding the needle. However, TRUS has some limitations, such as a weak ability to distinguish between benign and malignant tumours. Recent modifications designed to improve its performance and accuracy include three-dimensional ultrasound imaging (Ramon and Denis, 2007; Antunes *et al.*, 2014). Moreover, MRI-fused image technique was also developed to overcome the possibility of false diagnosis, since TRUS cannot usually guide a biopsy from some parts of

the prostatic transition zone, where around 30% of prostate cancer cases arise (Marberger *et al.*, 2012; Antunes *et al.*, 2014).

1.1.6.4. Prostate biopsy

Prostate biopsy is a test which involves screening prostate tissue under a microscope to detect any histological abnormalities. It is usually the last choice in the diagnosis guidelines, performed to confirm a positive diagnosis and more importantly to determine the exact stage of the disease. The accurate grading of prostate cancer is crucial in order to choose the most appropriate treatment for the patient (Ramon and Denis, 2007; Philippou *et al.*, 2014).

Prostate biopsy collection is usually performed with the guidance of TRUS, while a spring-loaded automatic biopsy gun is used to extract the specimens. Different prostate biopsy schemes are used to ensure systemic collection of samples from the prostate, but currently the one most commonly used is the extended biopsy scheme, with 12 cores (Stephen, 2012; Philippou *et al.*, 2014).

The histological grading of prostate cancer is performed by various methods; the most common method is the Gleason grading system (Philippou *et al.*, 2014). In 1966, Donald Gleason developed diagnostic procedure on the basis of histological images of specimens. Several changes have been made in the guideline since then. The grading system now has five major stages, where 1 is the mildest, as briefly described in Table 1-1 and Figure 1-4. However, instead of allocating the worst grade, the sum of the most dominant pattern and the next most dominant pattern is allocated to the tumour. A histological screening for the most abundant pattern of the tumour is usually done (primary grade), followed by a secondary grade for the next most frequent pattern of the tumour (secondary grade) for achieving more detailed diagnosis. The sum of these numbers should be between 2 to 10 where 2 is considered the mildest case (Shah and Zhou, 2012).

Table 1-1 Gleason grading system patterns (adapted from Shah and Zhou, 2012).

Prostate tissue grade	Major histological observation in the prostate tissues
Pattern 1	Oval uniform medium sized nodules aggregated but separated from each other.
Pattern 2	Almost like Pattern 1 but with more separated, less uniform nodules, and less arranged glands.
Pattern 3	Smaller, detached glands with more separation and variation in size and shape.
Pattern 4	Glandular units fused to each other with irregular shaped, perforated glands.
Pattern 5	Almost solid masses with no differentiation in glandular tissues.

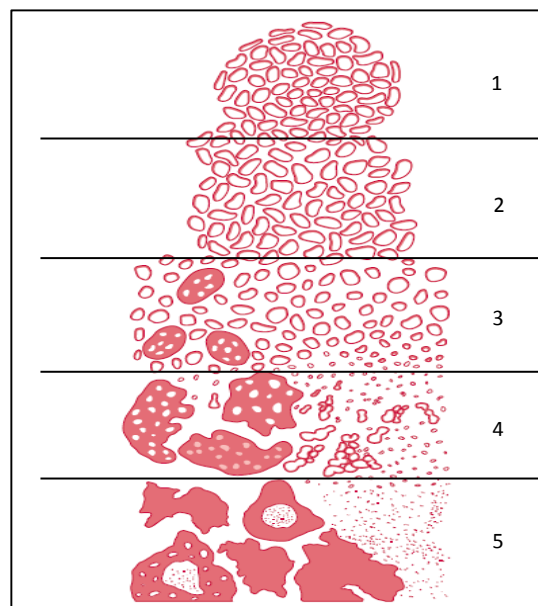


Figure 1-4 Modified Gleason grading system with five histological stages, where Grade 5 is the most advanced stage (Adapted from Shah and Zhou, 2012).

1.1.7. Treatments

Prostate cancer is usually diagnosed at the very late stages of the disease, which is one of the factors contributing to its high mortality rate in addition to the frequent failure of localized region prostate cancer cases therapy (Freytag *et al.*, 2007). Unfortunately, prostate cancer

patients rarely seek diagnosis during the localized stages of the disease, because most notice no symptoms other than the ones which resemble those of urinary tract infection (Philippou *et al.*, 2014).

In addition, prostate cancer treatment choices are limited; they are variable in their efficiency and associated side effects. The selection of the appropriate treatment plan depends mainly on the severity of the case, which determines the purpose of the treatment: either a total cure or prolongation of the patient's life and improved lifestyle. Patients diagnosed in the early stages of the disease have a better chance of total recovery, while the main goal is to improve and prolong the patient's life in the case of metastasis and relapse (Bagnall, 2014). However, most of the available treatment options are associated with major side effects and have limited ability to cure patients in the late stages of prostate cancer. Therefore, in light of the high and rising incidence of the disease, the search for new therapeutic approaches, including those applicable to metastasis cases, is crucial. (Bagnall, 2014).

1.1.7.1. Prostatectomy

Prostatectomy is a surgical procedure that is associated with the total eradication of the prostate gland and seminal vesicles. Radical prostatectomy is considered the treatment of choice for localized prostate cancer patients. However, it is not applicable to those with other health problems, since it constitutes major surgery (Bagnall, 2014).

Continuous monitoring is required after surgery to ensure the successful total removal of the tumour. Monitoring starts with a blood test for PSA, which is expected to be undetectable in blood samples after surgery, followed by histological screening of a biopsy extracted from the eradicated tumour site. If the prostatectomy does not succeed in complete removal of the tumour, radiotherapy is usually used as a second-line treatment.

Prostatectomy has been found to improve the survival rate of patients up to more than 10 years (Novara *et al.*, 2012). Nevertheless, it is associated with complications such as urination and

erectile dysfunctions, deep vein thrombosis and pulmonary embolism. These drawbacks reduce the favourability of this treatment option in applicable patients (Bagnall, 2014).

1.1.7.2. Radiotherapy

External beam teleradiotherapy (EBTR) is one of the options in the treatment of prostate cancer. Radiotherapy is a suitable treatment in all stages of prostate cancer, but with different purposes. Localized prostate cancer cases use EBTR to achieve total cure, while moderate to advanced (metastasis) cases undergo radiotherapy to control and localize the tumour and/or to control the pain (Bagnall, 2014).

The mechanism of action of EBTR is that ionized beams are focused on the tumour site to attack the DNA of the cancer cells. The affected cells lose their ability to divide due to the damage in their genetic material and, as a result, they undergo programmed cell apoptosis (Kulik and Dąbkowski, 2011). In order to avoid damage to the surrounding healthy cells, EBTR should be given in multiple small doses called fractions, since a single curative dose could lead to strong damage to the surrounding normal tissue. An initial MRI scan is also usually performed before the treatment, to improve the targeting of the beams on the tumour (Kulik and Dąbkowski, 2011; Bagnall, 2014).

Normal cells are less affected by radiotherapy because EBTR has higher selectivity for actively dividing cells, which makes normal cells automatically less affected by the radiation. Secondly, normal cells have high repairing ability that qualify them to restore after the radiation damages (Kulik and Dąbkowski, 2011).

1.1.7.3. Hormonal therapy

Androgen deprivation is another treatment option, since androgen hormones (testosterone and dihydrotestosterone (DHT)) have been found to be vital for prostate cancer cell proliferation. Hormone deprivation is considered the treatment of choice for metastasised tumours and

relapse prostate cancer. In addition, ‘localized’ and ‘localized advance’ tumours can be treated by hormonal therapy in combination with radiotherapy (Calabro and Sternberg, 2007).

The aim of the treatment is to block the testosterone hormone production in the patient’s body using various methods in order to reduce the testosterone level at the tumour site and decrease its effect on cancer cell growth. The approaches that are usually used to achieve a reduction in androgen hormones include orchiectomy and luteinizing hormone-releasing hormone (LHRH). Orchiectomy is the total removal of the testicles, which are the source of 95% of the testosterone in the male body. Testicles eradication results in a drop in testosterone level after only 12 hours following the operation. However, most patients are hesitant to undergo this operation, since it is irreversible and leads to changes in body shape (Bagnall, 2014). The method most commonly used to reduce androgen hormones levels is LHRH, which involves injecting the patient regularly every one to three months with a medication such as goserelin acetate or leuprorelin which suppresses the production of luteinizing hormone. Luteinizing hormone is released from the pituitary gland to stimulate the testicles to produce testosterone; by preventing its production, LHRH treatment reduces the production of testosterone (Schally and Block, 2010). A testosterone surge is a common side effect usually associated after the first injection of LHRH which could hamper the tumour regression.

The main limitation of androgen deprivation treatment is the development of resistance to hormone therapy and the subsequent recurrence of the disease in the form of hormone-refractory prostate cancer (HRPC) (Calabro and Sternberg, 2007; Bagnall, 2014).

1.1.7.4. Chemotherapy

Chemotherapy is one of the treatment choices for prostate cancer, especially in metastasis cases, although it is not highly favoured due to its severe side effects and low efficiency. It is considered the last treatment option, especially for patients who develop resistance to hormonal therapy, or relapsed patients with HRPC; its main purpose is prolonging the patient’s survival

(Calabro and Sternberg, 2007). The most common chemo-drug being used with prostate cancer is docetaxel which is an anti-mitotic drug that has been found to improve the survival rate especially for castration-resistant prostate cancer cases (Ryan *et al.*, 2013).

1.2. Gene therapy

Gene therapy is a new medical approach used to treat genetic and hereditary disorders such as cancer, Parkinson's disease, cystic fibrosis and others (Shan *et al.*, 2012). The United States Food and Drug Administration (FDA) defines gene therapy as any product which uses a transferred foreign genetic material to produce its effects by expressing and/or integrating the gene with the host cell genome for the purpose of cell modification both *in vivo* and *ex vivo*. The transferred gene is introduced to the host cell using a suitable vector such as a viral, bacterial or non-viral delivery system (Wirth *et al.*, 2013). It is based on delivering exogenous genetic material to host cells in order to resolve genetic mutation and regulate cellular processes (Shan *et al.*, 2012; Wang *et al.*, 2013).

1.2.1. History of gene therapy

The possibility of using gene therapy in humans arose in the early 1970s, when Rogers carried out the first human gene therapy. He transferred the arginase gene into twin girls suffering from urea cycle disorder, using the Shope papilloma virus as gene vector. The trial did not succeed and it later appeared that the viral vector did not encode the arginase gene (Wirth *et al.*, 2013).

In 1988, Rosenberg carried out an *ex vivo* trial by extracting tumour infiltrating lymphocytes (TILs) from metastatic melanoma patients. He used a retroviral vector to transfer the tumour necrosis factor (TNF α) gene into the extracted TIL cells, then reinjected them into the patients. The outcome was a decline in tumour growth with no sign of viable cancer cells at the site of injection, even after three weeks (Wirth *et al.*, 2013).

In 1990, the first gene transfer trial with a treatment purpose was approved by the US Food and Drug Administration (FDA). Blaese treated two children with adenosine deaminase deficiency using the *ex vivo* vaccine method, extracting white blood cells from the patients and introducing adenosine deaminase gene into them, then re-injecting them into the patients (Blaese *et al.*, 1995). There was individual variability in the outcome: one patient showed a good response to the treatment while the other did not. Nonetheless, this trial is considered the first successful experiment in the gene therapy field, whose promising results inspired others to proceed (Blaese *et al.*, 1995).

In 1999, a clinical gene therapy trial was performed to treat the 18-year-old Jesse Gelsinger who was suffering from partial ornithine transcarbamylase deficiency. A complication occurred after a high dose of the treatment, which caused an immediate response from the immune system and led to multiple organ failure. This highlights the risks of using viruses as gene vectors, as the incident was strongly linked to the viral vector used in this experiment (adenovirus) (Stolberg, 1999).

In 2003, the Chinese FDA approved the first gene therapy product to treat head-and-neck squamous cell carcinoma. Gendicine[®] is a non-replicative adenovirus that carries the p53 gene. This product created much controversy due to the lack of a phase III clinical trial (Ma *et al.*, 2009). Two years later, the Chinese FDA approved another gene therapy drug, Oncorine[®]. Oncorine[®] is used with chemotherapy to treat refractory nasopharyngeal cancer using a controlled replicative adenovirus.

In 2012, Glybera[®] was the first gene therapy to receive a recommendation for approval by the European Medicines Agency. It is an adeno-associated virus that carries the lipoprotein lipase gene to treat its severe deficiency by expressing the gene in muscle tissues.

Many gene therapy studies are currently underway worldwide, especially to treat cancer, which accounts for 60% of the total ongoing trials (Wirth *et al*, 2013).

1.2.2. Cancer gene therapy

Cancer is considered a genetic disorder, as various genetic mutations affect several genes in cancerous cells (Curiel and Douglas, 2005). Those mainly affected are tumour suppressor genes (e.g. P53 and nm23) and oncogenes (e.g. RAS, c-myc, bcl-2, and c-met) (Bookstein *et al.*, 1990; Mazhar and Waxman, 2004; Curiel and Douglas, 2005). Tumour suppressor genes are responsible for the regulation of normal cell death and cellular waste product cleaning; their inactivation by either total disappearance or mutation can promote cell malignancy. Oncogenes are responsible for consistent cell growth; their activation can boost cancer cell growth (Curiel and Douglas, 2005).

In prostate cancer, various genes are involved in the genetic mutations. For example, tumour suppressor genes p53 and retinoblastoma were found to be mutated in around 50% and 35% respectively of advanced prostate cancer cases. The main functions of p53 are to regulate the cell life cycle and repair any disruption in the DNA; when this gene is mutated, the result is uncontrolled cell growth (Bookstein *et al.*, 1990; Shalev *et al.*, 2001; Mazhar and Waxman, 2004). In addition, glutathione-S-transferase gene (p1) was found to be disrupted in some prostate cancer cases. The main cellular role of p1 is carcinogen detoxification and its inactivation leads to carcinogenesis (Shalev *et al.*, 2001; Mazhar and Waxman, 2004).

Different gene therapeutic strategies can be involved in prostate cancer treatment, such as gene apoptosis therapy, in which the transformed gene is replaced with one that regulates the cancer cells' death; immunomodulatory gene therapy, which uses genes to stimulate the immune system; and suicide gene therapy, which relies on introducing genes that cause changes to a chemical compound or enzyme to form toxic substances (Shalev *et al.*, 2001; Lu, 2009).

1.2.2.1. Apoptosis in gene therapy

Apoptosis is a normal physiological process that is programmed under certain circumstances to control cell death (Lu, 2009; Jia *et al.*, 2012). In normal cells, apoptosis is usually generated to eliminate cells that sustain genetic mutation or damage. Eliminating cellular apoptosis is one of the common problems generated due to genetic mutation in cancer cells, as it leads to cancer development. Therefore, using gene therapy to induce cellular apoptosis in cancer cells would be an effective treatment for cancer.

Tumour necrosis factor alpha (TNF α), tumour necrosis factor-related apoptosis-inducing ligand (TRAIL) and Fas ligand (FasL) are the most common cytokines to cause cellular apoptosis by binding to their specific death receptors (Walczak, 2013). Caspase activation, which occurs externally (by binding to the death receptor) or internally (via the mitochondria and death domain), is required for stimulating cell apoptosis (Wong, 2011; Jia *et al.*, 2012).

Apoptosis extrinsic activation occurs through the activation of the transmembrane death receptors (tumour necrosis factor receptors). The activation initiated by the specific binding of death ligands such as TNF protein family or Fas ligand (FasL) to their death receptors TNF-R1, TNF-R2 and Fas receptor respectively, which creates a particular binding site specific to the adaptor protein; this causes the formation of a death-inducing signalling complex (DISC), triggering the activation of caspase 8, which in turn causes cell apoptosis through activating effector caspases such as -3 and -6 that have the capability to recognizing proteins amino acids sequences that are involved in the main cellular physiological functions and cleave them at certain motifs to form substrate residues (Wong, 2011; Jia *et al.*, 2012).

Alternatively, the intrinsic activation pathway can arise in the cell itself, due to genetic damage, oncogene activation, or any stress condition. This pathway initiated from the mitochondria or endoplasmic reticulum. In mitochondrion, the mitochondrial membrane permeability is

controlled by a protein family called Bcl-2. After apoptotic stimulation, it causes the release of cytochrome-c followed by apoptosome, causing the release of the apoptotic peptidase activating factor 1 (Apaf-1) and as a result activating the initiator caspase -9 followed by the effector caspase 3 which initiates cell apoptosis (Wong, 2011).

Some cytokines are well known to cause apoptosis of inflamed and mutated cells (Wong, 2011); using this mechanism to suppress cancer has been found to have promising outcomes (Wang *et al.*, 1996; Tuting *et al.*, 1997; Jia *et al.*, 2012). Some common cytokines used for this purpose are TNF α , TRAIL and FasL.

1.2.2.1.1. Tumour necrosis factor alpha (TNF α)

TNF α is an inflammatory cytokine that produces many biological activities in the immune system, at inflammation sites, and in cell death and survival (Van Horssen *et al.*, 2006). To generate cell apoptosis, TNF α couples with its binding receptor (TNFR1), which is expressed in most tissues and leads to the activation of the death domain in the cytoplasm (TRADD) and Fas-associated death domain (FADD). This leads to the formation of DISC, which activates the pro-caspase 8, thereby causing DNA fragmentation and cell apoptosis (Chopra *et al.*, 2004; Tse *et al.*, 2012).

High level of TNF α causes cell apoptosis and necrosis, a property which can be employed to destroy cancer cells (Chopra *et al.*, 2004; Tse *et al.*, 2012). TNF α has been found to be efficient at inducing apoptosis when it is introduced externally to cells. Mauceri *et al.* (1996) used the TNF α gene to treat epidermoid carcinoma, together with targeted radiation therapy, and compared this with the same treatment in normal tissues in mice; the results showed highly selective tissue necrosis with no harm to normal tissue.

TNF α cytokine therapy was also tested against prostate cancer when Chopra *et al.* (2004) investigated the effects of TNF α on normal (NP) and cancerous (LNCaP) prostate cells *in vitro*,

the results for low doses of TNF α were promising, with significant (90%) LNCaP cell apoptosis and no effect on normal cells. Several articles have since been published, discussing the use of plasmid DNA encoding TNF α as an apoptotic agent with prominent finding after carrying this DNA to target different tumours including prostate cancer using targeted non-viral vectors as single therapy approach (Koppu *et al.*, 2010; Aldawsari *et al.*, 2011; Al Robaian *et al.*, 2014; Lim *et al.*, 2015).

1.2.2.1.2. Tumour necrosis factor-related apoptosis-inducing ligand

TRAIL or Apo2L is a cytokine that was first described by Wiley and colleagues in 1995. It is found in human tissues such as the spleen, prostate and ovaries. TRAIL binds to its specific receptors TRAILR1 (death receptor 4) and TRAILR2 (death receptor 5), causing activation of the death domain and cell apoptosis (Ashkenazi *et al.*, 1999; Norian *et al.*, 2011). In addition, TRAIL has also been found to bind with TRAILR3 (TRID/DcR1) and TRAILR4 (DcR2) decoy receptors which do not contain any cytoplasmic death domain and therefore cannot induce cell apoptosis. Thus, binding TRAIL to these receptors acts as an antagonist because it will not activate any cell death signalling. The existence of –R3 and –R4 in the cells is linked to their TRAIL apoptosis resistance (Griffith *et al.*, 2009).

The mechanism by which TRAIL induces apoptosis occurs mainly through the extrinsic pathway when TRAIL binds to –R1 or –R2 receptors which as a result stimulates TRAIL signalling cascade by forming death-inducing signalling complex (DISC). DISC includes several proteins such as FADD and pro-caspases 8 and 10. Therefore, after TRAIL binding and DISC activation, caspases 8 activation is initiated and so as caspases 3, 6, and 7. Caspases activation leads to the cleavage of target proteins responsible for preserving cellular function, resulting in cell apoptosis (Griffith *et al.*, 2009; Norian *et al.*, 2011).

The use of TRAIL as an agent to kill cancer cells arises from its preferential ability to induce cell apoptosis in cancer cells without harming normal healthy cells (Yu *et al.*, 2000; Farooqi and De Rosa, 2013). Ashkenazi *et al.* (1999) examined the apoptotic effect of TRAIL in various normal and cancerous cells. It was found to have good apoptotic activity against most cancer cells *in vitro* (32 of 39 cell types), and was not cytotoxic to normal cells. This criterion attracts the attention of numerous researchers to further investigate the anti-tumour activity of this cytokine. Moreover, TRAIL caused a significant reduction in tumour progression *in vivo*, with an accompanying increase in survival rate. Yu *et al.* (2000) also examined the effect of TRAIL cytokine *in vitro* in the androgen-insensitive prostate cancer cells (PC-3 and DU145). A TRAIL dose of 200 ng/ml resulted in 70% of cell death in both cell lines. The study also investigated the mechanism behind TRAIL effect, which was found to be the activation of caspase-8 and -3 by crosslinking and through the death receptors (DR4 and DR5).

Due to the successful outcomes obtained from using TRAIL cytokine as an apoptotic agent, Griffith *et al.* (2000) was the first group to introduce TRAIL cDNA instead of the cytokine delivered by adenovirus (Ad5-TRAIL) to examine its possible apoptosis effect against different cancer cells including prostate cancer PC-3 cells. *In vitro*, treating cells with Ad5-TRAIL showed similar antiproliferative effect obtained from using TRAIL cytokines, whereas other non-therapeutic DNA carried by the same carrier did not show any cytotoxic effect. The study also demonstrated the successful production of TRAIL protein in PC-3 cells after infecting it with Ad5-TRAIL using Western blot and flow cytometer. Later, numerous groups used adenovirus and adeno-associated virus as a carrier for the gene encoding TRAIL to target different cancer cells and tumours, including prostate in both *in vitro* and *in vivo* (Lin *et al.*, 2003; Seol *et al.*, 2003; Mohr *et al.*, 2004; Jiménez *et al.*, 2010). All of these showed the superiority of this gene in inducing cellular apoptosis *in vitro* and suppressing the tumour growth *in vivo*.

DNA encoding TRAIL was also complexed using different non-viral gene carriers for the purpose of avoiding the immunogenicity problem associated with using viral carriers. TRAIL was also examined in different studies as a single therapy approach for different cancer types. Chemically modified cationic dendrimers such as PPI and PAMAM have been used extensively to carry the plasmid encoding TRAIL (Koppu *et al.*, 2010; Lemarie *et al.*, 2012; Al Robaian *et al.*, 2014; Wang *et al.*, 2015; Gao *et al.*, 2016; Wang *et al.*, 2016); other studies have used cationic polymers as carriers for pTRAIL in order to form polyplex nanoparticles (Tzeng *et al.*, 2016; Wang *et al.*, 2016).

The route of administration of the polyplex or dendriplex, the number of injected doses, the DNA dose, and the fact that the gene therapy was a single approach or used with other treatments are all factors that play a key role in evaluating the outcome obtained from the *in vivo* studies. Intratumoral injection of DNA encoding TRAIL complexed with different carriers such as cationic dendrimer or polymer against breast cancer tumours was examined. The data demonstrated the capability of intratumoral injection of dendriplex (PAMAM: TRAIL) in preventing tumour growth (10 µg of DNA per injection) compared with polyplex (PEI: TRAIL) (Wang *et al.*, 2016). Similarly, Wang *et al.* (2015) targeted osteosarcoma intratumourally through PAMAM-triazine: pTRAIL dendriplex at N/P ratio 14:1 (10 µg pTRAIL per injection), which resulted in reduction in tumour size as well as slowing tumour growth rate.

However, some types of cancer cells develop resistance to TRAIL's apoptotic effect, caused by a mutation in the receptors responsible for the signalling pathway in the malignant cells, especially death receptors (Ashkenazi *et al.*, 1999; Norian *et al.*, 2011).

A combination treatment with different medications, chemotherapy, radiotherapy or another gene therapy has been examined extensively in the attempt to overcome TRAIL resistance (Kasman, 2007). However, the mechanism by which TRAIL resistance can be overcome is not

clarified. One mechanism could arise from the overexpression and activation of death receptors after treatment with chemo- or radiotherapy, which as a result improves sensitivity to the TRAIL apoptosis pathway (Farooqi and De Rosa, 2013). Voelkel-Johnson *et al.* (2002) tried to overcome the problem of TRAIL gene resistance in eight prostate cancer cell lines by combining gene therapy with doxorubicin, a chemotherapeutic drug hypothesized to play a role in improving the sensitivity of cancer cells to TRAIL. Cell death was significantly improved after the combination therapy in seven cell lines compared with each therapy alone. *In vitro* examination of TRAIL with the anticancer drug bortezomib in the LNCaP, LAPC4 and DU145 prostate cell lines also resulted in significant cell death (up to 90%) (An *et al.*, 2003). Shankar *et al.* (2005) and Kasman *et al.* (2007) combined TRAIL gene therapy with various chemotherapeutic drugs and found an improvement in the sensitivity of prostate cancer cells to the apoptotic effect of TRAIL, especially for the LNCaP and DU145 cell lines.

1.2.3. Gene delivery

In order to ensure the success of gene therapy, the therapeutic gene must successfully cross the cell membrane, and then integrate with the nucleus genome of the targeted cell. However, naked DNA cannot achieve this without undergoing degradation during its passage through the blood circulation and biological tissues (Taira *et al.*, 2005). Moreover, a charge repulsion can be created between the naked DNA and the cell membrane due to their common negative charge, which can hinder gene transfection inside the cell (Wang *et al.*, 2013).

These drawbacks can be overcome by using a suitable gene delivery system. Gene delivery can be simply defined as a process to introduce a foreign gene to a host cell using a gene carrier (Kamimura *et al.*, 2011). It involves the complexation of the gene of interest to a suitable gene delivery vector, in order to facilitate its transfection to the targeted cells (Wilson 1996; Taira *et al.*, 2005). The main challenge in gene delivery is to find an effective delivery system able

to target the required tissue and delivering the transferred gene to the cells without major side effects (Wang *et al.*, 2013).

Gene delivery confers several advantages on the complexed gene, such as protecting it from degradation in the blood circulation and increasing the targeting specificity to the required tissue. Several methods can be used to transfer genes, such as viral and non-viral vectors, and even naked DNA transferred by physical methods (Curiel and Douglas, 2005). Studies seeking more targeted and less toxic vehicles are ongoing.

1.2.3.1. Viral vectors

Viruses are highly efficient at transferring their own genomes to host cells; this unique ability has been invested to transfer therapeutic genes to specific cells (McTaggart and Al-Rubeai, 2002). Modified (replication-deficient) viruses are used as gene vectors to attenuate their ability to induce infection (Kamimura *et al.*, 2011).

The use of viruses as gene vectors has several advantages. First, viruses have a strong ability to pursue and attach to specific cells (targeting ability) and they exhibit great efficiency at introducing genetic material into cells (transfection). These targeting and transfection abilities ensure the transfer and penetration of the gene to the required cells. Second, viral vectors are found to integrate genes into the targeted cells for a longer period than non-viral vectors (Curiel and Douglas, 2005).

On the other hand, viral vectors are also associated with disadvantages such as immunogenicity (Hunt *et al.*, 2007); the immune system can identify a virus as a foreign substance and initiate an immune response against it, especially if the patient has been exposed to that virus before. This immune reaction can obstruct the function of the viral vector by attacking it in the bloodstream, reducing its probability of reaching the targeted cells and achieving successful gene penetration (Curiel and Douglas, 2005). In addition, viral vectors have limited ability to

condense and transfer large DNA molecules (Wang *et al.*, 2013). Other potential drawbacks could arise from using viruses as gene vectors are toxicity and oncogenicity (Shan *et al.*, 2012). Several viruses are used as gene vectors such as retroviruses, adenoviruses, adeno-associated viruses and the herpes simplex virus (Curiel and Douglas, 2005). The need for different viral vectors arises from the variety of genes to be delivered, where each gene has its own special criteria which requires the vector to fulfil these requirements (Selleck *et al.*, 2003). For example, genetic disorders usually demand long-term treatment, which requires a gene vector that is able to induce permanent gene expression and integration, such as an RNA-based virus (e.g. a retrovirus). In contrast, in suicide gene therapy, the therapeutic gene needs to be expressed for a short period without the need for its integration with the host cell genome, which makes transient vectors such as adenoviruses more suitable for this treatment approach (McTaggart and Al-Rubeai, 2002; Kamimura *et al.*, 2011).

1.2.3.2. Non-viral vectors

Non-viral delivery systems are based on the use of non-viral vectors such as liposomes or polymers to transfer the therapeutic gene to the required tissue. The delivery of the gene occurs via electrostatic interactions between the gene and the non-viral vector, which leads to the condensation of the gene with the vector (Wang *et al.*, 2013). Several advantages can arise from this complexation, such as protecting the gene from the surrounding environment, as well as preventing the degradation of DNA by the nuclease enzymes in the circulation (Ogris and Wagner, 2002; Wang *et al.*, 2013). In addition, it reduces the charge repulsion that arises from the charge similarity between the DNA and cell membrane, which in turn improves the penetrative ability of the gene inside the cells (McCrudden and McCarthy, 2013). Furthermore, non-viral vectors possess higher gene complexation ability for large DNA molecules when compared to viral vectors, due to their well-constructed chemical structure, while cationic

functional groups that are located at specific positions in the structure assist in complexing the DNA molecule.

On the other hand, viral vectors have been found to have a better targeting ability than non-viral vectors. However, the targeting ability of non-viral vectors can be improved via the use of a binding ligand that is designed to target a specific cell receptor in the targeted tissue (Wang *et al.*, 2013).

1.2.3.2.1. Cationic polymers

Cationic polymers are macromolecules that possess positive charges due to their high density in amine groups. Among the different types of cationic polymers developed in recent years are neutral polymers (e.g. chitosan), polypeptides (e.g. poly-L-lysine) and dendrimers (e.g. polyamidoamine). Some chemical modifications can be applied to these polymers in order to improve their efficiency as vectors and reduce their toxicity via the use of binding ligands (Wang *et al.*, 2013).

The concept of using polymers as drug or gene carriers was first developed in 1970 by Ringsdorf (Taira *et al.*, 2005). This can be achieved through the interaction between the polymer and DNA, where positively charged groups in the polymer tend to form an electrostatic attractive force with the negatively charged phosphates in the DNA. The molecule formed is called a polyion complex or polyplex and usually leads to the DNA condensing to around 10^{-3} of its actual size (Curiel and Douglas, 2005). Polymers tend to protect the complexed genetic material (DNA) from hydrolysis in the circulation or in the body tissue, giving it a longer half-life and better targeting (Curiel and Douglas, 2005).

Several criteria can affect the efficiency of the polyplex. For example, a higher molecular weight polymer provides superior condensation of the genetic material (Taira *et al.*, 2005). Another important factor that can contribute to polyplex efficiency is the charge ratio, which is a parameter used to calculate the nucleotide equivalence using the ratio of nitrogen (in the

polymer) to phosphate (in the DNA). The total charge should be positive in order to form a stable and effective polyplex (Männistö *et al.*, 2005). Although the charge ratio is important, it should to a certain extent be limited. A high total positive charge on the polyplex can have various side effects: a high charge ratio raises the systemic cytotoxicity of the polyplex and it can lead to a random interaction between the polyplex and biological membranes, thus attenuating the targeting ability and causing a loss of specificity (Mastrobattista and Hennink, 2012). In order to overcome these problems, a polypeptide such as PEG can be conjugated with the polyplex to reduce the overall charge ratio without affecting its gene complexation capability (Mastrobattista and Hennink, 2012). Alternatively, the high charge problem can be overcome by the use of newly designed cationic polymers with hydroxyl or amide groups, such as poly(vinyl alcohol) dimethylaminoacetal (PVA3), that are shown to have effective gene transfer, less toxicity and better DNA release in the cytoplasm. This effect can be explained by a decrease in the total positive charge or the formation of hydrogen bonds between the DNA and hydroxyl groups (Taira *et al.*, 2005).

1.2.3.2.1.1. Examples of cationic polymers

Poly-L-Lysine (PLL) is a polypeptide cationic polymer which is one of the early polymeric vectors used in gene delivery (Wang *et al.*, 2013). PLL contains high density of primary amines (Figure 1-5) that have a strong affinity to the negative ions at neutral pH, since most of them are ionized at pH 7.4 (Männistö *et al.*, 2005). The use of PLL as a gene carrier is associated with certain limitations. For example, its gene transfection ability is weak at the biological pH, due to the strong interaction between DNA and PLL, which obstructs the release of DNA to the cytoplasm. Additionally, the chemistry of PLL is associated with a certain toxicity because it contains amino groups. The modification of PLL with ligands can reduce its side effects and improve its ability as a gene carrier, especially in *in vivo* trials, since it is biodegradable (Männistö *et al.*, 2005; Wang *et al.*, 2013).

Another cationic polymer that is commonly used as a vector in gene delivery is polyethyleneimine (PEI). Its unique chemical structure, having a nitrogen atom to every three atoms, promotes its DNA complexation ability to form a stable polyplex, as well as a strong ability to condense large molecules (Figure 1-5) (Wang *et al.*, 2013). At pH 7.4, only 17% of the nitrogen groups in PEI are ionized. This gives PEI several advantages. It has a superior DNA condensation ability with a high gene transfection capability, since it can easily release DNA into the cytoplasm (Männistö *et al.*, 2005). Moreover, the low protonated PEI facilitates the endosomal escape of polyplex from the lysosome by means of the proton sponge effect (Wang *et al.*, 2013).

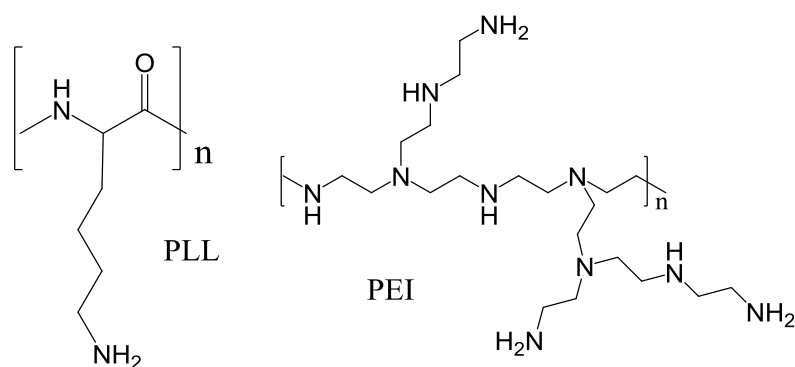


Figure 1-5 Chemical structure for the most common cationic polymers used in gene delivery (adapted from Taira *et al.*, 2005)

1.2.3.2.2. Dendrimers (dendritic polymers)

Dendrimers are three-dimensional branched macromolecules with a tree-like structure that were first synthesised in the late 1980s by Donald Tomalia. The name is taken from the Greek word *dendron*, which means ‘tree’. Since their discovery, dendrimers have been used in various applications in pharmacy, medicine and engineering (Klajnert and Bryszewska, 2001; Dufès *et al.*, 2005; Taira *et al.*, 2005). Their chemical structure is composed of two parts, a reactant core molecule which is considered the origin of the dendrimer, and highly branched polymers that

bind to the core in a very specific way to form a uniformly branched spherical macromolecule (Dufès *et al.*, 2005).

Dendrimer synthesis can be accomplished through either divergent or convergent pathways. Divergent synthesis is based on growing the dendrimer outwards, starting from a core of multifunctional groups that react with monomer molecules to form the first-generation dendrimer. Structural defect can arise from the use of this method if side reactions are incomplete. Convergent synthesis operates on the reverse principle of coupling the monomer groups to form dendrons, which then attach themselves to a multifunctional core molecule (Figure 1-6). This method yields dendrimers with a better three-dimensional structure (Klajnert and Bryszewska, 2001).

In either case, dendrimer synthesis occurs by a well-defined set of reactions leading to the formation of one generation, then repeating this sequence of reactions causes the formation of a new and higher generation. Each new dendrimer generation is twice the size of the previous one and has twice as many binding sites (Klajnert and Bryszewska, 2001; Dufès *et al.*, 2005).

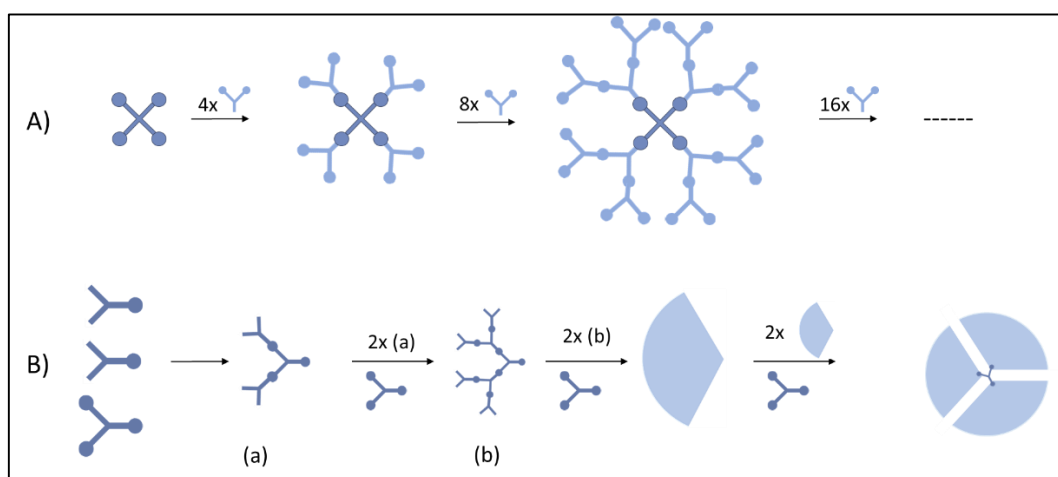


Figure 1-6 Different methods used in dendrimer preparation A) divergent synthesis method, which initiated upward and B) convergent method which started backward (adapted from Klajnert and Bryszewska, 2001)

The use of dendrimers in gene delivery is restricted to cationic dendrimers such as polyamidoamine (PAMAM) and diaminobutyric polypropylenimine (DAB). Cationic dendrimers tend to complex the genetic material by initiating an electrostatic interaction between the phosphate groups on the DNA and the amino groups on the dendrimer, which leads to the formation of dendriplex nanoparticles (Dufès *et al.*, 2005). Among their advantages over regular polymers, dendrimers have a significant gene transfection ability which increases with higher generations (Taira *et al.*, 2005). Their tree-like shape also increases the surface area of the molecule and creates inner cavities, thus improving their DNA complexation and encapsulation capability. DNA complexation with dendrimers is also affected by reaction properties such as pH, salt and buffer capacity. Additionally, dendrimers have been found to be non-immunogenic molecules, which makes them suitable gene carriers for *in vivo* experiments (Dufès *et al.*, 2005; Kim *et al.*, 2007).

On the other hand, dendrimers have some level of toxicity which also increases with higher generations. This toxicity arises from the high positive charge ratio of the molecule. It also depends on the surface charge, so that primary amines are more toxic than secondary or tertiary amines (Dufès *et al.*, 2005). In order to overcome this limitation, conjugation with a peptide, acetylation and alkylation can reduce dendrimer toxicity and promote delivery specificity by lowering the charge ratio (Shan *et al.*, 2012).

PAMAM and DAB are the most common cationic dendrimers used in gene delivery. The remainder of this subsection outlines their chemical structure and synthesis. Structurally, PAMAM has two main parts, the first being the reactive core molecule, which is usually the source of structural difference in PAMAM dendrimers; it can be a trivalent core such as ammonia (NH₃) or a tetravalent core, e.g. ethylenediamine. Changing the core molecule leads to the formation of a different dendrimer shape, charge and density. The second part of the PAMAM structure is the branches, formed from reacting methylacrylate with the ammonia

core, followed by the binding of ethylenediamine (Figure 1-7) (Dufès *et al.*, 2005; Taira *et al.*, 2005).

The core molecule of the DAB dendrimer is butylenediamine. Its synthesis starts when this core molecule is reacted with acrylonitrile, followed by the hydrogenation of the nitrile groups to primary amines. This process is repeated until the required dendrimer size is achieved (Figure 1-8). The molecule is usually called DAB_x, where x is the number of positively charged amines in the surface (Dufès *et al.*, 2005).

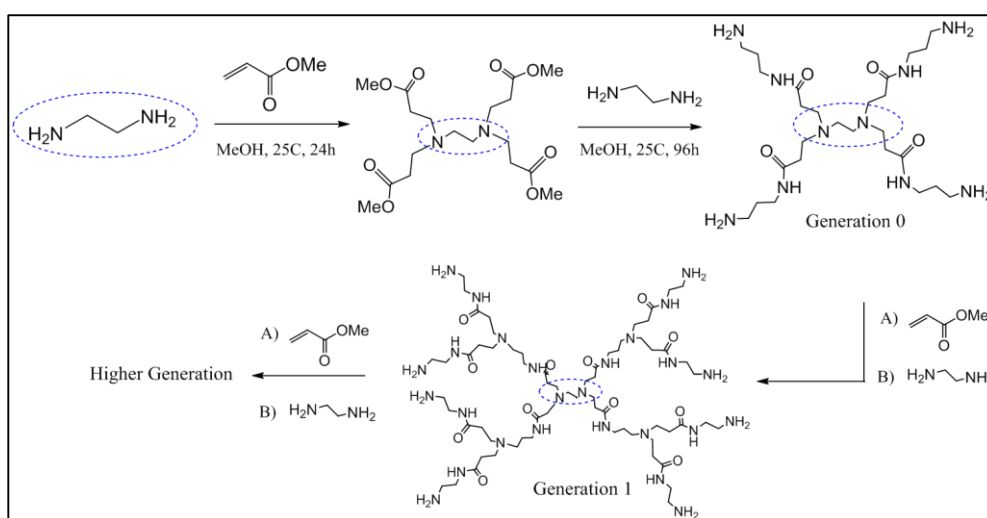


Figure 1-7 Synthesis of PAMAM dendrimer and chemical structure of its different generations (adapted from Dufès *et al.*, 2005).

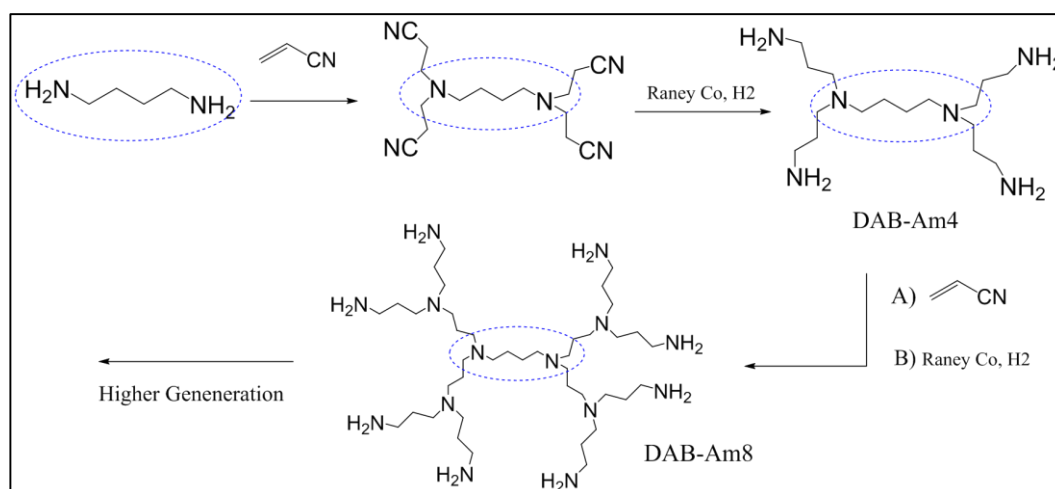


Figure 1-8 Synthesis of DAB dendrimer (adapted from Dufès *et al.*, 2005).

1.2.3.2.2.1. Diaminobutyric polypropylenimine (DAB)

Among dendrimers, PAMAM has been examined extensively as a gene carrier, whereas DAB has been more rarely considered, due to the high cytotoxicity of its high generations. Studies of the use of DAB dendrimers as gene carriers have tended to focus on the high generations, with few testing the use of low generations in gene delivery. Recently, however, polypropylenimine low generations (DAB-Am4, 8 and 16) were found to have low cytotoxicity, making them potentially attractive as non-viral vectors for genetic materials (Zinselmeyer *et al.*, 2002; Kim *et al.*, 2007; Zhang *et al.*, 2014).

Zinselmeyer and colleagues (2002) evaluated the transfection efficacy and the cytotoxicity of various generations of polypropylenimine dendrimers. From the data obtained, as the size of DAB increases, its DNA complexation ability improves. DAB third generation (DAB-Am16) was found to complex the DNA completely in a helical turn, whereas lower generations were partially bound to the DNA molecule. Furthermore, the toxicity of polypropylenimine dendrimers is reported to increase with increasing molecular weight, due to the high charge density generated, leading to uncontrolled binding between the dendrimer molecule and the cellular anions. Fortunately, DNA complexation with the dendrimer leads to the reduction of this cytotoxicity due to the decline in the total charge of the dendriplex formed. However, the cytotoxicity of DAB dendrimers generations 3, 4, and 5 will only partially decrease. Finally, the study demonstrates that among the different generations of DAB, the optimum gene transfer activity occurs with DAB-Am16 (Zinselmeyer *et al.*, 2002). This suggests that third-generation DAB is the most appropriate polypropylenimine molecule for use as a gene carrier, due to its efficiency in DNA binding, its transfection ability and the controllable toxicity level, which is reduced dramatically by gene binding. In this study, the third-generation polypropylenimine dendrimer (DAB-Am13) was selected as the gene vector.

1.3. Cancer targeting

1.3.1. Passive targeting

A tumour needs blood and oxygen to grow, but when it reaches a specific size, the surrounding blood vessels become incapable of nourishing the tumour mass adequately. The tumour cells start to shrink and die; these shrinking cells then release growth factors that trigger angiogenesis, i.e. the growth of new capillaries which supply blood to the tumour (Bertrand *et al.*, 2014). The new capillaries are incompletely grown and tend to take an irregular shape, with disruption to the epithelial and basal membranes, causing them to have high permeability towards the surrounding tissues. These abnormal vessels acquire an extensive blood supply for the outer cortex of the tumour but with minimal supply to the core, associated with semi-necrotic effects (Ogris and Wagner, 2002; Bertrand *et al.*, 2014). In addition, the lymph nodes in tumour sites do not function properly, as they cannot perform systemic filtration of the extracellular fluids; the result is that diffusion of macromolecules and colloids back to the circulation is obstructed (Bertrand *et al.*, 2014).

Passive targeting is a naturally occurring process that arises from the unique pathophysiology of the tumour site. Due to the nature of the blood vessels formed and the disruption of the lymph nodes' function, macromolecules and nanoparticles (NPs) tend to accumulate in the tumour tissues. This is called the enhanced permeability and retention (EPR) effect or passive targeting (Bertrand *et al.*, 2014). Its efficiency is affected by several factors, such as the vascular permeability of the tumour blood vessels and the size of macromolecules, which controls their diffusion to the cancer tissue. Most blood vessels in cancer tissues have a diffusion permeability between 200 and 2000 nm depending on the location and the type of the tumour (Bertrand *et al.*, 2014).

Passive targeting is also associated with certain drawbacks, such as low targeting specificity, which reduces the therapeutic efficiency of the transferred nanomedicine because of its

restricted access to the targeted tissue. Low targeting can also increase the expression of systemic side effects of the transferred cytotoxic agents (Won *et al.*, 2012). Some methods have been used to improve targeting specificity. For example, the introduction of a perfusion pressure during the intravenous administration of the drug improves the targeting of NPs to the cancer site. The administration of vasodilator medication also brings some improvement in passive targeting by increasing the vascular permeability of the tumour vessels to the macromolecules (Won *et al.*, 2012). A reliance on passive targeting alone to transfer nanoparticles is not sufficient to overcome the systemic side effects and weak targeting. Therefore, active targeting should be used in addition to passive targeting, to improve the targeting capability of the nanoparticles.

1.3.2. Active targeting

Active targeting is a method whereby nanoparticles are designed specifically to target an organ, tissue, or cell by chemically conjugating the nanoparticle with a specific compound called a ligand, which has the ability to bind to a special binding site in the targeted tissue. The ligand could be a protein, vitamin, antibody, nucleic acid, or even sugar, while the targeted binding site could be a receptor, sugar, protein, or lipid that is highly expressed in the targeted tumour site (Bertrand *et al.*, 2014).

Several factors affect the efficiency of active targeting. First, the chosen ligand should have specific overexpressed receptors on the targeted cells in order to ensure a particular targeting and reduce the possibility of non-specific binding. It is important to mention that some ligands have the ability to bind to more than one type of receptor, which could increase the chance of non-specific binding (Bertrand *et al.*, 2014). In addition, the conjugation reaction of the ligand with the nanoparticle has a major impact on the stability of the complex formed. It is always preferable to perform the conjugation reaction with the polymer before condensing the genetic material. This one-step reaction has the advantages of low probability of side reactions, with

straightforward purification of the final polymer formed which results in better control of the polyplex properties.

The binding that occurs between the delivered ligand-NPs and targeted receptor facilitates the uptake of NPs inside the cell through receptor-mediated endocytosis. The ligand-nanoparticle enters the cell cytoplasm together with the receptor and is trapped in an endosome (Wagner *et al.*, 1994; Ogris and Wagner, 2002). The acidic endosomal environment (low pH) triggers the release of the nanoparticle to the nucleus, while the receptor and ligand either lyse or return to the cell membrane and separate from each other.

The genetic material finds its way to the nucleus through three possible pathways:

- During cell division, when the nucleus membrane lyses and allows the genetic material to migrate inside the nucleus. This is the common pathway with cancer cells, since they possess high growth rate.
- The passage of DNA through the nuclear membrane pores, which can normally accommodate molecules with a maximum diameter of 9 nm (Pérez-Martínez *et al.*, 2011).
- Active transport, which based on introducing chemical compounds that enhance the passage of transgenes, making it possible to introduce the gene to the nucleus (transfer carriers) (Ogris and Wagner, 2002; Pérez-Martínez *et al.*, 2011). This method is based on binding nuclear localization signals such as basic amino acids to receptors in the nuclear membrane; active transport can help in transporting molecules of up to 30 nm in diameter (McCrudden and McCarthy, 2013).

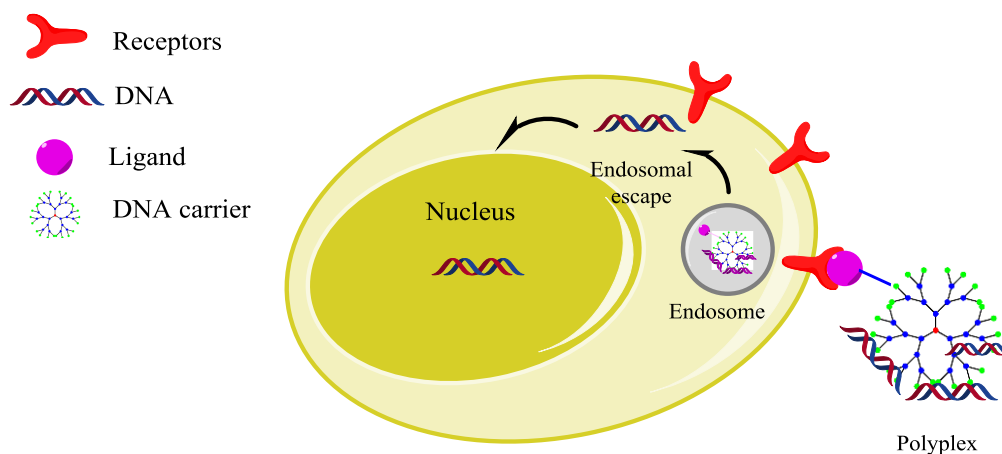


Figure 1-9 Active tumour cell targeting (by receptor-mediated endocytosis) (adapted from Wagner *et al.*, 1994)

1.4. Delivery barriers

Several factors affect the delivery of polyplex, lipoplex and dendriplex nanoparticles to their specific targeted cancer sites, especially if the treatment is taken by intravenous administration, which is the only choice in the treatment of metastasis (Ogris and Wagner, 2002). These factors can be classified as systemic and cellular barriers.

1.4.1. Systemic barriers

Systemic barriers are any factors that obstruct the delivery or binding of a nanomedicine to its targeted cells, from its administration until it reaches the required site. In the bloodstream, nanoparticles (NPs) face a number of barriers, especially after intramuscular or intravenous administration.

Due to their net positive charge, nanoparticles could undergo non-specific binding to negatively charged molecules such as immunoglobulin M, complement C3 and other proteins in the circulation by electrostatic interactions, which can lead to the dissociation of the NPs before reaching the target site (Ogris and Wagner, 2002; McCrudden and McCarthy, 2013). This is usually overcome by conjugating the NPs with an anionic hydrophilic molecule such

as poly PEG, to reduce their total positive charge, and therefore decreases non-specific aggregation and improves transfection ability (McCrudden and McCarthy, 2013).

Another issue that can arise during gene delivery is the intake of the non-viral vector by the immune cells in the bloodstream which identify it as foreign particles (Ogris and Wagner, 2002). Non-viral vectors are usually less immunogenic compared with viral. Nevertheless, a non-viral delivery system that is complexed with DNA molecules can still face an immune reaction due to the unmethylated CpG sites in the condensed gene. The immune response can be diminished by eliminating unnecessary CpG sites from the complexed gene or by reducing the administration dose (McCrudden and McCarthy, 2013).

Furthermore, the final systemic targeting barrier is the extracellular matrix that is formed in the cancerous tissues and composed of several proteins and collagen which obstructs the permeability of the nanoparticles through the tissue, impeding them from reaching the targeted cells (Ogris and Wagner, 2002).

1.4.2. Cellular barriers

Cellular barriers can be categorized as any factors that arise at the cellular level and lead to a reduction in the efficiency of the gene therapy. The first cellular obstacle that could face NPs when they approach the targeted cells is the transfection efficiency, which mostly occurs via conjugating a suitable ligand to the NP. The binding of the ligand to its specific receptor in the cell membrane allows the transfection of the NP via receptor-mediated endocytosis, a cellular biological process whereby a specific molecule can enter or leave the cell with the assistance of a specific receptor in the cell membrane. The endocytosis process or endocytic pathway can be considered a barrier to gene delivery, since its efficiency can be affected by several complications, such as the size of the NP. It has been observed that NPs smaller than 50 nm show significant uptake by the cells through endocytosis, compared with NPs larger than 50 nm, with an optimum size being 25 nm (Gao *et al.*, 2005).

The second cellular barrier take place during the uptake of the NP inside a cell, when the NP-ligand-receptor complex is trapped inside an endosomal sack. In the endosome, NPs and genetic material may undergo degradation by lysosomal nucleases and low pH environment (Ogris and Wagner, 2002; Pérez-Martínez *et al.*, 2011). In overcoming this limitation, NPs tend to escape from the endosome through the proton sponge effect, which is initiated by the acidic pH of the endosome. The low pH increases the ionization of the NPs (cationic polymer or dendrimer), then the ionized polymer attracts protons to the endosome, leading to an increase in the osmotic pressure and causing endosomal swelling and disruption, which releases the therapeutic gene in the cytoplasm (Pérez-Martínez *et al.*, 2011; McCrudden and McCarthy, 2013).

Finally, after endosomal escape, up to 99% of the DNA may be degraded by cytoplasmic nuclease if it persists for a long time in the cytoplasm. The last obstacle to gene delivery is the effective passage of the delivered DNA through the nuclear envelope (lipid bilayer nuclear membrane). Normally, nuclear transportation is controlled by the nuclear pore complex (NPC), which is permeable to molecules with size less than 70 kDa (10 nm in diameter) (McCrudden and McCarthy, 2013).

Two methods are used to transfer genes into the nucleus and reduce the possible degradation in the cytoplasm. The first is passive transport, which occurs during cell division, where the nuclear envelope lyses, allowing the genetic material to be transported to the nucleus. This is the most common method in cancer cases, since cancer cells actively divide. The second is active transport, where nuclear localization signals (NLS) are used to binds to NPC to allow larger DNA molecules to pass through these pores (Pérez-Martínez *et al.*, 2011). Working to improve these methods may minimize the cytoplasmic degradation and induce better gene expression in the nucleus. For instance, covalent and non-covalent binding of the DNA or its carrier to NLS peptides or proteins could improve the active importation of DNA to the

nucleus; but it is not clear whether or not these peptides will be separated from the DNA after gene transfer, which could result in the biological effect of the expressed gene being changed or lost. In general, dendrimers are shown to have a better gene transfection to both cell and nucleus than other non-viral delivery systems, although research is ongoing on how to improve it (Pérez-Martínez *et al.*, 2011).

1.5. Aim and objectives

Prostate cancer is considered one of the leading causes of death among all cancer types. Unfortunately, no single treatment is associated with high efficiency without toxicity or major side effects, especially in the late stages of the disease (metastasis). These side effects mostly arise due to poor targeting of the cancer tissue. It is crucial to find new therapies for prostate cancer with high selectivity to overcome systemic side effects.

Gene therapy is one of the new treatment approaches under investigation for different cancer types. The main factors reducing the efficiency of gene therapy is the lack of a suitable delivery system that is successfully able to deliver and transfect the therapeutic gene to the cancer site. The aim of this study is the synthesis of different novel non-viral gene delivery carriers with specific tendency to target prostate cancer. We hypothesize that conjugating the cationic dendrimer 3-diaminobutyric polypropylenimine with different targeting ligands that their receptors are overexpressed in prostate cancer cells, may significantly improve the therapeutic efficacy *in vitro* and *in vivo*. The objectives of this study are therefore:

- To synthesise and characterise lactoferrin- and peptide- bearing 3-diaminobutyric polypropylenimine (DAB) dendrimer as targeted gene carriers for prostate cancer.
- To evaluate *in vitro* the targeting capability and therapeutic efficiency of the delivery system after condensing plasmid DNA previously known to cause cell apoptosis, such as tumour necrosis factor (TNF α), tumour necrosis factor-related apoptosis-inducing ligand (TRAIL) or interleukin 12 (IL-12).
- To evaluate the therapeutic efficacy of the synthesized dendriplexes *in vivo*, following intravenous administration to mice bearing prostate tumours.

Chapter 2 : Synthesis and characterisation of lactoferrin- and peptide- bearing polypropylenimine dendrimers.

2.1. Introduction

Gene therapy is one of the promising approaches in treating cancer. However, nucleic acids undergo degradation in the blood stream. Thereby, the success of gene therapy depends on finding a suitable gene carrier that is capable on efficiently condense the gene of interest and safely delivers it to the targeted cells, which is by itself a challenging problem due to the lack of safe and effective carriers. Non-viral gene delivery carriers are one of the prominent vectors in complexing DNA. They are superior over viral vectors because of the immunogenicity obstacle that is usually associated with using viruses. In addition, non-viral vectors have the capacity in packing large DNA molecules whereas the maximum packing capacity of adenovirus, a commonly used viral vector is 7.5 kb (Gene therapy net, 2017). In addition, the high control in the design of non-viral vectors is considered an advantage because it yields a structure with well-defined properties (Kim *et al.*, 2007; Zhang *et al.*, 2014).

Dendrimers in particular have gained special attention as effective gene carriers. Diaminobutyric polypropylenimine (DAB) is a promising example which has been found to be very effective in gene transfer. The low generations of DAB dendrimer, especially the third and second generations were found to have effective gene transfection with low cytotoxicity (Zinselmeyer *et al.*, 2002; Schätzlein *et al.*, 2005). The efficacy of DAB as gene carrier depends on the successful transfection of the therapeutic gene to the required site. The third generation of DAB (DAB-Am16) has been proven to have the optimal gene transfection capability among the different polypropylenimine dendrimer generations. However, to avoid non-specific binding in the circulation after intravenous administration, surface modification of DAB dendrimer with specific targeting ligands such as proteins or peptides that specifically target receptors that are overexpressed on the cancer cells seems to be most effective (Schätzlein *et al.*, 2005; Taira *et al.*, 2005). Lactoferrin, prostate specific membrane antigen (PSMA) and integrin receptors are found to be extensively expressed on prostate cancer cells to different

extents. Targeting these receptors using specific coupling ligands should theoretically increase the targeting ability of the modified nanomedicine.

2.1.1. Prostate cancer targeting ligands

2.1.1.1. Lactoferrin

Lactoferrin (Lf) is an iron-binding, single chain glycoprotein of the Tf family with a molecular weight of 80 kDa and 703 amino acid sequence, with 60% similarity in its chemical structure to Tf (Adlerova *et al.*, 2008). The main function of Tf and Lf is to control the free iron level in the blood and body fluids respectively. High iron level would increase the risk of bacterial invasion as well as free radical generation, which was produced from the conversion of ferrous ion (Fe^{2+}) to ferric ion (Fe^{3+}) in the body (Wally and Buchanan, 2007).

Lactoferrin is an iron transfer molecule that facilitates the iron uptake by cells due to its superior iron-binding capability to ferric ions (Fe^{3+}) over Tf (Huang *et al.*, 2008). There are three Lf isoforms: lactoferrin- α , lactoferrin- β and lactoferrin- γ , but only lactoferrin- α has iron-binding ability (Adlerova *et al.*, 2008). Some studies demonstrate that the binding site of Lf to LRs is located in the N terminal (between the amino acids 1 to 90) (Levay and Viljoen, 1995). Two main criteria make lactoferrin a suitable ligand to target cancer tissues. First, lactoferrin shows a strong ability to bind to transferrin receptors, which are found in highly proliferating cancerous tissues (Adlerova *et al.*, 2008). Second, Lf has been found to have numerous properties such as antimicrobial, antioxidant and more importantly anticancer effects on its own. Therefore, the iron transfer protein lactoferrin (Lf) is one of the possible ligand choices that is expected to boost the targeting capability of DAB (Elfinger *et al.*, 2007; Wei *et al.*, 2012; Ye *et al.*, 2013). Based on these publications, lactoferrin has been chosen for use in this study as a targeting ligand for prostate cancer.

2.1.1.2. Prostate specific membrane antigen

Prostate specific membrane antigen (PSMA) is an integral transmembrane glycoprotein with a molecular size of 100 kDa. It was first identified on the prostate epithelial membrane in 1987, when a newly developed antibody (7E11) was successfully used to recognise the N-terminus of the protein in prostate tissue; hence its common name (Horoszewicz *et al.*, 1987; Kinoshita *et al.*, 2006). Alternative names for PSMA are N-acetylated-alpha-linked acidic dipeptidase (NAALADase), folate hydrolase (FOLH1) and glutamate carboxypeptidase II (GCPII), reflecting its physiological function in the body. Its chemical structure can be divided into three main parts (Figure 2-1): the external part consisting of 707 amino acids, the transmembrane part made of 24 amino acid and the internal part consisting of 19 amino acids (Chang, 2004; Kasten *et al.*, 2013). The N-terminus of the glycoprotein is localised in the cytoplasmic part of the protein. The extracellular portion is highly glycosylated and has four main domains, C to F. Domain E was found to be the catalytic part related to the metabolic activities (metallopeptidases) of PSMA (Rawlings and Barrett, 1997).

While the functions of PSMA are still not completely clarified, some normal functions have been characterised as being generated from the extracellular domain of PSMA (Goodman *et al.*, 2007). PSMA has enzymatic activity as glutamate carboxypeptidase, which is an enzyme encoded by the folate hydrolase 1 gene (FOLH1). This enzyme has a role in folate hydrolysis in the small intestine, where it facilitates folate uptake through the hydrolysis of dietary folylpoly- γ -glutamates and polyglutamylated folate. Additionally, GCPII functions as a catalyst for the hydrolysis of N-acetyl-L-aspartyl-L-glutamate (NAAG), which is a neuropeptide that binds to N-methyl-D-aspartate and metabotropic glutamate receptors in the brain, to N-acetyl-L-aspartate (NAA) and to L-glutamate. L-glutamate is an even more potent neurotransmitter than NAAG and its accumulation leads to excitotoxicity, due to the continuous degradation of neurons, which can cause neurodegenerative problems such as

stroke (Kinoshita *et al.*, 2006; Mesters *et al.*, 2006). Although PSMA expression is correlated with the progress of the clinical stages of prostate cancer its function in the prostate remains unclear (Goodman *et al.*, 2007; Yao *et al.*, 2010).

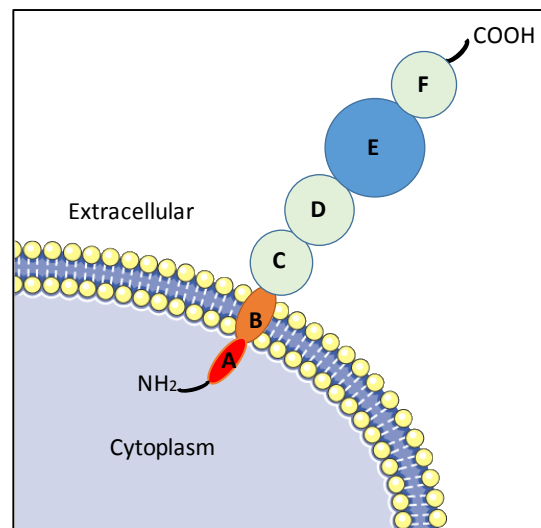


Figure 2-1 General structure of prostate specific membrane antigen divided into external, transmembrane and internal parts (adapted from Chang, 2004).

Therapeutically, PSMA could be used as a targeting ligand by conjugating its binding antibodies or peptides with the nanoparticles containing the therapeutic drug or gene, which would improve the ability of the complex to target the cancer cells without affecting normal tissues (Liu *et al.*, 1998; Chang, 2004). On the other hand, PSMA serum level could be used as a test in prostate cancer diagnosis. The possibility of using PSMA as a diagnostic marker for prostate cancer arises from two main properties: its high specificity for prostate tissues and its high release in both the early and late stages of the disease (Chang, 2004; Kasten *et al.*, 2013).

Various studies have used PSMA antibodies or parts of them as ligands for targeting prostate cells which can be applied for therapeutic and diagnostic applications. Among the factors making antibody ligands preferable to other targeting ligands are their high specificity to the

targeted receptors. More importantly, it could induce an immune reaction against the targeted cancer cells, although it could also cause unwanted immune responses (Kuchenthal and Maison, 2010). In 1990, the first PSMA- targeted imaging agent has been approved by the US FDA (ProstaScint[®]) (Ghosh and Heston, 2004). It is composed of a monoclonal antibody (mAb 7E11), which found to have limited sensitivity and specificity because its binding epitope is in the internal part of PSMA. Second-generation PSMA antibodies have also been developed with the ability to bind to different epitopes of the extracellular moiety of PSMA, thereby increasing their specificity and sensitivity to PSMA (Bouchelouche *et al.*, 2010).

Prostate tissue can also be targeted by designing special inhibitors that have the affinity to bind to PSMA. Kasten and his research group used the PSMA inhibitor CTT54 as a targeting ligand by conjugating it with PEGylated gold nanoparticles (CTT54-PEG-AuNPs). The targeted formulation showed a high, significant selectivity to target PSMA-positive cells LNCaP compared with PC-3 cells. The study also tested the affinity of the delivery system, compared with CTT54 alone, to bind to PSMA in LNCaP cells. The results indicated significant competitive targeting of the designed nanoparticle to LNCaP cells, even after blocking the cells with CTT54 (Kasten *et al.*, 2013).

Alternatively, small peptides can be used to target PSMA as well. They have less immunogenicity *in vivo* than antibodies and they are relatively inexpensive. Aggarwal *et al* (2006) used a random phage library to identify some peptides with the ability to selectively bind to the extracellular domain of PSMA, then synthesized them using the standard solid phase Fmoc. Among the synthesised peptides, WQPDTAHHWATL (Peptide2) is a 12 amino acid peptide that was found to target PSMA selectively (Aggarwal *et al.*, 2006). We hypothesise that conjugating this new peptide with the gene carrier DAB-Am16 would improve the targeting capability of the dendriplex, as well as the cellular uptake of the therapeutic gene through receptor-mediated endocytosis.

2.1.1.3. Integrins

Integrins are transmembrane glycoprotein receptors that link the cytoskeletons of cells with the extra cellular matrix (ECM). Each integrin receptor consists of two proteins, the alpha (α) and beta (β) subtypes, that bind non-covalently to each other to form a unique transmembrane heterodimer with a specific ligand binding site. There are currently around 24 heterodimers known to be generated from the binding of 18 different α -subunits and eight β -subunits (Figure 2-2) (Barczyk *et al.*, 2010). Integrins can generally be divided into two main types: the RGD binding integrins such as $\alpha v\beta 3$, $\alpha v\beta 5$, $\alpha v\beta 6$, $\alpha v\beta 8$ and $\alpha 5\beta 1$, and the non-RGD binding integrins such as collagen and laminin (Sutherland *et al.*, 2012).

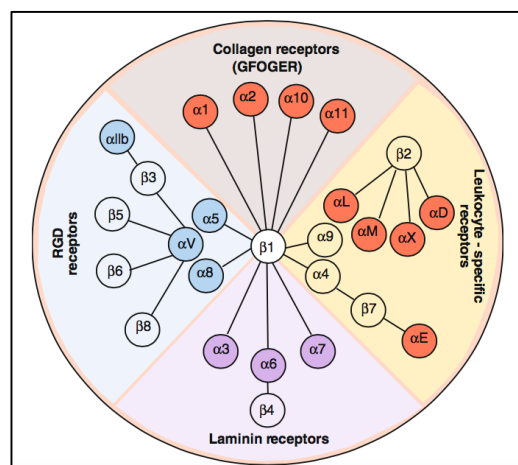


Figure 2-2 Integrins receptors family (Adapted from Barczyk *et al.*, 2010)

In normal tissues, integrins act as adhesion, migration and signalling molecules, connecting the cells to the ECM by binding with proteins such as fibronectin, vitronectin and collagen (Liu *et al.*, 2008; Marelli *et al.*, 2013). These adhesive molecules assist the connection between the adjacent cells and surrounding ECM by creating tunnel-like junctions, maintained by integrins, which facilitate the passage of ions and small molecules between cells and which form and break as needed (Bonkhoff, 1993; Suyin *et al.*, 2013). Integrins also act as signalling molecules between cells in a tissue and between the cells and the ECM. This happens by creating a

signalling pathway to maintain homeostasis in normal physiological processes such as wound healing (Dunehoo *et al.*, 2006; Barczyk *et al* 2010).

Several integrins have been found to be strongly expressed in cancerous tissues, indicating that they play a role in cancer progress. Integrin expression affects the growth and cell proliferation in rudimentary tumours via various mechanisms such as controlling the expression of cell cycle proteins, binding with some components in the ECM to promote migration and invasion to other organs, and activating some matrix-degrading proteases such as matrix metalloprotease 2 (MMP2), which tends to modify surrounding tissues to enrol them in angiogenesis (Desgrosellier and Cheresch, 2010).

Several integrin receptors have been found to be overexpressed in prostate cancer cells, with a differentiation in their expression as the cancer progresses such as $\alpha\nu\beta_3$ where it is extensively expressed in PC-3 but not LNCaP cells, as $\alpha\nu\beta_3$ tends to adhere to vitronectin in the ECM (Zheng *et al.*, 1999), whereas other receptors were detected only in cancer tissues, not in normal ones such as $\alpha\nu\beta_6$ (Azare *et al.*, 2007). Moreover, $\alpha_6\beta_4$ and $\alpha_6\beta_1$ were found to have variable roles in prostate cancer, $\alpha_6\beta_4$ was found to assist the attachment of normal cells to the basement membrane explaining its low expression in prostate cancer cells, whereas $\alpha_6\beta_1$ found to be overexpressed in cancerous cells due to its involvement in cancer cells migration (Davis *et al.*, 2001; Stevenson *et al.*, 2007; Suyin *et al.*, 2013). $\alpha_5\beta_1$ is expressed in both normal and cancerous cells and has been found to have a role in PC-3 cell adhesion (Stachurska *et al.*, 2012). Therefore, selecting a suitable peptide to target overexpressed integrin receptors would be a good way to improve the active targeting capability of the nanoparticles.

Two peptides have been selected to target PC cells by targeting integrin receptors that are overexpressed in prostate cancer. EETI-II 2.5F is an RGD peptide designed by Kimura and colleagues (2009) to target integrin receptors overexpressed in cancer: $\alpha\nu\beta_5$, $\alpha\nu\beta_3$, $\alpha_{11b}\beta_3$ and

$\alpha_5\beta_1$. Moore *et al.* (2013) used this peptide as an imaging probe in brain tumour targeting. Its targeting capability was examined *in vivo* and *ex vivo*, and it was found to pick up $\alpha_5\beta_1$ in particular. Our study used the active binding site of the EETI-II 2.5F peptide (PRPRGDNPPLT) as a targeting ligand for prostate cancer.

The second binding ligand, YESIKVAVS, synthesised by Stevenson *et al.* (2007) to target $\alpha_6\beta_1$ and $\alpha_6\beta_4$, was selected to target PC due to the overexpression of these peptides in prostate cancer cells, as mentioned above.

2.1.2. Structural elucidation

2.1.2.1. Nuclear magnetic resonance

Nuclear magnetic resonance (NMR) is an important technique for the structural identification of organic compounds. The principle of NMR is based on the magnetic properties of certain nuclei that have an odd atomic number (the magnetic moment and angular momentum, or spin) (Lampman *et al.*, 2008; Watson, 2012).

Proton NMR (^1H -NMR) is the most commonly analysed isotope, due to its sensitivity and the diverse structural information that can be obtained from it. Two-dimensional NMR spectroscopy is a more advanced technique for interpreting chemical structures which has become possible due to developments in NMR instruments. In 2D NMR spectra, the X and Y axes are usually proton and carbon frequencies that comprise together providing a map which is interpreted by matching which peaks on the X axis correspond to peaks on the Y axis. (Lampman *et al.*, 2008; Watson, 2012).

The nuclear Overhauser effect (NOE) is a technique used to determine inter- and intramolecular distances through space, not through chemical bonds, i.e. how close two protons are to each other. NOE can detect protons separated by spatial distances up to 5 Å. When

protons are close to each other in space, they tend to interact through magnetic dipoles; if one of the protons is irradiated, the signals of the surrounding nucleus will change accordingly.

Diffusion-ordered spectroscopy (DOSY) is another NMR technique used to separate the NMR signals of different compounds in a mixture by measuring the Brownian molecular motion of these compound in a particular solvent in terms of the diffusion coefficient (DC). The diffusion of the molecules depends on several factors such as their shape and size, as well as the viscosity of the solvent and the temperature at which the test is performed. The 2D-DOSY NMR spectrum plots the regular ^1H -NMR chemical shift against the diffusion constant, which is determined by introducing the sample to a gradient of pulses of radio frequency, thus determining the change in the movement of the molecules in the sample.

2.1.2.2. Matrix assisted laser desorption/ionization-time of flight

Matrix-assisted laser desorption/ionization (MALDI) is a mass spectroscopy ionisation technique first reported by Hillenkamp and Karas in 1988. The sample to be analysed is uniformly mixed with a matrix, which is usually a UV-absorbing weak organic acid such as α -cyano-4-hydroxycinnamic acid or 2,5-dihydroxy benzoic acid. The mixture is then exposed to laser light, usually at UV wavelength, which heats the matrix strongly enough to vaporise it, together with the sample molecules. The role of the matrix in MALDI is substantial; its ability to absorb the laser light is directly linked to its ability to promote the vaporisation of the sample. Additionally, the matrix ionises the sample by acting as proton donor or receiver, thus creating a positive or negative ionisation mode for the sample (Lewis *et al.*, 2000). Therefore, selecting the most appropriate matrix depends mainly on the physical and chemical properties of the sample.

After ionisation and evaporation of the sample, fragmented ions are separated according to their mass; time of flight (TOF) is the most common ion separator linked to MALDI (Watson, 2012).

MALDI-TOF has been found to be the most suitable mass spectroscopy technique for peptides, proteins and dendrimers, as it yields an accurate mass determination for such compounds (Lewis *et al.*, 2000; Peterson *et al.*, 2003; Yellepeddi, 2013). However, achieving the optimal spectrum is strongly dependent on the selection of a matrix, as mentioned above. Protein and peptide samples are usually ionised by protonation, the most common matrices used with them being cinnamic acid derivatives such as α -cyano-4-hydroxycinnamic acid. Dendrimers, on the other hand, are usually best ionised by cationization, most commonly using a 2,5-dihydroxybenzoic acid matrix (Shion and Ellor, 2007).

2.1.3. DNA complexation study

DNA complexation or condensation is a method utilized in gene delivery to chemically complex the DNA with the designed vector, which is usually a cationic polymer or dendrimer. This complexation occurs via electrostatic interactions between the amino group in the cationic vector and the phosphate moieties in the DNA.

Several benefits are usually associated with DNA condensation in gene delivery. The cellular uptake of the complexed gene is found to be higher than that of free DNA, due to the reduction in the repulsive forces between the genetic material and the membrane of the targeted cell, as both of them are charged negatively. In addition, DNA complexation generates a safe environment for the genetic materials; it protects the DNA from non-specific binding with any cationic molecules and enzymatic degradation in the bloodstream (Taira *et al.*, 2005).

The efficiency of the prepared vector in condensing the required DNA can be assessed by conducting an assay such as PicoGreen[®] and agarose gel retardation assays (Aldawsari *et al.*, 2011; Lim *et al.*, 2015).

2.1.3.1. PicoGreen® assay

PicoGreen® is a reagent that fluoresces when coupled with a double-stranded DNA (dsDNA). Among several fluorescent agents investigated, PicoGreen® has been found to be highly sensitive in detecting and quantifying even small amounts of DNA (around 25 pg/ml), which is extremely beneficial for biological applications such as the quantification of purified DNA, or diagnostic techniques such as identifying DNA contamination in pharmaceutical products. In addition, the high selectivity of PicoGreen® minimises the probability of inaccuracy in dsDNA quantification, since it has very low affinity with single-stranded DNA and RNA, which will thus lead to much less fluorescence (Singer *et al.*, 1997).

PicoGreen® assay was conducted to determine the efficiency of the designed vectors in complexing the required genes, based on the fact that the more efficiently the vector complexes with the DNA through electrostatic interaction, the less free DNA the PicoGreen® will find to couple with and the less fluorescence will be detected (Singer *et al.*, 1997). Thus, the intensity of fluorescence induced by the PicoGreen® reagent provides a measure of the level of DNA complexation with the dendrimer.

2.1.3.2. Gel retardation assay

Gel retardation or electrophoresis is a technique for separating macromolecules of different sizes and charges. The charged molecules migrate with different intensities towards the oppositely charged pole when placed in an agarose or polyacrylamide gel plate under an electric field. The speed of migration depends on external factors such as the field applied, the viscosity and porosity of the matrix and the temperature. It is also affected by internal factors such as the net charge density, the hydrophobicity, the charge to mass ratio and the size and shape of the molecules. Different charged molecules will migrate with different speeds forming separated zones (Westermeier, 2005; Reddy and Raju, 2012).

This method was used in this study to evaluate the ability of the designed vector to complex with the DNA. The agarose gel is sprayed with a specific fluorescent dye such as ethidium bromide after the migration ends. The concept of the method is that free DNA molecules will be separated from the complexed ones, since they migrate at different speeds under the applied electrical field. Thus, the free DNA will induce fluorescence under the UV light when it binds to ethidium bromide, while complexed DNA with the designed vector will show less fluorescence (Westermeier, 2005; Reddy and Raju, 2012).

2.1.4. Photon correlation spectroscopy

The size of the nanoparticle is an important physical factor influencing other properties of the nanoparticle, such as its distribution time or half-life, phagocytosis by immune cells and intratumoural accumulation. Firstly, the size of the nanoparticle has a direct impact on its half-life in the blood circulation; longer circulating time will lead to additional accumulation of the nanoparticle at the cancer site. The clearance of nanoparticles depends on their size; particles of less than 5 nm are usually cleared rapidly via extravasation or renal clearance, whereas larger particles tend to accumulate primarily in the liver and spleen, this tendency being proportional to the increase in size. On the other hand, large nanoparticles tend to move with the blood flow, avoiding the vessel walls as they become heavier; therefore, their transport from the circulation to the cancer site tends to be lower than that of smaller molecules, which tend to move laterally in the blood vessels and exhibit higher diffusion. The clinical outcomes of these two criteria are contradictory, so that large particles have a better half-life but slower diffusion than smaller ones. Thus, nanoparticles should be of a size which is not too large to prevent adequate distribution nor too small for them to be cleared rapidly (Toy *et al.*, 2014). Tang *et al.* (2014) investigated the effects of size in nanomedicines used to treat cancer. Of the three sizes examined (20 nm, 50 nm and 100 nm), they found 50 nm to be optimal, as nanoparticles of this size had the highest accumulation and retention in both primary and metastatic tumours.

Photon correlation spectroscopy (PCS) is a light-scattering technique that is used to study the physical properties of samples (size and charge). Its principle was introduced by Tyndall in the mid-19th century. The particles in a colloidal solution undergo Brownian motion, meaning that the diffusing particles are in constant random movement due their multiple collisions with the molecules of the liquid; PCS relies on the dynamic light scattering (DLS) of these particles in the solution. As the colloidal particles are in Brownian motion, a beam of light (usually laser) to which they are subjected will scatter at different angles. The total scattered intensity of light wavelengths is detected by a photomultiplier tube, together with the light scattering angle. This scattered light will fluctuate with time due to the Brownian motion of the particles; therefore, the continuously changing scattering of light through the solution over time provides evidence of the motion of the particles and their hydrodynamic size distribution (Tscharnuter, 2000). The diameter of the particles can be calculated by measuring their velocity (diffusion coefficient, D) at a given temperature and viscosity (Filella *et al.*, 1997; Tscharnuter, 2000).

Another relevant physical property is the zeta (ζ) potential, which can be defined as the electrostatic potential generated between a nanoparticle and the diffusion layer of a colloidal system (Honary and Zahir, 2013). It is used to calculate the surface charge of the nanoparticles in a colloidal system. Zeta potential affects several properties of the delivery system, such as its long-term stability due to nanoparticle-nanoparticle interaction, and the cellular uptake efficiency of the nanodrug formed due to nanoparticle-cell interaction. Thus, the zeta potential should be adjusted to attain a certain level of nanoparticle stability as well as effective cellular uptake. The electrokinetic potential difference between the medium and the nanoparticles tends to create a balance that should ideally prevent the aggregation of the particles in the solution. Several studies states that to obtain good stability, the zeta potential should be either higher than -30 mV or lower than 30 mV (Bhattacharjee, 2016), while others propose a narrower range of $25 \text{ mV} \leq \zeta \leq -25 \text{ mV}$ (Durymanov *et al.*, 2015). On the other hand, in nanoparticles designed

for gene delivery, the zeta potential should be slightly positive. The cellular uptake of the nanoparticles to the targeted cells is also affected by the zeta potential: a high value (above 30 mV) may lead to non-specific binding with the surrounding cell membranes, while a low one (+/-5 mV) can cause particles to aggregate with low uptake profile (Honary and Zahir, 2013). For a better understanding of zeta potential, any charged particles dispersed in aqueous solution will start to adsorb oppositely charged ions and molecules in the solution, forming an electrical double layer (EDL) around them. The first layer is composed of the most predominant ions with opposite charge to the particle, then the second (diffuse) layer has a lower electrostatic power, being composed of both similarly and oppositely charged ions (Bhattacharjee, 2016). To measure the zeta potential, an external electrical field is applied to the sample by means of two electrodes, causing charged particles to migrate to the oppositely charged electrode. The interface between the diffuse layer and the dispersant around it during electrophoresis is the shear plane. The value of the zeta potential then reflects the potential difference between the electrical double layer of the particle and the shear plane. The direction and velocity of migration are also involved in the determination of zeta potential. The velocity of the particles can be determined by calculating the change in light scattering due to the Doppler shift; the electrical potential of particles at the shear plane (the zeta potential) is proportional to their velocity (Tucker *et al.*, 2015; Bhattacharjee, 2016). The zeta potential can be then measured via the Henry equation:

$$\zeta = \frac{U\eta}{\epsilon f(ka)} \quad (1)$$

where ζ is the zeta potential, U is the electrical mobility, ϵ is the solvent dielectric constant, η is solvent viscosity and $f(ka)$ is the Henry coefficient.

The sample should be suspended in a solvent with known refractive index and dielectric constant, then transferred to a special cuvette, where it is subjected to laser light and an electric

field at the same time. The particles will migrate to the opposite electrode and the scattered light angle will thus fluctuate, allowing velocity to be determined from the frequency shift (Shimko *et al.*, 2012).

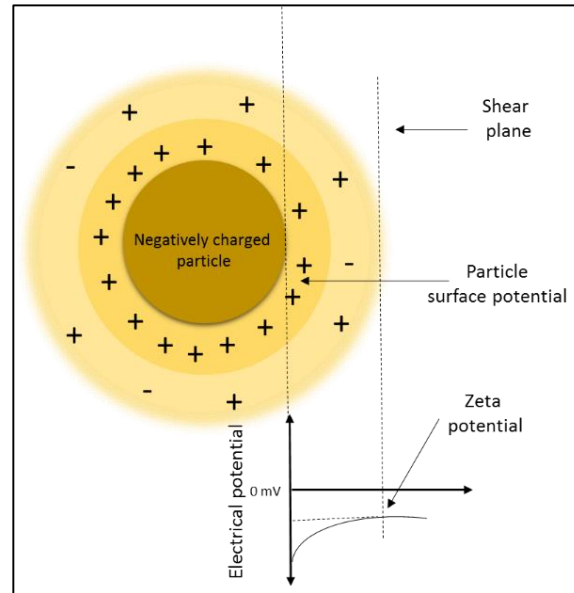


Figure 2-3 Zeta potential of charged particles (adapted from Shimko *et al.*, 2012)

The characteristics of the solvent where the nanoparticles were dissolved, have significant impact in the zeta potential of these nanoparticles such as the pH and ionic strength. The zeta potential will vary with pH since it directly affects the ionisation state of the particles (Bhattacharjee, 2016). Generally, the degree of ionisation is linked with the difference between the logarithmic acid dissociation constant, pK_a , of the dissolved particles and the pH of the solution. In the case of the cationic dendrimer polypropylenimine (DAB), the terminal primary amine groups have pK_a values between 9.5 and 10, so that around 90% of these groups will be ionized if the pH of the solution is one degree lower (Shao *et al.*, 2011), thereby affecting the zeta potential accordingly. The ionic strength of the dissociation solution also has an impact on the zeta potential: as ionic strength increases, the EDL will be compacted with ions and the zeta potential will decrease accordingly (Bhattacharjee, 2016).

2.1.5. Atomic force microscopy

Atomic force microscopy (AFM) is a technique used to measure surface structures with high resolution and accuracy. Since its development in 1980, AFM has become a useful technique in many fields including chemistry, biology, nanotechnology and medicine. It can be used to image samples of various types and textures, ranging from hard metallic nanoparticles to soft human cells. However, an AFM image is not an actual image formed from focusing light on the surface of an object; instead, it is created by physically touching the sample surface with a probe (Eaton and West, 2010). In nanomedicine, AFM is usually used to examine the shape and size of nanoparticles (Li *et al.*, 2000).

The principle of AFM is based on placing the sample on a moving stage, then gently scanning over it using a sharp probe mounted on a flexible cantilever, making it sensitive to any small changes in the sample surface. The information thereby collected on changes in the height of the surface allows the building of a detailed map. The probe is monitored by a magnification system which records its motion.

AFM is considered superior to alternative microscopy techniques such as SEM and TEM, because it is able to produce images in three dimensions (on the X, Y and Z axes), whereas the other microscopies generate images on two axes only. The image resolution of AFM is considered high; it can approach 0.1 nm, thanks to the use of sharp probes. In addition, AFM requires minimum sample preparation and is suitable for scanning most types of sample, while TEM and SEM require the special preparation of samples and particular measurement conditions such as a vacuum. On the other hand, AFM cannot be used to generate an image larger than 100 μm because it would take too long for the probe to physically cover a larger area. Indeed, AFM requires a longer scanning period than either of the other two microscopies.

2.1.6. Objectives

The objective of this chapter is to investigate the impact of conjugating different ligands (Lactoferrin, Peptide2 and Peptide4) to diaminobutyric polypropylenimine (DAB) dendrimer on its physicochemical characteristics such as DNA condensation, size, zeta potential and morphology.

The first part of the study is the synthesis of lactoferrin- and peptide - bearing DAB dendrimer. Thereafter, the physical characterisation of the synthesised dendriplexes will be investigated in this chapter, starting from structure elucidation using different techniques (NMR, LC-MS, and MALDI-TOF) and examining the DNA condensation tendency of the dendriplexes using fluorescence spectrophotometry and electrophoretic mobility assay. In addition, the physical characteristics such as morphology, size and charge of the nanoparticles will be investigated using transmission electron microscopy and photon correlation spectroscopy.

2.2. Materials and methods

2.2.1. Materials

Table 2-1 List of materials used in chapter 2.

Materials	Supplier
Ampicillin	Sigma-Aldrich, UK
Dialysis tubing, benzoylated	Sigma-Aldrich, UK
Diaminobutyric polypropylenimine hexadecaamine dendrimer (DAB-Am16)	Sigma-Aldrich, UK
5,5'-dithiobis(2-nitrobenzoic acid) (Ellman's)	Sigma-Aldrich, UK
Ethidium bromide	Sigma-Aldrich, UK
Ethylenediaminetetraacetic acid (EDTA)	Sigma-Aldrich, UK
EndoFree Plasmid Giga Kit	Qiagen, UK
pCMVsport β -galactosidase	Life Technologies, UK
2-Iminothiolane (Traut's reagent)	Sigma-Aldrich, UK
Isopropanol	Sigma-Aldrich, UK
L-Cysteine	Sigma-Aldrich, UK
Lactoferrin, bovine colostrum	Sigma-Aldrich, UK
Maleimide PEG 3.5K succinimidyl carboxymethyl ester	JenKem, USA
<i>N</i> -(γ -maleimidobutyryloxy)succinimide ester (GMBS)	Polypeptide Group, France
Methoxy PEG 2K succinimidyl carboxymethyl ester	JenKem, USA

Methanol	Sigma-Aldrich, UK
Passive lysis buffer	Promega, UK
Peptide2 (CQWPDTAHHWATLC)	Biomatik, Canada
Peptide4 (CPRPRGDNPLTCGGKKK)	Biomatik, Canada
PicoGreen [®] dsDNA reagent	Life Technologies, UK
Phosphate buffer saline	Sigma-Aldrich, UK
Snakeskin [®] Dialysis tubing, 3.5 K MWCO	ThermoFisher, UK
Snakeskin [®] Dialysis tubing, 7 K MWCO	ThermoFisher, UK
Na ₂ HPO ₄	Sigma-Aldrich, UK
NaH ₂ PO ₄	Sigma-Aldrich, UK

2.2.2. Methods

2.2.2.1. Plasmid DNA synthesis and purification

The plasmid DNAs used in the experiments were prepared according to the following procedure. Plasmid encoding the gene of interest was grown in *E. coli* bacteria (250 µl) using sterile conical flasks containing 650 ml Luria broth (L-Broth) and 650 µl ampicillin solution. The cultures were kept at 37 °C for 24 h with continuous shaking to create suitable growth conditions for the bacteria. The bacterial suspensions formed were then centrifuged at speed of 6000 rpm (6048 g) for 20 minutes and the bacteria pellets were collected.

Plasmid DNA extraction and purification was performed using a Qiagen® endotoxin-free Giga Plasmid Kit according to the manufacturer's instructions. DNA extraction was performed using P1 and P2 buffers to induce cell lysis as follows. The bacterial pellets were reconstituted using 125 ml of re-suspension buffer P1 at pH 8 containing ethylenediaminetetraacetate (EDTA) and ribonuclease A (RNase A). EDTA affects the cell membrane integrity through its action as a chelating agent for divalent ions such as Mg²⁺ and Ca²⁺, which disrupt the cellular envelope structure and thus promote cell membrane lysis (Tsugama *et al.*, 2011), while RNase A assists in the degradation of RNA to prevent it from contaminating the DNA. Next, 125 ml of alkaline lysis buffer P2, containing sodium hydroxide (NaOH) and sodium dodecyl sulphate (SDS), was added and kept for five minutes. The high pH of the alkaline buffer (pH 12) alters the nature of the DNA, while the anionic detergent SDS promotes cell membrane lysis by binding with the lipid components of the membrane (Shafa and Salton, 1960). The suspension formed was then neutralised using 125 ml of 3M potassium acetate at pH 5.5 (P3) before filtration using the QIA filter provided.

The last stage of DNA synthesis was purification, which was achieved using the Qiagen® endotoxin-free Giga Plasmid Kit to collect pure DNA without any cellular components such as protein, RNA, or any cell membrane debris. The purification process depends on the use of

anion exchange cartridges, where the positively charged resin molecules in the column interact with the DNA molecules, as these have an intense negative charge. The cartridge was first equilibrated with 75 ml of neutral buffer (pH 7) in order to ensure that all cationic groups in the resin were ionized and capable of binding with the DNA. The lysate was then introduced to the cartridge and washed using 600 ml of QC buffer to elute any impurities in the solution. Finally, the DNA was collected from the cartridge using highly basic buffer at pH 8.5 by adding 100 ml of QN buffer. This high pH buffer causes deionization of the cartridge resin cationic groups, thus breaking the electrostatic interactions between the DNA and the resin and causing the complete elution of the DNA (Watson, 2012). The DNA collected was precipitated using 70% methanol, then redissolved in 5% glucose solution. The concentration of the DNA collected was measured using UV absorbance spectrophotometry (GeneQuant RNA/DNA calculator) at a wavelength of 320 nm.

2.2.2.2. Conjugation of lactoferrin, Peptide2, and Peptide4 to DAB dendrimer

Diaminobutyric polypropylenimine hexadecaamine (DAB-Am16) dendrimer was purchased from Sigma-Aldrich and conjugated to Lf, Peptide2, and Peptide4 using a novel method adapted from Hermanson (2013). DAB-Am16 was dissolved in 50 mM sodium phosphate and 0.15 M sodium chloride buffer at a concentration of 10 mg/ml (pH 7.4). In a separate container, a stock solution of *N*-(γ -maleimidobutyryloxy) succinimide ester (GMBS) was prepared by dissolving 40 mg of GMBS in 1 ml of dimethyl sulfoxide (DMSO). From the stock, specific volumes of GMBS solution equivalent to 2, 4, 6, 8, 10 and 12-fold moles excess over the DAB amount were taken. The dendrimer and GMBS solutions were then mixed together with continuous stirring for one hour at room temperature and the final compounds were purified using benzoylated dialysis tubing with molecular weight cut-off (MWCO) of 2000 at room temperature using 500 ml of 50 mM sodium phosphate and 0.15 M sodium chloride buffer as the dialysis solution and changed twice during dialysis. After 24-hour dialysis, the solution was

frozen dried using Christ® freeze dryer for 48 hours. The powder formed was collected and characterised using high resolution mass spectrometry, MALDI-TOF and NMR.

The ligand lactoferrin was modified first to hold a sulfhydryl group, so that it would react with the maleimide site of GMBS. The reaction was achieved by mixing the protein of interest with 10-fold moles excess of 2-iminothiolane (Traut's reagent) (Figure 2-4). Lactoferrin protein (10 mg) was first dissolved in 1 ml of 50 mM sodium phosphate buffer with 0.15 M sodium chloride (pH 8) at a concentration of 10 mg/ml. In a separate container, Traut's reagent stock solution was prepared by dissolving 2 mg of the reagent in 1 ml distilled water to obtain a 14.5 mM concentration. Next, 76.55 µl of Traut's stock was reacted with the lactoferrin solution for one hour at 20 °C. The modified Lf was filtered using a Vivaspin-4 centrifuge tube with a MWCO of 5000 Da for 15 minutes at 7500 rpm (6477.4 g).

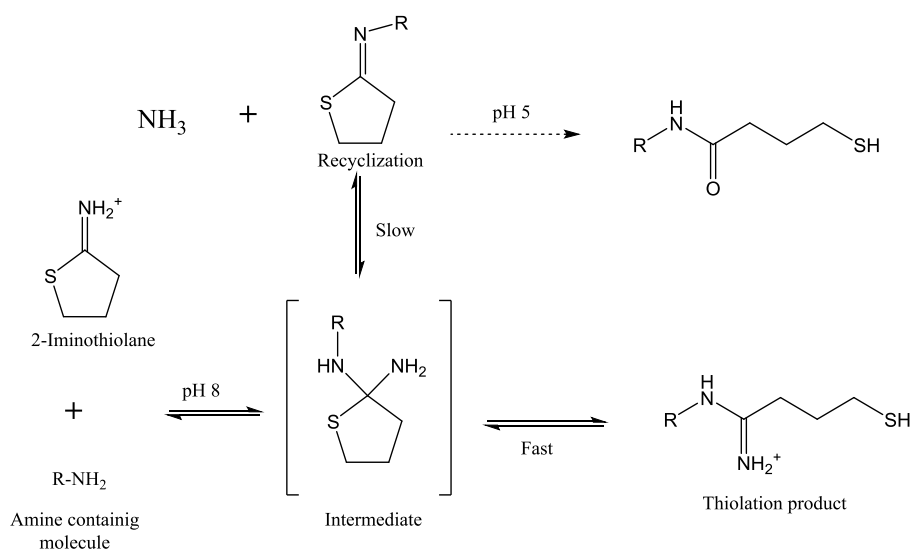


Figure 2-4 Protein modification reaction steps with Traut's reagent (2-Iminothiolane) to carry free sulfhydryl group (Adapted from Hermanson, 2013)

Table 2-2 summarizes the peptides to be used as targeting ligands in this study. All the peptides were synthesised in Biomatik and requested to be modified with the amino acid cysteine in their N-terminus (Biomatik, Canada). As cysteine amino acid holds free sulfhydryl group and has a high tendency to react with the maleimide group in the cross-linker, there is no need to

modify the peptides structure using Traut's reagent. Equivalent mole ratio of Peptide2 (CWQPDTAHHWATL) and Peptide4 (CPRPRGDNPLTCGGKKK) to DAB molecules (1:1 mole ratio) was used in this reaction (9.2 mg and 11.2 mg respectively).

The modified protein (10 mg) was then immediately used in the bioconjugation reaction with DAB cross-linker at 20 °C for four hours with continuous mixing. DAB-Lf was filtered using the Vivaspin tube in the same conditions as described above to remove any unreacted dendrimer, followed by a desalting procedure using a SnakeSkin[®] dialysis tube with a MWCO of 3500 Da using 1L distilled water as dialysis solution at 25 °C changed twice during 24 hours of a dialysis period, to purify the complex and remove any buffer salts.

For DAB-Pep2 and DAB-Pep4 formulations, 9.3 mg of Peptide2 and 11.2 mg of Peptide4 were dissolved in 1 ml of 50 mM sodium phosphate buffer with 0.15 M sodium chloride (pH 7.4) and reacted with DAB cross-linker at 20 °C for four hours with continuous mixing. The purification and desalting steps were done together via dialysing these dendrimers against 1L distilled water at 25 °C changed twice during 24 hours and using dialysis tubing with MWCO 2000 Da or 3500 Da respectively for DAB-Pep2 and DAB-Pep4 to remove any unreacted peptide molecules and desalt the final product. The collected solution was then freeze-dried using Christ[®] freeze dryer for 48 h and the yielded powder was collected.

The modified dendrimers were structurally identified by NMR spectroscopy (Jeol Oxford NMR AS 600 spectrometer) and matrix assisted laser desorption/ionisation-time of flight (MALDI-TOF) mass spectroscopy (Axima CFR, Kratos, Shimadzu). NMR samples were prepared by dissolving 12 mg of the dendrimer in 600 µl of deuterated water (D₂O). MS samples were prepared by dissolving 1 mg of the sample in 1:1 water/acetonitrile mixture, then performing a series of dilutions and finally mixing 1 µl of the sample stock with 9 µl ionisation matrix (sinapinic acid or dihydroxybenzoic acid). For high molecular weight samples such as DAB-Lf and free Lf the matrix selected was sinapinic acid, whereas lower molecule weight

samples such as DAB dendrimer, DAB-GMBS, DAB-Pep2 and DAB-Pep4 were mixed with dihydroxybenzoic acid.

The other peptides listed in Table 2-2 were eliminated from the study due to solubility issues during the synthesis. Peptide1 has seven hydrophobic amino acids in its sequence affecting its solubility in aqueous solutions. During the bioconjugation reaction with DAB, Peptide1 was dissolved first in DMSO, then gradually added to DAB-GMBS solution, however, the solution became turbid once Peptide1 was added. Therefore, for the purpose of improving the peptide solubility, Peptide1 was modified with basic amino acid moiety (-GGKKK) in its C-terminus, as suggested in Kato et al (2006) (Table 2-2). The solubility of the new peptide (named Peptide3) was partially improved in aqueous solutions, but the same problem still occurred when reacting DAB-GMBS with Peptide3.

Table 2-2 List of the peptides proposed for use as targeting ligands

Name	Sequence	Targeting receptor/s	Reference
Peptide1	YESIKVAVS	Integrin ($\alpha v \beta 3$)	(Stevenson <i>et al.</i> , 2007).
Peptide2	CWQPDTAHHWATL	PSMA	(Wu <i>et al.</i> , 2010; Aggarwal <i>et al.</i> , 2006)
Peptide3	CYESIKVAVSGGKKK	Modified form of peptide1	(Kato <i>et al.</i> , 2006)
Peptide4	CPRPRGDNPLTCGGKKK (RGD peptide)	The active site of the cyclic peptide EETI 2.5 F Integrin targeting ($\alpha v \beta 5$, $\alpha v \beta 3$, $\alpha_{11b} \beta 3$ and $\alpha 5 \beta 1$)	(Kimura <i>et al.</i> , 2009; Moore <i>et al.</i> , 2013)

2.2.2.2.1. PEGylation of Peptide2- bearing DAB dendrimers

For the purpose of improving the physiochemical properties of the peptide-bearing DAB dendrimers, different PEGylation patterns were used to modify DAB-Pep2 dendrimer and identify the best PEGylation reaction that would be used in the future for similar formulations. The aim of these reactions was to evaluate the use of different crosslinkers to conjugate the third generation DAB dendrimer with the targeting ligand Peptide2; in this study we originally used the short crosslinker *N*-(γ -maleimidobutyryloxy)succinimide ester (GMBS) or a polyethylene glycol chain crosslinker with a molecular weight of 3500 g/mole (PEG3.5 kDa). Following the synthesis of DAB-Pep2 and DAB-PEG3.5k-Pep2 respectively using these crosslinkers, another reaction was performed to PEGylate some of the amine groups on the periphery of the dendrimer by reacting a 4-mole excess of polyethylene glycol chain with a molecular weight of 2000 g/mole (PEG2 kDa) over DAB. The content of each reactant in these polymers is listed in Table 2-3.

First, the crosslinker used in conjugating DAB with Peptide2 was changed from GMBS to NHS-PEG (3.5k)-maleimide as follows: 10 mg of DAB-Am16 was dissolved in 1 ml 50 mM sodium phosphate buffer and 0.15 M NaCl (pH 7.4) and reacted with 20 mg of NHS-PEG (3.5)-maleimide (equivalent to one mole excess of DAB) for one hour at 20 °C. The reaction was dialysed using 3500 MWCO SnakeSkin[®] tubes against 1000 ml of the buffer for 24 hours at 25 °C. Peptide2 (9.3 mg) was then reacted with DAB-PEG 3.5 in a molar ratio 1:1 for four hours at 20 °C. The final compound was purified through dialysis using 3500 MWCO SnakeSkin[®] tubes against 1000 ml of water changed twice during 24 hours at 25 °C.

Another PEGylation reaction was performed using the above formulations, DAB-Pep2 and DAB-PEG3.5k-Pep2, as follows: 47 mg of NHS-PEG2k-methoxy (molecular weight 2000 Da) was dissolved in 2 ml sodium phosphate buffer (pH 7.4), then added gradually over DAB-Pep2 (20 mg) or DAB-PEG3.5k-Pep2 (30 mg) formulations and left to react for 8 hours at 20 °C

before being dialysed against one litre of distilled water using SnakeSkin[®] dialysis tubing (MWCO 7000) for 24 hours at 25 °C. The dialysis solution was changed twice during that period. This dialysis process should ensure the extraction of any unreacted PEG molecules as well as any dendrimer that binds to fewer than three PEG molecules. All synthesised formulations were characterised by ¹H-NMR (AV600).

Table 2-3 Chemical compositions of Peptide2- bearing DAB dendrimer formulations

Name	Dendrimer	Crosslinker	PEGylation	Peptide2	Estimated molecular weight (Da)
DAB-Peptide2	G3 DAB (10 mg)	2 moles excess GMBS (3.3 mg)	NO	1 mole excess (9.3 mg)	3250
DAB-PEG3.5k-Peptide2	G3 DAB (10 mg)	1 mole excess NHS-PEG3.5-maleimide (20 mg)	NO	1 mole excess (9.3 mg)	6700
DAB-PEG2k-Peptide2	G3 DAB (10 mg)	2 moles excess GMBS (3.3 mg)	4 moles excess of PEG 2000 (47 mg)	1 mole excess (9.3 mg)	9000
DAB-PEG2k-PEG3.5k-Peptide2	G3 DAB (10 mg)	1 mole excess NHS-PEG3.5-maleimide (20 mg)	4 moles excess of PEG 2000 (47 mg)	1 mole excess (9.3 mg)	12700

2.2.2.2.2. PEGylation of DAB-Peptide4 dendrimer

By comparing the PEGylation ratios used to modify DAB-Pep2, the use of a 4-mole excess of PEG2000 was selected as the optimal method for improving the physiochemical properties of DAB-Pep2, as will be demonstrated in the results section. This method was followed in the synthesis of DAB-Pep4 to form DAB-PEG2k-Pep4 as follows: DAB dendrimer was reacted with the crosslinker GMBS, followed by the addition of Peptide4 (11.4 mg) in a similar way to that mentioned in Section 2.2.2.2. Next, 47 mg of NHS-PEG2k-methoxy was dissolved in 2 ml 50 mM sodium phosphate buffer with 0.15 M sodium chloride (pH 7.4) and reacted with DAB-Pep4 for 8 hours at 20 °C. The final compound, DAB-PEG2k-Pep4, was purified by

dialysing the reaction against distilled water (1000 ml) for 24 hours at 25 °C using SnakeSkin® dialysis tubing with MWCO of 7000 Da.

2.2.2.3. Characterization of DAB-Lf and DAB-Pep2 dendriplexes

2.2.2.3.1. PicoGreen® assay

The ability of the DNA to complex with the Lf-bearing DAB and peptides - bearing DAB was assessed by PicoGreen® assay. PicoGreen® reagent is a fluorescent stain of nucleic acid used to quantitatively determine the amount of double-stranded DNA. The degree of fluorescence that occurs when it complexes with the dsDNA can be measured via fluorescence spectrophotometer, while unbound PicoGreen® reagent displays less fluorescence. Accordingly, when the DNA forms electrostatic interactions with the dendrimers, the fluorescence of the PicoGreen® will decrease, due to the low number of binding sites with the DNA (Koppu *et al.*, 2010; Aldawsari *et al.*, 2011).

Following the protocol provided by the supplier, PicoGreen® reagent was diluted 200 times using Tris-EDTA buffer (pH 7.5). One ml of the dendrimer-DNA at various DAB: DNA ratios (20:1, 10:1, 5:1, 2:1, 1:1, 0.5:1 and 0:1) was added to one ml of the diluted PicoGreen® reagent at a constant DNA concentration of 10 µg/ml per cuvette throughout the experiment. The intensity of PicoGreen® fluorescence was measured at various time frames using a Varian Cary Eclipse Fluorescence spectrophotometer (Palo Alto, California) (λ_{exc} : 480 nm, λ_{em} : 520 nm). The results were displayed as the percentage of DNA condensation as follow:

$$\% \text{ DNA condensation} = (100 - (F_{\gamma} \times 100)) \quad (2)$$

Where F_{γ} is the reduced fluorescence values which measured by dividing the fluorescence of the sample with the fluorescence of free DNA as follows:

$$F_{\gamma} = (F_t - F_{PG}) / (F_0 - F_{PG}) \quad (3)$$

F_t = fluorescence of the polymer-DNA complexes

F_0 = fluorescence of the DNA alone

F_{PG} = fluorescence of PicoGreen

For the purpose of investigating the influence of the lactoferrin protein in the condensation capacity of nanomedicine formulated (DAB-Lf), the same PicoGreen experiment was conducted using lactoferrin protein only without conjugating it to DAB. Various Lf: DNA weight ratios were used (20:1, 10:1, 5:1 and 2:1) using similar DNA concentration (10 $\mu\text{g/ml}$). The sample was then mixed with 1 ml of PicoGreen[®] solution and its fluorescence was measured using fluorescence spectrophotometer with the same wavelength mentioned above.

2.2.2.3.2. Agarose gel retardation assay

The ability of the dendrimer conjugates to complex with the DNA was assessed by agarose gel retardation assay. DAB-Lf, DAB-PEG2k-Pep2 and DAB-PEG2k-Pep4 dendriplexes were prepared at different dendrimer: DNA weight ratios from 20 to 0.5 with a fixed DNA concentration of 20 $\mu\text{g/ml}$. After mixing with the loading buffer, the samples (15 μL) were loaded on a 1X Tris-Borate-EDTA (TBE) (89 mM Tris base, 89 mM boric acid, 2 mM Na₂-EDTA, pH 8.3) buffered 0.8% (w/v) agarose gel containing ethidium bromide (0.4 $\mu\text{g/mL}$), with 1x TBE as a running buffer. The DNA size marker was HyperLadder I. The gel was run at 50 V for one hour and then photographed under UV light.

2.2.2.3.3. Dendriplex size and zeta potential measurement

The size and zeta potential of the DAB-Lf, DAB-Pep2 and DAB-Pep4 dendriplexes were measured for the different dendrimer: DNA weight ratios (20:1, 10:1, 5:1, 2:1, 1:1, 0.5:1, 0:1) by photon correlation spectroscopy and laser Doppler electrophoresis using a Malvern Zetasizer Nano-ZS (Malvern, UK). The samples were prepared by complexing 50 μg of the plasmid per sample with the required amount of the dendrimer based on the ratio required. The

sample size was then immediately measured using disposable micro cuvette; zeta measurements were then performed for the same sample using folded capillary cell.

The size and zeta potential of the PEGylated dendrimers DAB-PEG2k-Pep2 and DAB-PEG2k-Pep4 were also measured following the same procedure mentioned above. Additionally, the size and zeta potential of DAB-PEG3.5k-Pep2 and DAB-PEG2k-PEG3.5k-Pep2 polyplex were also measured for the weight ratios 20:1, 10:1 and 5:1.

2.2.2.3.4. Atomic force microscopy

DAB-Lf dendriplex was analysed via atomic force microscopy (AFM) to review the size and shape of the nanoparticles formed. DAB-Lf dendrimer (250 µg) was complexed with DNA encoding β-galactosidase (50 µg) in a ratio of 5:1 using glucose 5% as solvent. The solution was diluted 100 times using distilled water, then 5 µl of the dilute solution was placed on a mica surface and left to air-dry at room temperature.

DAB-PEG2k-Pep2 and DAB-PEG2k-Pep4 dendriplexes were analysed as well via AFM as follow: 1 mg of the dendrimer was complexed with 50 µg DNA encoding β-galactosidase in a dendrimer: DNA ratio of 20:1 using glucose 5% solution as solvent. The solution was diluted 10 times using distilled water, then 5 µl of the dilute solution was placed on a mica surface and left to air-dry at 20 °C.

The scanning mode used was PeakForce Tapping[®] mode at room temperature using Bruker ScanAsyst-Air probe (Camarillo, California). The data were collected by a Dimension Fast Scan AFM (Bruker) equipped with an Icon scanner with nominal tip radius of 2 nm and nominal spring constant of $k = 0.4$ N/m. All data were analysed using the NanoScope Analysis 1.5 software (Bruker), while height images were corrected by first order flattening.

2.3. Results

2.3.1. Conjugation of lactoferrin and Peptide2 to DAB dendrimer

The synthesis of DAB-Lf, DAB-Pep2, and DAB-Pep4 was achieved in two steps; the first step was linking the dendrimer with a heterobifunctional cross-linker followed by conjugating the ligand of interest to the intermediate product formed (DAB-crosslinker). DAB-Lf, DAB-Pep2 and DAB-Pep4 yielded around 50% and 60% of final product respectively. The synthesis was verified by NMR and MALDI-TOF, each step being investigated separately to confirm its success.

Peptide-bearing DAB dendrimer were then subjected to extra modification by introducing PEG polymer in the periphery of the dendrimer to form DAB-PEG2k-Pep2 and DAB-PEG2k-Pep4 which yielded respectively around 64% and 75% of the final product. The successful synthesis of the final step of the reaction was confirmed via $^1\text{H-NMR}$ and DOSY NMR.

2.3.1.1. DAB-GMBS

The conjugation between the DAB-Am16 and the cross-linker GMBS was performed at various multiples (2, 4, 6, 8, 10 and 12) of molar excess of cross-linker over the amount of DAB present. Each ratio was then analysed by $^1\text{H-NMR}$ and based on the spectra produced, DAB-GMBS ratios with six-, four- and two-fold molar excess were taken to the next step of synthesis.

The optimum conjugate (formed with two-fold molar excess of GMBS over DAB) was then characterised via $^1\text{H-NMR}$, COSY, HMBC and HSQC. $^1\text{H-NMR}$ of DAB-cross-linker (Figure 2-5, Figure 2-10 and Table 2-4) confirmed the coupling between DAB and GMBS as follows: $^1\text{H-NMR}$ (D_2O): δ DAB ($\text{N-CH}_2\text{-CH}_2\text{-CH}_2\text{-CH}_2\text{-N}$) at 1.48 ppm (a), δ DAB ($\text{N-CH}_2\text{-CH}_2\text{-CH}_2\text{-N}$) at the peak at 1.64 ppm (b); δ DAB ($\text{N-CH}_2\text{-CH}_2\text{-CH}_2\text{-NH}_2$) at 1.79 ppm (c); δ DAB ($\text{N-CH}_2\text{-CH}_2\text{-CH}_2\text{-NH}$) at 2.48 ppm; δ DAB ($\text{N-CH}_2\text{-CH}_2\text{-CH}_2\text{-N}$) at 2.55 ppm (d); δ DAB

(N-CH₂-CH₂-CH₂-NH₂) at 2.91 ppm (e). The peaks corresponding to the cross-linker protons in the same spectrum are as follows: protons for carbon (h) at 2.21 ppm; for carbon (g) at 2.98 ppm; protons for carbon (i) at 3.15 ppm; maleimide group protons (j) at 6.23 ppm; and finally, amide proton at 8.15 ppm (k). The full characterisation of DAB-GMBS based on 2D-NMR can be seen in Table 2-4. All NMR spectra were analysed using Mestrenova[®] NMR software.

Table 2-4 DAB-GMBS characterisation using 2D-NMR (COSY, HMBC and HSQC)

Number from Figure 2-5	Proton Chemical Shift (ppm)	Carbon Chemical Shift (ppm)	Long Distance Coupling HMBC
a	1.48	21.2	C ₂
d	2.55	49.9	C _{4, 7, 10, etc.}
b	1.64	23.7	C _{2, 3, 5, 6, 8, 9, etc.}
f	2.48 (q)	50.41	C _{9, 10}
g	2.98 (t)	50.99	C _{13, 14}
h	2.21	21.79	C _{12, 14, Amide carbonyl}
i	3.15	53	C _{12, 13, Maleimide carbonyl}
j	6.23	128.2	Maleimide carbonyl
c	1.79	37.9	C _{2, 3, 5, 6, 8, 9, etc., C₁₇}
e	2.91 (t)	53.09	C _{2, 3, 5, 6, 8, 9, etc., C₁₆}
k	8.15	-	-

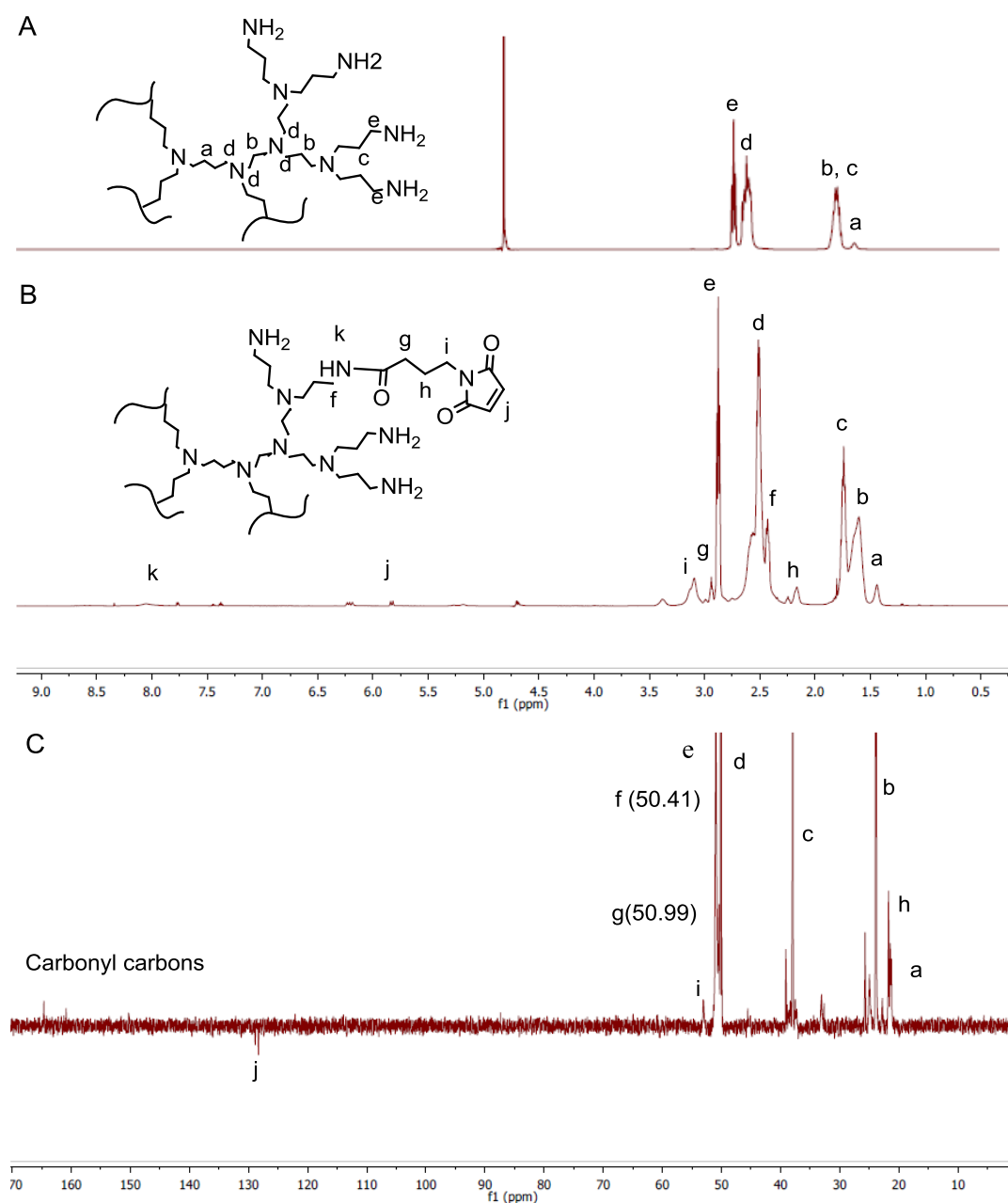


Figure 2-5 NMR spectra of DAB (A) and DAB-cross-linker (B: $^1\text{H-NMR}$, C: $^{13}\text{C-NMR}$)

It can be observed that the DAB peaks in the DAB-GMBS spectrum (Figure 2-5, B) are shifted compared with the peaks in the $^1\text{H-NMR}$ spectrum of DAB only (Figure 2-5, A). The characteristic broad peak at 1.48 ppm is for the protons in the CH_2 groups (b), shielded between the other CH_2 groups in DAB and shifted forward to be more shielded compared with the DAB spectrum, where it was detected at 1.60 ppm. On the other hand, the peaks at 2.55 and 2.91

ppm, corresponding to the protons on CH₂ groups (d) and those on CH₂ group (e) respectively, are seen to have moved back slightly to be more deshielded compared with the DAB spectrum, where they appear at 2.45 and 2.58 ppm respectively. These shifts in the peaks are mainly due to the change in DAB structure after its conjugation with GMBS.

The presence of the maleimide peaks at 5.85 and 6.23 ppm in the DAB-GMBS spectrum indicates the successful conjugation between DAB and GMBS, although its integration is relatively small, which can be explained by the very large difference in the numbers of protons integrated for each peak in the spectrum, whereas DAB-related peaks are highly intensive with protons compared to the conjugated cross-linker peaks, that have two protons under each peak at most. Amide proton peak which appears as broad small peak (k) at 8.15 ppm is another confirmation of the successful linkage between DAB and GMBS. Furthermore, the GMBS peaks in the spectrum do not represent the prospective spin-spin splitting, which could be for the same reason as that given above, as well as the partial overlapping of these peaks with the dominant DAB peaks, since they tend to appear in fairly similar chemical shifts.

For the purpose of investigating the ratio of GMBS molecules being conjugated to each DAB molecule, DAB-GMBS ¹H-NMR integration was measured using the Mestrenova[®] NMR software. The area under a particular peak gives a measure of the number of protons correlated to that peak relative to the other peaks in the spectrum; therefore, comparing the integration intensities of two peaks, one with known proton intensity and one which is to be investigated, could be a good method of determining the coupling ratio between two reactants. In order to obtain reasonable data, the chosen peaks should be completely separate from the other peaks in the spectrum. The first peak selected is correlated to the DAB molecule and the other correlated to the GMBS moiety, in order to estimate the ratio of coupling between DAB and GMBS. The peaks selected were the DAB peak (a) at 1.44 ppm, which is known to represent four protons, as this peak corresponds to the DAB core molecule, and peak (h) at 2.17 ppm,

corresponding to the middle CH₂ group in the GMBS molecule. The two peaks had almost similar integrations (1 and 0.93 respectively) (Figure 2-6). This is an indication that there are four protons represented in peak (h), corresponding to two GMBS molecules.

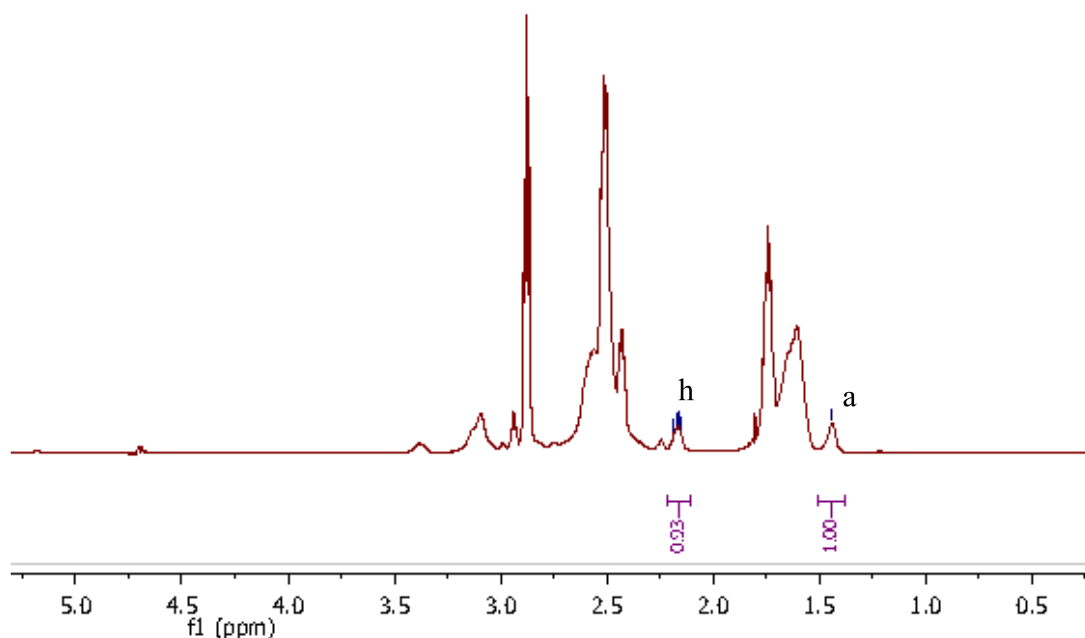


Figure 2-6 Peaks integration in the spectrum of DAB-GMBS molecule

The LC-MS spectrum of DAB-GMBS shown in Figure 2-7 also confirmed successful conjugation. DAB-crosslinker was subjected to liquid chromatography using C18 reverse phase column, to ensure separation of DAB-crosslinker from unbounded DAB, then the sample was characterised by mass spectroscopy to measure accurately the mass of the compound. DAB-crosslinker with two- and six-fold molar excess of GMBS over DAB was analysed via LC-MS. The 6-molar ratio showed considerable coupling between the DAB and the GMBS at around four to seven GMBS molecules per DAB molecule (Figure 2-7, Table 2-5). On the other hand, the sample with lower molar ratio excess of GMBS showed evidence of single-to-double binding of GMBS to the dendrimer molecule.

Successful DAB-GMBS linkage was also characterised by MALDI-TOF (Figure 2-8). The spectrum obtained showed four characteristic peaks explained in details in Table 2-6. These

results demonstrate that DAB was successfully conjugated with one to two GMBS cross-linker and thus that the first step of the synthesis was successful. However, some of the obtained m/z were higher than the expected weight by one or two which could be due to the impact of ^{13}C isotope on the overall molecular weight.

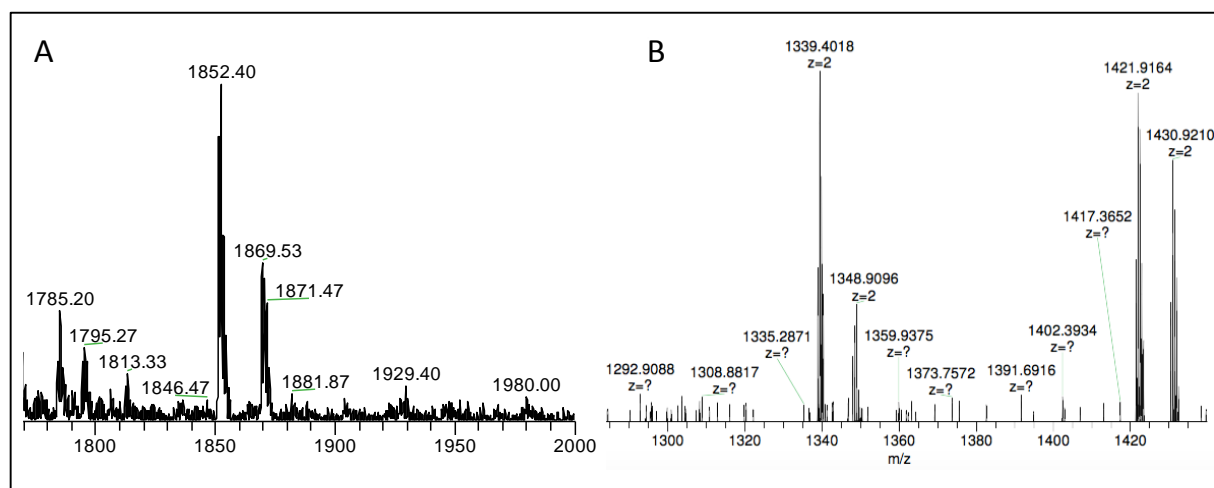


Figure 2-7 Mass spectroscopy spectrum of DAB-GMBS using two (A) and six-molar excess (B) of GMBS over DAB.

Table 2-5 LC/MS spectra analysis for DAB-GMBS at Figure 2-7

Sample	m/z	Charge	Molecular weight (Da)	Compound	Adduct
A	1852.4	1	$(1851.79 \times 1) + \text{H}$	DAB dendrimer linked to one GMBS group	N/A
A	1869.5	1	$(1851.79 \times 1) + \text{H} + 18$	DAB dendrimer linked to one GMBS group	H ₂ O
B	1339.4	2	$[1680.7 + (166 \times 6) = 2676.8]$	DAB dendrimer linked to six GMBS groups	N/A
B	1348.9	2	$[1680.7 + (166 \times 6) = 2676.8] + \text{H} + 18$	DAB dendrimer linked to two GMBS groups	H ₂ O
B	1421.9	2	$[1679.7 + (166 \times 7) = 2841.8]$	DAB dendrimer linked to seven GMBS groups	N/A

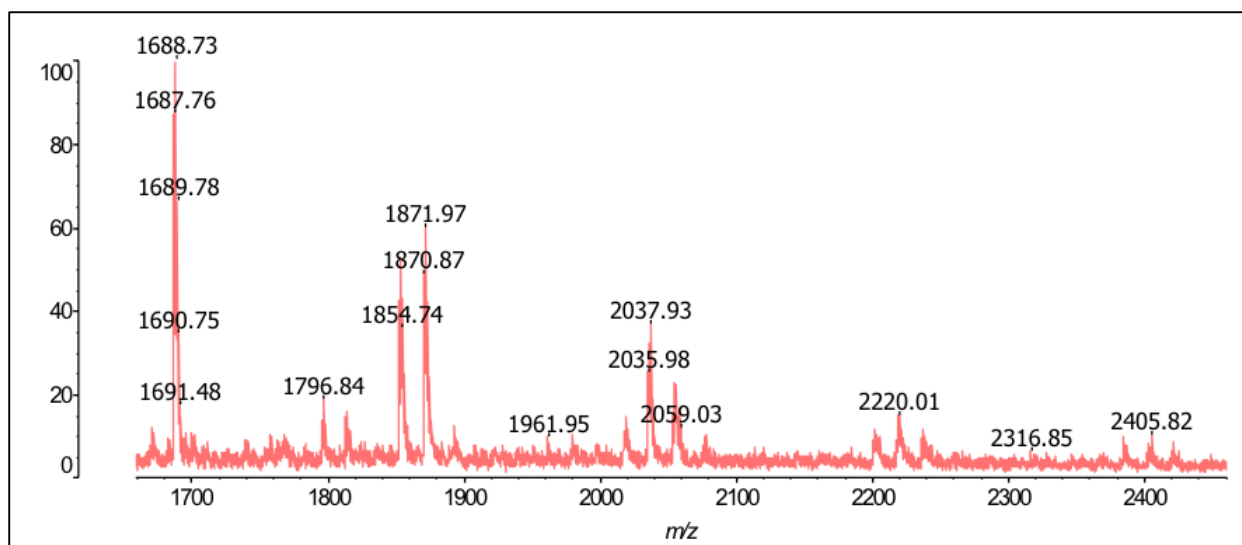


Figure 2-8 MALDI-TOF spectrum of DAB-GMBS showing one to two GMBS molecules linked to each dendrimer molecule.

Table 2-6 MALDI-TOF spectrum analysis of DAB-GMBS

No	m/z	Charge	Molecular weight (Da)	Compound	Adduct
1	1687.78,	1	$(1686.79 \times 1) + H$	DAB dendrimer + H	N/A
2	1854.74	1	$(1852.79 \times 1) + H$	DAB dendrimer linked to one GMBS group	N/A
3	1871.97	1	$(1851.97 \times 1) + 21$	DAB dendrimer linked to one GMBS group	Sodium ion
4	2037.93	1	$(2016.79 \times 1) + 21$	DAB dendrimer linked to two GMBS groups	Sodium ion
5	2059.03	1	$(2016 \times 1) + 39$	DAB dendrimer linked to two GMBS groups	Potassium ion
6	2220.01	1	$(2181 \times 1) + 39$	DAB dendrimer linked to three GMBS groups	Potassium ion

2.3.1.2. DAB-Lactoferrin

The final step in the synthesis of DAB-Lf was verified by the $^1\text{H-NMR}$ spectrum (Figure 2-9) which shows all the peaks corresponding to the DAB-GMBS conjugate, including the maleimide peaks. It is important to note here that the detection of high molecular weight protein via NMR is a very complicated procedure. The $^1\text{H-NMR}$ spectra of proteins tend to show uncharacteristic overlapped peaks because of the very different proton environments and the dynamic helical structure of such compounds, as can be seen in the lactoferrin spectrum (Figure 2-9, A) (Kwan *et al.*, 2011). However, there is still some evidence of the successful modification of the dendrimer. Firstly, in DAB-Lf $^1\text{H-NMR}$ spectrum (Figure 2-9, B), the peaks corresponding to DAB-cross-linker in the region between 1.5 and 3.5 ppm remain at high intensity even after the filtration methods that were used in the synthesis procedure, which should insure the removal of any unreacted molecules from the final product. Thus, these peaks correspond to DAB-cross-linker conjugated with protein molecules, supporting the successful coupling of DAB-Lf. Some Lf moieties are detected in the $^1\text{H-NMR}$ spectrum at 0.8 (l), 3.5 (m) and 8.5 (n).

MALDI-TOF mass spectroscopy was also used to confirm the successful synthesis of DAB-Lf. Figure 2-11-A shows the average molecular weight of DAB-Lf at a peak of 84537.5 m/z. This is compared with lactoferrin alone as a standard sample (Figure 2-11-B), which shows the lactoferrin peak at 82751.31 m/z. The difference between the two spectra indicates the successful conjugation of the protein to the dendrimer.

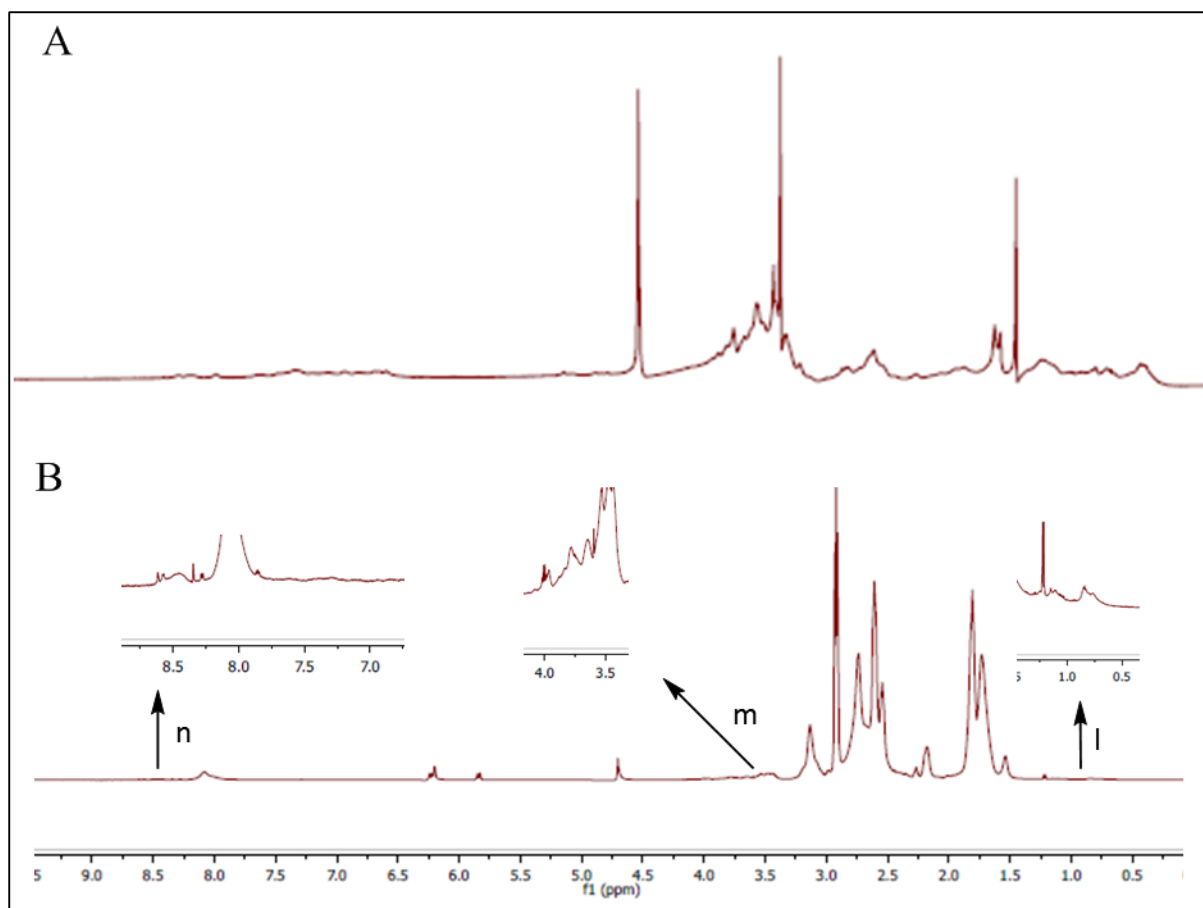


Figure 2-9 $^1\text{H-NMR}$ spectra of A) Lactoferrin protein and B) DAB-Lf, where (l, m and n) are lactoferrin residues.

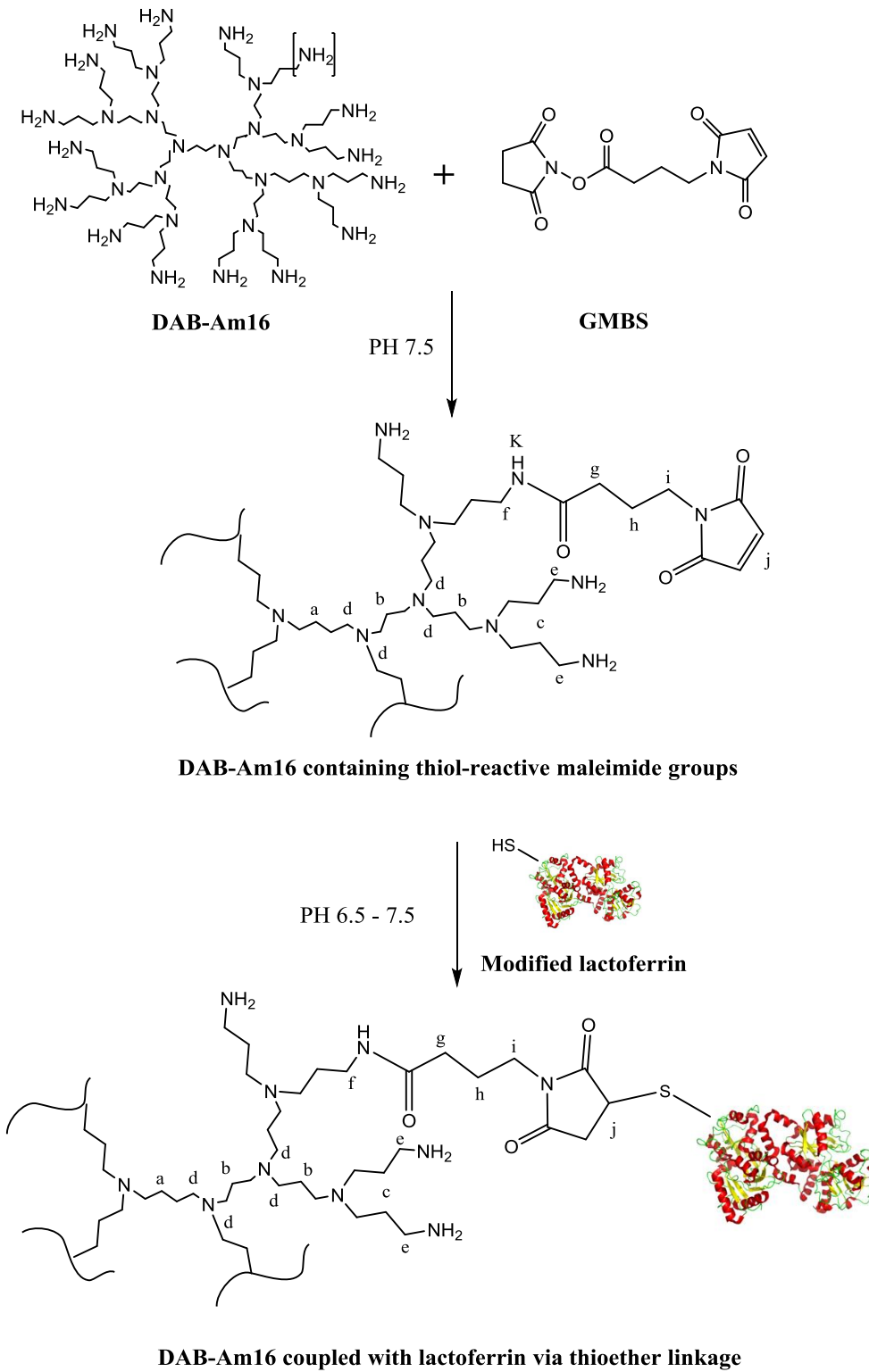


Figure 2-10 Conjugation reaction steps of DAB-Lf

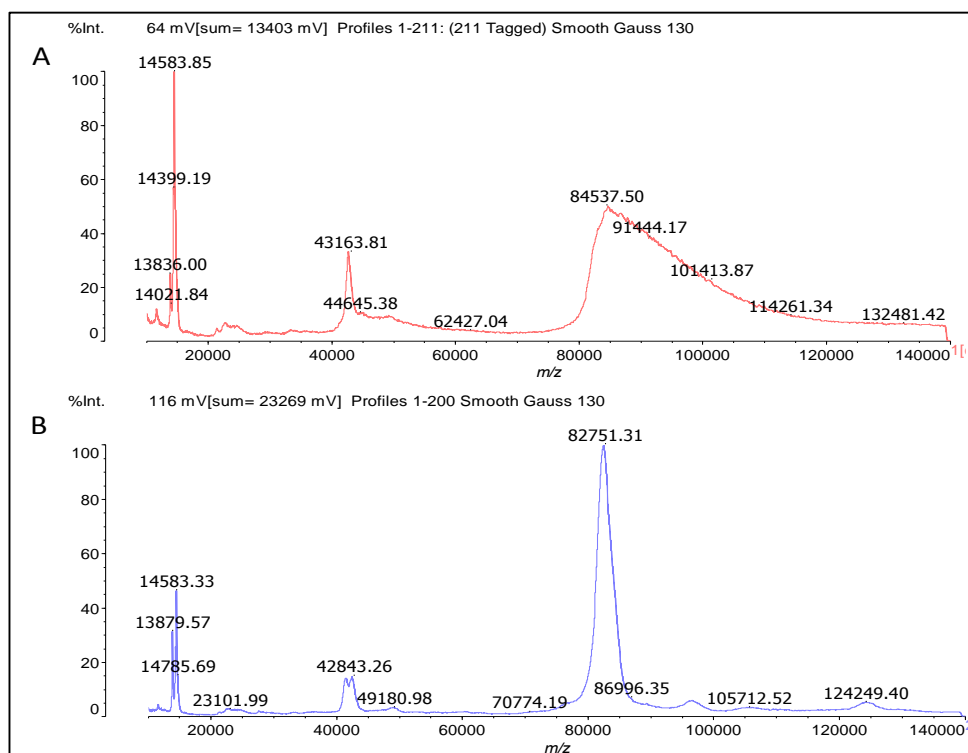


Figure 2-11 MALDI-TOF mass spectrometry of the dendriplex DAB-Lf (A) and lactoferrin alone (B) as standard sample.

2.3.1.3. Peptide2 - bearing DAB dendrimer

The successful synthesis of the novel nanoparticle DAB-Pep2 was confirmed by two different analytical methods: NMR and MALDI-TOF. $^1\text{H-NMR}$ analysis of Peptide2 revealed characteristic peaks for some of the amino acids in the sequence of the peptide such as leucine (L), threonine (T), alanine (A) and tryptophan (W); similar peaks were detected in the DAB-Pep2 spectrum with some changes in intensity and location, as described in Table 2-4. The detection of these peaks in the DAB-Pep2 spectrum (Figure 2-12) provides positive evidence of the successful conjugation between Peptide2 and DAB, beside the significant peaks corresponding to DAB-GMBS as described above (section 2.2.1). However, detecting the covalent bond formed by the reaction of the sulfhydryl group in the peptide (SH) and the maleimide group in DAB-GMBS is not applicable via $^1\text{H-NMR}$ as well as common 2D NMR (COSY, HMBC, & HSQC).

Therefore, in order to gain a better understanding of the mechanism of coupling between the peptide and the DAB-GMBS molecule, additional 2D-NMR experiments were conducted. They rely on detecting the spatial distance between two protons, instead of searching for covalent bond evidence, which is not applicable to our compounds.

Peptide2 and DAB-Pep2 were subjected to NOESY to reveal any through-space distance between DAB-GMBS and Peptide2. The ^1H -NMR spectra of Peptide2 and DAB-Pep2 show strong overlapping between the peaks, especially in the area between 1.5 and 3.5 ppm; this makes interpreting the spectra more complicated. Therefore, Peptide2 alone was first subjected to NOESY to determine the space correlations between the amino acid protons in the peptide, so as to eliminate them and reveal any actual correlation between the peptide and the dendrimer peaks in the DAB-Pep2 spectrum.

The DAB-Pep2 NOESY spectrum shows a clear correlation between some of the amino acids in the peptide and the dendrimer protons (Figure 2-13). The figure also revealed space correlations between the DAB dendrimer protons (b and c) and the beta and gamma protons in the alanine and threonine amino acids respectively in the Peptide2 sequence. Such peaks are indicative of the space correlation between Peptide2 and DAB-GMBS, which is not in itself proof of a covalent linkage, but instead confirms the existence of such a bond that causes these two molecules to be sufficiently close in space to allow their respective protons to sense each other's spin resonances.

In addition, Peptide2, DAB-Pep2 and DAB-PEG2k-Pep2 were subjected to DOSY NMR to measure their distribution coefficient (DC) in a specific environment (90% H_2O and 10% D_2O) at the same temperature (Figure 2-14). DAB-Pep2 had a lower DC ($1.81 \times 10^{-10} \text{ m}^2/\text{s}$) than Peptide2 ($2.55 \times 10^{-10} \text{ m}^2/\text{s}$), while PEGylated DAB-Pep2 had the lowest value ($1.25 \times 10^{-10} \text{ m}^2/\text{s}$). This is to be expected, as molecules of higher molecular weight tend to have a lower DC, indicating that DAB-PEG2k-Pep2 had a slower Brownian motion in the solution than

DAB-Pep2, which in turn diffused more slowly than the peptide alone. More importantly, DAB-PEG2k-Pep2 and DAB-Pep2 DOSY spectra confirmed the purity of these compounds, each spectrum has a single peak, representing a single compound diffused in the solution. This is a very important confirmation for the successful conjugation as well as the purity of the solution.

MALDI-TOF analysis indicated the successful synthesis of DAB-Pep2 as well; it shows a peak at 3131.07 m/z, which is believed to correspond to DAB-Pep2. DAB-GMBS has a molecular weight between 1851 and 2016 Da as determined earlier by MALDI-TOF (Figure 2-8); adding this to the weight of Peptide2, which is 1565 Da, would result in a compound with a molecular weight around 3433 m/z. However, the MALDI-TOF spectrum showed a weight of 3131.07 m/z (Figure 2-15). This reduction in molecular weight could be due to some fragmentation in one of the branches of the DAB dendrimer, as the stability of polymers, including dendrimers, can be diminished during MALDI-TOF analysis (Subbi *et al.*, 2005).

Table 2-7 List of Peptide2 characteristic peaks in the ¹H-NMR spectrum of DAB-Peptide2

Location in the sequence N to C terminal	Name	Significant peaks in DAB-Peptide2	Reference
2 & 10	Tryptophan (W)	1. Phenolic protons (6.95, 7.05, 7.2, 7.3 ppm). 2. NH proton in the indole group (7.7 and 7.8 ppm).	Graça <i>et al.</i> , 2008; Wishart <i>et al.</i> , 2018
6 & 12	Threonine (T)	1. Protons correlated to CH ₃ at 1.05 and 1.15 ppm, doublet.	Gowda <i>et al</i> 2015; Wishart <i>et al.</i> , 2018
7 & 11	Alanine (A)	1. Protons correlated to CH ₃ at 1.17 and 1.2 ppm, doublet.	Gowda <i>et al</i> 2015; Wishart <i>et al.</i> , 2018
8 & 9	Histidine (H)	1. Protons correlated to the carbons in the imidazole ring at 6.29 and 7.15 ppm, doublet.	Gowda <i>et al</i> 2015; Wishart <i>et al.</i> , 2018
13	Leucine (L)	1. Protons correlated to the two CH ₃ groups at 0.77 and 0.8 ppm, doublet.	Gowda <i>et al</i> 2015; Wishart <i>et al.</i> , 2018

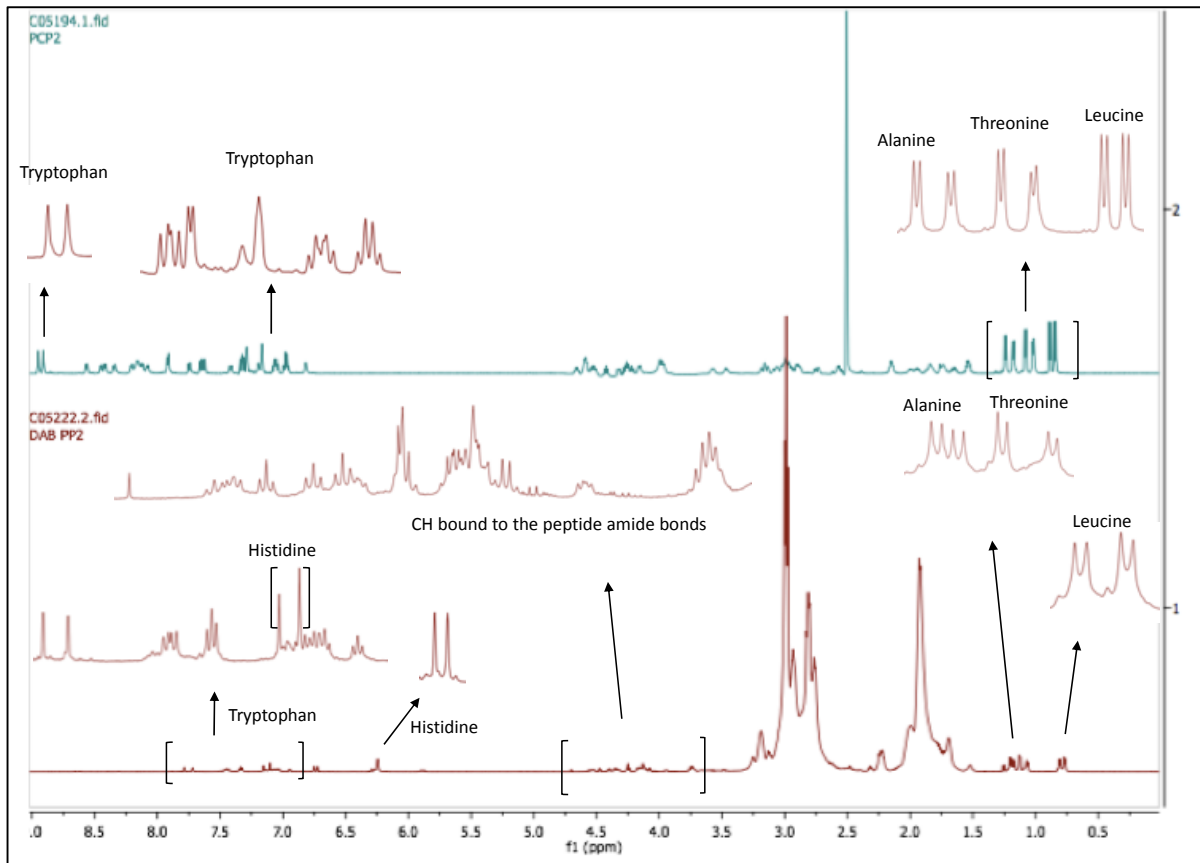


Figure 2-12 $^1\text{H-NMR}$ spectra of Peptide2 (A) and DAB-Peptide2 (B)

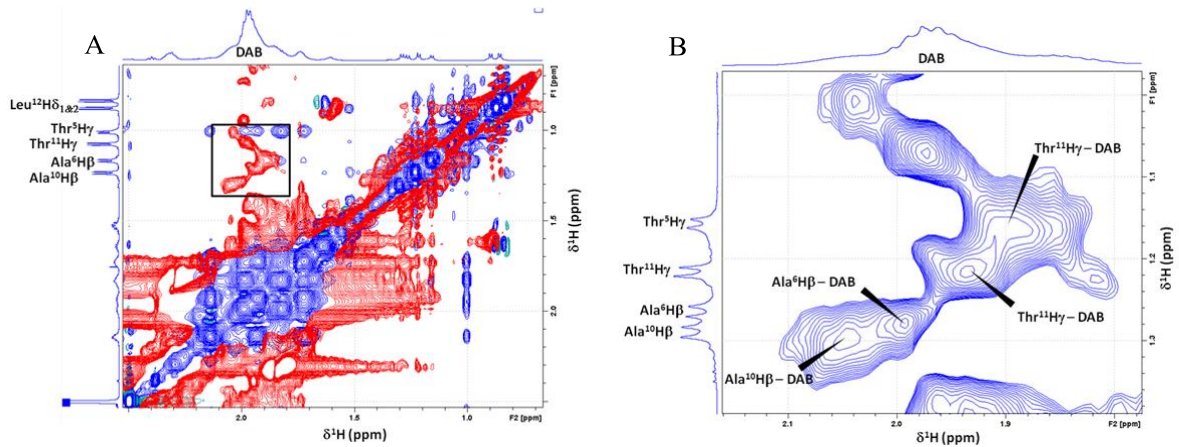
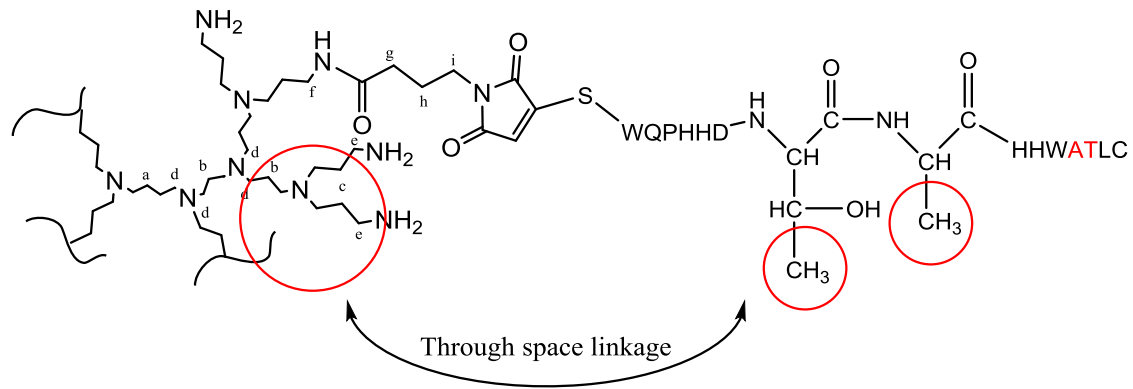


Figure 2-13 Evidence for through-space contact between the Peptide2 and DAB components of DAB-Peptide2. A) Overlay of the 0.5-2.5 ppm region of the 2D [^1H , ^1H] NOESY NMR spectrum for PEP2 (blue) and the DAB-PEP2 conjugate (red). B) 2D [^1H , ^1H] NOESY NMR spectrum for DAB-Peptide2 in 90% H_2O / 10% D_2O

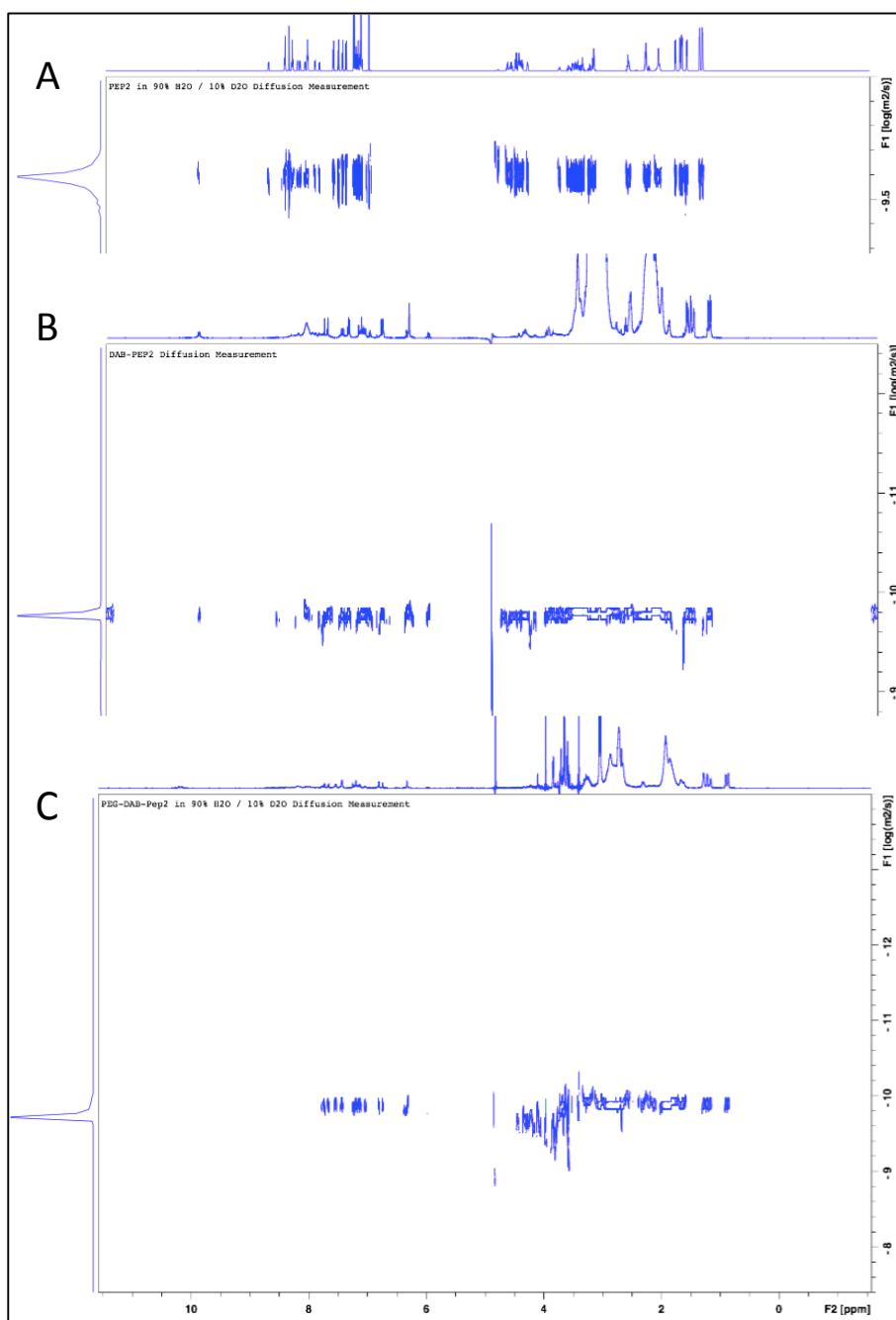


Figure 2-14 DOSY spectra of Peptide2 (A), DAB-Peptide2 (B) and DAB-PEG2k-Peptide2 (C) using 90% H₂O and 10% D₂O as solvent.

Table 2-8 Diffusion coefficient of Peptide2, DAB-Pep2 and DAB-PEG2k-Pep2

Name	Diffusion coefficient (m ² /s)
Peptide 2	2.55 x 10 ⁻¹⁰
DAB-Pep2	1.81 x 10 ⁻¹⁰
DAB-PEG2k-Pep2	1.25 x 10 ⁻¹⁰

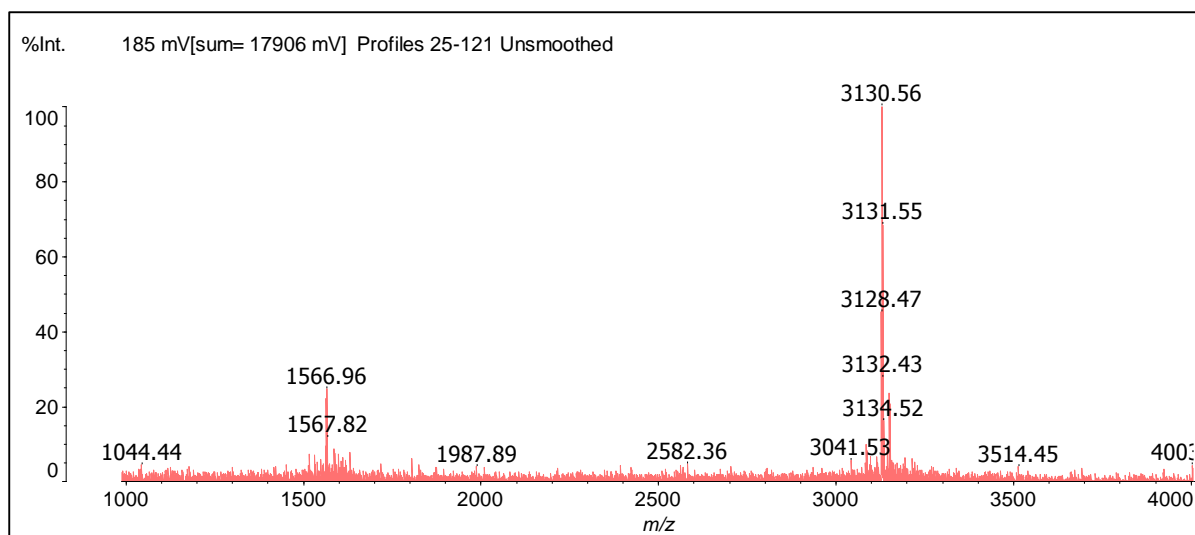


Figure 2-15 MALDI-TOF spectrum of DAB-Peptide2

2.3.1.4. PEGylation of DAB-Peptide2 dendrimer

2.3.1.4.1. DAB-PEG2k-Peptide2

The successful synthesis of DAB-PEG2k-Pep2 was investigated primarily by $^1\text{H-NMR}$. The successful conjugation of the NHS-ester in the PEG polymer with the DAB primary amine groups was measured by detecting the PEG peaks in the $^1\text{H-NMR}$ spectrum as follows: (600 MHz, D_2O) δ : singlet methoxy protons ($\text{CH}_3\text{-O-PEG}$) at 3.29 ppm (a), triplet PEG protons at 3.65 ppm (b), singlet ($\text{PEG-O-CH}_2\text{-CO}$) at 3.85 ppm (Figure 2-16). The NMR data are in line with the PEG spectra at Jeong *et al* (2008).

The number of PEG 2kDa molecules conjugated to each DAB molecule was estimated by measuring the integration of specific peaks on both DAB and PEG in the $^1\text{H-NMR}$ spectrum then comparing them as follows: the core of the DAB molecule (diaminobutane) has its protons peak at 1.52 ppm, which is well known to represent four protons (Zhang *et al.*, 2014); starting the spectrum integration with this peak would help in the estimation of the number of PEG molecules attached. The methoxy proton peaks had integration values around three (2.96);

therefore, they are expected to be $4 \times 3 = 12$ protons covered under these peaks. This is an indication that four PEG molecules have successfully reacted with DAB (Figure 2-16).

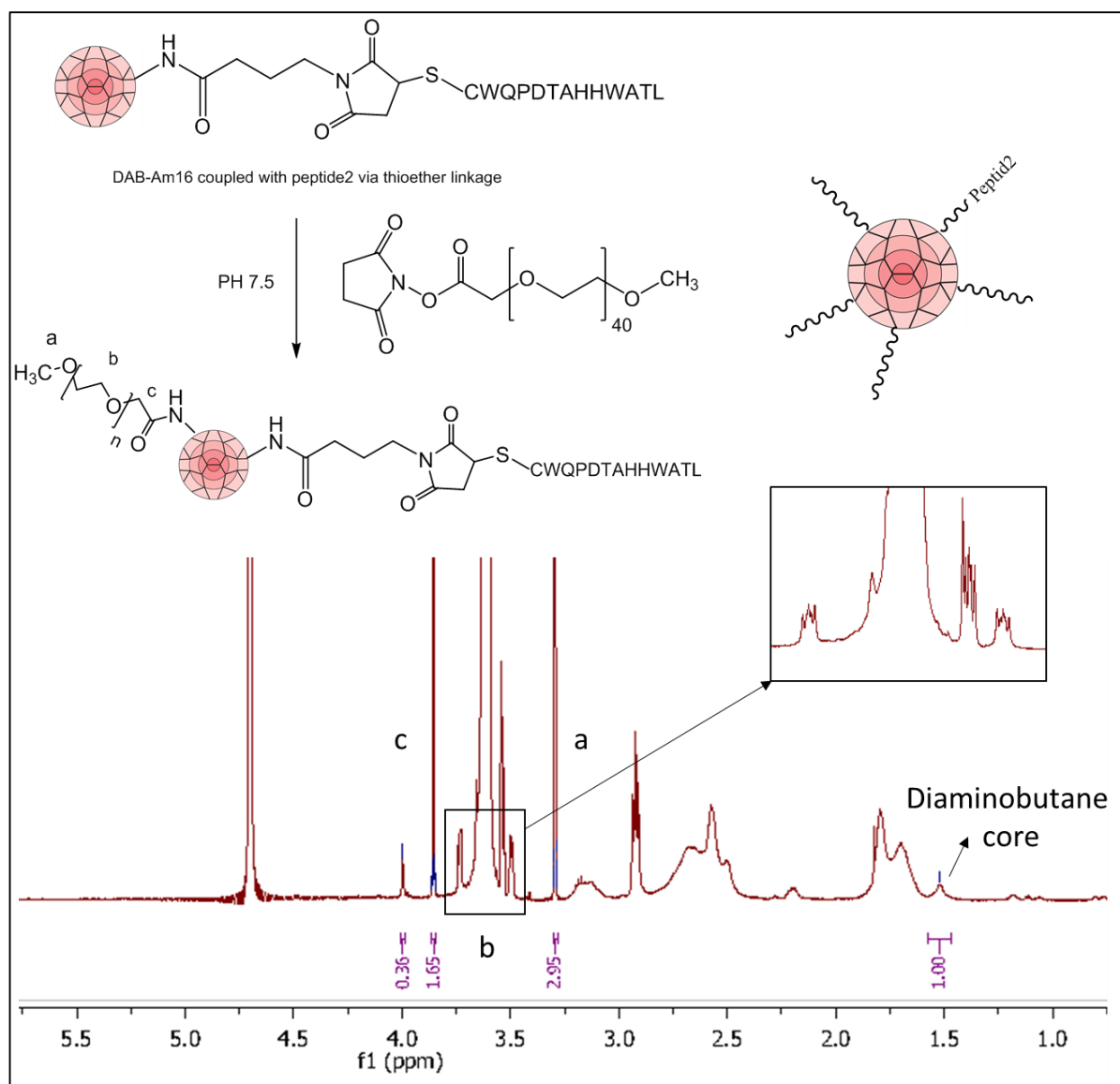


Figure 2-16 The final synthesis step of DAB-PEG2k-Peptide2 dendrimer and its corresponding 1H -NMR spectrum

2.3.1.4.2. DAB-PEG3.5-Peptide2

The successful conjugation of the NHS ester group in the NHS-PEG3.5-maleimide with the DAB amine group, followed by the conjugation of Peptide2, was measured by detecting PEG and Peptide2 peaks in the 1H -NMR spectrum as follows: (600 MHz, D_2O) δ : singlet peak of

CO-CH₂-O-PEG protons at 3.98 ppm (a), triplet PEG protons at 3.74 ppm (b), triplet peak of NH-CO-CH₂-CH₂-maleimide protons at 3.53 ppm (c), triplet peak of NH-CO-CH₂-CH₂-maleimide protons at 3.43 ppm (d) and doublet peaks of maleimide protons at 5.96 and 6.36 ppm (e) (Figure 2-17). Peptide2 peaks can be seen in the DAB-PEG3.5k-Pep2 spectrum between 0.6 and 1.2 ppm and from 6.7 to 7.75 ppm, which are similar to the peaks detected in the DAB-Pep2 spectrum (Figure 2-12 and Table 2-7).

One PEG 3.5 kDa molecule was found to be coupled with each DAB molecule; this was estimated by comparing the integration of the diaminobutane peak at 1.65 ppm and the peak at 3.98 ppm (a), corresponding to the protons of the PEG molecule. The integration indicates that peak (a) covers two protons (CO-CH₂-O-PEG) and thus that only one PEG molecule was linked to DAB as expected.

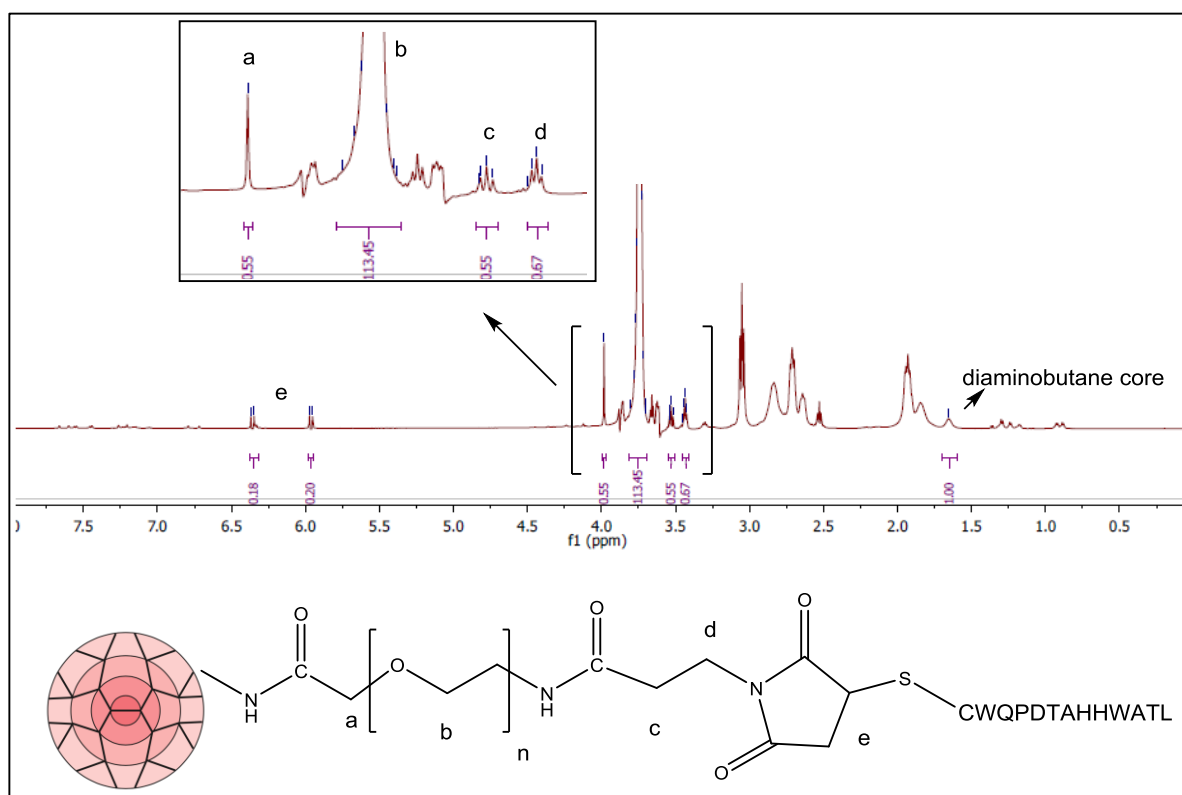


Figure 2-17 DAB-PEG3.5-Peptide2 ¹H-NMR spectrum and structure

2.3.1.4.3. DAB-PEG2k-PEG3.5k-Peptide2

Another PEGylated DAB-Pep2 molecule was prepared by reacting extra PEG 2kDa branches in DAB as well as using PEG 3.5kDa as crosslinker between DAB and Pep2. The successful synthesis of this formulation was confirmed by $^1\text{H-NMR}$ (Figure 2-18) as follows: (600 MHz, D_2O) δ : singlet peak of methoxy protons ($\text{CH}_3\text{-O-PEG}$) at 3.27 ppm (a), singlet peak of $\text{CO-CH}_2\text{-O-PEG}$ protons at 3.98 ppm (b), triplet PEG protons at 3.6 ppm (c), triplet peak of $\text{NH-CO-CH}_2\text{-CH}_2\text{-maleimide}$ protons at 3.40 ppm (e), triplet peak of $\text{NH-CO-CH}_2\text{-CH}_2\text{-maleimide}$ protons at 3.30 ppm (d) and doublet peaks of maleimide protons at 5.96 and 6.36 ppm (f).

It was estimated that one PEG 3.5kDa molecule was linked to DAB, using the same technique as explained in Section 2.3.1.4.2. In addition, it was estimated that around three PEG 2kDa molecules were conjugated with the DAB primary amine groups, as can be integrated from the spectrum: the integration of the methoxy proton peak is 2.49, indicating that it covers $4 \times 2.49 = 9$ protons, which indicates around three methoxy groups and therefore three PEG 2kDa molecules.

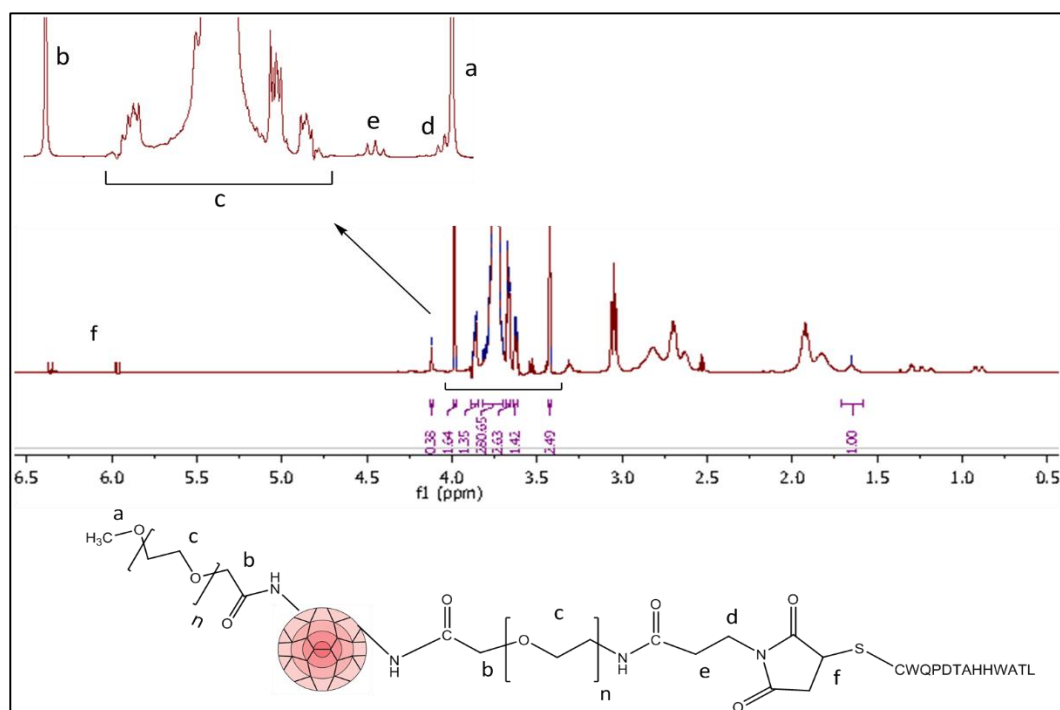


Figure 2-18 $^1\text{H-NMR}$ spectrum of DAB-PEG2k-PEG3.5k-Peptide2.

2.3.1.5. Peptide4- bearing DAB dendrimer

The successful synthesis of DAB-Pep4 was confirmed first by $^1\text{H-NMR}$, which revealed some peaks characteristic of Peptide4 such as threonine at 1.15 ppm (d) and leucine at 0.85 ppm (dd) (Figure 2-19, B), as well as some small peaks between 3.25 and 5 ppm which correspond to alkane protons adjacent to the amide bonds through the peptide sequence. The detected amino acids peaks were compared and confirmed with the one in Gowda *et al* (2015). The spectrum also showed DAB-GMBS peaks, as demonstrated before. The DAB-PEG2k-Pep4 spectrum showed some peaks corresponding to Peptide4 as well as the dendrimer peaks and some significant peaks for PEG molecules as follows: (600 MHz, D_2O) δ : singlet methoxy protons ($\text{CH}_3\text{-O-PEG}$) at 3.35 ppm (a), triplet PEG protons at 3.65 ppm (b), singlet ($\text{PEG-O-CH}_2\text{-CO}$) at 3.90 ppm (Figure 2-19,C). The spectra also show the amino acid peaks: threonine γ protons at 1.15 ppm as doublet, leucine δ protons at 0.83 and 0.87 ppm as doublets and leucine γ proton at 1.40 ppm as multiplet.

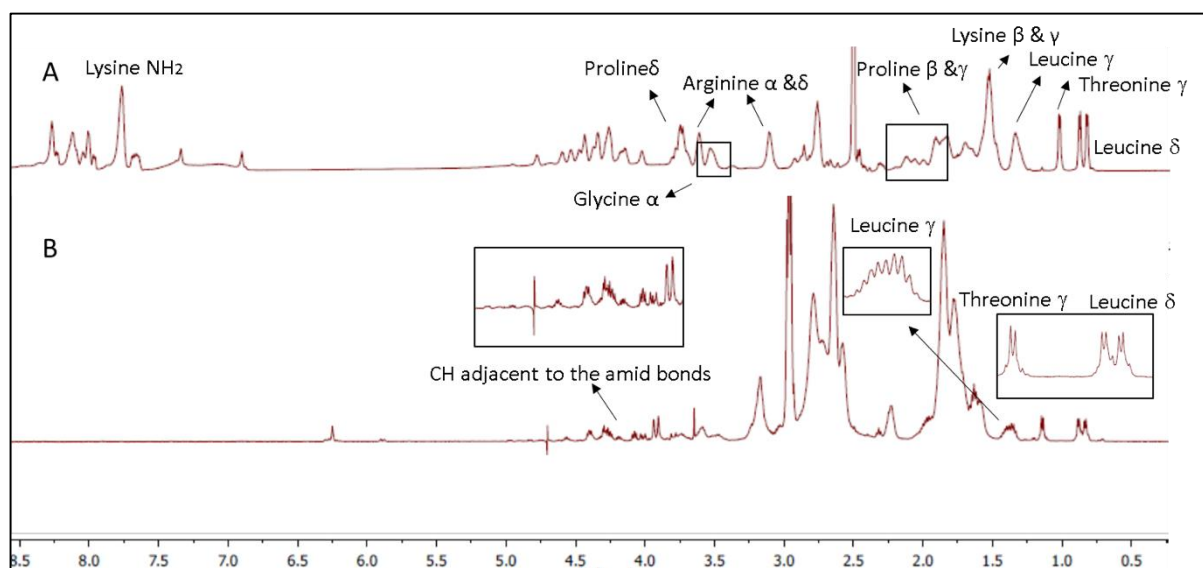


Figure 2-19 $^1\text{H-NMR}$ spectra of Peptide4 (A) and DAB-Peptide4 (B)

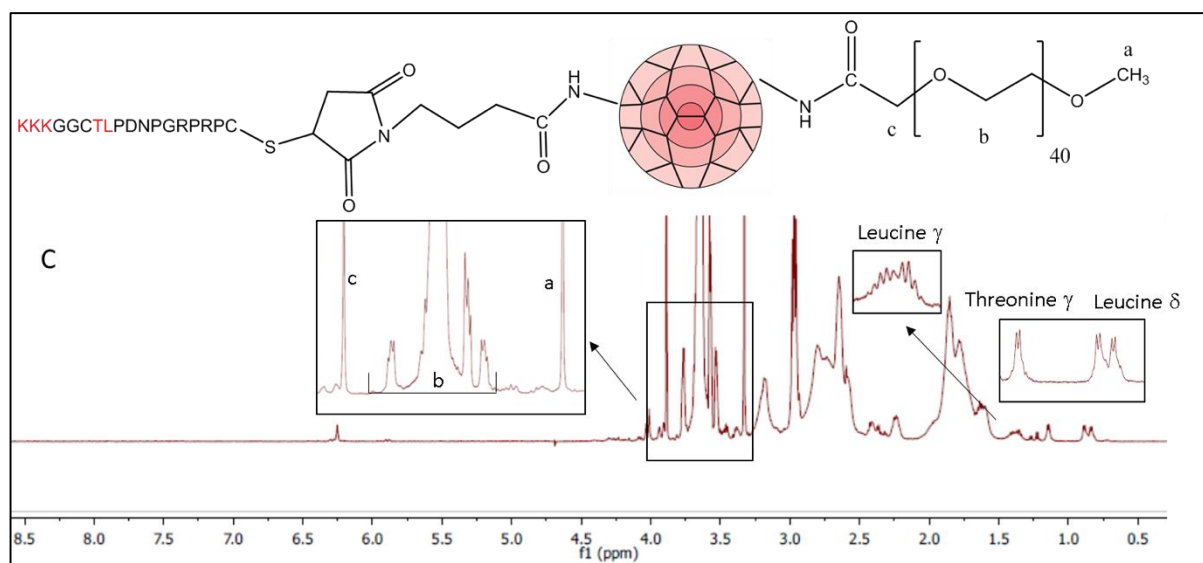


Figure 2-20 ¹H-NMR spectra of DAB-PEG2k-Peptide4

Table 2-9 List of Peptide4 characteristic peaks in the ¹H-NMR spectrum of DAB-Peptide4 and DAB-PEG2k-Peptide4

Location in the sequence N to C terminal	Name	Significant peaks in DAB-PEG2k-Peptide4	Reference
11	Leucine (L)	1. Protons correlated to the protons in the two sigma carbones (CH ₃) at 0.83 and 0.90 ppm, doublet. 2. Protons correlated to the protons in gamma carbone (CH) at 1.4 ppm, multiplet.	Gowda <i>et al</i> 2015; Wishart <i>et al.</i> , 2018
12	Threonine (T)	1. Protons correlated to the protons in gamma carbone (CH ₃) at 1.15 ppm, doublet.	Gowda <i>et al</i> 2015; Wishart <i>et al.</i> , 2018
16, 17 & 18	Lysine (K)	1. Protons correlated to the protons in sigma and gamma carbones (CH ₂) at 1.65 ppm, doublet.	Gowda <i>et al</i> 2015; Wishart <i>et al.</i> , 2018

2.3.2. Characterization of lactoferrin- and peptide- bearing DAB dendriplexes

2.3.2.1. PicoGreen[®] assay

2.3.2.1.1. DAB-Lf

DNA condensation tests were conducted on several DAB-Lf nanoparticles synthesised with various excess molar concentrations of GMBS over DAB (6, 4 and 2). The DNA condensation of the 6 and 4-fold excess of GMBS over DAB were able to condense 53.74% and 69.15% of the DNA respectively at their highest concentrations (DAB-Lf: DNA 20:1), while the two-molar excess of GMBS had a much better DNA condensation capability of around 78%, at dendrimer: DNA weight ratios of 10:1 and higher (Figure 2-21). DNA condensation occurred instantly and was found to be stable for at least 24 h. In addition, at the 5:1 weight ratio, more than 70% of the DNA was complexed, whereas at 2:1 there was a sharp drop in condensation to only 12% of the DNA. The remaining dendrimer weight ratios showed very poor ability to complex the DNA.

For the purpose of measuring the interference or the effect of lactoferrin in condensing the DNA, Lactoferrin protein was examined for its DNA condensation ability. The data showed that lactoferrin has a relatively weak ability in condensing DNA, where 35% of the DNA was condensed at the highest ratio (20:1) (Figure 2-22), whereas Lf: DNA ratio 5:1 condenses 7% of the DNA. This result actually indicates that the DNA conjugation capability of DAB-Lf nanoparticles is generated from the DAB dendrimer conjugated with the Lf ligand, whereas Lf has minor effect on the DNA conjugation.

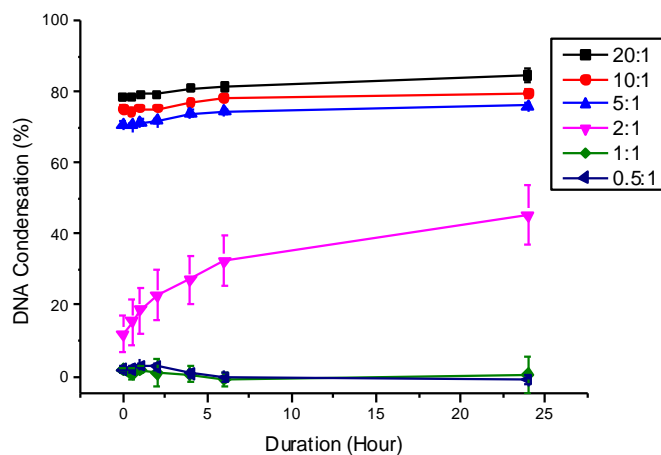


Figure 2-21 DNA condensation to DAB-Lf at various DAB-Lf: DNA weight ratios (n=4)

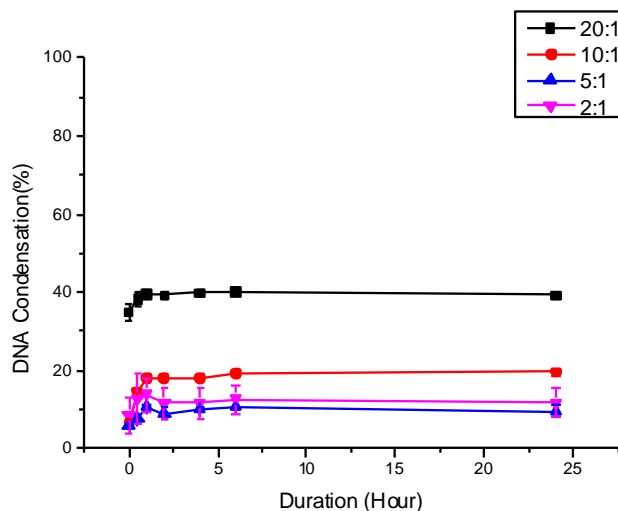


Figure 2-22 DNA condensation to Lactoferrin at various Lf: DNA weight ratios (n=4)

2.3.2.1.2. DAB-Peptide2 and DAB-PEG2k-Peptide2

The DNA condensation capability of DAB-Pep2 and DAB-PEG2k-Pep2 was examined using different weight ratios of the dendrimer over DNA. For DAB-Pep2 dendriplex, the data obtained showed a high DNA condensation ability at all weight ratios examined, with the lowest condensation ability being recorded for the lowest DAB-Pep2: DNA weight ratio (0.5:1), where 69.16% of the DNA was complexed. Ratios from 20:1 to 2:1 resulted in the condensation of more than 80% of the DNA. The condensation capability was persistent, with

signs of improvement over time until complete complexation of the DNA was reached after 24 hours for all the examined ratios (Figure 2-23, A).

For DAB-PEG2k-Pep2, on the other hand, the DNA condensation ability at all weight ratios examined was decreased compared with DAB-pep2. The weight ratios 10:1 and 20:1 were found to condense more than 70% of the DNA whereas 5:1 ratio was able to complex around 65% of the DNA. The remaining lower ratios failed to complex the DNA efficiently. The condensation capability of DAB-PEG2k-Pep2 was persistent, with no sign of any improvement over time (Figure 2-23, B)

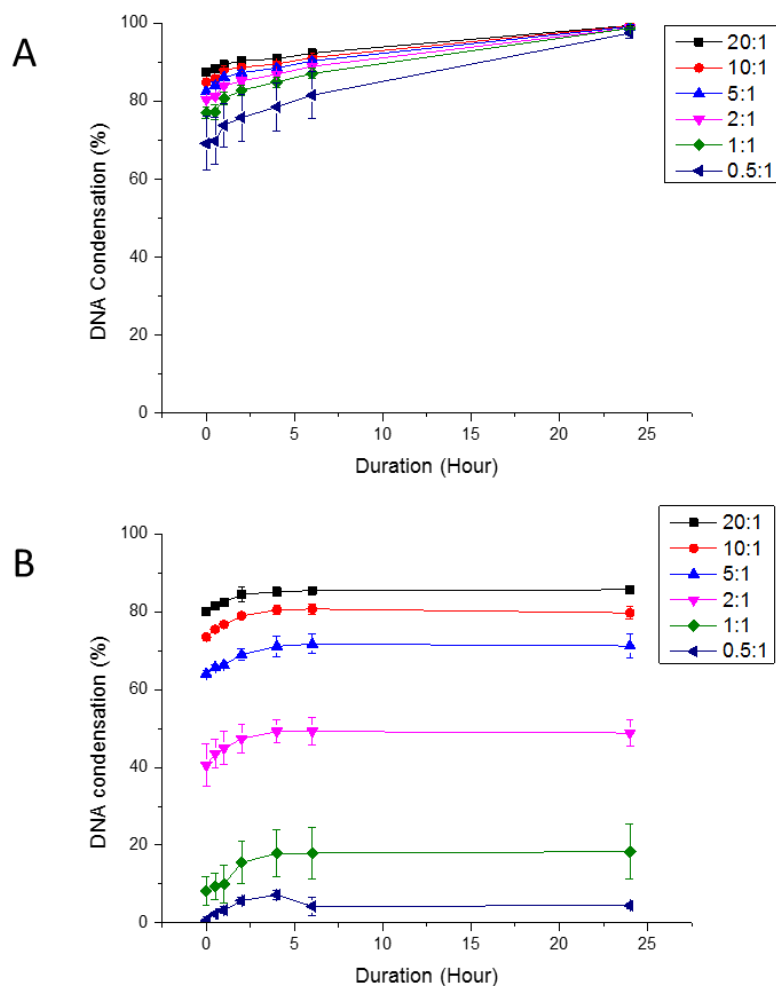


Figure 2-23 DNA condensation to DAB-Pep2 (A) and DAB-PEG2k-Pep2 (B) dendriplexes at various dendrimer: DNA weight ratios (n=4)

2.3.2.1.3. DAB-PEG2k-Peptide4

The DNA condensation capability of DAB-PEG2k-Pep4 dendrimer was found to be high for the dendrimer: DNA weight ratios 5:1 and above, which condensed more than 75% of the DNA. For the weight ratio 2:1, the dendrimer was able to condense 65% of the DNA with gradual improvement in the condensation abilities during time. For the lower weight ratios, the condensation capability was reduced significantly. DNA condensation was persistent with some sign of improvement over time for the high ratios (Figure 2-24).

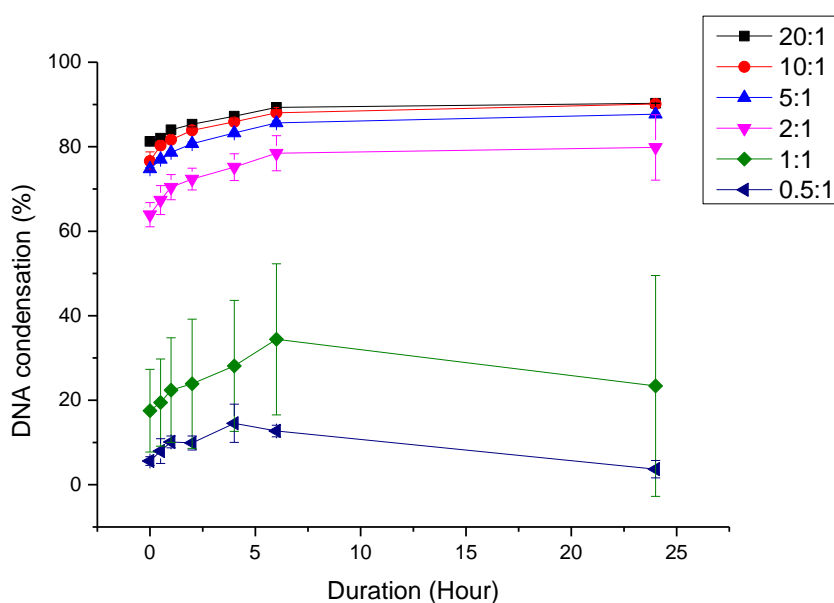


Figure 2-24 DNA condensation to DAB-PEG2k-Peptide4 dendriplex at various dendrimer: DNA weight ratios (n=4)

2.3.2.2. Gel retardation assay

Gel retardation assay was conducted to assess the ability of the modified dendrimers DAB-Lf, DAB-PEG2k-Pep2 and DAB-PEG2k-Pep4 in condensing DNA. Various weight ratios of dendrimer to DNA were used, from 20 to 0.5, while the DNA concentration was kept stable in the whole experiment at 20 $\mu\text{g/ml}$.

2.3.2.2.1. DAB-Lf

DAB-Lf: DNA weight ratios of 20:1, 10:1 and 5:1 resulted in complete DNA complexation by the DAB-Lf, with partial condensation at 2:1 and minor DNA complexation at 1:1 and 0.5:1 (Figure 2-25). These results are in line with the findings of the PicoGreen[®] assay detailed above.

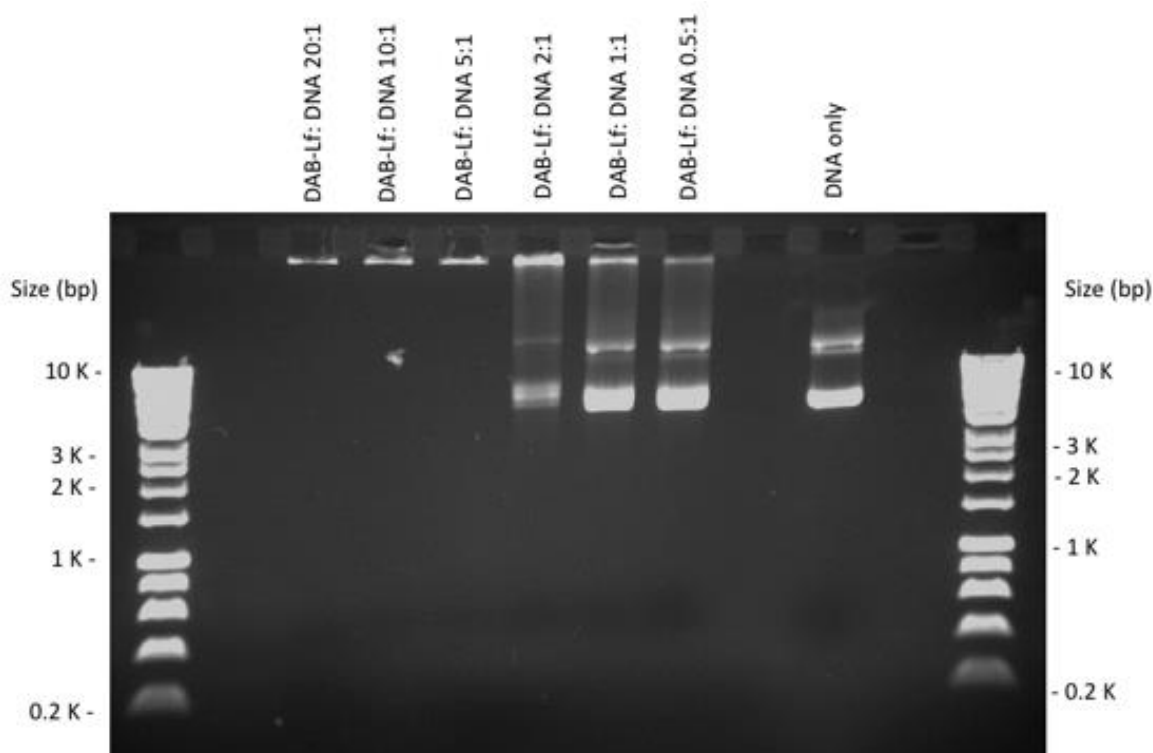


Figure 2-25 Gel retardation assay of DAB-Lf dendriplexes at various dendrimer: DNA weight ratios (20:1, 10:1, 5:1, 2:1, 1:1, 0.5:1) and DNA only as control.

2.3.2.2.2. DAB-PEG2k-Peptide2

The PEGylated polymer DAB-PEG2k-Pep2 was found to condense the DNA completely at the weight ratios of 20:1, 10:1 and 5:1, as the gel showed no migrated DNA, demonstrating the ability of the polymer at these ratios to capture the DNA completely, preventing it from migrating into the gel. At the 2:1 weight ratio, some DNA migrated into the gel, indicating a partial tendency for this ratio to condense the DNA, whereas at the lower ratios of 1:1 and 0.5:1 there were migrated bands closely resembling those of the free DNA, indicating the failure of these ratios to complex the DNA.

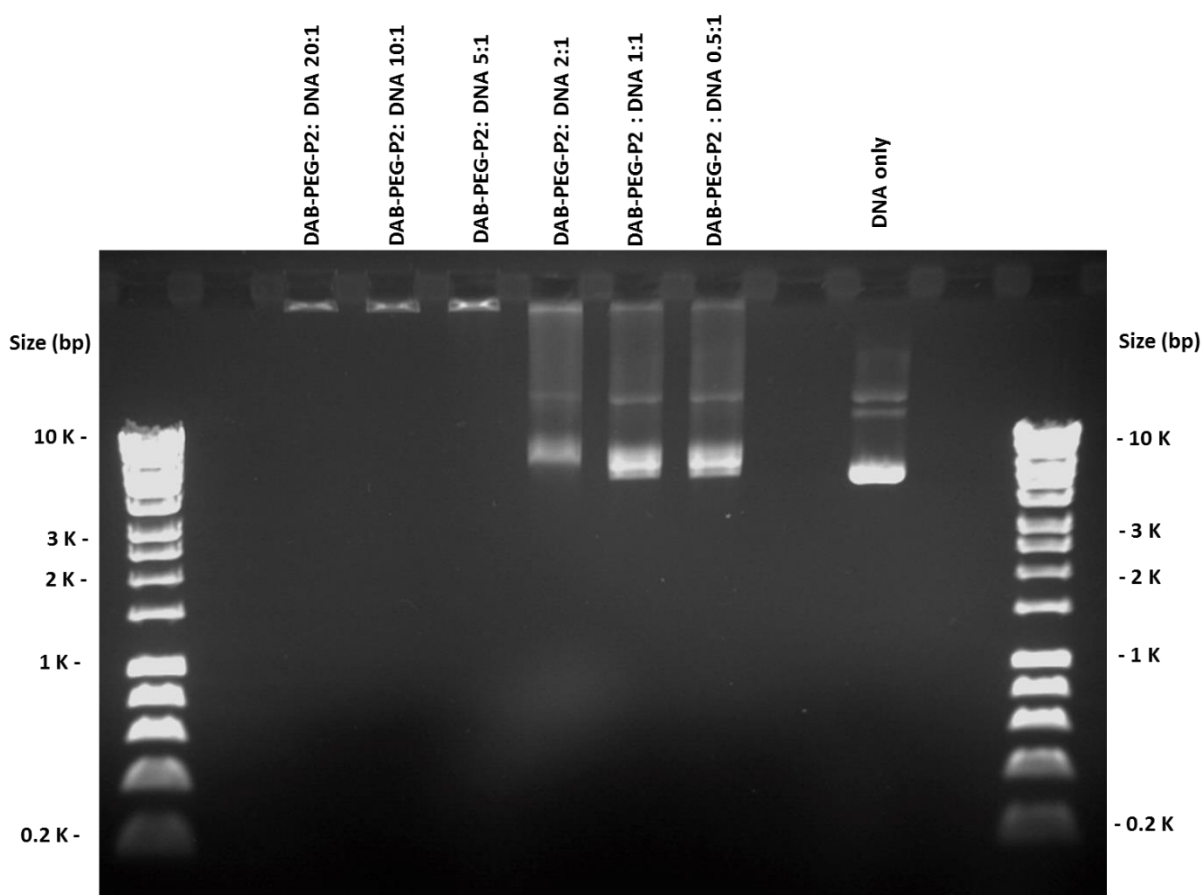


Figure 2-26 Gel retardation assay of DAB-PEG2k-Peptide2 dendriplexes at various dendrimer: DNA weight ratios (20:1, 10:1, 5:1, 2:1, 1:1, 0.5:1) and DNA only as control.

2.3.2.2.3. DAB-PEG2k-Peptide4

DAB-PEG2k-Pep4 was found to condense the DNA completely at the two high weight ratios of 20:1 and 10:1, where no DNA mark was detected in the gel, while at the 5:1 ratio some DNA was observed to have migrated into the gel, although no DNA band was detected. This could be explained by the ability of DAB-PEG2k-Pep4 to condense the DNA at this ratio, but with less efficacy than at the higher ratios, allowing the complex to migrate into the gel but with no free or uncomplexed DNA being detected at the end. At the ratio of 2:1, the polymer showed a partial tendency to condense the DNA, as a small free-DNA band was detected in the gel, whereas at the lowest ratios of 1:1 and 0.5:1, the result was the same as for DAB-PEG2k-Pep2, where migrated bands similar to those of free DNA indicated that the DNA had not been complexed.

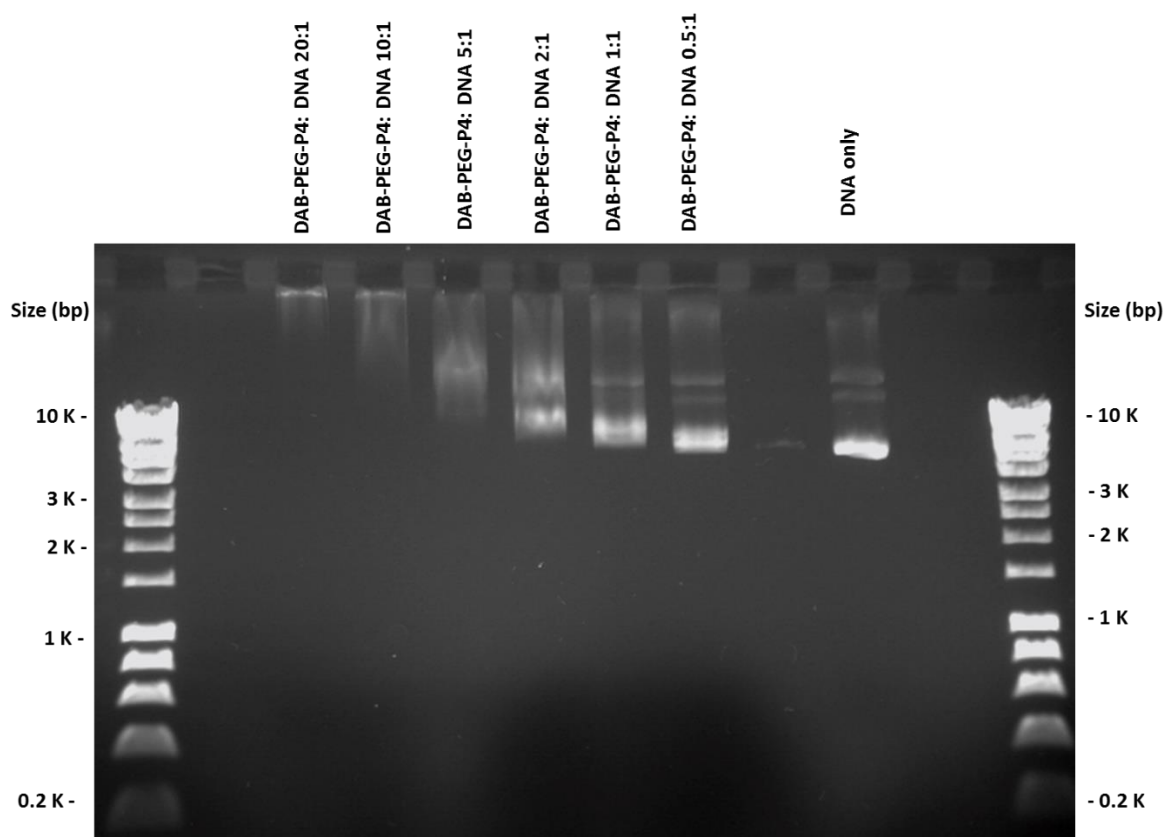


Figure 2-27 Gel retardation assay of DAB-PEG2k-Peptide4 dendriplexes at various dendrimer:DNA weight ratios (20:1, 10:1, 5:1, 2:1, 1:1, 0.5:1) and DNA only as control.

2.3.2.3. Size and zeta potential

The particle size and zeta potential of the lactoferrin- and Peptide2 - bearing DAB dendriplex were examined at various dendrimer: DNA weight ratios ranging from 0.5 to 20, while the DNA concentration was kept constant at 50 µg/ml.

2.3.2.3.1. DAB-Lf

Lactoferrin-bearing DAB dendriplex had an average size less than 205 nm at all weight ratios used. The particle size was found to be smaller with higher dendrimer: DNA weight ratios, suggesting that higher ratios of DAB-Lf: DNA are more efficient in condensing DNA, resulting in smaller complexes (Figure 2-28-A). Thus, at a dendrimer: DNA ratio of 0.5:1 the DAB-Lf particles were found to be the largest, with an average size of 200.72 ± 6.89 nm (polydispersity: 0.223), while at a 20:1 to 5:1 weight ratio the size was almost stable with an average of 66.37 ± 0.96 nm (polydispersity: 0.216) and 65.17 ± 0.75 nm (polydispersity: 0.150) respectively. Unconjugated DAB dendriplex (5:1) was found to have an average particle size of 94.95 ± 1.79 nm, showing that the conjugation of DAB did not prevent the complexation of DNA, however, it improves the condensation capability of the modified molecules giving smaller dendriplex size.

Zeta potential results for the dendriplexes showed almost steady positive charge at the weight ratios 20:1 to 2:1 followed by dramatic decrease in the positive potential at the dendrimer: DNA weight ratio 1:1, and a negative potential at 0.5:1 (Figure 2-28-B). Similarly, the zeta potential of DAB-Lf before its complexation with DNA was found to be positive as well (19.6 mV), which is expected at that stage because cationic dendrimers are highly charged molecules at this environment (Glucose 5% solution, pH 6.5). Thus, the high charge on DAB assists its complexation capability with the DNA molecules. However, the charge of DAB-Lf dendriplex remains positive and even higher than that of the dendrimer alone for some ratios. This could

be due to the formation of a nanoparticle from numerous DAB-Lf molecules that act on complexing one large DNA molecule resulting in forming nano-sized particles with positive potential. This is considered an advantage, because it facilitates the uptake of the dendriplex via receptor-mediated endocytosis, which is expected to occur after the conjugation of the dendrimer to its targeting ligands.

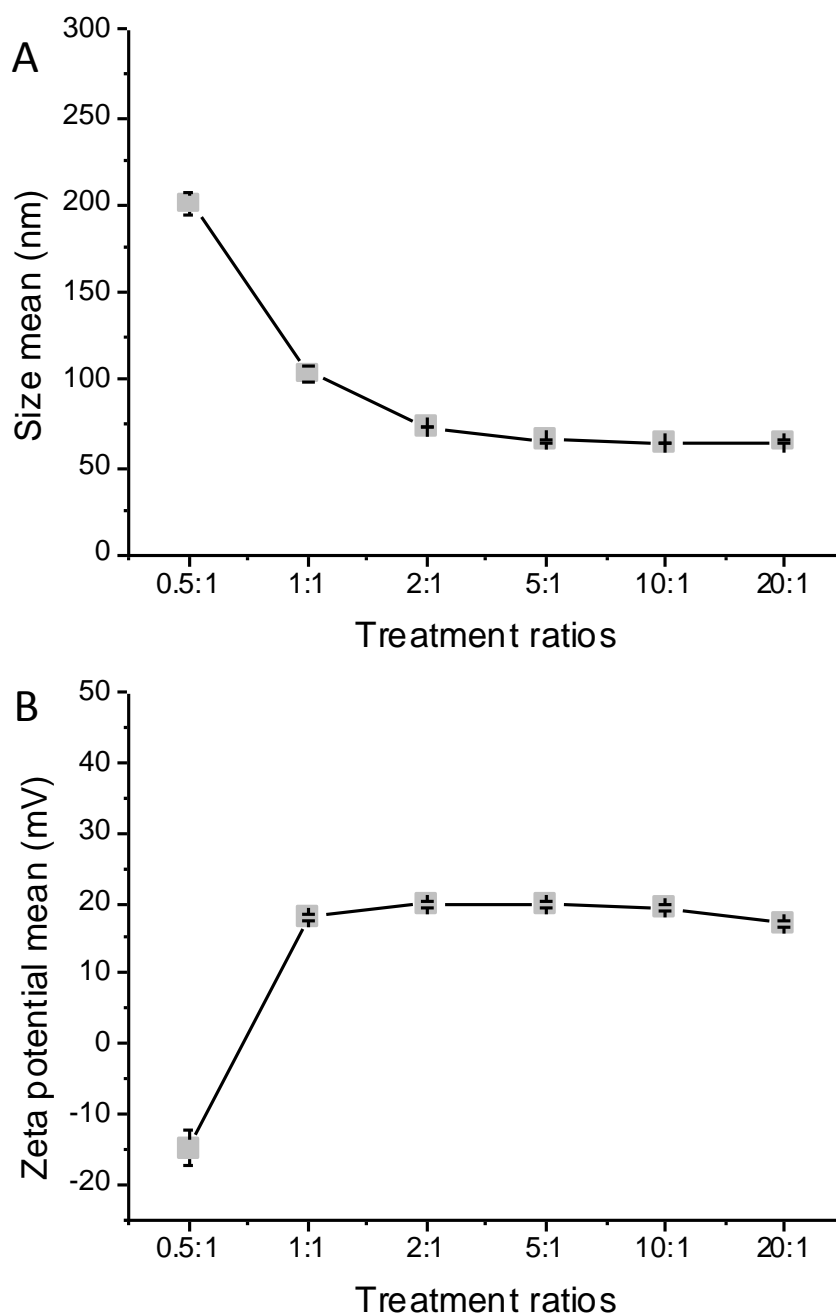


Figure 2-28 Average size (A) and zeta potential (B) of DAB-Lf dendriplexes at various dendrimer: DNA weight ratios (n=9)

2.3.2.3.2. DAB-Peptide2

Peptide2- bearing DAB dendriplex was found to have an average size lower than 250 nm at all weight ratios examined. The data showed a gradual increase in particle size with the decrease in DAB-Pep2: DNA weight ratio (Figure 2-29). No significant difference in the size was detected among the weight ratios from 20:1 to 1:1. The highest weight ratio of DAB-Pep2 (20:1) resulted in the formation of the smallest particles, with a mean size of 59.86 ± 0.67 nm (polydispersity: 0.22) and the largest size resulted from a weight ratio of 0.5:1, where mean size was 215.03 ± 25.82 nm (polydispersity: 0.17).

DAB-Pep2: DNA weight ratios from 20:1 to 2:1 have a constant positive potential of more than 30 mV. There was a significant reduction in the potential at the 1:1 weight ratio (27.99 ± 1.57 mV) and a negative zeta potential of -7.82 ± 4.23 mV at the weight ratio 0.5:1.

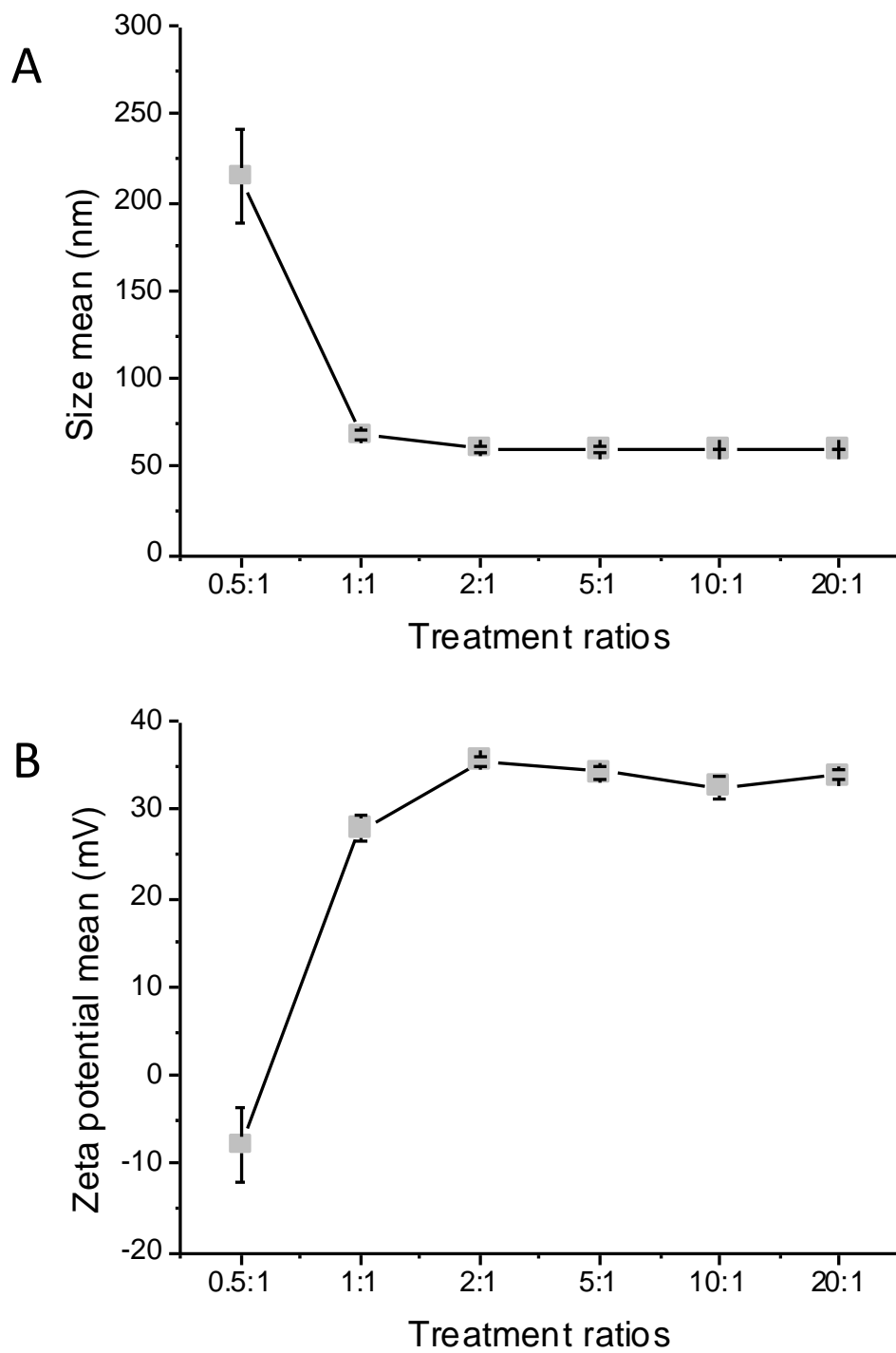


Figure 2-29 Average size (A) and zeta potential (B) of DAB-Peptide2 dendriplexes at various dendrimer: DNA ratios (n=9)

2.3.2.3.3. PEGylated DAB-Peptide2

After the various PEGylated forms of DAB-Pep2 had been prepared, it was important to measure their size and zeta potential in order to determine the impact of PEG on the physical characteristics of these polymers. Generally, after the PEGylated forms of DAB-Pep2 (DAB-PEG2k-Pep2, DAB-PEG3.5k-Pep2 and DAB-PEG2k-PEG3.5k-Pep2) had been complexed with the DNA, none of the dendriplexes showed a significant change in size at a weight ratio of 5:1 and above, with the exception of DAB-PEG2k-PEG3.5k-Pep2, which had a dendriplex size of approximately 100 nm for the same weight ratios (Figure 2-30 and Table 2-10).

On the other hand, the zeta potential of the Peptide2 PEGylated dendriplexes (DAB-PEG2k-Pep2, DAB-PEG3.5k-Pep2 and DAB-PEG2k-PEG3.5k-Pep2) was significantly reduced after reacting different ratios of PEG polymer with DAB dendrimer and Peptide2. Adding a 4-mole excess of PEG at a molecular weight of 2kDa (DAB-PEG2k-Pep2) significantly reduced the zeta potential of the dendriplex from 33.93 ± 0.56 mV to 23.28 ± 0.96 mV at a weight ratio of 20:1. Changing the crosslinker used to conjugate DAB with Peptide2 from GMBS to NHS-PEG3.5K-maleimide also resulted in a significant reduction in the zeta potential to only 3.87 ± 0.084 mV, which was expected because the PEG chain had almost double the molecular weight of DAB. The third PEGylated polymer, DAB-PEG2k-PEG3.5k-Pep2, also had a low positive zeta potential of 5.24 ± 0.21 mV, but with a significant increase in particle size due to the impact of PEG polymers and PEG crosslinker.

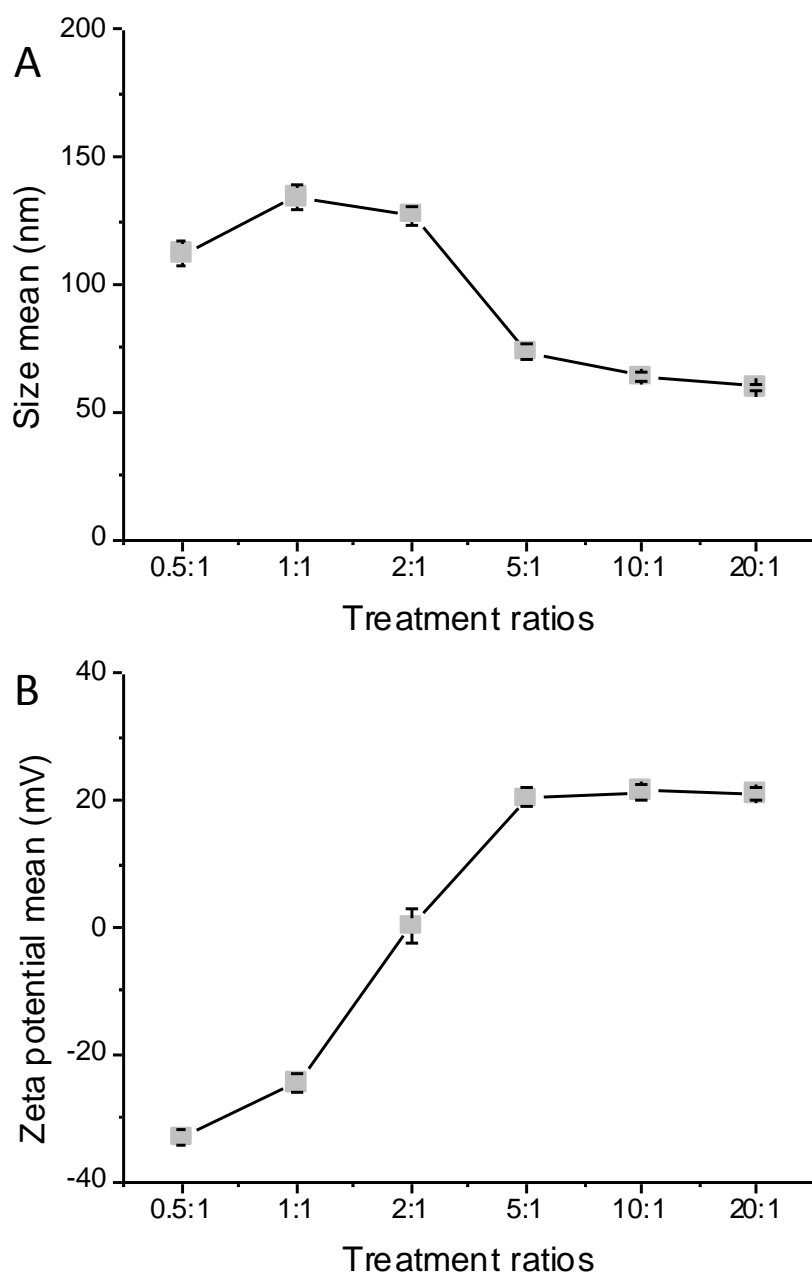


Figure 2-30 Average size (A) and zeta potential (B) of DAB-PEG2k-Peptide2 dendriplexes at various dendrimer: DNA ratios (n=9)

Table 2-10 Size and zeta characterisation for the different PEGylated forms of Peptide2-bearing DAB dendrimers

Polymer: DNA weight ratio	DAB-Peptide2		DAB-PEG2k- Peptide2		DAB-PEG3.5- Peptide2		DAB-PEG2k- PEG3.5k-Peptide2	
	Size (nm)	Zeta (mV)	Size (nm)	Zeta (mV)	Size (nm)	Zeta (mV)	Size (nm)	Zeta (mV)
20:1	59.87 ± 0.67	33.93 ± 0.56	64.86 ± 1.7	23.28± 0.96	64.64 ± 0.24	3.87 ± 0.084	93.27 ± 0.16	5.24 ± 0.21
10:1	59.99 ± 0.54	32.65 ± 1.19	65.84 ± 1.5	23.77 ± 1.08	67.85 ± 0.21	5.29 ± 0.17	100.3 ± 0.89	4.04 ± 0.18
5:1	60.02 ± 1.3	34.23 ± 0.88	72.69 ± 1.9	22.84 ± 1.16	72.67 ± 0.41	4.55 ± 0.26	126.8 ± 0.68	0.93 ± 0.15

2.3.2.3.4. DAB-PEG2k-Peptide4

Peptide4- bearing PEGylated DAB dendriplex was found to have an average size less than 120 nm at all weight ratios examined. The data showed a gradual increase in particle size with the decrease in DAB-PEG2k-Pep4: DNA weight ratio. No significant difference in the size was detected between the weight ratios 20:1 to 5:1, followed by significant increase in the size at the low ratios 2:1 and lower (Figure 2-31). The highest weight ratio of DAB-PEG2k-Pep4 (20:1) resulted in the formation of the smallest particles, with a mean size of 52.38 ± 6.27 nm (polydispersity: 0.121).

DAB-PEG2k-Pep4: DNA weight ratios from 20:1 to 5:1 have almost a constant positive potential of a value around 20 mV. Significant reduction in the potential was detected at the weight ratio 2:1 with a potential of $(1.87 \pm 5.81$ mV) and a negative zeta potential of -29.98 ± 12.48 mV and -36.67 ± 12.16 mV for the weight ratios 1:1 and 0.5:1 respectively.

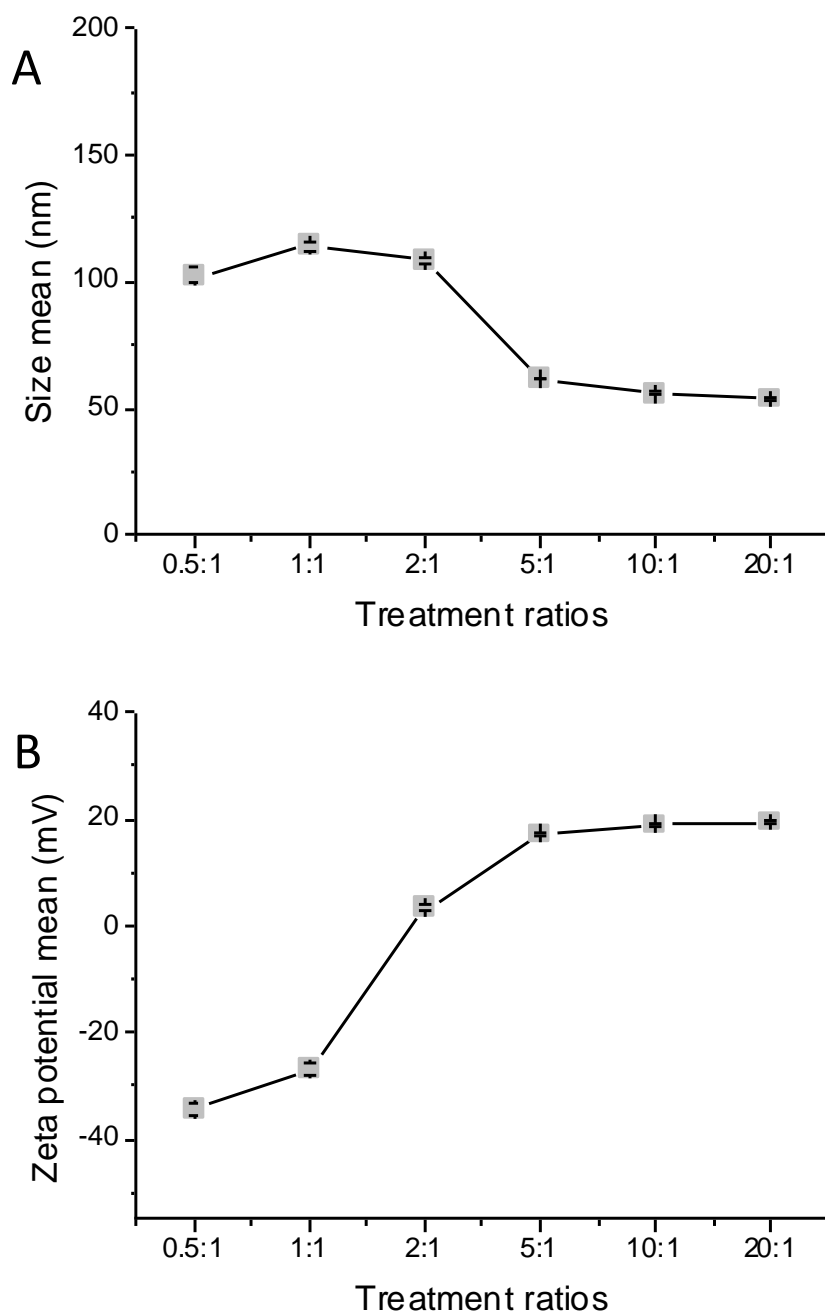


Figure 2-31 Average size (A) and zeta potential (B) of DAB-PEG2k-Peptide4 dendriplexes at various dendrimer: DNA ratios (n=9)

2.3.2.4. Atomic force microscopy

2.3.2.4.1. DAB-Lf

The images obtained by AFM (three per sample) were scanned at scanning sizes of 7 μm and 3 μm . They showed the particles being diffused through the plate with no sign of aggregation. The particles appeared spherical, with a mean diameter of 66.5 ± 41.9 nm (mean of data obtained from three images). These findings are in line with the data collected by photon correlation spectroscopy, which showed a mean particle size of 62.48 ± 0.16 nm. The particles appeared larger in the AFM images than when measured by photon correlation spectroscopy because the AFM samples were spread and dried on a mica surface to facilitate the probe scanning process. Dried particles tend to undergo surface adherence, causing them to enlarge in diameter with a corresponding reduction in height, resulting in the disk shape (Figure 2-32). By contrast, the photon correlation spectroscopy samples were measured in solution; the particles tended to be diffused in the solvent without any kind of restriction to their shape and therefore to their diameter.

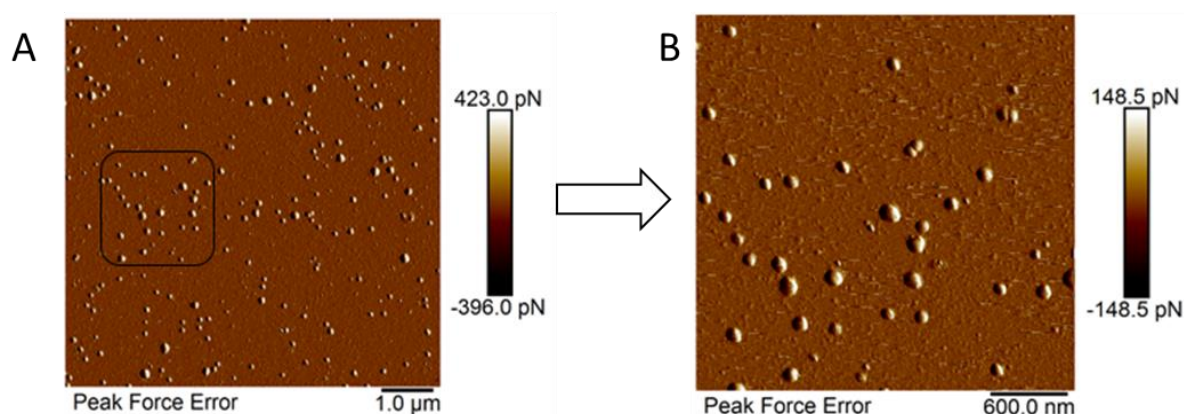


Figure 2-32 AFM force image of DAB-Lf dendriplex (weight ratio 5:1). (Images size: A) 7 μm and B) 3 μm).

2.3.2.4.2. DAB-PEG2k-Peptide2

The images obtained by AFM (three per sample) were scanned at scanning sizes of 10 μm and 3 μm . The AFM images of the DAB-PEG2k-Pep2 dendriplex showed a composed and diffused spherical particles with no sign of aggregation. At a weight ratio of 20:1 the mean size of the particles was 67.27 ± 14.73 nm, in line with the data obtained from photon correlation spectroscopy that showed the size of the same dendriplex at 64.86 ± 1.7 nm. The change in size between the AFM and DLS is expected as AFM sample where dried on mica surface before analysis.

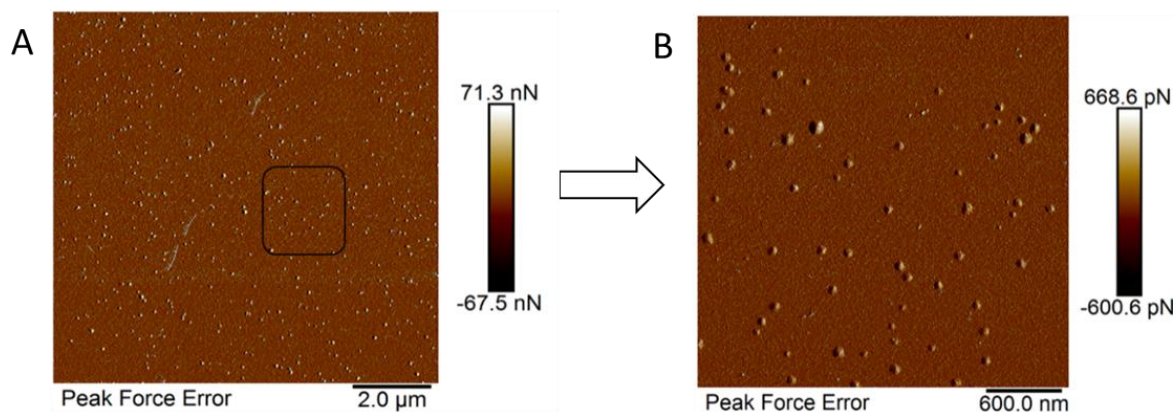


Figure 2-33 AFM force image of DAB-PEG2k-Peptide2 dendriplex (weight ratio 20:1). (Images size: A) 10 μm and B) 3 μm).

2.3.2.4.3. DAB-PEG2k-Pep4

The images obtained by AFM (three per sample) were scanned at scanning sizes of 10 μm and 3 μm . AFM images showed particles being diffused through with simple level of aggregates formulated. At a weight ratio of 20:1 the mean size of the particles was 81.83 ± 21.9 nm, which is significantly higher than the value obtained by photon correlation spectroscopy which gave a mean size of this dendriplex 52.38 ± 6.27 nm. The significant change in size between the AFM and DLS could be due to the particles aggregation as the spectroscopy may measure the diameter of two adjacent particles and consider it as one.

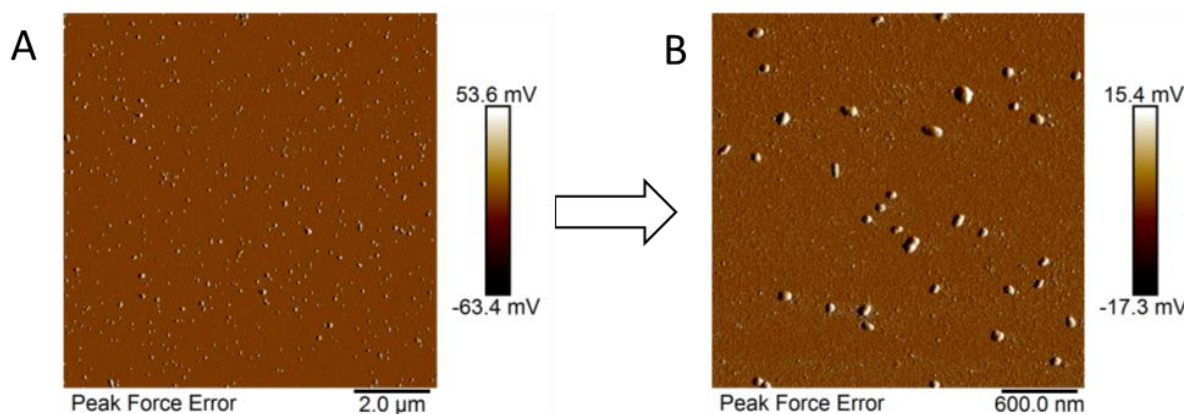


Figure 2-34 AFM force image of DAB-PEG2k-Peptide4 dendriplex (weight ratio 20:1).(Images size: A) 10 μm and B) 3 μm).

2.4. Discussion

Non-viral delivery systems have gained much attention in recent years for their efficiency in encapsulating genetic materials. They are an outstanding alternative to viral vectors due to their prominent advantages, such as low immunogenicity and high performance in carrying large DNA molecules (Kim *et al.*, 2007). Cationic dendrimers in particular are found to be efficacious in gene condensation. They carry high positive charges, usually resulting from the amine groups that are distributed throughout the dendrimer structure in a fixed pattern. Their tree-like structure also means that dendrimers tend to condense DNA in a very constructive way via electrostatic interaction, so that each DNA molecule tends to curl round and inside the dendrimer branches, resulting in highly complexed dendriplexes and low particle sizes (Ogris and Wagner, 2002; Kim *et al.*, 2007; McCrudden and McCarthy, 2013; Wang *et al.*, 2013). The use of dendrimers as gene carriers has several advantages in cancer tissue targeting. Because the genetic material is condensed by electrostatic interactions, it is protected from enzymatic degradation during its passage through the bloodstream. Dendriplex formation results in a decrease in the prominent negative charge of the DNA, which improves targeting, as DNA repulsive forces with the cell membrane would otherwise obstruct its transit through the cell wall (Dufès *et al.*, 2005).

In this study, diaminobutyric polypropylenimine hexadecaamine (DAB-Am16) was selected as the gene carrier. Several publications demonstrate its efficiency in condensing DNA molecules with relatively low toxicity and superior transfection ability (Zinselmeyer *et al.*, 2002; Schätzlein *et al.*, 2005). Furthermore, our research group conducted several prior studies using the same dendrimer and findings were encouraging (Koppu *et al.*, 2010; Al Robaian *et al.*, 2014; Lim *et al.*, 2015).

Using DAB only as a gene carrier will protect the DNA from degradation and improve its half-life in the circulation, thus ameliorating its accumulation in the cancer site through passive targeting. However, this is not sufficient for improving the targeting of the dendriplex and reduce systemic side effects. Active targeting should therefore be investigated by modifying the DAB gene vector with a specific ligand that has particular receptors in the targeted cells in order to improve dendriplex accumulation at the required site and promote its cellular uptake.

Conjugating dendrimers with a targeting ligand is a prominent method of non-viral vector modification. The iron-binding proteins transferrin and lactoferrin are potential targeting ligands for prostate cancer due to the very strong expression of their receptors in most cancer cells (Tortorella and Karagiannis, 2014). In work previously published by the research group, transferrin was used as a ligand to DAB for the targeting of prostate cancer cells. The conjugated DAB-Tf nanoparticle was complexed with various therapeutic genes and was found to target cancer cells efficiently (Al Robaian *et al.*, 2014).

Lactoferrin, on the other hand, has been found to be expressed in several cancerous tissues including prostate (VanSande and VanCamp, 1981; Barresi and Tuccari, 1984; Tuccari and Barresi, 2011). In addition, its concentration is higher in undifferentiated than in differentiated prostatic carcinoma tissues, with low expression in benign prostatic hypertrophy. Moreover, lactoferrin has been found to have the valuable ability to bind as well as transferrin to iron-dependent receptors called general receptors, which are expressed extensively in several cancer tissues, making it a potential ligand of choice to target prostate cancer cells (Adlerova *et al.*, 2008).

Similarly, PSMA was found to be overexpressed in different prostate cancer tissues with a minimum sign of detection in normal cells (Kinoshita *et al.*, 2006). Various previous studies have targeted PSMA using antibodies, proteins or peptides. A study by Aggarwal *et al.* (2006)

detected a peptide sequence that selectively binds to PSMA and inhibits its function. The 12-amino acid peptide which we refer to as Peptide2 in this report (WQPDTAHHWATL) was selected as a targeting ligand in our study.

The third targeting strategy selected for this study was to target integrin receptors. While these have several roles in normal tissues, there are some, including $\alpha v\beta_5$, $\alpha v\beta_3$, $\alpha_{IIb}\beta_3$ and $\alpha_5\beta_1$, which have been found to be overexpressed in various cancer tissues including prostate cancer (Fornaro *et al.*, 2001; Suyin *et al.*, 2013). They are reported to play major roles in cancer angiogenesis, metastasis and cell proliferation (Desgrosellier and Cheresh, 2010). The synthetic RGD-peptide EETI-II 2.5F was developed by Kimura and colleagues (2009) to target these receptors. In this study, we used the active binding site of this peptide with the sequence PRPRGDNPPLT as a targeting ligand for integrin receptors and refer to it as Peptide4. For the purpose of improving the chemical properties of Peptide4, it was modified with some amino acids on its C-terminal. Two glycine amino acids were added to act as spacers, followed by three lysine amino acids as polar basic amino acids to improve the water solubility of the peptide; this method has been followed before to improve the solubility of various peptides and proteins (Kato *et al.*, 2007)

Based on the above information, we hypothesised that the modulation of DAB with the iron-binding protein lactoferrin, PSMA targeting peptide WQPDTAHHWATL, or integrin targeting peptide PRPRGDNPPLT would improve its targeting and transfection efficiency to prostate cancer cells, thus improving the therapeutic efficiency of the dendriplex both *in vitro* and *in vivo*.

Previous studies reported the use of lactoferrin with different types of cationic polymers to target several tissues in the body (Elfinger *et al.*, 2007; Huang *et al.*, 2008; Ye *et al.*, 2013; Lim *et al.*, 2015). Using lactoferrin as a targeting ligand is also of interest because of its anticancer properties mentioned earlier in the introduction (Fujita *et al.*, 2004; Shimamura *et al.*, 2004;

Gibbons *et al.*, 2011). On the other hand, there were few articles mentioning Peptide2 and Peptide4 as ligands to target PSMA and integrin respectively. Wu *et al* (2010) used Peptide2 to target PSMA after being modified with some amino acids, whereas Moore *et al* (2013) used the RGD-peptide EETI-II 2.5F as imaging probe to target brain tumours.

In our study, the conjugation of lactoferrin, Peptide2 and Peptide4 to DAB-Am16 was achieved by a bioconjugation reaction using GMBS as a cross-linker (Hermanson, 2013). GMBS is a heterobifunctional cross-linker with an NHS ester at one end and a maleimide group at the other. Thus, a two-step synthesis technique was used in order to direct the conjugation reaction towards a selected part of the coupling molecule. The NHS ester was first directed to react with the primary amine group in DAB to form amide linkages, followed by the addition of the targeting ligand (lactoferrin, Peptide2, or Peptide4). Lactoferrin had been modified earlier with a sulfhydryl group, to react with the maleimide, yielding a thioether bond whereas the peptides were ordered to hold cysteine amino acid on their N-terminus as it holds free sulfhydryl group. The internal spacer created by GMBS is an approximately 10.2 Å cross-bridge between the DAB and conjugated ligand. Based on the molar ratio between the reactants, the primary amine groups in DAB were coupled with GMBS molecules, while the remaining primary amines are available to complex electrostatically with the therapeutic gene. The main advantage of this method is that it prevents the polymerisation that usually occurs when using homobifunctional cross-linkers. In addition, it offers great control of the resultant conjugate size by controlling the molar ratio of the reactants at each step (Hermanson, 2013).

In contrast to this multi stepped method, Lim *et al.* (2015) synthesised DAB-Lf in a faster one-step reaction, using dimethyl suberimidate as a homobifunctional cross-linker. While this technique has the advantage of being fast, it yields compounds whose properties are not closely controlled. Variations may occur in the coupling between the reactant compounds, resulting in

possible asymmetry in the nanoparticles formed. The stepwise nature of our modified method overcomes this disadvantage.

DAB-Lf and DAB-Pep2 synthesis yielded around 50% and 60% of the formulation and were confirmed via NMR and MS. By comparing the spectra of unreacted DAB and DAB-GMBS, the detection of the peak at 6.23 ppm in $^1\text{H-NMR}$ of DAB-GMBS indicates the successful coupling between the dendrimer and the cross-linker, as well as the other GMBS corresponding peaks at 2.21, 2.98 and 3.15 ppm, since any additional unreacted GMBS molecules will be washed away after the 24 h dialysis, indicating with certainty that these peaks are for the coupled cross-linker. Moreover, the appearance of the amide proton peak at 8.15 ppm is a clear confirmation of the successful binding between the primary amine and the NHS-ester of the cross-linker. This was confirmed as well by 2D-NMR (COSY, HMBC and HSQC) and mass spectroscopy. The binding ratio between DAB and GMBS was one to two, as established by $^1\text{H-NMR}$ integration measurement as well as MALDI-TOF. In DAB-GMBS $^1\text{H-NMR}$, the integration of peak (a) at 1.45 ppm which was found to be correlated to four protons was compared with the integration of the peak at 2.21 ppm (h). The fact that the two peaks showed almost similar integration is an indication of the binding of two GMBS molecules to DAB. This was confirmed by MALDI-TOF analysis, which showed peaks at masses equivalent to one to two GMBS molecules being bound to DAB.

In the same manner, the successful conjugation between the intermediate product (DAB-cross-linker) and the modified lactoferrin was assured primarily via $^1\text{H-NMR}$. $^1\text{H-NMR}$ is not very efficient at analysing high molecular weight proteins, due to the poorly resolved broad peaks generated by such samples, making the interpretation the spectral data more complicated (Kwan *et al.*, 2011). Nevertheless, the distinctive integration of the DAB-cross-linker peaks between 1.5 and 3.5 ppm supports the successful formation of the intended nanoparticles, since the final compound yielded was filtered by two different methods, using a Vivaspin centrifuge

tube with a MWCO of 5000 Da, followed by a dialysis process with a tube with a MWCO of 3500 Da. Thus, any unconjugated DAB-cross-linker would be washed away from the final product. Therefore, the peaks detected in the DAB-Lf spectrum correspond to the DAB molecules that were successfully coupled with the protein, yielding a molecular weight around 85 kDa.

MALDI-TOF has been found to be the preferred method of analysing samples containing proteins (Rader *et al.*, 2014). Sample analysis via MALDI-TOF also confirmed the success of conjugation by producing a characteristic peak with the average mass of 84537.5 m/z. There was a difference in average masses between the peaks in the DAB-Lf and Lf MS spectra of around 1786.19 m/z, which is close to the weight of the DAB-cross-linker (1851.79). This difference between the theoretical value and what was actually detected in the spectrum is to be expected, as this method is based on detecting an average mass and not a specific one, especially in such high molecular weight sample, whereas MALDI sensitivity decreases with high molecular weight proteins (Trauger *et al.*, 2002). Additionally, samples of such high molecular weight have a complex structure, which makes their precise analysis by mass spectroscopy very difficult (Trauger *et al.*, 2002). Thus, the mass spectrum data gathered is considered positive evidence of effective binding between the protein and the dendrimer.

For the second formulation, the conjugation between DAB-GMBS and Peptide2 was confirmed via ¹H-NMR, NOESY, DOSY and MALDI-TOF. For NMR data, several characteristic peaks from the Peptide2 sequence were detected with noticeable displacement of peaks to the more shielded region in comparison with the peptide spectrum, which could be ascribed to the impact of the dendrimer proton-rich environment of the peptide protons. The maleimide peaks were also found to be slightly deshielded in the DAB-Pep2 spectrum compared with the DAB-GMBS spectrum; this could be due to their linkage to the sulphur group and the formation of thioether linkage, which has high electronegativity, causing the protons to be deshielded. On

the other hand, 2D NMR spectrums did not show any actual peaks related to the thioether linkage formulation between the peptide and the dendrimer. However, this effect is to be expected and it would not contradict the success of the conjugation for different reasons. Firstly, the linkage between Peptide2 and DAB dendrimer occurs through the conjugation between the sulfhydryl group in the cysteine amino acid and the maleimide group in the DAB-GMBS molecule, so all the peaks expected to be visible under ^1H -NMR due to this conjugation are the maleimide protons which already exist in DAB-GMBS, as well as the cysteine protons, which cannot be distinguished due to their location in the region between 2.9 and 4.6 ppm, where they overlap with many other peaks related to DAB and Peptide2 (Chen *et al.*, 2013). Therefore, given that degree of structural complexity, HMBC and HSQC cannot be used to confirm the conjugation. Secondly, to acquire good 2D spectra, H & C NMR spectra should first be obtained. However, the C-NMR spectrum of DAB-Pep2 was very weak and did not show all expected peaks, due to the high carbon density in the compound; indeed, all 2D experiments requiring C-NMR, such as HMBC and HSQC, will yield deficient information. Thus, some important relations between the peaks could not be confirmed, simply because they could not be detected, rather than because they did not exist.

Analysing dendrimers by 2D NMR will enhance understanding of the coupling between the polymer and the targeting ligand by investigating the complex supramolecular interactions in close spatial distance (Banerjee *et al.*, 2004; Markowicz *et al.*, 2012). 2D ^1H - ^1H NOESY NMR would be able to detect any through-space coupling up to 4 to 6 Å between the source proton and the proton of interest, which would usually be in one molecule. Our aim with the DAB-Pep2 dendrimer was to confirm the positive coupling between the dendrimer and the peptide, whereas it was not possible to detect the thioether bond that is expected to be generated between the maleimide group and the sulfhydryl group, due to the complexity of the NMR spectrum obtained. However, evidence that the targeting ligand (Peptide2) and DAB dendrimer were in

close proximity to each other indirectly confirms the existence of the covalent bond between them, as this kind of correlation would occur only between protons in one molecule; in this case, DAB-Pep2. The NOESY data confirmed correlations of the methyl protons in the alanine and threonine amino acids in Pep2 with the DAB protons; this is considered evidence of the successful coupling of these two molecules.

Another 2D NMR experiment (DOSY) was performed to measure the diffusion coefficient (DC) and so to confirm the successful synthesis of DAB-Pep2 and DAB-PEG2k-Pep2 by detecting any change in the Brownian motion of Peptide2 after conjugation with DAB dendrimer and after PEGylation. It also confirmed the purity of these dendrimers.

DOSY NMR spectra of Peptide2, DAB-Pep2 and DAB-PEG2k-Pep2 showed that the DC of Peptide2 was higher than DAB-Pep2. The reduction in DC is evidence of enlargement of the molecule, making it diffuse more slowly in any particular solvent due to its higher molecular weight. As expected, DAB-PEG2k-Pep2 had the lowest DC, indicating the slowest Brownian motion and the highest molecular weight. DOSY spectra of DAB-Pep2 and DAB-PEG2k-Pep2 also revealed the existence of one compound in each spectrum, providing important confirmation of the purity of the modified dendrimers DAB-Pep2 and DAB-PEG2k-Pep2.

MALDI-TOF data for DAB-Pep2 showed a peak which is believed to correspond to DAB-Pep2, although the m/z of 3131 which was obtained was different from the expected value of 3416. It is likely that a loss of one of the DAB molecule branches caused this decrease in molecular weight. This illustrates one of the difficulties in analysing synthetic polymers in general, since most mass spectroscopy techniques available would lead to some sort of degradation (Montaudo *et al.*, 2006).

The literature reports previous uses of polyethylene glycol in the modification of dendrimers (PEGylation) to improve their physicochemical properties. PEG is usually covalently attached to the periphery of a cationic dendrimer for three common purposes: either to reduce its toxicity

or its immunogenicity or to increase the circulating time (Natali and Mijovic, 2009). Depending on the number of peripheral amine groups and the generation of the dendrimer, there tends to be some level of toxicity, which is the main reason for the modest representation of these formulations in clinical applications. Modifying dendrimers to carry PEG is the most common way to reduce their cytotoxicity (Lee and Larson, 2011).

The purpose of modifying DAB-Pep2 with different PEG molecules was to improve the physiochemical properties of this dendriplex and reduce its cytotoxicity, as will be shown below. All of the PEGylated dendrimers, DAB-PEG2k-Pep2, DAB-PEG3.5k-Pep2 and DAB-PEG2k-PEG3.5k-Pep2, were characterised by ¹H-NMR to confirm their successful synthesis. DAB was conjugated with the targeting ligand Peptide2 using either of two heterobifunctional crosslinkers, GMBS and PEG3.5 kDa, to form DAB-Pep2 and DAB-PEG3.5k-Pep2 respectively. In addition, excess PEGylation was performed by reacting a 4-mole excess of PEG 2 kDa over DAB to form DAB-PEG2k-Pep2 and DAB-PEG2k-PEG3.5k-Pep2. All of these PEGylated dendrimers were synthesised principally in order to determine the optimal formula for PEGylating DAB-Pep2. These PEGylated formulations were subjected to preliminary ¹H-NMR screening to confirm their synthesis, followed by measurements of size and zeta potential, then they underwent preliminary *in vitro* screening for DNA transfection capability. Finally, one of the formulations was selected for further characterisation and for *in vitro* and *in vivo* studies. The methods selected were then adopted for the synthesis of the remaining peptide-bearing DAB dendrimers.

Hashemi *et al.* (2015) and Stasko *et al.* (2007) used PEG of molecular weight 3400 and 2000 to PEGylate the G5 DAB dendrimer in order to reduce its toxicity. However, I could not find an article discussing the modification of the third generation DAB dendrimer as its cytotoxicity is well known to be relatively low (Zinselmeyer *et al.*, 2002). This has also been demonstrated as well before by our research group (Koppu *et al.*, 2010; Aldawsari *et al.*, 2011). The main

aim of PEGylation in the present study was to modify the physical characteristics of the formulated DAB-Pep2 dendriplex, whose zeta potential was shown to be relatively high compared with values given in the literature; we assumed that conjugating DAB-Pep2 with PEG molecules would reduce this high potential and therefore its relative cytotoxicity.

The final formulation synthesised in this study was Peptide4-bearing DAB dendrimer with PEG2kDa molecules reacted in the periphery of DAB (DAB-PEG2k-Pep4). This polymer was synthesised in three consecutive steps following the method used to synthesise DAB-PEG2k-Pep2 as follows: DAB dendrimer was first reacted with the crosslinker, then with one mole equivalent of the targeting ligand Peptide4 and finally with a 4-mole excess of PEG2KDa over DAB. The successful synthesis of DAB-Pep4 followed by DAB-PEG2k-Pep4 was assured by preliminary ¹H-NMR. The spectra of DAB-Pep4 and DAB-PEG2k-Pep4 demonstrate the existence of Peptide4 in these formulations by detecting the threonine and leucine amino acid peaks in the range of 0.5 to 1.5 ppm and by detecting the DAB-GMBS and PEG peaks. Further NMR experiments are required to confirm the covalent binding of these reactants.

The ability of the formulations DAB-Lf, DAB-Pep2, DAB-PEG2k-Pep2 and DAB-PEG2k-Pep4 dendriplex in condensing DNA was measured by PicoGreen[®] and gel retardation assays. These experiments were conducted after ensuring the successful formulation of the nanoparticles to analyse their ability in condensing the DNA and form a stable dendriplexes, ensuring that the DAB modification did not negatively affect its high capacity to condense the DNA.

The DAB-Lf complexes that were synthesised from intermediates having 6- and 4-fold excess molar concentration of GMBS over DAB had weak condensation capability, due to the extensive binding between the DAB and GMBS molecules, which reduces the availability of primary amine groups in the DAB molecule to complex with the DNA. In contrast, in the case of the two-molar excess of GMBS, the DAB-Lf formed was able to condense around 80% of

the DNA at a 10:1 ratio. However, a lower DAB ratio was required to condense the same percentage of DNA, indicating that DAB modification slightly reduces the DNA encapsulation ability of the dendrimer, but to an acceptable extent, whereby DAB-Lf can still effectively condense the DNA.

The DAB-Pep2 formulation was found to condense the DNA molecules even at low weight ratios, with condensation of up to 68% at 0.5:1. It appears that the DAB-Pep2 dendrimer has superior DNA condensation capability over DAB-Lf. One possible explanation for this effect is the considerable difference between the molecular weight of the targeting ligands used in these formulations; Peptide2 has a molar mass of 1565, while lactoferrin has a molecular weight of 82 kDa. However, PEGylating DAB-Pep2 with a 4-mole excess of PEG2000 resulted in a significantly reduced DNA condensation capability. DAB-PEG2k-Pep2 showed more than 65% of DNA condensation capability for the weight ratios 5:1 and above, whereas at lower ratios it failed to condense the DNA properly. The reduction in the DNA condensation capability of DAB-PEG2k-Pep2 compared to DAB-Pep2 is mainly related to the altered physiochemical properties of the dendriplex, such as size and zeta potential, as will be clarified below.

DAB-PEG2k-Pep4 was found to complex the DNA highly efficiently even at the weight ratio 2:1, where more than 60% of the DNA was condensed. This value is significantly higher than the efficiency of DAB-Lf and DAB-PEG2k-Pep2 at condensing DNA at the same weight ratio. In addition, comparing the DNA condensation capability of the two PEGylated formulations DAB-PEG2k-Pep2 and DAB-PEG2k-Pep4 shows that the latter is superior at polymer: DNA weight ratios of 10:1 and 5:1, with an almost similar percentage at the 20:1 weight ratio, condensing more than 80% of the DNA.

The physical properties of the dendriplexes such as the size, shape and potential have a direct influence on its therapeutic efficacy. Various dendrimer: DNA weight ratios showed a strong ability to condense the DNA, with the optimum ratio for *in vivo* experiments depending on several factors such as cytotoxicity, size and charge of the dendriplex formed. In cancer tissues, the vascular permeability of the tumour blood vessels is generally higher than in normal vessels, because they are incomplete and irregularly formed. Any molecule of 3 nm or smaller is able to pass through the cells of the vessel wall (transcellular uptake). On the other hand, macromolecules diffuse paracellularly, through the pores in the vessels (Yuan *et al.*, 1995; Azzi *et al.*, 2013). Thus, the particle size of the dendriplex contributes with its transvascular transport to the tumour site (Yuan *et al.*, 1995). The pore size of the blood vessels in most cancer types is between 200 and 2000 nm (Bertrand *et al.*, 2014). In addition, increasing the size of the nanoparticles improves the half-life and the circulation time of the dendriplex, thus increasing its accumulation in the targeted tissue through the effect of passive targeting (Taira *et al.*, 2005).

Therefore, it is extremely important to ensure that the dendriplex generated has an overall size less than the pore size of the targeted tissue, so that it is able to diffuse transvascularly to the targeted tissue. At the same time, it must be large enough to withstand clearance from the body and thus remain longer in the circulation.

There is a large discrepancy in the optimal size of the nanoparticles, which varies mainly according to the nature of the nanomedicine as a polymer, liposome or gold nanoparticles. There are no studies specifically addressing the influence of dendriplex size; however, some articles discussed the optimal size of nanoparticles in general (Durymanov *et al.*, 2015). Tang *et al.* (2014) investigated the optimal size of nanomedicines to target cancer tissues and found that 50 nm particles assembled better on primary and metastatic cancer sites compared with 20 and 200 nm particles.

Zeta potential is another physical characteristic that has a direct influence on the stability of the nanomedicine and *in vivo* cellular targeting. To obtain a stable nanoformulation, the zeta potential should usually be lower than -25 mV or higher than 25 mV (Durymanov *et al.*, 2015). This will prevent the aggregation of nanoparticles due to the Van der Waals interaction. However, to avoid non-specific tissue binding *in vivo*, it is believed that the zeta potential should be lower than 30 nm (Honary and Zahir, 2013).

At DAB-Lf dendriplex weight ratio of 20:1 the average particle size was 67 nm (polydispersity 0.284) and it increased as the DAB-Lf ratio decreased, reaching 200 nm at a 0.5:1 dendrimer:DNA weight ratio. Thus, all the particles formed at the different ratios were of an appropriate size to be able to reach the target site. The nanoparticles shape and size were also investigated via AFM; spherical nano-sized particles were detected at the weight ratio 5:1, supporting the data obtained by PCS. The size of DAB-Lf is believed to be very suitable for further *in vitro* and *in vivo* studies, as discussed earlier. The zeta potential of DAB-Lf found to have a positive potential at all weight ratios from 20:1 to 1:1, while the lowest ratio of 0.5:1 had a negative zeta potential, indicating the inability of the dendrimers to condense the DNA at this low ratio. The DAB-Lf potential is considered to lie in an acceptable range, being positive, so assisting its attraction to the cell membrane, but not high enough to cause non-specific binding *in vivo* based on the values discussed above (Honary and Zahir, 2013; Durymanov *et al.*, 2015).

At weight ratios of 20:1 to 1:1, the size of the second formulation, DAB-Pep2, was between 50 and 70 nm, followed by a sharp elevation in size at a ratio of 0.5:1, indicating the failure of this ratio to fully condense the DNA. The PEGylated forms of Peptide2-bearing DAB dendrimers DAB-PEG2k-Pep2 and DAB-PEG3.5k-Pep2 showed no significant alteration in dendriplex size at high weight ratios of 20:1, 10:1 or 5:1, whereas the other formulation, DAB-PEG2k-PEG3.5k-Pep2, resulted in a significantly higher dendriplex size compared with DAB-

Pep2, even at the highest weight ratio of 20:1. This suggests the inability of this formulation to properly condense the DNA, even at this high ratio.

The zeta potential of DAB-Pep2 was found to be positive for the weight ratios 20:1 to 1:1, with values between 35 to 28 mV. This zeta potential, which is considered high according to the literature, could lead to non-specific binding during *in vivo* treatment. Therefore, the synthesis of Peptide2-bearing DAB dendrimer was modified to carry PEG molecules for the purpose of reducing the zeta potential and thus non-specific binding and toxicity. The zeta potential of these PEGylated formulations was significantly reduced compared with DAB-Pep2. DAB-PEG2k-Pep2 had a potential around 20 mV, which is half the potential of DAB-Pep2 and is in line with the ranges discussed in the literature. The other PEG formulations, DAB-PEG3.5k-Pep2 and DAB-PEG2k-PEG3.5k-Pep2, had zeta potentials around 5 and 0 mV respectively for the weight ratios 20:1 to 5:1. According to Honary and Zahir (2013), these values would lead to the accelerated sedimentation of the dendriplex due to the absence of charge repulsion between the molecules.

The reduction in the zeta potential of the PEGylated formulations did not dramatically affect the size of the nanoplexes formed in the case of DAB-PEG2k-Pep2 or DAB-PEG3.5k-Pep2, in contrast to the case of DAB-PEG2k-PEG3.5k-Pep2, where the enlargement in size was associated with neutral potential. This could be due to the extensive use of PEG molecules in the formulation compared with the other two, where only half the amount was consumed. An alternative explanation is the use of a crosslinker of high molecular weight, PEG 3.5kDa, which has double the molecular weight of the gene carrier DAB-Am16.

From the data obtained, we selected DAB-PEG2k-Pep2 as the PEGylated form of DAB-Pep2 for further characterisation in both *in vitro* and *in vivo* studies. DAB-PEG2k-Pep2 meets the requirements for optimal size (Tang *et al.*, 2014) and has an acceptable positive potential which is less than the potential of the positive controls DAB and DAB-PEG. AFM images of DAB-

PEG2k-Pep2 at the weight ratio of 20:1 confirmed the formation of spherical nanoparticles of a size similar to that determined by DLS analysis.

Building on the overall findings of PEGylating DAB-Pep2, we decided to PEGylate an integrin-targeting formulation to carry a 4-mole excess of PEG2KDa (DAB-PEG2k-Pep4). The size of this formulation was below 50 nm at the highest weight ratios of 20:1, 10:1 and 5:1, giving an indication of the ability of this formulation to effectively condense the DNA to a small size. Lower ratios resulted in significant enlargement, which could be an indication of inability at these ratios to effectively complex the DNA. However, the sizes detected at all of the ratios examined are deemed suitable for further *in vitro* and *in vivo* studies. The positive zeta potential of the top ratios (5:1 and above) is an indication of the efficient condensation of the DNA, which is supported by the PicoGreen[®] assay findings as well as the size measurements. Conversely, at lower ratios the zeta potential values were considerably reduced and became negative, suggesting the inability to condense the DNA at these ratios, as uncomplexed DNA has a negative zeta potential. This finding is supported by the large sizes measured at these ratios and by the weak condensation ability detected by the PicoGreen assay.

Chapter 3 : *In vitro* evaluation of lactoferrin- and peptide - bearing DAB dendrimers

3.1. Introduction

In order to study the effectiveness of nanomedicines and to predict their toxicity in humans, they should go first through various experiments in cell culture, which are usually developed to examine the efficacy of these formulations before doing any animal studies. These experiments involve testing human or animal cells and tissues in a controlled environment (*in vitro*), defined as techniques for performing experiments or processes in a managed environment that takes place outside the living organism (Ravi *et al.*, 2015).

The history of *in vitro* studies starts in the late nineteenth century, when several researchers focused on developing methods for cell and tissue culture. In 1951, the first cancer cell line HeLa, was successfully cultured after being serendipitously discovered during the analysis of a cervical biopsy from a cancer patient. HeLa establishment makes culturing cells and tissues outside the human body possible and numerous cell lines are currently available (Rodríguez-Hernández *et al.*, 2014). Cell culture technology has developed considerably in the last two decades and it is now considered a reliable technique that is used in all pharmaceutical and medical studies (Ravi *et al.*, 2015).

In vitro experiments help in understanding the complexity of the cellular physiology of the organ concerned as well as the biochemical responses to the treatments being tested. The main feature that makes *in vitro* study a favourable technique is the ability to control the physiochemical environmental features of the experiment such as the pH, osmolarity, gas level (O₂ and CO₂), temperature and humidity. Cells are usually placed in an environment that simulates the physiological conditions from which they were isolated (Freshney, 2006; Ravi *et al.*, 2015).

Therapeutically, a complete exposure of the nanomedicine is ensured in *in vitro* experiments, which is not the case with most *in vivo* experiments, where 90% of the drug will be distributed among the bodily organs before starting to accumulate in the targeted tissue. On the other hand,

in vitro cell cultures are usually associated with the differentiation of some characteristics compared with the original tissue they were extracted from, because the cells adapt to changes that occur during culturing. Therefore, the results obtained from *in vitro* experiments only partially represent the actual response that would be seen after systemic administration of the drug, in respect of its toxicity and therapeutic effect (Freshney, 2006).

3.1.1. Transfection assay

Transfection is the process of introducing a genetic material to specific cells, mostly with the assistance of non-viral vectors. The principle of the assay is based on quantifying the expression of the protein encoded by DNA as evidence for its successful override of the different cellular barriers. It is usually performed to test the capability of the delivery system in improving the uptake of the nucleic acids by the cells and nucleus. In order to determine the efficiency of the transfection, it is necessary to use a reporter gene such as β -galactosidase or luciferase which can be quantified (Groth *et al.*, 1998; Griffith and Wolf, 2002).

β -galactosidase is an enzyme able to cleave lactose to galactose or glucose. In 1972, Miller described a quantitative assay for measuring the β -galactosidase activity in cells, based on the ability of β -galactosidase to break down the colourless o-nitrophenyl- β -D-galactopyranoside (ONPG) to yield o-nitrophenol (ONP), which is yellow. The assay quantifies this process using spectrophotometry (Figure 3-1). Based on Miller's assay concept, β -galactosidase gene is now widely used as a reporter gene for testing gene expression in cells.

The Miller assay was modified to be employed colorimetrically, measuring the transfection of DNA (β -galactosidase gene) by the targeted cells. The cells were first treated with the β -galactosidase encoding DNA complexed with the designed vector, then they underwent lysis. ONPG reagent was then introduced to the lysate and incubated for a period of time to let the cleavage of ONPG to ONP proceed. From the degree of absorbance of the ONP formed, the

amount of β -galactosidase transferred to the cells can be measured (Miller, 1972; Griffith and Wolf, 2002; Zhao *et al.*, 2011).

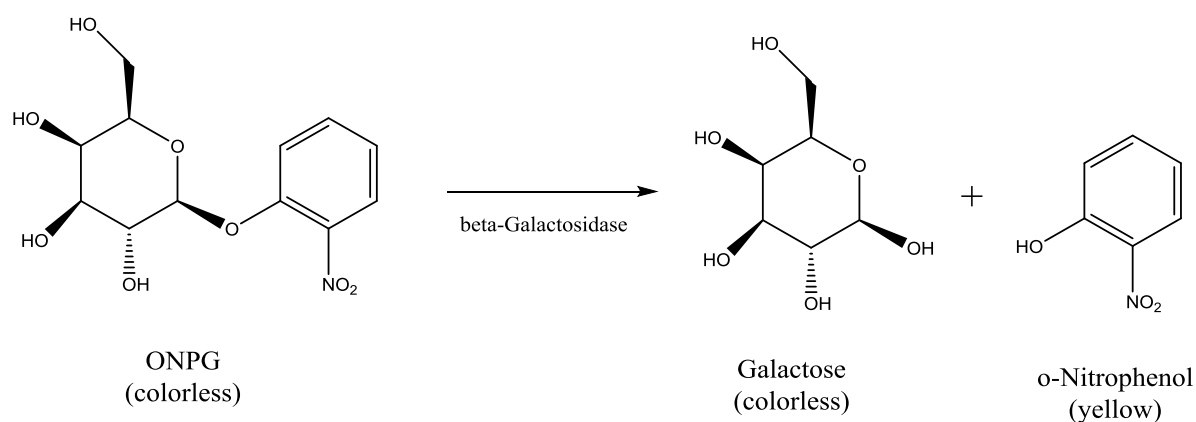


Figure 3-1 Hydrolysis reaction of o-nitrophenyl- β -D-galactopyranoside (adapted from Miller, 1972).

3.1.2. Confocal microscopy

Confocal microscopy is an advanced imaging technique used in the analysis of biological specimens up to a thickness of 100 μ m. The principal features of confocal microscopy are illustrated in Figure 3-2. The sample is scanned point by point and only a very small part of the specimen is analysed. The source of light (laser) is scanned across the sample by means of a dichroic mirror and movable lenses. The samples analysed are usually stained with fluorescent dye such as Vectashield DAPI. When excited by the laser light, this emits a range of wavelengths that are reflected back to the lenses and dichroic mirror, before passing through a pinhole which excludes the out-of-focus light so that only a specific wavelength is detected. The detector is usually a photomultiplier tube (PMT) that is capable of detecting emissions ranging from 400 to 750 nm, (in the UV, visible and near-IR spectral regions) (Semwogerere and Weeks, 2005; Ray and Dey, 2011; Nwaneshiudu *et al.*, 2012).

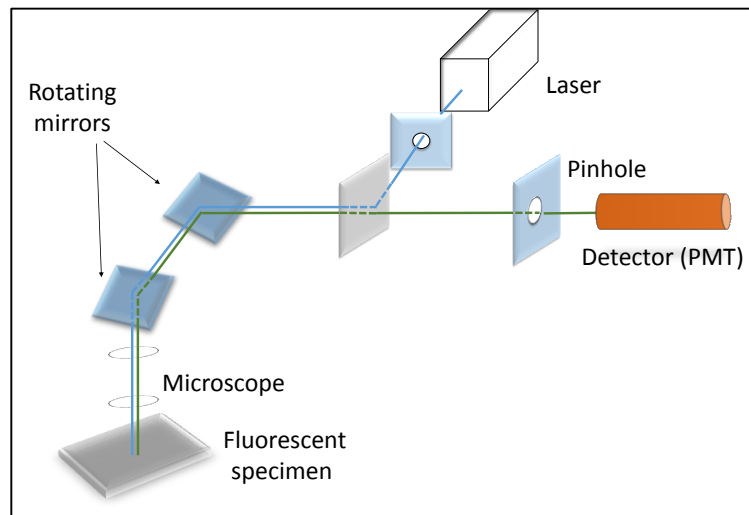


Figure 3-2 Confocal microscopy basic setup (adapted from Semwogerere and Weeks, 2005)

Several advantages make confocal microscopy superior to other imaging techniques. The important feature of the microscope is considered to be its high confocality, which is the ability to analyse a thin and sharply defined section of the sample, between 0.5 to 1.5 μm thick. In addition, the images displayed in the confocal microscopy are sharper and have better contrast compared with fluorescence microscopy. This is achieved by eliminating most of the light from the specimen that is outside the focal plane. Confocal microscopy is also able to eliminate out-of-focus wavelengths (haze) within the sample, thus increasing its ability to collect a plane of focused wavelengths only (Semwogerere and Weeks, 2005; Ray and Dey, 2011).

There are some drawbacks to imaging specimens by confocal microscopy such as the time-consuming and the limited resolution (about 200 nm) by the diffraction of the light source, which appears as a faint disk at the scanned spot (Semwogerere and Weeks, 2005; Ray and Dey, 2011; Nwaneshiudu *et al.*, 2012).

3.1.3. Anti-proliferation assay

Tetrazolium reduction assay is a colorimetric experiment developed by Mosmann in 1983 and used to measure the *in vitro* cytotoxic effect of a gene or drug by measuring the percentage of cell viability (Mosmann, 1983; Pozzolini *et al.*, 2003; Angius and Floris, 2015). 3-(4,5-

Dimethylthiazol-2-yl)-2,5-diphenyltetrazolium bromide (MTT) is a yellow water-soluble salt usually prepared as a solution with a concentration between 0.2 and 0.5 mg/ml. It undergoes an incubation period of one to four hours after being added to the cells. The principle of the assay is the ability of the live cells to reduce the yellow MTT reagent to form a purple lipophilic precipitate of formazan, which can be measured at an absorbance wavelength of 570 nm after dissolution in DMSO. The reduction reaction occurs in the mitochondria of viable cells through the cleavage of the tetrazolium ring in the MTT by the coenzyme nicotinamide adenine dinucleotide (NADH) (Figure 3-3). Dead cells lose the ability to convert MTT to formazan; thus, the absorbance of the dissolved formazan is proportional to the percentage of viable cells (Liu *et al.*, 1997; Riss *et al.*, 2013).

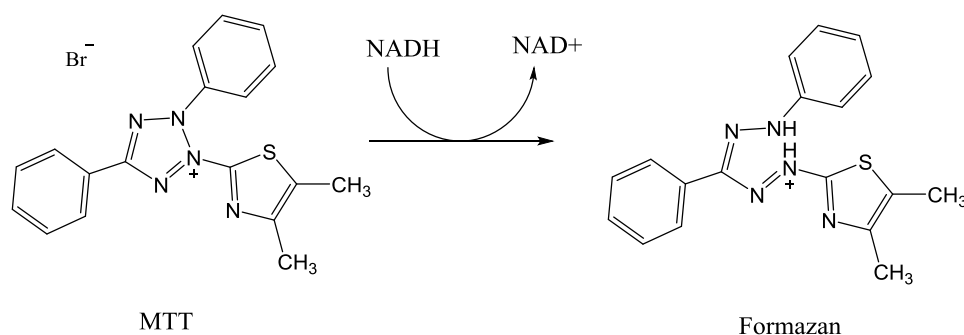


Figure 3-3 Reduction reaction of 3-(4,5-dimethylthiazol-2-yl)-2,5-diphenyltetrazolium bromide (MTT) to form the lipophilic compound formazan.

3.1.4. Fluorescence activated cell sorting (FACS)

A flow cytometer is a quantitative measuring instrument that has been used since the 1970s and which has undergone major development since the 1990s, having many applications in biotechnology, immunology and drug discovery (Chattopadhyay *et al.*, 2008). The main criterion placing the flow cytometer among the most important apparatus is its capacity for multiparameter analysis of each particle or cell in a sample in a very short time, screening thousands of cells per second. The underlying principle is immunofluorescence, which allows

the visualization of cell features by binding these features to the fluorescence emitted by molecules when stimulated by light via different channels (McCoy, 2002). In order to be able to allocate the measurement of a specific biochemical or biological property to the cells being examined, various fluorescent probes and dyes are used to target specific epitopes in the cell and thus to quantify the population of cells, intracellular properties, immune activities and many other properties (McCoy, 2002). As many cytometric assays use more than one fluorochrome to investigate different features of cells, it is important to ensure that each fluorochrome used has a distinct emission wavelength that does not interfere with the other fluorochromes, in order to obtain a precise result.

3.1.5. Cellular uptake mechanism

The targeting ligand which was selected to be conjugated with DAB dendrimer for the purpose of improving its targeting capability is expected to have major impact on the dendriplex internalisation to the targeted cells. Therefore, investigating the internalisation mechanism of the dendriplex will provide confirmation of the successful synthesis of the dendrimer, as well as confirming the hypothesis that conjugating the DNA carrier with this ligand would improve the dendriplex uptake by the targeted cells. The iron binding protein lactoferrin is thought to bind to the cells via its specific receptors LfR1 and LfR2, as well as the general transferrin receptor (VanSande and VanCamp, 1981). The mechanism by which lactoferrin enters the cells is thought to be receptor-mediated endocytosis (Tuccari and Barresi, 2011). Similarly, PSMA was reported previously to cause an uptake for targeted nanoparticles through receptor-mediated endocytosis (Goodman *et al.*, 2007; Zhang *et al.*, 2016). Xiang *et al* (2013) used folate to target PSMA, the cellular uptake of the targeted liposomes was found to decrease by 40% after pretreating the cells with chlorpromazine, a blocker for clathrin-mediated endocytosis pathway.

Endocytosis is an essential procedure in eukaryotic cells that controls many biological processes such as nutrient uptake and intracellular signalling (Hansen and Nichols, 2009). Endocytosis can be split into two main pathways. These are phagocytosis (macropinocytosis), which usually accounts for the uptake of large molecules (> 200 nm) and pinocytosis, which in turn has two main pathways: either clathrin-mediated endocytosis (CME) or clathrin-independent endocytosis (CIE).

CME is the most common pinocytosis pathway, through which diverse cargoes are internalized. This occurs through three main steps: clathrin pit formation, followed by early and late endosome formation (McMahon and Boucrot, 2011). A clathrin adaptor such as adaptor protein 2 (AP-2) complex facilitates the binding of clathrin protein in the membrane in order to cluster the receptor and its correlating protein ligand to clathrin-coated pits. The GTPase dynamin then grip the coated pits and forms clathrin-coated vesicles, which facilitate the entrance of the ligand and form an endosome (early vesicles) (Figure 3-4) (Liu and Shapiro, 2003; Grant and Sato, 2006). Clathrin is then removed and recycled back to the cytoplasm to start a new endocytosis cycle (McMahon and Boucrot, 2011).

Clathrin-independent endocytosis is an alternative pathway to CME. In CIE, the cellular glycolipids have a tendency to mediate cell membrane budding and lead to endocytosis. The best known mediators in CIE are caveolae, which are lipid rafts present mainly in endothelial cells and involved in various transport processes such as endocytosis, potocytosis and transcytosis. Among these, endocytosis is the most common mechanism, due to the abundance of dynamin. The exact mechanism of caveolar endocytosis is not yet clear, although the budding formation is similar to that of CME, involving dynamin (Liu and Shapiro, 2003; Nabi and Le, 2003).

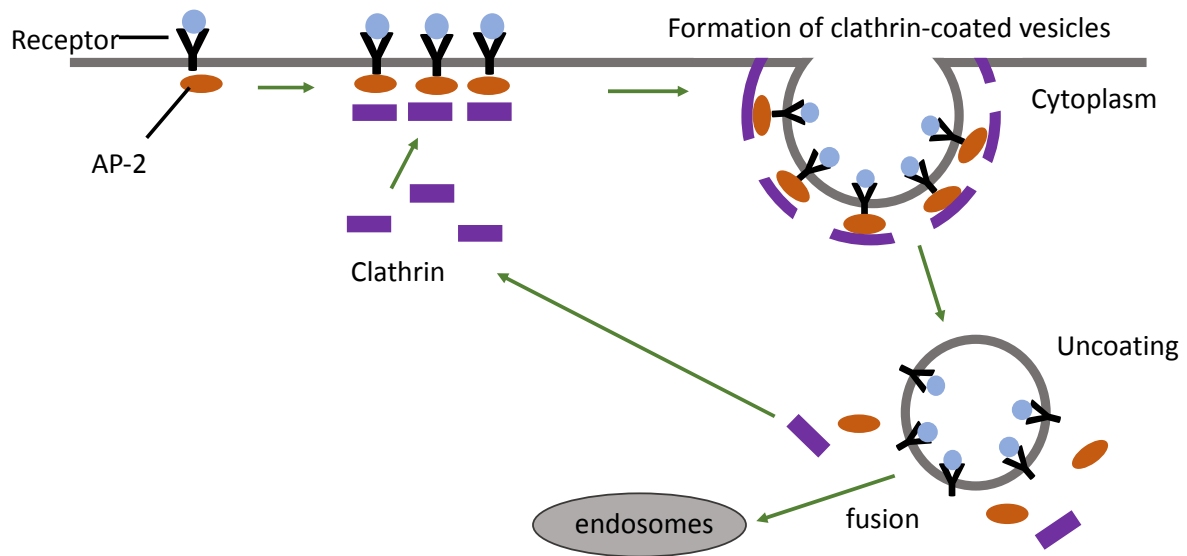


Figure 3-4 Clathrin-mediated endocytosis pathway (adapted from Grant and Sato, 2006).

Therefore, for the purpose of confirming the cellular uptake mechanism, different blockers of the most common uptake mechanisms were examined *in vitro*. For blocking CME, phenylarsine oxide was selected. This is a membrane-permeable protein-tyrosine phosphatase (PTPase) inhibitor which prevents vesicle formation and the internalisation of cell membrane receptors, as well as pinocytosis at the cell surface (Gerhard *et al.*, 2003). This criterion makes it a well-known inhibitor of CME, which is the pathway believed to be linked to transferrin and lactoferrin endocytosis (Dutta and Donaldson, 2012). Another receptor-mediated endocytosis blocker is filipin, which prohibits any caveolae-dependent endocytosis by binding to cholesterol, which is a major component of caveolae, thereby preventing the caveolae from functioning (Schnitzer *et al.*, 1994).

A further mechanism of endocytosis is macropinocytosis, which applies to the uptake of large molecules by forming irregular vesicles of 0.2 μm in diameter. The most common inhibitors of this pathway are colchicine and cytochalasin D (Liu and Shapiro, 2003).

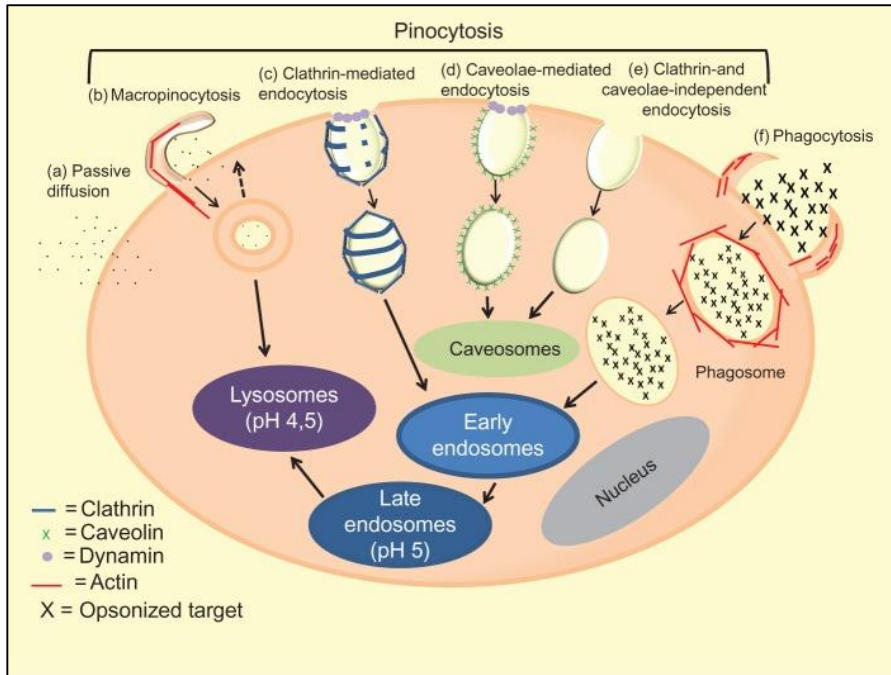


Figure 3-5 Common mechanisms of cellular uptake (adapted from Panariti *et al.*, 2012)

3.1.6. Objectives

In the previous chapter, we reported the successful synthesis of the nanocarriers DAB-Lf, DAB-Pep2, DAB-PEG2k-Pep2 and DAB-PEG2k-Pep4. In this chapter, we will examine their ability to improve the cellular uptake of the DNA being carried. We will also investigate the therapeutic efficiency obtained from using these carriers for different therapeutic DNA (TNF α , TRAIL and IL-12) and compare these results with the effects obtained by using the unmodified carrier DAB.

We hypothesised that the conjugation with the targeting ligands lactoferrin, Peptide2 and Peptide4 would increase the therapeutic efficacy of the DAB-Lf, DAB-Pep2 and DAB-Pep4 dendriplexes by improving the active targeting of the nanoparticles, thereby enhancing the delivery of the therapeutic DNA to prostate cancer cells. Furthermore, we hypothesised that conjugating PEG molecules with DAB-Pep2 and DAB-Pep4 would result in improving the physical characteristics by reducing the overall zeta potential of the dendriplexes as demonstrated in Chapter 2. The various aspects covered in this chapter include investigating the transfection and cellular uptake of the dendriplexes, their anti-proliferative effect and finally the mechanism of uptake by the cells. Three different prostatic cancer cell lines (PC-3, DU145 and LNCaP cells) were used in these experiments to emulate different metastatic stages of the disease.

3.2. Materials and methods

3.2.1. Materials

Table 3-1 List of materials used in chapter 3.

Materials	Supplier
Ammonium chloride	Sigma-Aldrich, UK
Ampicillin	Sigma-Aldrich, UK
Bovine serum albumin	Sigma-Aldrich, UK
Colchicine	Sigma-Aldrich, UK
Dimethyl sulfoxide (DMSO)	Sigma-Aldrich, UK
3-(4,5-dimethylthiazol-2-yl)-2,5-diphenyl-tetrazolium bromide (MTT)	Sigma-Aldrich, UK
DU145 prostate cancer cell line	European Collection of Cell Cultures , Salisbury, UK
Ethylenediaminetetraacetic acid (EDTA)	Sigma-Aldrich, UK
EndoFree Plasmid Giga Kit	Qiagen, UK
Filipin complex from <i>Streptomyces filipinesis</i>	Sigma-Aldrich, UK
Fluorescein isothiocyanate isomer I	Sigma-Aldrich, UK
Foetal bovine serum	Biosera, UK
N-2-hydroxyethylpiperazine-N-2-ethane sulfonic acid (HEPES; 10 mM)	Life Technologies, UK
Isopropanol	Sigma-Aldrich, UK
L-glutamine	Sigma-Aldrich, UK
Label IT [®] Fluorescein Nucleic Acid Labelling kit	Cambridge Biosciences, UK
LNCaP prostate cancer cell line	European Collection of Cell Cultures , Salisbury, UK

Minimum Essential Medium Eagle (MEM)	Sigma-Aldrich, UK
Mouse TNF alpha ELISA kit	Invitrogen, UK
2-nitrophenyl- β -D-galactopyranoside (ONPG)	Sigma-Aldrich, UK
Passive lysis buffer	Promega, UK
PC3M-luc-C6 human prostate cancer cell line	Caliper Life Sciences, USA
Penicillin-streptomycin	Sigma-Aldrich, UK
Peptide2 (CWQPDTAHHWATL)	Biomatik, Canada
Peptide4 (CPRPRGDNPPPLTCGGKKK)	Biomatik, Canada
Phenylarsine oxide	Sigma-Aldrich, UK
Phosphate buffered saline tablet	Sigma-Aldrich, UK
Plasmid encoding β -galactosidase (pCMVSPORT β -galactosidase)	Life Technologies, UK
Plasmid encoding TNF α (pORF9- mTNF α)	InvivoGen, USA
Plasmid encoding TRAIL (pORF- mTRAIL)	InvivoGen, USA
Plasmid encoding IL-12 (pORF- mIL-12)	InvivoGen, USA
Poly-L-lysine	Sigma-Aldrich, UK
Roswell Park Memorial Institute (RPMI)	Sigma-Aldrich, UK
Sephadex [®] G-10	Sigma-Aldrich, UK
Sodium pyruvate	Life Technologies, UK
Trypsin	ThermoFisher, UK
Triton-X	Sigma-Aldrich, UK
Vectashield [®] 4',6-diamidino-2-phenylindole (DAPI)	Vector Laboratories, UK

3.2.2. Methods

3.2.2.1. Cell lines

The cell lines used in the experiments were all human prostate cancer cells extracted during different stages of the disease and from different metastasized organs such as lymph node, bone and brain.

3.2.2.1.1. PC-3

PC-3 is a human prostatic cancer cell line derived from a bone metastatic site in a 62-year-old Caucasian male. Due to the lack of androgen receptors in the cell membrane, PC-3 cells have been found to be androgen-insensitive, allowing them to survive even in androgen-deprived media. In addition, PC-3 cells do not release PSA and do not express PSMA in their cell membrane (Tai *et al.*, 2011; Liu *et al.*, 2012). However, PSA and PSMA mRNA were detected in these cells (Takahashi *et al.*, 1999).

PC-3 tumour cells have been found to be highly oncogenic and usually produce poorly differentiated tumours categorized as grade IV adenocarcinoma (Russell and Kingsley, 2003).

3.2.2.1.2. DU145

DU145 is an epithelial prostatic cell line that is derived from a metastatic brain site in a 69-year-old Caucasian male (Stone *et al.*, 1978). DU145 cells have a low response to androgen hormones due to the lack of androgen receptors in their cell membrane. Although DU145 cells were proven to carry DNA encoding PSA (Takahashi *et al.*, 1999), they do not produce PSA and do not express PSMA in their cell membrane (Takahashi *et al.*, 1999; Ghosh *et al.*, 2005). The metastatic potential of DU 145 cells has been found to be lower than PC-3 cells, thus, it has less invasive capability.

3.2.2.1.3. LNCaP

LNCaP is a cancerous epithelial cell line of human prostatic adenocarcinoma extracted from a metastatic lymph node of a 50-year-old Caucasian male (Russell and Kingsley, 2003).

Numerous androgen receptors are expressed in the cell membrane, explaining the high sensitivity of these cells to androgen hormones such as testosterone and dihydrotestosterone. LNCaP cells also overexpress PSMA and secrete prostate specific antigen (PSA) (Horoszewicz *et al.*, 1983; Liu *et al.*, 2004; Jin *et al.*, 2014).

In addition, LNCaP cells have been found to have weak oncogenicity compared with other prostate cancer cell lines. As a result, they initiate tumours that are slower growing and less invasive when injected into nude mice, unless co-injected with stromal cells (Tai *et al.*, 2011).

3.2.2.2. Cell culture

All the *in vitro* experiments were conducted using prostate cancer cell lines (PC-3, DU145 and LNCaP) purchased frozen from the European and American collections of cell cultures.

PC-3 and DU145 cells were grown in Minimum Essential Medium (MEM) as monolayers in a T75 flask, while LNCaP cells were grown in Roswell Park Memorial Institute Medium (RPMI). These media were supplemented with 10% (v/v) foetal bovine serum, 1% (v/v) L-glutamine and 0.5% (v/v) penicillin-streptomycin, plus 10 mM HEPES (5 ml) and 1 mM sodium pyruvate (5 ml) for LNCaP cells only. The cell culture flasks were kept in the incubator at 37 °C and 5% carbon dioxide in a humid atmosphere.

3.2.2.3. Transfection assay

Transfection assay was performed to test the efficacy of the dendrimers in improving the cellular uptake of the DNA to the targeted cells by complexing the dendrimer with DNA encoding β -galactosidase enzyme.

PC-3, DU145 and LNCaP cells were seeded in 96 well plates at a concentration of 2000 cells per well and incubated for 72 h at 37 °C and 5% CO₂. They were then treated with DNA encoding β -galactosidase complexed with the dendriplex of interest (DAB-Lf, DAB-Pep2, PEGylated DAB-Pep2, or DAB-PEG2k-Pep4) in quintuplicate at various dendrimer: DNA

weight ratios (20:1, 10:1, 5:1, 2:1, 1:1 and 0.5:1). Naked DNA was used as negative control and DAB: DNA (5:1) was used as a positive control since it resulted in optimum DNA expression in previous study (Schätzlein *et al.*, 2005). The DNA concentration was kept constant through the experiment at 10 µg/ml (1 µg/well). After treatment, the cells were incubated for 72 h before the analysis. At the analysis day, the medium was removed from the wells before 50 µl/well of 1X passive lysis buffer (PLB) was added to each well and incubated for at least 20 min at 37 °C to ensure complete cell lysis. The lysed cells were tested for β-galactosidase expression by adding 50 µl of ONPG solution. The ONPG solution with the concentration 1.33 mg/ml was prepared fresh just before the analysis using 2X assay buffer (sodium dibasic phosphate 60mM; magnesium chloride 1mM; β-mercaptoethanol 50mM; pH 7.3) as solvent. Plates were then incubated for two hours at 37 °C, protected from light. The absorbance was taken at 405 nm using a plate reader (Thermo Lab Systems, Multiscan Ascent, UK) and the resultant absorbances were converted to concentrations using a β-galactosidase standard curve.

3.2.2.4. Cellular uptake

3.2.2.4.1. Confocal microscopy

The cellular uptake of the DNA complexed to the dendrimer was assessed by imaging the targeted cells using confocal microscopy after treatment with the dendriplex. Cellular uptake is a qualitative assay that aims to evaluate the efficiency of the dendrimer in targeting the cells and introducing the genetic material. In 6-well plates, two coverslips were added above each other in a star shape in each well before the plates were seeded with PC-3, DU145 and LNCaP cells. The cells were seeded directly on the coverslips at a concentration of 10^4 cells per well, with a total volume of 3 ml/well, and incubated for 24 h at 37 °C. They were treated with fluorescein-labelled, β-galactosidase-encoding DNA that was complexed with DAB-Lf, DAB-Pep2 or DAB-PEG2k-Pep2 using the optimal dendrimer: DNA weight ratio obtained from their

transfection assays. Control wells were also prepared: DAB: DNA at 5:1, as a positive control for DAB-Lf, DAB-PEG: DNA 20:1, as a positive control for DAB-PEG2k-Pep2, plasmid DNA only and untreated cells as negative controls. The concentration of the DNA (2.5 µg/well) was kept constant during the experiment. The treated cells were incubated for 24 h at 37 °C and 5% CO₂. The cells were then washed three times with 3 ml phosphate buffered saline (PBS) and the cells were fixed with 3 ml 3.7% w/v formaldehyde solution for 10 min at 25 °C. Wells were then washed twice with 3 ml PBS and incubated at room temperature with 3 ml 0.1% Triton-x solution for 5 min before adding 3 ml of 1% w/v bovine serum albumin in PBS for 30 min at 37 °C to reduce the non-specific binding. One unit of Alexa Fluor[®]647 dye was diluted with 200 µl of PBS before being added on the wells and incubated for 20 min at 25 °C. The wells were then washed for the last time with 3 ml PBS before mounting the coverslip on a glass slide. DAPI (HardSet-1500) was used as a visualizing fluorescent dye to stain the nucleus of the cells, while the cell walls were stained with Alexa Fluor[®]647 probe. DAPI is excited by the 405 nm laser line (emission bandwidth: 415-491 nm), fluorescein is excited by the 543 nm laser line (emission bandwidth: 550-620 nm), and Alexa Fluor[®]647 is excited by the 633 nm laser line (emission bandwidth: 650-685 nm). The prepared samples were then visualized under a Leica TCS SP5 confocal microscope.

3.2.2.4.2. Fluorescence-activated cell sorting (FACS)

PC-3, DU145 and LNCaP cells were seeded at a density of 16×10^4 cells per well in 6-well plates and incubated for 72 hours before being treated with 5 µg/well of fluorescein-labelled DNA complexed with the dendrimer of interest (either DAB-Lf in a dendrimer: DNA weight ratio of 5:1, DAB-Pep2 2:1, or DAB-PEG2k-Pep2 20:1). Other wells were treated with DAB: DNA or DAB-PEG: DNA as positive controls and DNA only as a negative control. The treated plates were incubated for 24 h at 37 °C, protected from light. The wells were then washed three times with 3 ml PBS. Trypsin was then added (250 µl per well) and the plates were incubated

for 5 minutes at 37 °C followed by the addition of 500 µl per well of FACS buffer (PBS buffer with 0.5% BSA and 2mM EDTA). Samples were transferred to polystyrene round-bottomed tubes and the fluorescence intensity was measured by FACSCanto[®] flow cytometer (BD, Franklin Lakes, NJ) to determine the amount of gene expression inside the cells after being complexed with the dendriplex. Ten thousand cells were counted for each sample as gated events. Standard solutions from BD Calibrate[®] Beads (un-labelled beads, fluorescein isothiocyanate (FITC) and phycoerythrin (PE) labelled beads) were prepared to calibrate the instrument before analysing the samples. DNA fluorescence emission was detected, as it proportionally reflects the amount of the cellular uptake of the DNA. Their mean fluorescence intensity was analysed with FACSDiva[®] software (BD, Franklin Lakes, NJ).

3.2.2.5. Cellular uptake mechanism

The cellular uptake mechanism of DAB-Lf dendriplex was investigated using different inhibitors of the most common cellular uptake mechanisms (Huang *et al.*, 2009; Pang *et al.*, 2012; Somani *et al.*, 2015). PC-3, DU145 and LNCaP cells were seeded in 6-well plates (1x10⁵ cells per well) and incubated at 37 °C for 24 or 72 hours. Cells were pretreated with free lactoferrin (80 µM), colchicine (10 µmol/L), phenylarsine oxide (10 or 20 µmol/L), filipin (5 or 10 µg/mL) and poly-L-lysine (40 µg/mL) for 15 minutes at 37 °C. DAB-Lf: fluorescein-labelled DNA dendriplex was then added to the wells at a weight ratio of 5:1 and incubated for one hour at 37 °C. The fluorescein labelled-DNA concentrations used in this experiment were 2.5 and 5 µg/well for qualitative and quantitative analyses by confocal microscopy and flow cytometry respectively. Samples were prepared for the analysis by confocal imaging and FACS as previously described in sections 3.2.2.4.1 and 3.2.2.4.2 respectively.

3.2.2.6. Peptide2 binding efficacy

This assay was conducted for the purpose of examining the efficacy of Peptide2 in binding to the different prostate cancer cells. Peptide2 was chosen for use in this study as a targeting ligand to PSMA, which is believed to be overexpressed in the LNCaP cell line but not in PC-3 and DU145 cells. Therefore, and in order to compare the uptake affinity of Peptide2 to the positive and negative PSMA-expressing cells, Peptide2 was conjugated with fluorescein isothiocyanate (FITC). The labelling of Peptide2 with FITC was carried using the method described by Zheng *et al* (2014) with some modifications as follow:

Peptide2 (10 mg) was dissolved in 3 ml of sodium carbonate buffer at pH 9. FITC stock was prepared by dissolving 5 mg of FITC in 2 ml DMSO. The 2 ml FITC stock which is equivalent to two-mole excess of FITC over Pep2 was added gradually (20 µl in each addition) to Peptide2 solution with continuous mixing. The reaction took place for 8 hours at 4 °C in the dark with continuous mixing. Ammonium chloride (13.3 mg, 50 mM) was then added and the reaction was incubated for 2 hours at 4 °C in the dark. The formulated conjugate Peptide2 -FITC was separated from the excess unreacted FITC by size exclusion chromatography using Sephadex[®] G-10. Peptide2 -FITC was collected first as it eluted faster from the column, while unreacted FITC was collected last. The collected solution was then desalted by dialysis against 1000 ml distilled water for 48 h at 4 °C using a benzylated dialysis tubing with MWCO 2000 Da as a filter and the dialysis solution was changed every 12h. The conjugation reaction was confirmed using MALDI-TOF to detect the molecular weight of Pep2-FITC.

PC-3, DU145 and LNCaP cells were seeded in 6-well plates (16×10^4 cell/well) and incubated for 72 hours before being treated with different concentrations of FITC-Pep2 (10 µg, 50 µg and 100 µg per well), with untreated wells acting as negative controls. The cells were incubated for 15 min, followed by triplicate washes of PBS (3 ml each). Cells were then suspended by adding 250 µl trypsin for 5 min followed by 500 µl of FACS buffer (PBS buffer with 0.5% BSA and

2mM EDTA). Samples were transferred to round-bottomed polystyrene tubes and the fluorescence intensity was measured immediately using a FACSCanto® flow cytometer (BD, Franklin Lakes, NJ).

3.2.2.7. Enzyme-linked immunosorbent assay

This assay was conducted to examine the efficiency of the modified dendrimer DAB-PEG2k-Pep2 in carrying the therapeutic DNA encoding TNF α inside the cells and the ability of the DNA to transfect inside the nucleus to produce the cytokine of interest (mTNF α).

PC-3, DU145 and LNCaP cells were seeded in a 24-well plate at density of 35×10^3 cells per well and incubated for 48 hours before being treated with DAB-PEG2k-Pep2 dendriplex complexed with DNA encoding TNF α at a ratio of 20:1 and a DNA concentration of 2 μ g/ml in a volume of 1 ml per well. The cell medium was then collected after 12, 24, 48, 72, 96, 120, 144 and 168 hours of treatment and frozen at -80 °C until analysis. The concentration of mouse TNF α protein produced was measured using an enzyme-linked immunosorbent kit (ELISA), following the instructions provided (Invitrogen by Thermo Fisher, UK). The absorbance was taken at 450 nm using a plate reader (FlexStation3 multi-mode microplate reader, Molecular Devices, California, USA) and the resultant absorbance converted to concentration using mTNF α standard curve.

3.2.2.8. Tetrazolium reduction assay (MTT)

The anti-proliferative activity of the synthesised dendrimers (DAB-Lf, DAB-Pep2, DAB-PEG2k-Pep2 and DAB-PEG2k-Pep4) complexed with plasmid DNA encoding TNF α , TRAIL, or IL-12 was assessed using a standard MTT assay.

PC-3, DU145 and LNCaP cells were seeded in quintuplicate at a density of 2000 cells/well in 96-well plates and incubated at 37 °C for 72 to 96 h. The cells were then treated with the DAB-Lf dendriplex at a dendrimer: DNA weight ratio of 5:1 using various DNA concentrations

ranging from 200 to 0.05 $\mu\text{g/ml}$, using naked DNA as a negative control, while DAB: DNA 5:1 ratio served as a positive control. The cytotoxicity of the prepared nanocarrier DAB-Lf and DAB only was also examined by the same method, treating the seeded cells with 1000 to 0.25 $\mu\text{g/ml}$, which is equivalent to the amount of DAB-Lf used in the anti-proliferation assay.

For DAB-PEG2k-Pep2 dendrimer, PC-3 and DU145 cells were used in this assay as PSMA-negative cells and LNCaP PSMA-positive cells respectively. Cells were treated with DAB-PEG2k-Pep2: DNA weight ratio of 20:1 using various DNA concentrations ranging from 100 to 0.06 $\mu\text{g/ml}$, using naked DNA as a negative control, while DAB: DNA 5:1 ratio and DAB-PEG: DNA 20:1 served as a positive control. The cytotoxicity of DAB-PEG2k-Pep2, and DAB-PEG only were also examined by treating the cells with 2000 to 1.2 $\mu\text{g/ml}$ of the polymer, which is equivalent to the amount used in the anti-proliferation assay.

The plates were incubated for 72 h at 37 °C and 5% CO₂, then 50 μl of 0.5% MTT solution was added to the medium and incubated at 37 °C protected from light for four hours. The medium was then replaced with 200 μl of DMSO per well to dissolve the precipitated formazan. The absorbance of the dendriplex was measured at 570 nm using a plate reader (Thermo Labsystems, Multiscan Ascent) and the growth inhibitory concentration for 50% of the cells (IC₅₀) was measured. A dose-response curve was plotted between the percentage of the live cells and the logarithm of the DNA concentration used to obtain the IC₅₀ values.

3.2.2.9. Statistical analysis

All experimental results were expressed as means \pm standard error of mean (S.E.M). Statistical significance was detected using one-way ANOVA test followed by Tukey test for multiple comparison using Minitab[®] and OriginPro[®] software. Significant differences were considered when P value become equal or lower than 0.05.

3.3. Results

3.3.1. Transfection assay

Transfection assay was conducted in order to compare the gene transfection efficacy of the targeted carriers with the unconjugated dendriplex. It also assisted in identifying the optimum dendrimer: DNA weight ratio to yield the best transfection effect in each modified dendrimer synthesised. Three prostate cancer cell lines (PC-3, DU145 and LNCaP) were examined and treated with different weight ratios.

3.3.1.1. DAB-Lf

Lactoferrin-bearing DAB dendrimer was found to improve gene transfection compared with unconjugated DAB in the all cell lines tested. The results showed that the increase in the weight ratio of the dendrimer was not related to the increase in β -galactosidase gene transfection (Figure 3-6).

The PC-3 and DU145 cell lines were found to have improved gene transfection after using DAB-Lf compared with unconjugated DAB, by a factor of 2.7 and 2.4 respectively. PC-3 cells showed a remarkable gene expression at DAB-Lf: DNA weight ratios of 10:1 and 5:1, with concentrations $8.31 \times 10^{-3} \pm 0.48$ U/ml and $10.5 \times 10^{-3} \pm 0.43$ U/ml respectively, compared with $5.17 \times 10^{-3} \pm 0.46$ U/ml for unconjugated DAB; there was then a sharp drop in transfection ability at weight ratios of 2:1 and lower, while a 20:1 ratio yielded gene transfection analogous to that of the DAB positive control, with a concentration of $4.62 \times 10^{-3} \pm 0.40$ U/ml. DU145 cells underwent optimum transfection at the weight ratios 10:1 and 5:1, with a concentration of $2.22 \times 10^{-3} \pm 0.23$ U/ml and $1.99 \times 10^{-3} \pm 0.18$ U/ml.

LNCaP cell line showed significant elevation in gene transfection after treatment with DAB-Lf at a weight ratio 20:1 only ($2.324 \times 10^{-3} \pm 0.20$ U/ml), whereas the remaining ratios showed no improvement in gene transfection compared with the unconjugated DAB ($1.54 \times 10^{-3} \pm 0.14$ U/ml).

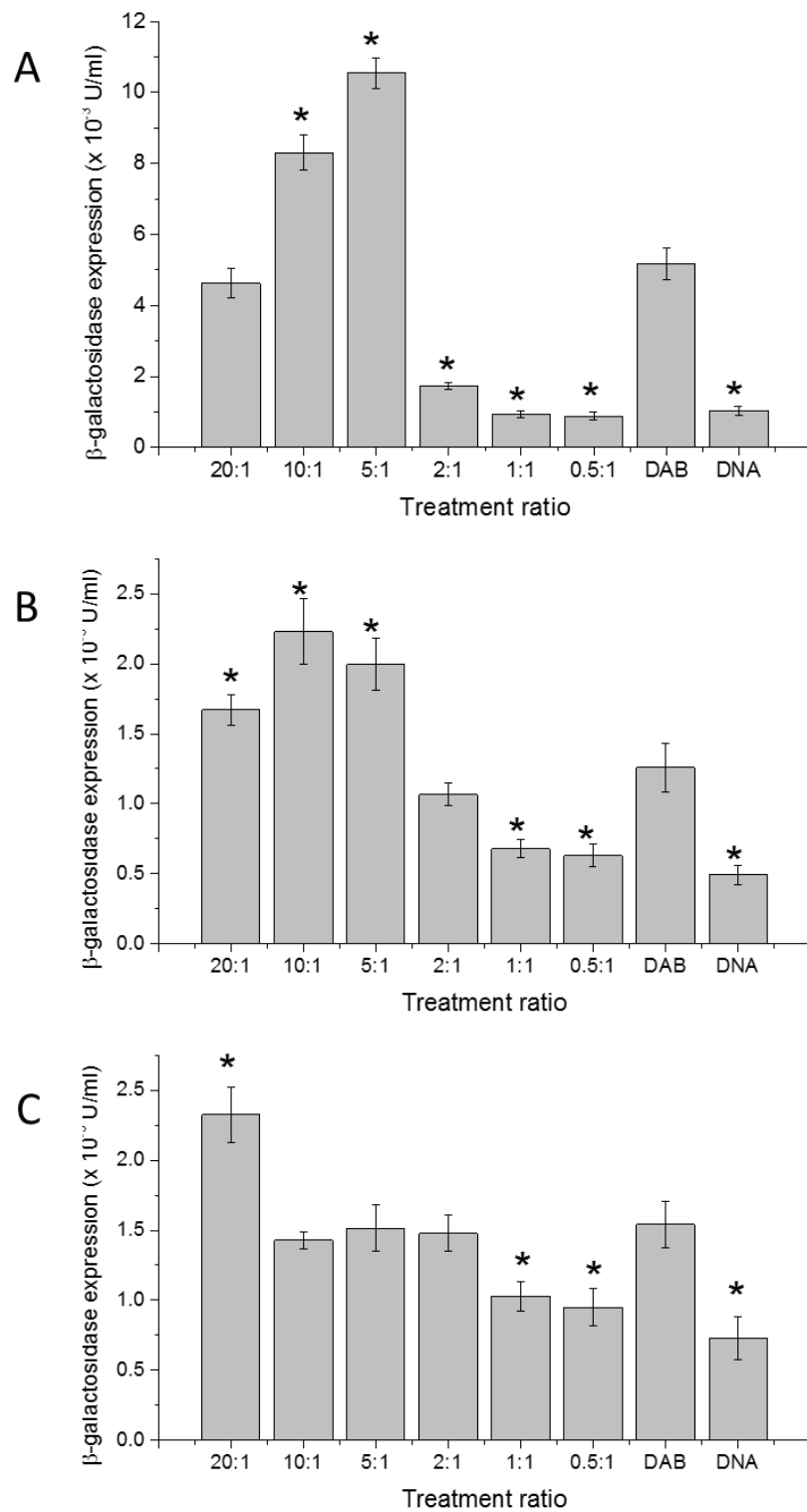


Figure 3-6 Transfection efficiency of DAB-Lf dendriplex in PC-3 (A), DU145 (B) and LNCaP cells (C). Results were expressed as the mean \pm SEM of three replicates (n=15). The data were analysed by one-way ANOVA; *: $P \leq 0.05$ versus the positive control DAB.

3.3.1.2. DAB-Peptide2

Peptide2 -bearing DAB dendrimer complexed with DNA encoding β -galactosidase resulted in variable gene expression tendency based mainly on the weight ratio used (Figure 3-7). For the PC-3 cell line, the three DAB-Pep2: DNA weight ratios 10:1, 5:1 and 2:1 showed a significant increase in β -galactosidase expression compared with unmodified DAB, while the remaining ratios resulted in either similar or lower expression. However, the optimum expression was achieved using the 5:1 ratio with a 1.52-fold improvement over unmodified DAB, resulting in β -galactosidase concentration of $9.63 \times 10^{-3} \pm 0.19$ U/ml and $6.32 \times 10^{-3} \pm 0.19$ U/ml for DAB-Pep2 and DAB respectively. On the other hand, the DU145 cell line showed a significant increase in the transfection efficacy of DAB-Pep2 at the 2:1 weight ratio, up to 1.8-fold over DAB, with a β -galactosidase concentration of $5.89 \times 10^{-3} \pm 0.48$ U/ml. The other ratios failed to show any significant improvement in gene expression, being similar to that obtained from unmodified DAB. For LNCaP cells, the three weight ratios 10:1, 5:1 and 2:1 resulted in significant increase in β -galactosidase expression compared with unmodified DAB, while the lower ratios resulted in low gene expression.

Although 2:1 ratio was not the optimal weight ratio for the PC-3 and LNCaP cell lines, it was the only one showing significant expression with DU145 cells. Therefore, this weight ratio was selected for use in further *in vitro* experiments.

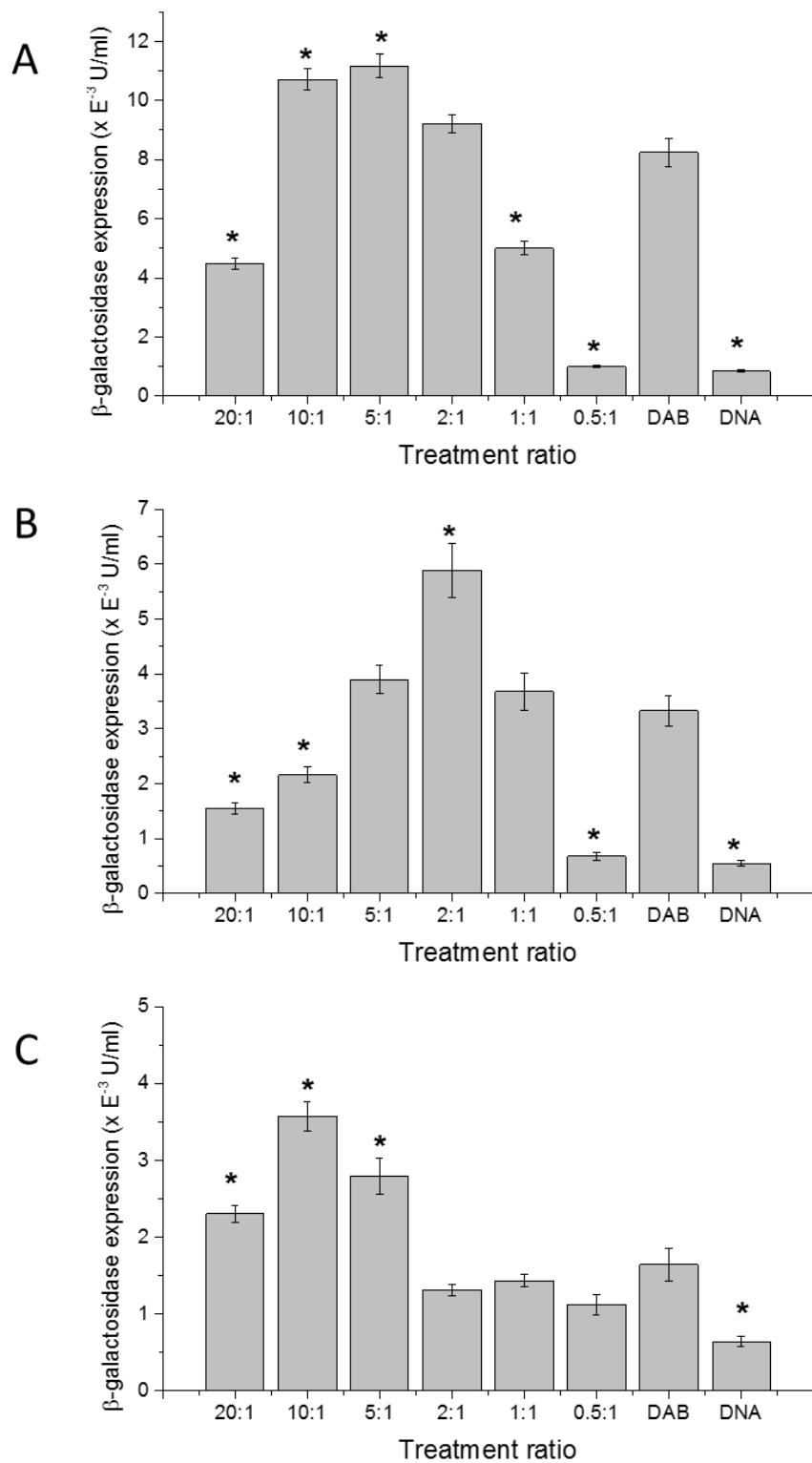


Figure 3-7 Transfection efficiency of DAB-Peptide2 dendriplex in PC-3 (A), DU145 (B) and LNCaP cells (C). Results were expressed as the mean \pm SEM of three replicates (n=15). The data were analysed by one-way ANOVA; *: $P \leq 0.05$ versus the positive control DAB.

3.3.1.3. DAB-PEG2k-Peptide2

After DAB-Pep2 had been PEGylated with a four-mole excess of NHS-PEG2000-methoxy, a transfection assay was performed to examine the capability of this new dendrimer in improving the gene expression in PSMA-positive cells. For the cell lines PC-3 and DU145, the new dendrimer showed no improvement in transfecting the DNA at any of the ratios examined compared with the positive controls DAB-PEG: DNA (20:1) and DAB: DNA (5:1), which resulted in superior DNA transfection efficacy. On the other hand, the PSMA-positive cell line (LNCaP) showed a significant (2.7-fold) improvement in DNA transfection at the weight ratio of 20:1 ($2.78 \pm 0.11 \times 10^{-3}$ U/ml) compared with the positive control DAB-PEG 20:1 ($0.99 \pm 0.10 \times 10^{-3}$ U/ml). Significant 2-fold and 1.48-fold improvements in gene expression over DAB-PEG were also recorded at weight ratios of 10:1 and 5:1 respectively, with transfection values of $1.98 \pm 0.12 \times 10^{-3}$ U/ml and $1.47 \pm 0.09 \times 10^{-3}$ U/ml. The other control, DAB 5:1, also resulted in lower transfection values compared with the three top weight ratios of DAB-PEG2k-Pep2 in LNCaP cells, showing a β -galactosidase concentration of $1.27 \pm 0.09 \times 10^{-3}$ U/ml.

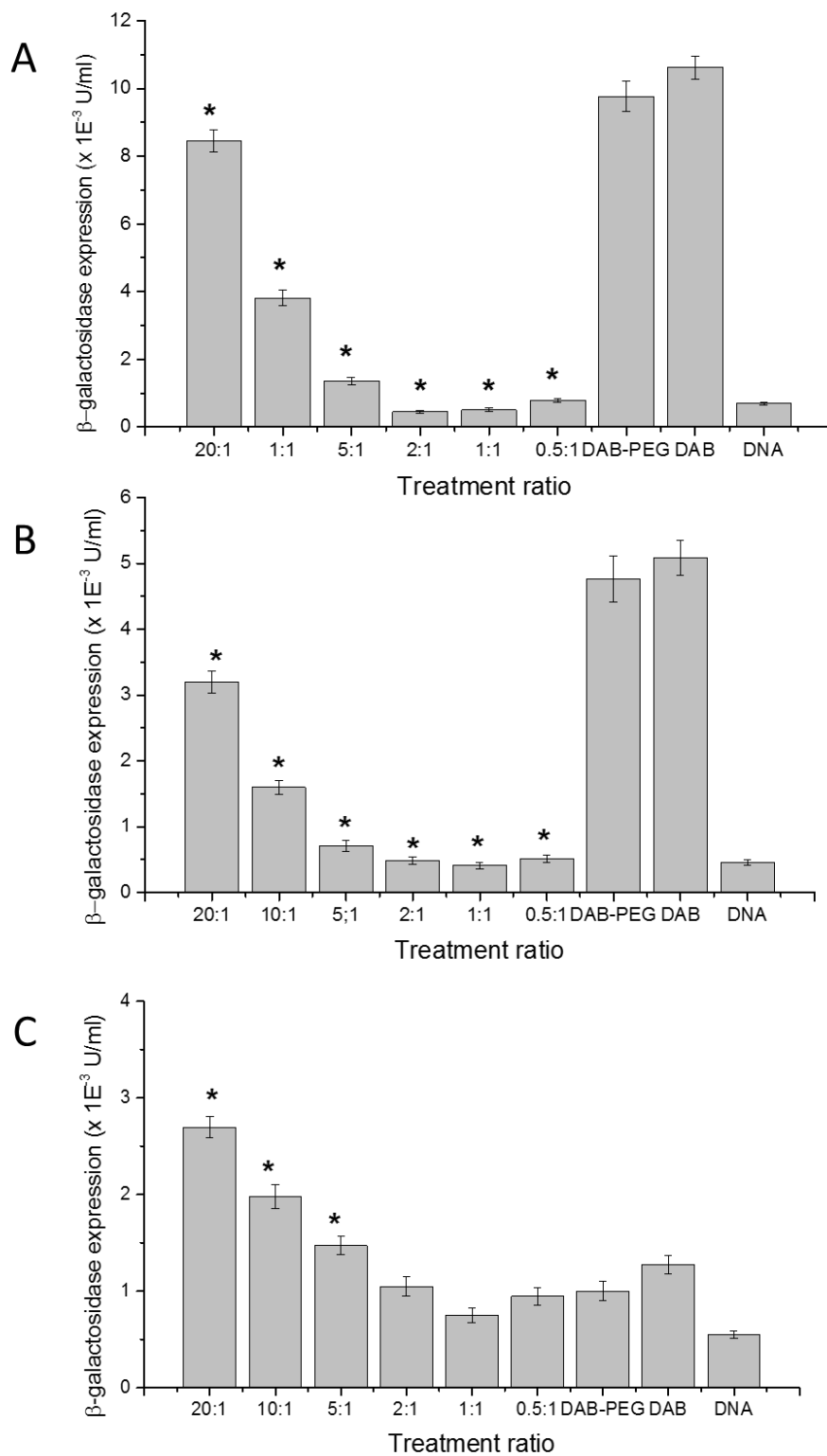


Figure 3-8 Transfection efficiency of DAB-PEG2k-Peptide2 dendriplex in PC-3 (A), DU145 (B) and LNCaP cells (C). Results were expressed as the mean \pm SEM of three replicates (n=15). The data were analysed by one-way ANOVA; *: $P \leq 0.05$ versus the positive control DAB-PEG.

3.3.1.4. DAB-PEG3.5-Peptide2

Using the long crosslinker NHS-PEG3.5K-malimide to conjugate DAB dendrimer with the targeting ligand Peptide2 resulted in no clear pattern of the transfection efficacy of the DAB-PEG3.5k-Pep2 dendriplex. For the PC-3 cell line, the weight ratio 20:1 gave a significant improvement in dendriplex transfection, with a value of $16.2 \pm 0.24 \times 10^{-3}$ U/ml compared with the positive control DAB ($12.7 \pm 0.28 \times 10^{-3}$ U/ml). In contrast, DU145 cells showed almost no transfection at the same ratio and there was no improvement in transfection as a result of the inclusion of Peptide2 in the dendriplex. PSMA-positive cells (LNCaP) showed no significant improvement in the transfection of DAB-PEG3.5k-Pep2 dendriplex compared with the positive control DAB-PEG at any of the ratios examined.

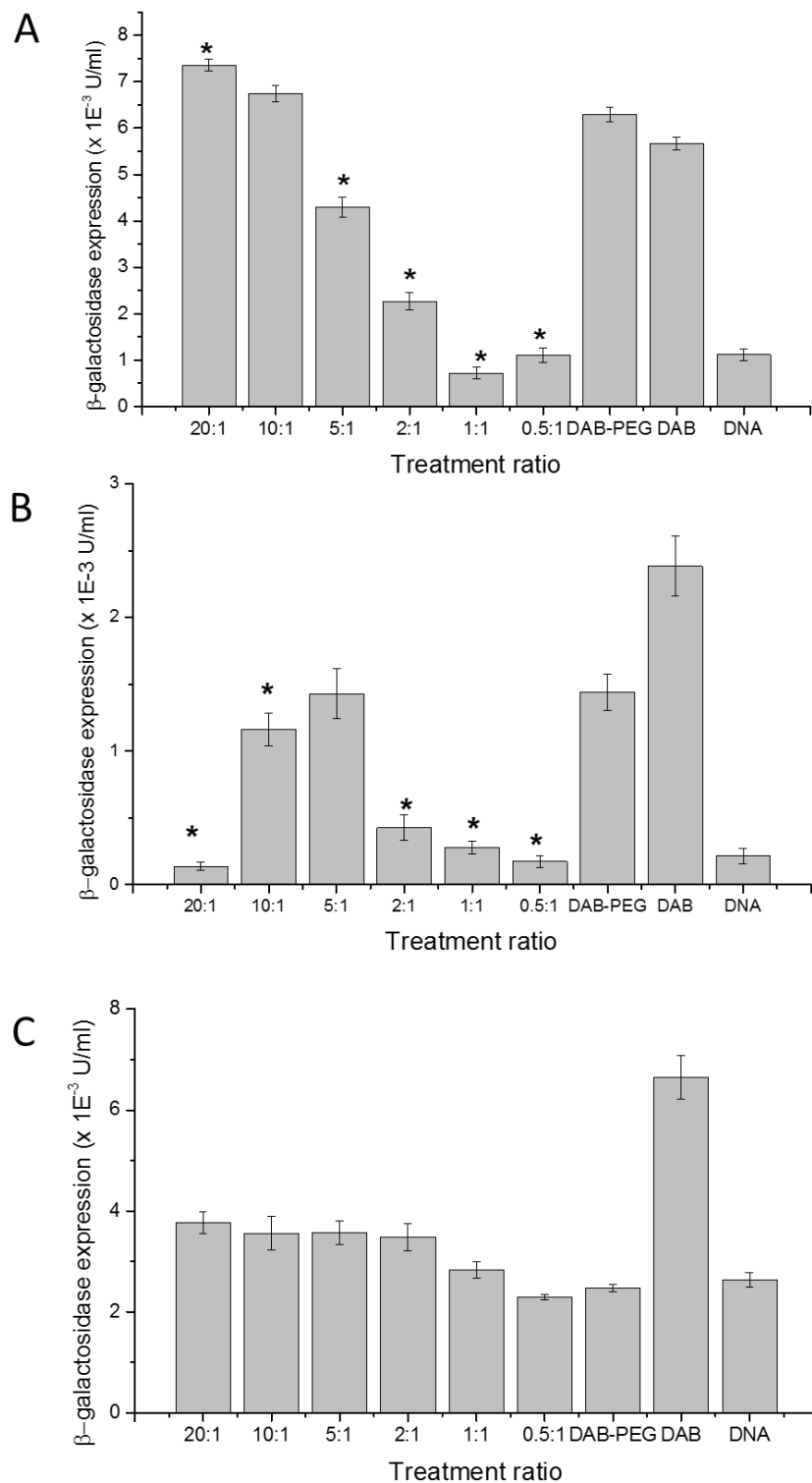


Figure 3-9. Transfection efficiency of DAB-PEG3.5-Peptide2 dendriplex in PC-3 (A), DU145 (B) and LNCaP cells (C). Results were expressed as the mean \pm SEM of three replicates (n=15). The data were analysed by one-way ANOVA; *: $P \leq 0.05$ versus the positive control DAB-PEG.

3.3.1.5. DAB-PEG2k-PEG3.5k-Peptide2

The DAB-PEG2k-PEG3.5k-Pep2 polymer showed no improvement in the transfection of the complexed DNA in any of the cell lines examined, including the PSMA-positive LNCaP cells. This failure could be related to the modest DNA complexation capability of this polymer, which directly affects its physical characteristics such as its size and zeta potential.

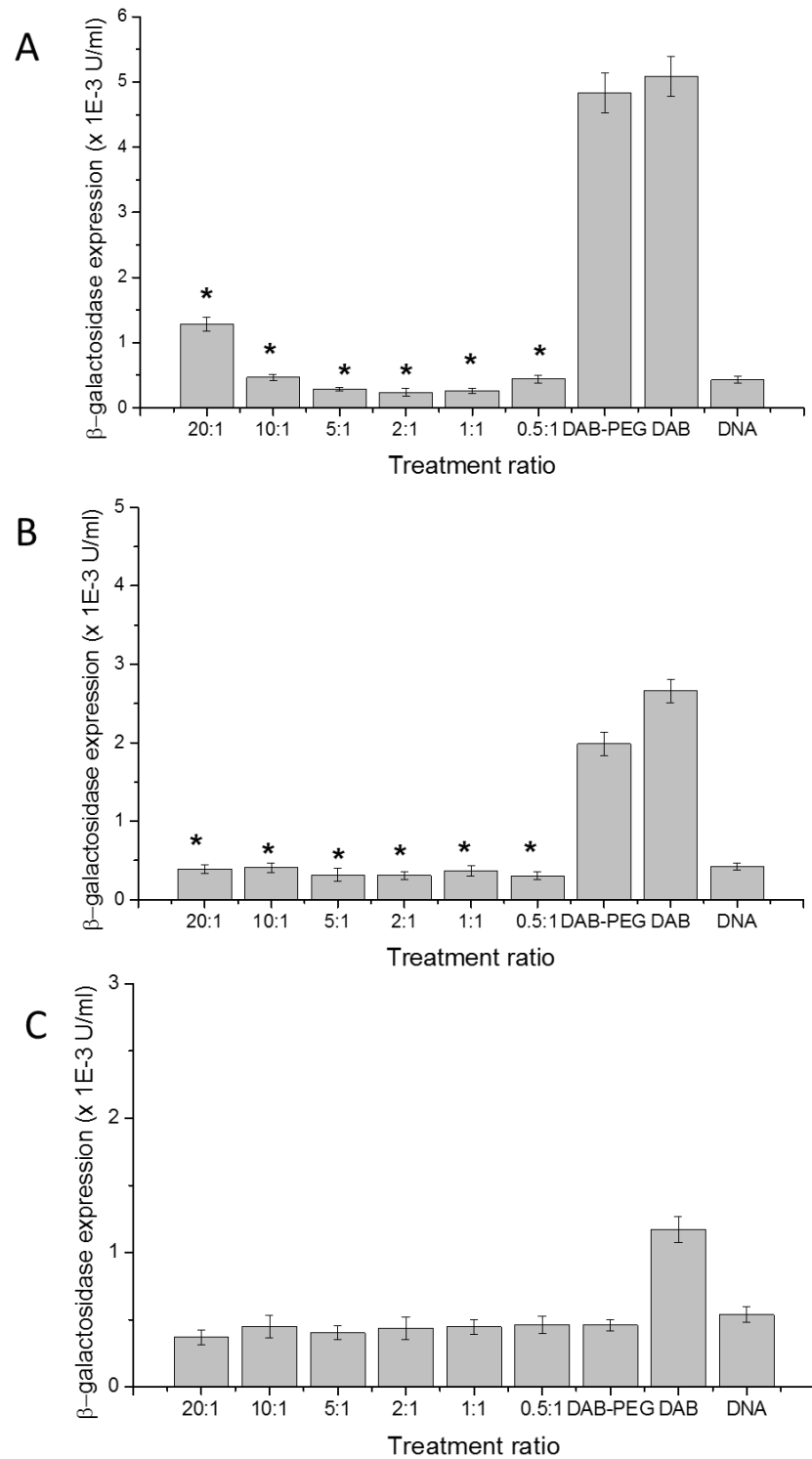


Figure 3-10 Transfection efficiency of DAB-PEG2k-PEG3.5k-Peptide2 dendriplex in PC-3 (A), DU145 (B) and LNCaP cells (C). Results were expressed as the mean \pm SEM of three replicates (n=15). The data were analysed by one-way ANOVA; *: $P \leq 0.05$ versus the positive control DAB-PEG.

3.3.1.6. DAB-PEG2k-Peptide4

Peptide4-bearing DAB-PEG was first examined by transfection assay to estimate the improvement in the gene expression after using this new dendrimer as an indication for the successful targeting to integrin receptors in prostate cancer cells. The new dendrimer showed no improvement in transfecting the DNA in any of the cell lines and at any of the ratios examined, compared with the positive controls DAB-PEG: DNA (20:1) and DAB: DNA (5:1), indicating the failure of Peptide4 to improve the cellular uptake of this dendriplex. Another control used in this assay was DAB-PEG: DNA (10:1). At that specific ratio, DAB-PEG2k-Pep4 showed significantly enhanced transfection results than DAB-PEG in both PC-3 and DU145 cell lines, yet both values were significantly lower than for the DAB: DNA control, eliminating them from comparison because the main aim in using the targeted formulation was to obtain higher uptake and transfection compared with the third generation DAB-Am16.

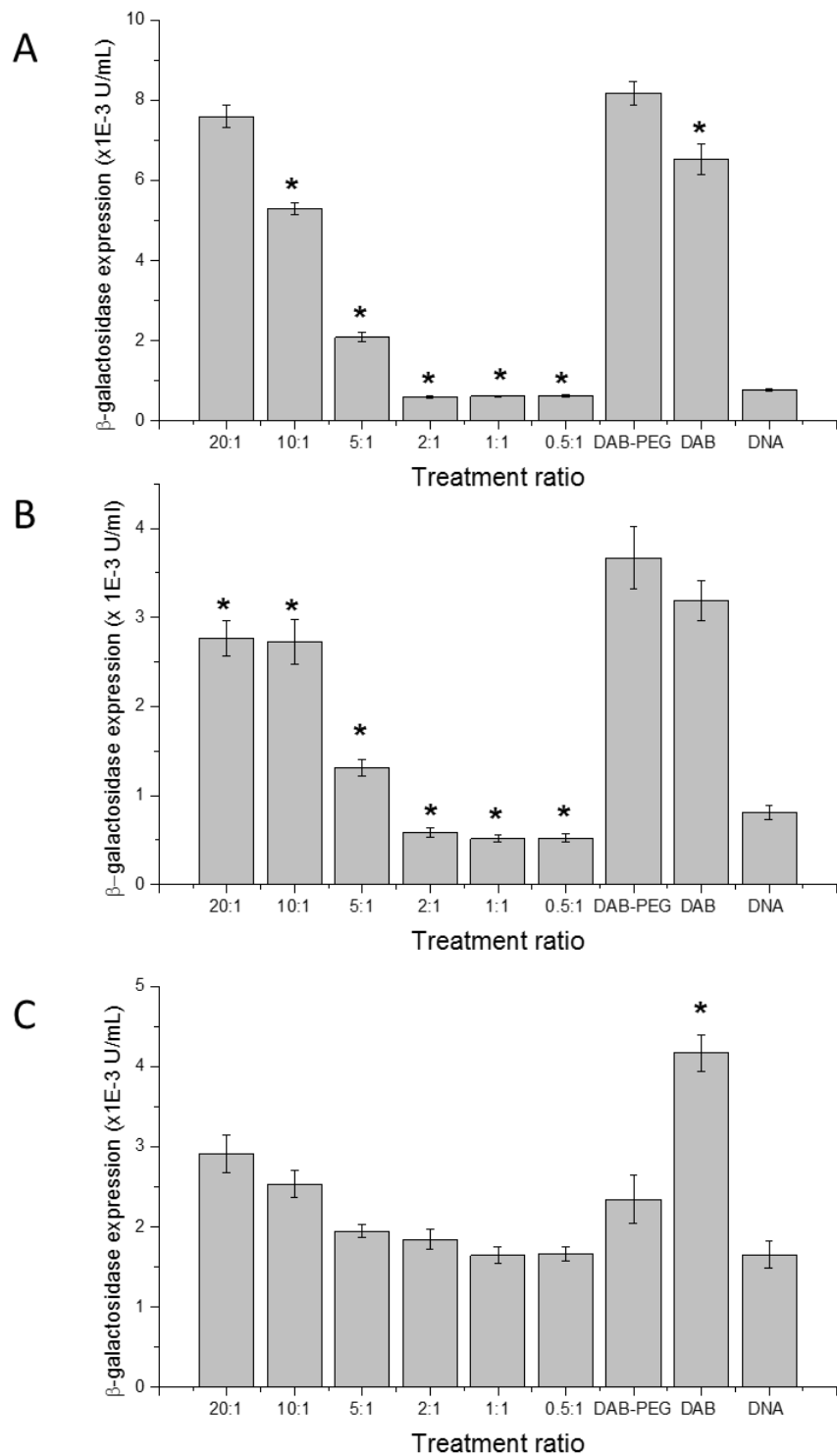


Figure 3-11 Transfection efficiency of DAB-PEG2k-Peptide4 dendriplex in PC-3 (A), DU145 (B) and LNCaP cells (C). Results were expressed as the mean \pm SEM of three replicates (n=15). The data were analysed by one-way ANOVA; *: $P \leq 0.05$ versus the positive control DAB-PEG.

3.3.2. Cellular uptake

3.3.2.1. Confocal microscopy

Confocal microscopy was used to qualitatively investigate the cellular uptake of the plasmid DNA, labelled with the fluorescent dye (fluorescein-labelled DNA encoding β -galactosidase) by the targeted cells after their complexation with DAB-Lf, DAB-Pep2 and the PEGylated form of DAB-Pep2 (DAB-PEG2k-Pep2).

3.3.2.1.1. DAB-Lf

The DAB-Lf: DNA weight ratio selected for this study was 5:1 as was the optimal ratio in the transfection assay, especially for PC-3 and DU 145 cells. Fluorescein-labelled DNA was found to be diffused in the cell cytoplasm of PC-3 and DU145 cells after treatment, with less diffusion for LNCaP cell line (Figure 3-12). PC-3 cells showed the most abundant DNA uptake. Cells treated with unconjugated DAB complex also showed DNA uptake inside the cells, but with less intensity compared with those treated with DAB-Lf dendriplex. In contrast, naked DNA showed minimum fluorescence on the cytoplasm of all of the cell lines tested, as expected.

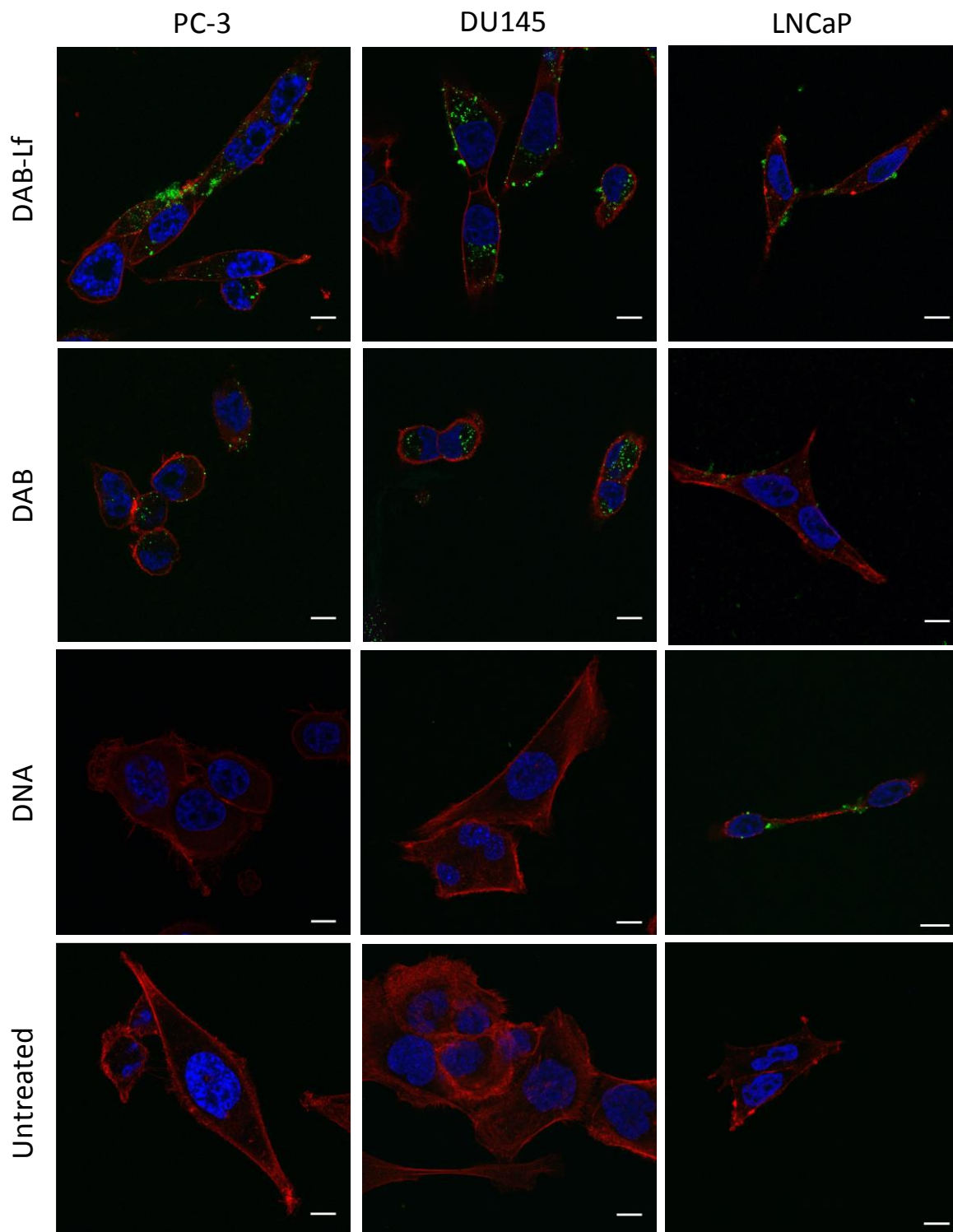


Figure 3-12 Confocal microscopy images for the cellular uptake of fluorescein-labelled DNA at a concentration of 2.5 $\mu\text{g}/\text{well}$, complexed with DAB-Lf, DAB or uncomplexed, after incubation for 24 hours with PC-3, DU145 and LNCaP cells. Blue: nuclei stained with DAPI (excitation: 405 nm laser line, bandwidth: 415-491 nm), green: fluorescein-labelled DNA (excitation: 543 nm laser line, bandwidth: 550-620 nm), red: Alexa Fluor[®]647 probe (excitation: 633 nm laser line, bandwidth: 650-690 nm) (Bar size 10 μm).

3.3.2.1.2. DAB-Peptide2

DAB-Pep2 at a dendrimer: DNA weight ratio of 2:1 was selected for this experiment as it was the optimal ratio in the transfection study. For all the cell lines treated, green fluorescence corresponding to the fluorescein-labelled DNA was distributed inside the cytoplasm and around the membranes of cells that have been treated with DAB-Pep2 and DAB dendriplexes. A stronger fluorescein intensity was seen in the cells treated with DAB-Pep2 dendriplex compared with the positive control, DAB: DNA 5:1. In contrast, cells treated with naked DNA showed no sign of cellular uptake in either cell line (Figure 3-13).

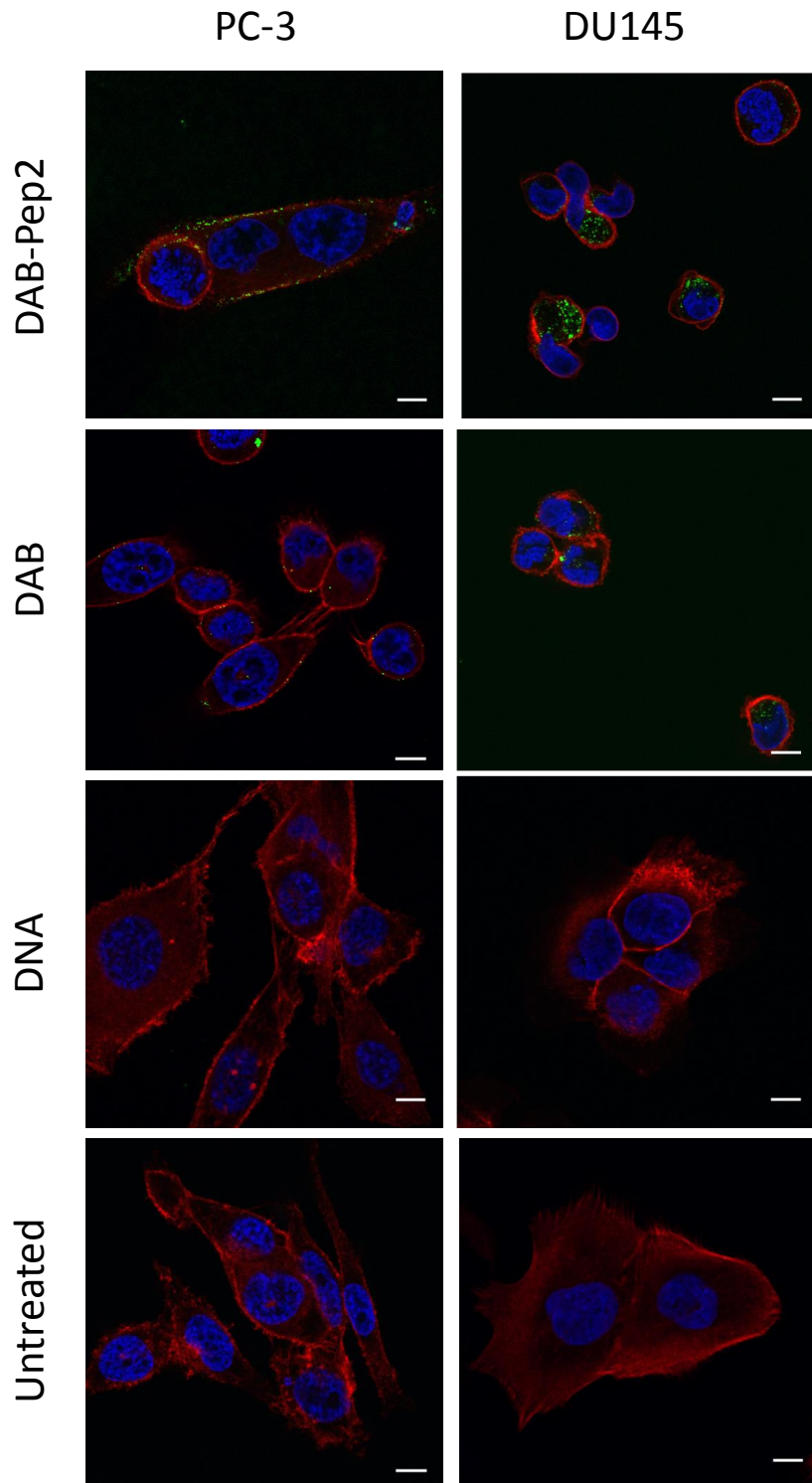


Figure 3-13 Confocal microscopy images for the cellular uptake of fluorescein-labelled DNA at a concentration of 2.5 $\mu\text{g}/\text{well}$, complexed with DAB-Peptide2, DAB or uncomplexed, after incubation for 24 hours with PC-3 and DU145 cells. Blue: nuclei stained with DAPI (excitation: 405 nm laser line, bandwidth: 415-491 nm), green: fluorescein-labelled DNA (excitation: 543 nm laser line, bandwidth: 550-620 nm), red: Alexa Fluor[®]647 probe (excitation: 633 nm laser line, bandwidth: 650-690 nm) (Bar size 10 μm).

3.3.2.1.3. DAB-PEG2k-Peptide2

DAB-PEG2k-Pep2 dendriplex at the weight ratio 20:1 was selected for *in vitro* experiments, as it showed optimal transfection in the PSMA-positive control cells (LNCaP). The PC-3 cell line was used in this experiment as a model for PSMA-negative cells. The cells were treated with DAB-PEG2k-Pep2: DNA (20:1) and with DAB-PEG: DNA at the same ratio as positive control and DNA only as negative control. In LNCaP cells, the images showed green fluorescence being distributed inside the cytoplasm of the cells treated with DAB-PEG2k-Pep2 and DAB-Pep2, with more intense fluorescence in the cells treated with DAB-PEG2k-Pep2, suggesting that Peptide2 had improved the cellular uptake of the dendriplex. In the PC-3 cell line, the green fluorescence was found to be distributed inside the cytoplasm of the cells treated with DAB-PEG2k-Pep2 and DAB-PEG.

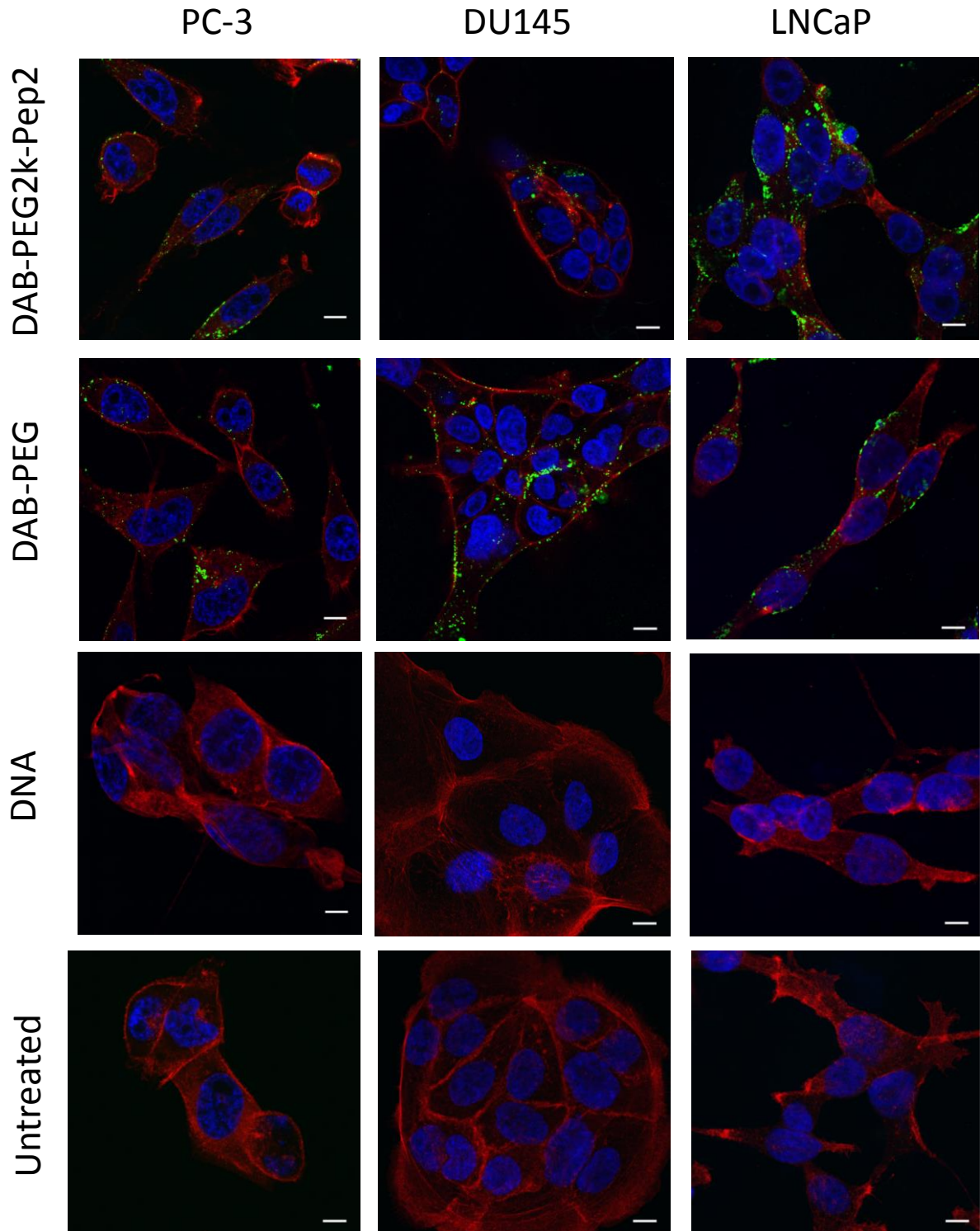


Figure 3-14 Confocal microscopy images for the cellular uptake of fluorescein-labelled DNA at a concentration of 2.5 $\mu\text{g}/\text{well}$, complexed with DAB-PEG2k-Peptide2, DAB-PEG or uncomplexed DNA, after incubation for 24 hours with PC-3, DU145 and LNCaP cells. Blue: nuclei stained with DAPI (excitation: 405 nm laser line, bandwidth: 415-491 nm), green: fluorescein-labelled DNA (excitation: 543 nm laser line, bandwidth: 550-620 nm), red: Alexa Fluor[®]647 probe (excitation: 633 nm laser line, bandwidth: 650-690 nm) (Bar size 10 μm).

3.3.2.2. Fluorescence-activated cell sorting (FACS)

Flow cytometry is a quantitative assay used to examine the cellular uptake of DNA by measuring its fluorescence emission in different prostate cancer cell lines. The three cell lines PC-3, DU145 and LNCaP resulted in significant high fluorescence intensity following treatment with the DAB-Lf, DAB-Pep2 and DAB-PEG2k-Pep2 dendriplexes compared with unmodified DAB dendriplex.

3.3.2.2.1. DAB-Lf

PC-3 cells showed the highest cellular uptake of the DAB-Lf dendriplex, with a mean of 9004.3 ± 241.1 a.u., which is twice as high as the fluorescence emission of the unconjugated DAB dendriplex. Similarly, DU145 and LNCaP cells resulted in significant fluorescence emissions after treatment with DAB-Lf dendriplex compared with the DAB dendriplex, with rates of 1.6 and 1.5 times higher in fluorescence intensity respectively (Figure 3-15 and Figure 3-16). Lactoferrin-bearing DAB dendriplex had a fluorescence mean of 5227 ± 251 a.u. and 5535 ± 532 a.u. compared with the unconjugated DAB, with 3261 ± 677 a.u. and 3671 ± 120 a.u. for the DU145 and LNCaP cell lines respectively. Uncomplexed DNA did not result in any cellular uptake for all cell lines examined, indicating the failure of the DNA to be taken by cells without the assistance of a carrier.

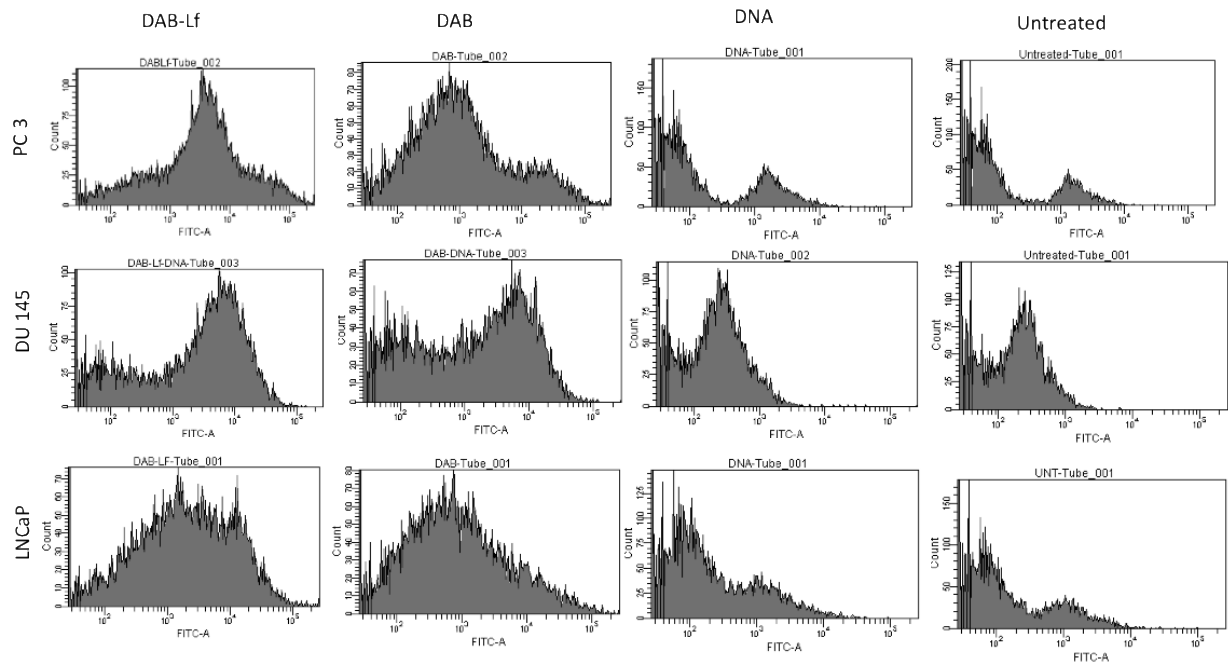


Figure 3-15 Flow cytometry histograms showing fluorescence emission intensity as a quantitative measurement of the cellular uptake of fluorescein-labelled DNA complexed with DAB-Lf and DAB in A) PC-3, B) DU145 and C) LNCaP prostate cancer cell lines.

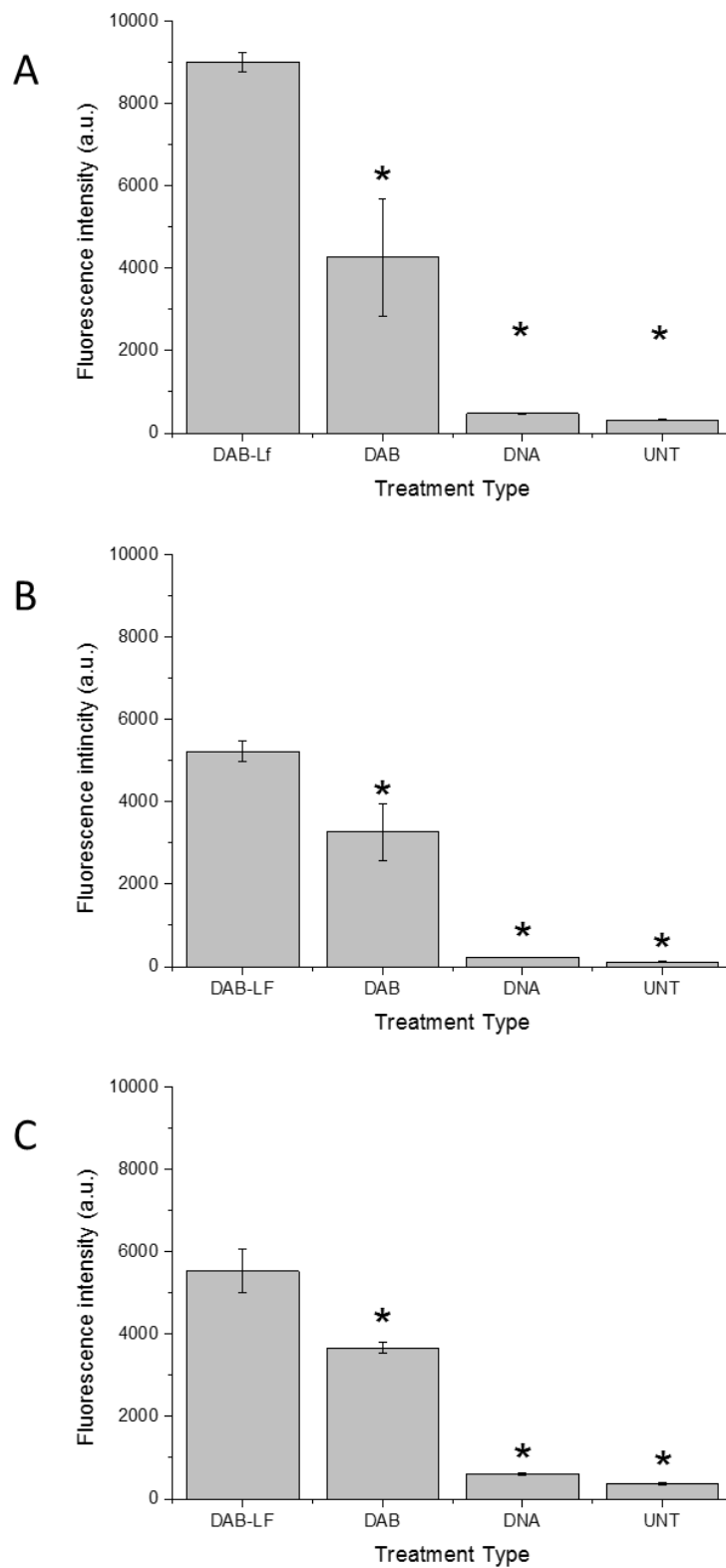


Figure 3-16 Fluorescence emission intensity as a quantitative measurement of the cellular uptake of fluorescein-labelled DNA complexed with various carriers in various prostate cancer cell lines (PC-3, DU145 and LNCaP) (n=3). *: $P \leq 0.05$ versus the highest cellular uptake.

3.3.2.2.2. DAB-Peptide2

In the case of the DAB-Pep2 formulation, PC-3 and DU145 cell lines showed significant increase in the uptake of fluorescein-labelled DNA compared with unmodified DAB (Figure 3-18). In PC-3 cells, DAB-Pep2 treatment resulted in a 1.54-fold increase in DNA uptake compared with unmodified DAB, with total mean fluorescence of 15017 ± 614 a.u. and 9776 ± 454 a.u. respectively. For DU145 cells, DAB-Pep2 dendriplex had a 2.54-fold increase in uptake, with a fluorescence intensity of 12464 ± 299 a.u. compared with 4909 ± 135 a.u. for DAB: DNA. On the other hand, there was no significant increase in the fluorescence intensity between DAB-Pep2 and DAB dendriplexes in LNCaP cells.

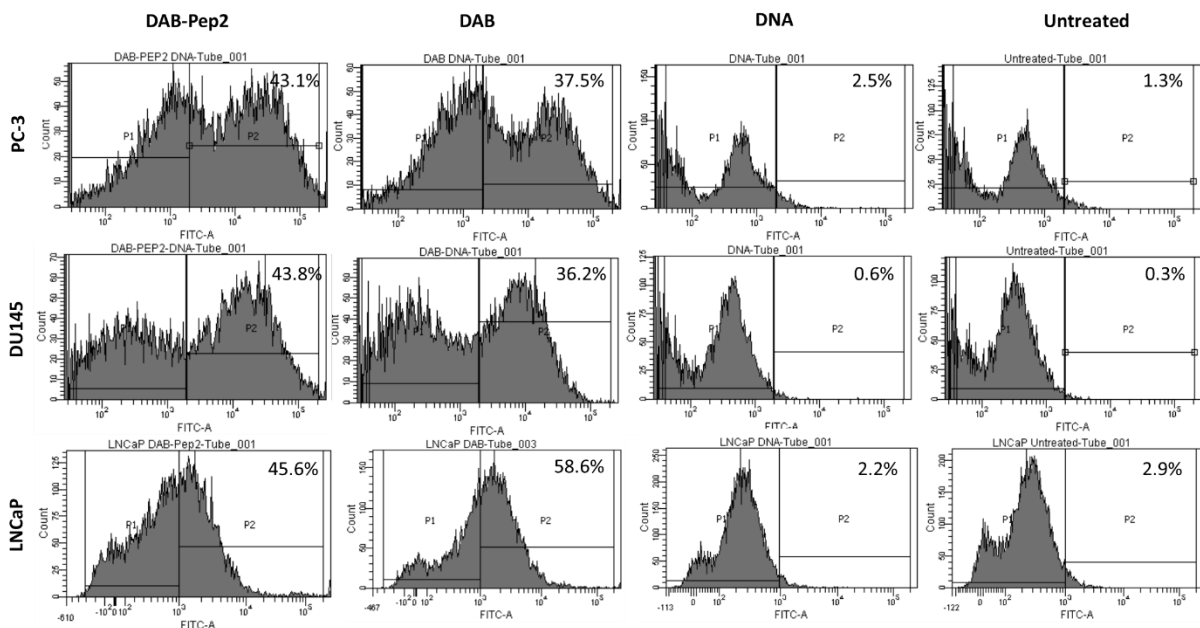


Figure 3-17 Flow cytometry histograms showing fluorescence emission intensity as a quantitative measurement of the cellular uptake of fluorescein-labelled DNA complexed with DAB-Peptide2 and DAB in A) PC-3, B) DU145 and C) LNCaP prostate cancer cell lines.

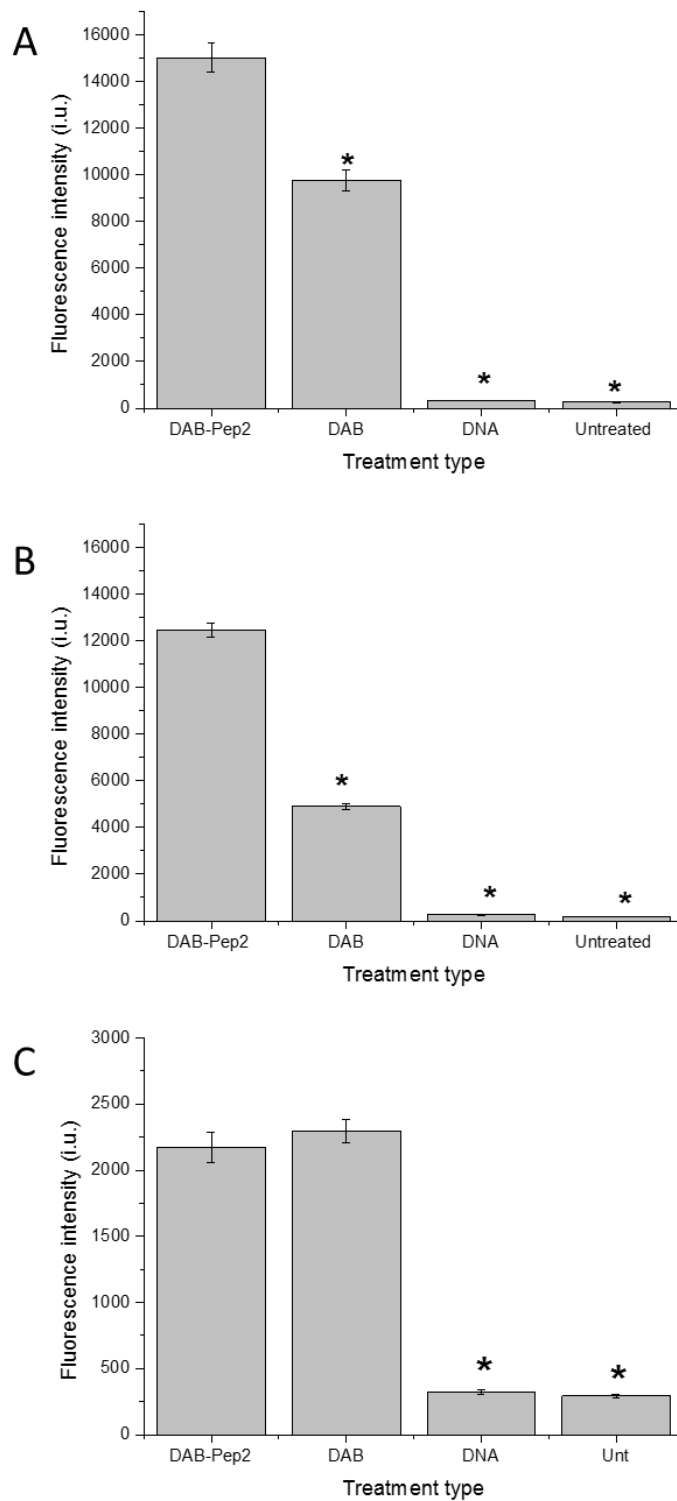


Figure 3-18 Fluorescence emission intensity as a quantitative measurement of the cellular uptake of fluorescein-labelled DNA complexed with DAB-Peptide2, DAB, or uncomplexed in PC-3 (A), DU145 (B) and LNCaP (C) cell lines (n=3). *: $P \leq 0.05$ versus the highest cellular uptake.

3.3.2.2.3. DAB-PEG2k-Peptide2

In the PSMA-positive LNCaP cell line, DAB-PEG2k-Pep2 dendriplex showed a significant improvement in cellular uptake, with a mean fluorescence intensity of 5045 ± 242 a.u. compared with 3695 ± 237 a.u. for the same dendriplex without Peptide2 (DAB-PEG). DNA only failed to show any cellular uptake, with a mean fluorescence value of 145.3 ± 13.9 a.u. PSMA-negative cell lines, PC-3 and DU145, responded to the treatment differently. In PC-3 cells, the uptake of fluorescein-labelled DNA complexed with DAB-PEG2k-Pep2 was significantly lower than that of the DAB-PEG dendriplex, the respective fluorescence intensity values being 3030 ± 282 a.u. and 4608 ± 266 a.u., whereas DU145 cells treated with DAB-PEG2k-Pep2 showed a significant improvement in fluorescence intensity (5467 ± 703 a.u.) over DAB-PEG dendriplex (2605 ± 695 a.u.).

There was no significant difference in the percentage of cells successfully taking up by DAB-PEG2k-Pep2 and DAB-PEG dendriplexes, yet, the intensity of the uptake was significantly different as demonstrated above.

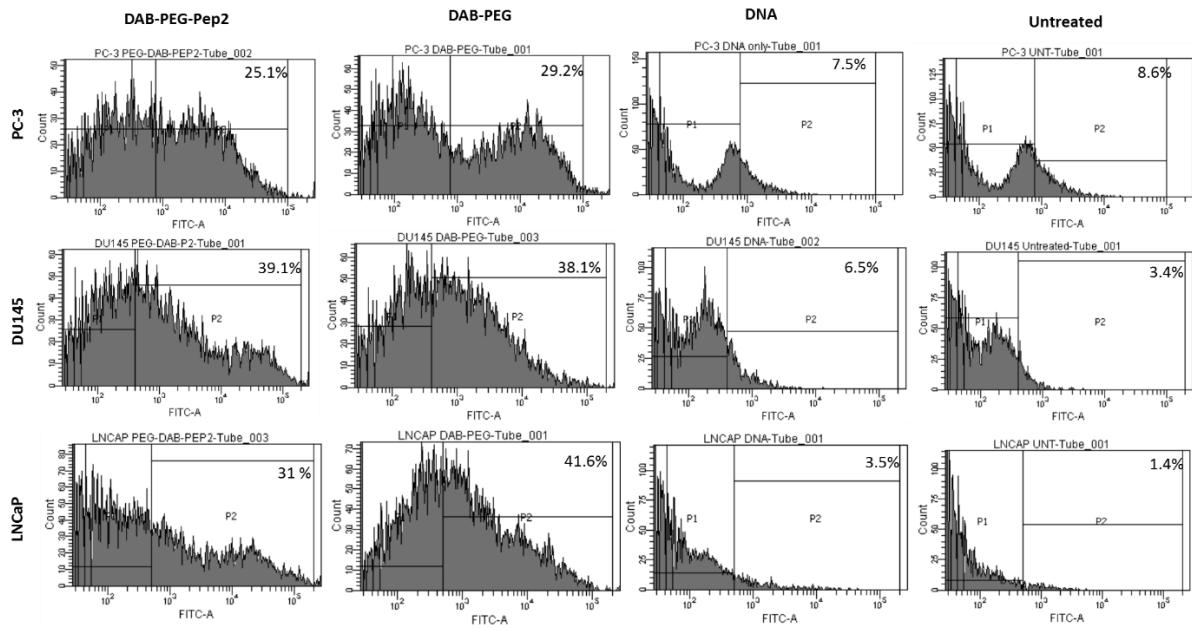


Figure 3-19 Flow cytometry histograms showing fluorescence emission intensity as a quantitative measurement of the cellular uptake of fluorescein-labelled DNA complexed with DAB-PEG2k-Peptide2 or DAB-PEG in PC-3, DU145 and LNCaP prostate cancer cell lines. The P2 gating area show the percentage of cells that took up each specific treatment in a total of 10000 events.

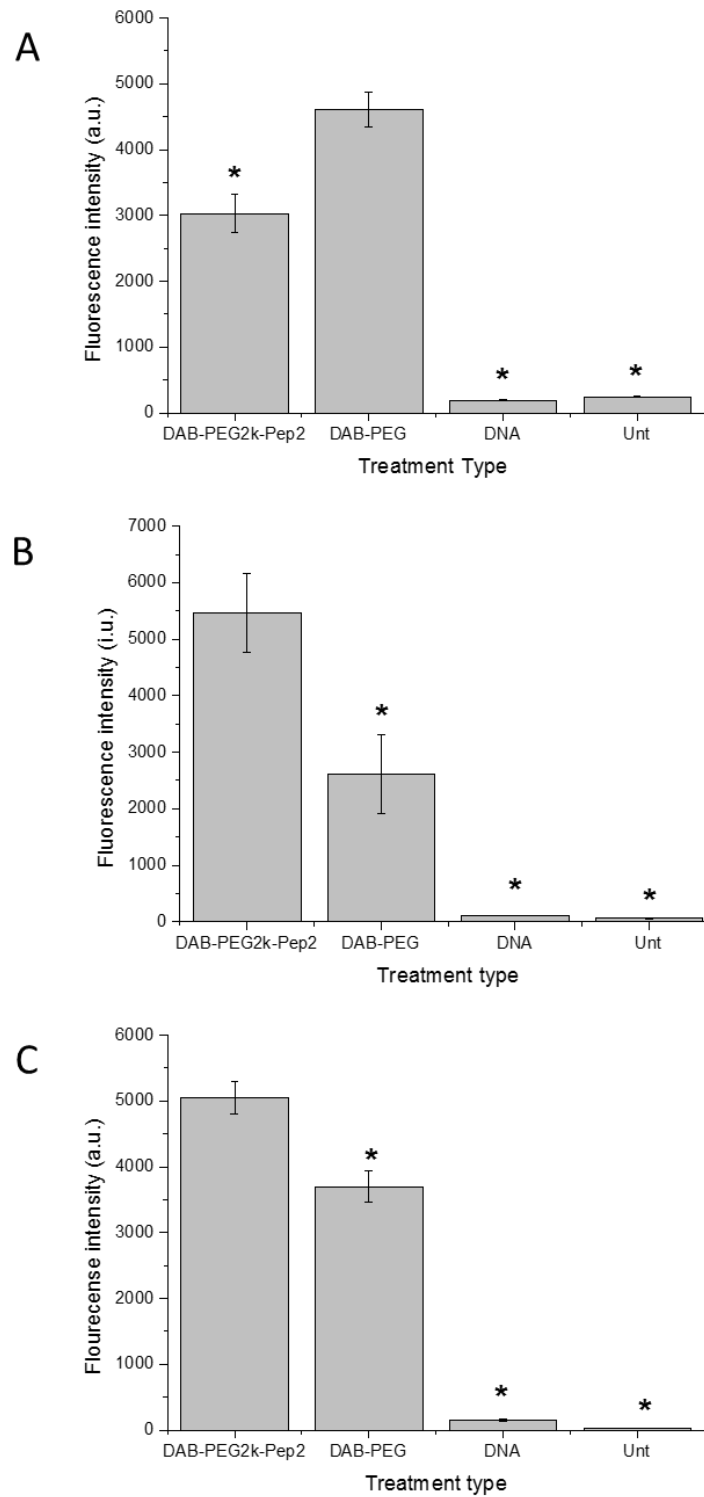


Figure 3-20 Fluorescence emission intensity as a quantitative measurement of the cellular uptake of fluorescein-labelled DNA complexed with DAB-PEG2k-Peptide2, DAB-PEG, or uncomplexed in PC-3 (A), DU145 (B) and LNCaP (C) (n=3). *: $P \leq 0.05$ versus the highest cellular uptake.

3.3.3. Mechanism of cellular uptake

3.3.3.1. DAB-Lf

DAB-Lf dendriplex was pre-treated with different cellular uptake inhibitors to investigate and confirm the mechanism of dendriplex uptake by the cells. For the three cell lines examined, pre-treating the cells with poly-L-lysine resulted in almost complete blocking of the uptake of DAB-Lf dendriplex, while 80 μ M of free lactoferrin resulted in approximately 60% inhibition of the uptake of DAB-Lf dendriplex compared with the positive control (DAB-Lf dendriplex). Pre-treating the cells with different doses of phenylarsine oxide (Ph.O) resulted in cellular uptake reduction of around 60% and 80% for the PC-3 cell line. In DU145 cells, the low dose of Ph.O (10 μ M) did not cause an uptake reduction whereas the higher dose (20 μ M) led to 30% reduction in DAB-Lf dendriplex cellular uptake. Similarly, pre-treating PC-3 cells with 5 and 10 μ g/ml of filipin (Fil) showed similar percentage of cellular uptake reduction (70%). In DU145 cells, the low dose of Fil did not cause any reduction in the cellular uptake, while 10 μ g/ml Fil caused 90% reduction in the dendriplex uptake. On the other hand, colchicine pre-treatment showed no sign of affecting the uptake of the dendriplex (Figure 3-21).

In the PC-3 and DU145 cell lines, 40 μ g/ml of the cationic polymer poly-L-lysine resulted in complete suppression of dendriplex uptake, with a mean fluorescence intensity of 239.6 ± 8.83 a.u. and 93.66 ± 6.43 a.u. respectively. These values were not significantly different from the negative control samples (untreated cells). In LNCaP cells, 61.9% reduction in uptake was recorded after pre-treating the cells with PLL, with a mean fluorescence of 473.6 ± 19.1 a.u. Pre-treatment with free lactoferrin resulted in more than 3-fold decrease in the uptake of DAB-Lf dendriplex compared with the positive control, with a fluorescence intensity of 482.0 ± 20.2 a.u. for PC-3 cell line, and more than 2.5-fold reduction compared with the positive control showing mean values of 2120 ± 44.3 a.u. and 497.0 ± 39.5 a.u. for DU145 and LNCaP cells

respectively. The result of Ph.O pretreatment (10 μ M) was 51.8% inhibition of dendriplex uptake, with a fluorescence intensity of 766.0 ± 22.6 a.u., amounting to a two-fold lower uptake by PC-3 cells. The same dose of Ph.O did not lead to such inhibition in DU145 and LNCaP cells, it caused 1.2- and 1.3-fold reduction in the uptake with fluorescence intensity values of 4585 ± 169 a.u. and 974.0 ± 29.6 a.u. respectively. Increasing the dose of Ph.O to 20 μ M causes a significant reduction in the cellular uptake of the dendriplex by up to 4.7-fold and 1.7-fold following treatment with DAB-Lf dendriplex in PC-3 and DU145 cell lines respectively. Similarly, pre-treating the cells with 5 μ g/ml Filipin produced a roughly 3.2-, 1.3- and 1.4-fold reductions in uptake by PC-3 (597.0 ± 13.4 a.u.), DU145 (4334 ± 636 a.u.), and LNCaP cells (910.0 ± 104 a.u.). Higher dose of Fil (10 μ g/ml) caused a significant improvement in DNA uptake inhibition with 3.4-fold and 9-fold reduction in DNA uptake for PC-3 and DU145 cell lines and fluorescence intensity values of 1082 ± 66.7 a.u. and 380.7 ± 36.9 a.u. respectively.

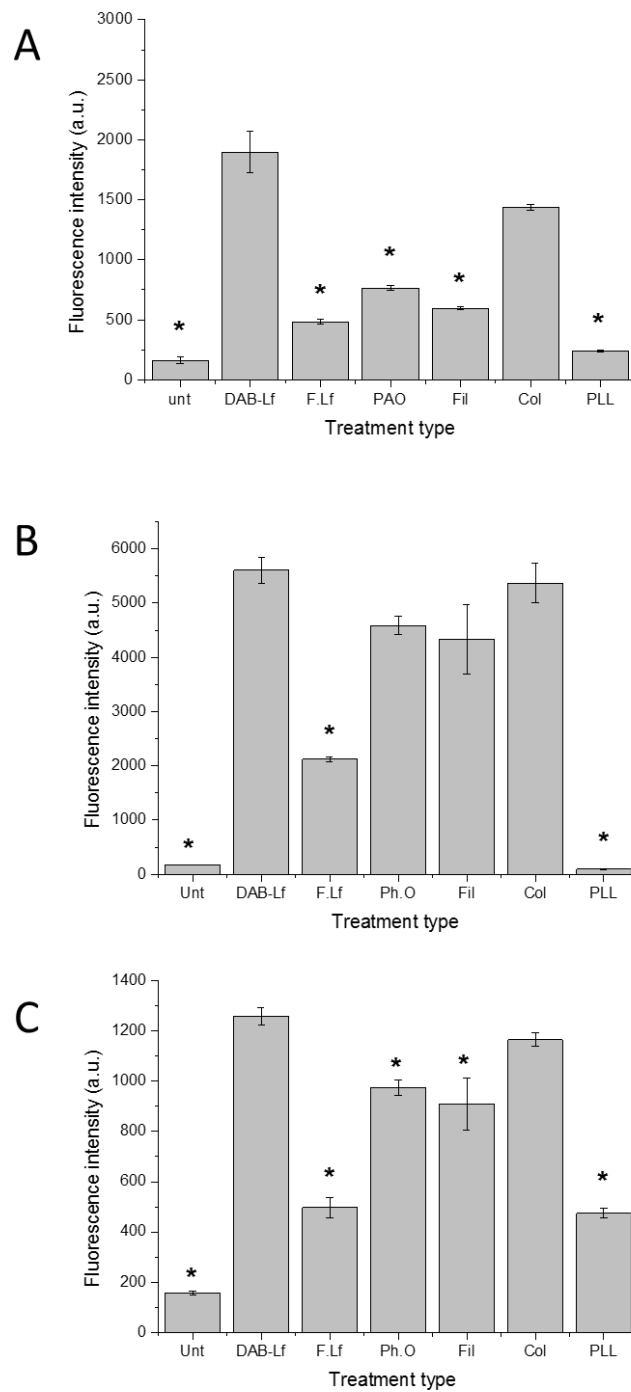


Figure 3-21 Flow cytometry quantification of the cellular uptake of fluorescein-labelled DNA complexed to DAB-Lf dendrimer in PC-3 (A), DU145 (B) and LNCaP (C) prostate cancer cell lines after pre-treating them with different uptake inhibitors: free lactoferrin (Lf), phenylarsine oxide (Ph.O), filipin (Fil), colchicine (Col) and poly-L-lysine (PLL) (n = 3), *: p < 0.05 compared with DAB-Lf dendriplex without pre-treatment.

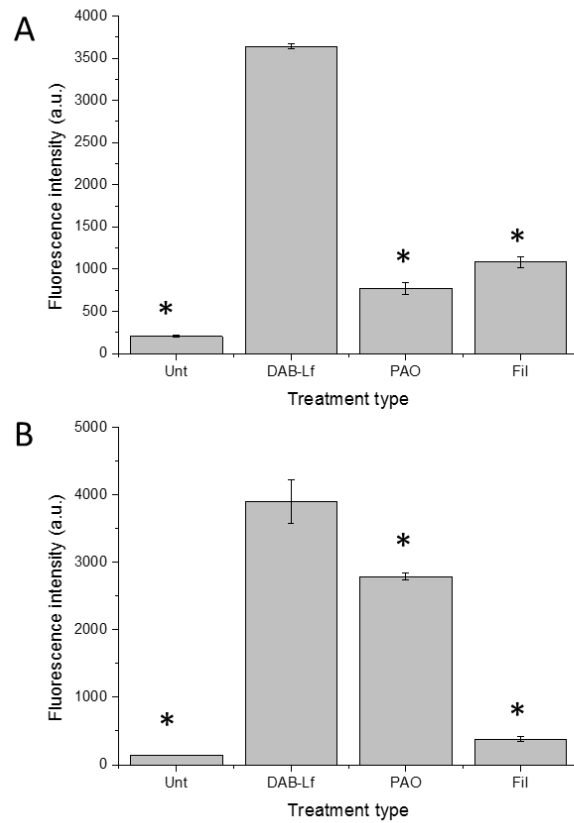
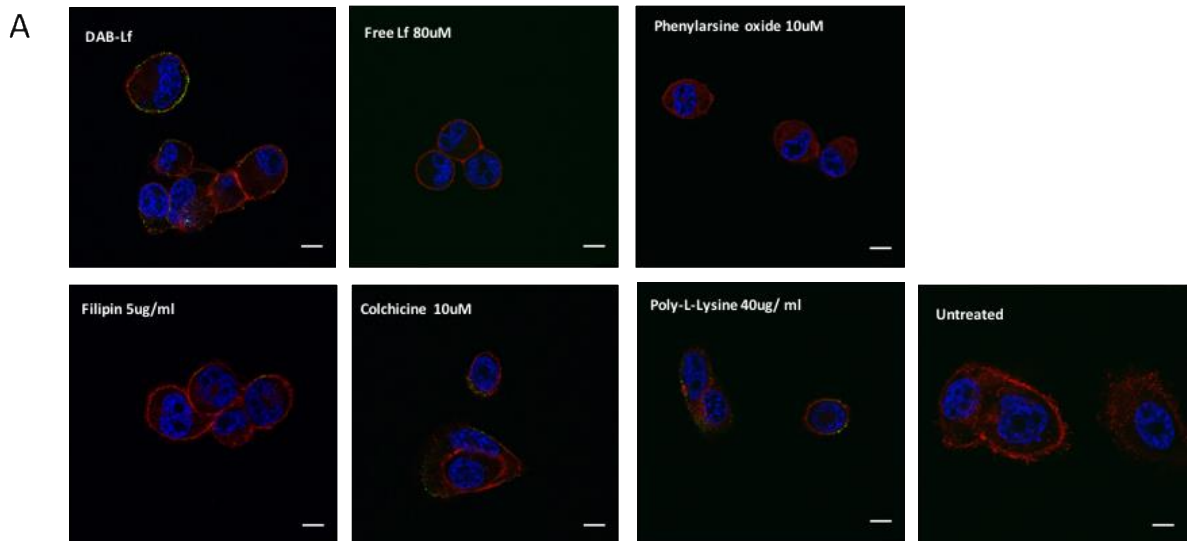


Figure 3-22 Flow cytometry quantification of the cellular uptake of fluorescein-labelled DNA complexed to DAB-Lf dendrimer in PC-3 (A) and DU145 (B) cells after pre-treating them with phenylarsine oxide (Ph.O) 20 μ M, and filipin (Fil) 10 μ g/ml (n = 3), *: p < 0.05 compared with DAB-Lf dendriplex without pre-treatment.



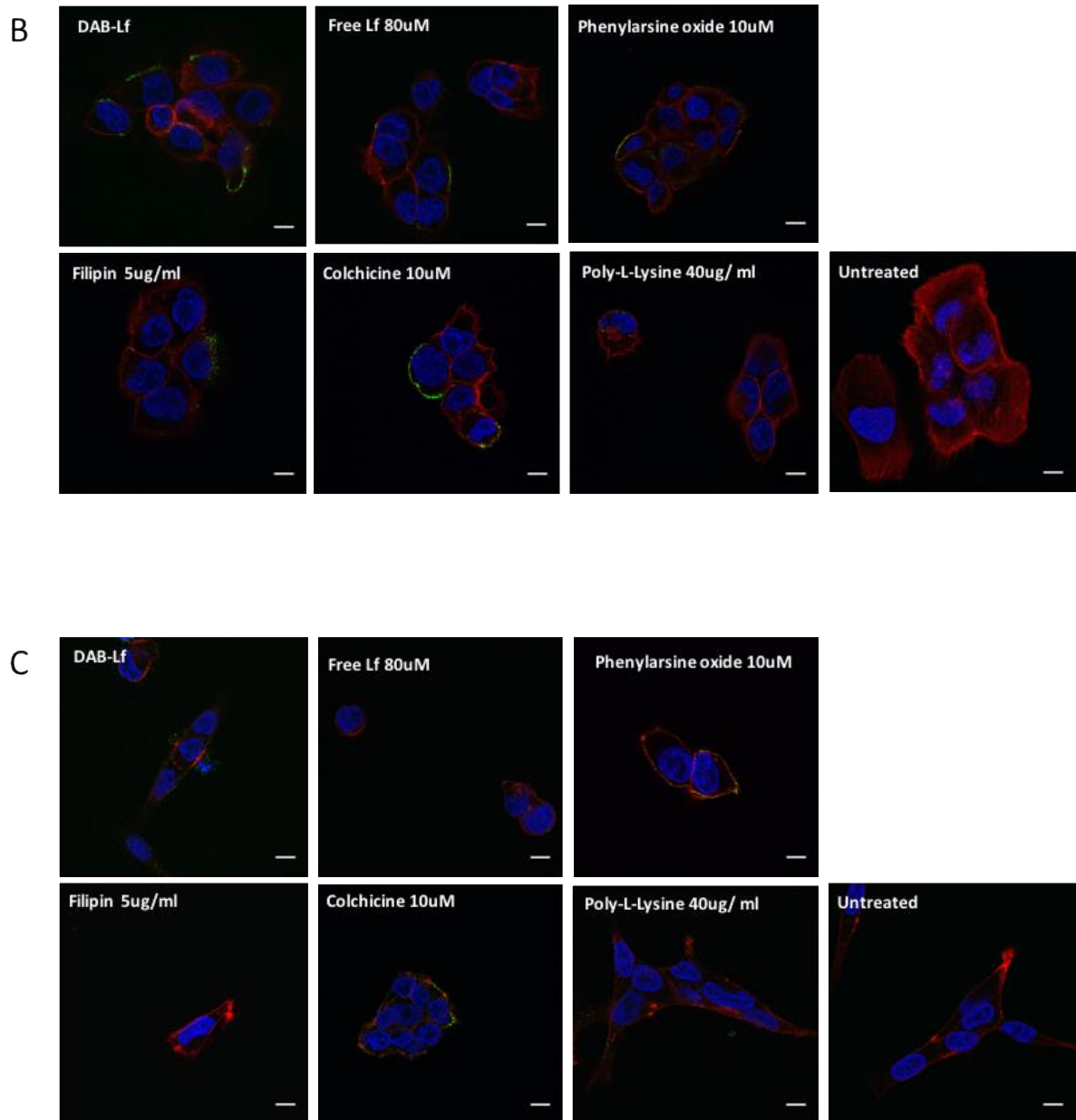


Figure 3-23 Confocal microscopy imaging of A) PC-3, B) DU145 and C) LNCaP cells, showing the cellular uptake of fluorescein-labeled DNA (2.5 $\mu\text{g}/\text{well}$) complexed with DAB-Lf, after pre-treatment with various cellular uptake inhibitors: poly-L-lysine (PLL), phenylarsine oxide (Ph.O), filipin (Fil), colchicine (Col) and free lactoferrin (Lf) (B). Blue: nuclei stained with DAPI (excitation: 365 nm, emission bandwidth: 435–485 nm), green: fluorescein-labeled DNA (excitation: 470 nm, emission bandwidth: 515–555 nm), red: Alexa Fluor[®] 647 probes (excitation: 633 nm laser line, bandwidth: 650-690 nm) (Bar: 10 μm).

DAB-Lf dendriplex cellular uptake inhibition by several inhibitors of different apoptosis pathways was qualitatively measured by confocal microscopy as well. In the PC-3 cell line, after treatment with DAB-Lf dendriplex pretreated with poly-L-lysine and colchicine, the confocal images showed a similar diffusion of the DNA around the cell membrane in comparison with the positive control. The other blockers seemed to cause some degree of uptake inhibition, as relatively minimal green fluorescence was detected in the cells compared with the control. All of the data are consistent with the FACS experiment measurements, except for poly-L-lysine, as cells pretreated with it showed no sign of uptake inhibition (Figure 3-23, A).

In DU145 and LNCaP cells, pre-treating the cells with PLL, phenylarsine oxide, filipin and free lactoferrin resulted in a decrease in fluorescein-labeled DNA uptake as indication for uptake inhibition in comparison with the positive control. By contrast, there was no sign of uptake inhibition in cells pre-treated with colchicine, as the fluorescence detected was almost similar to the positive control (Figure 3-23, B and C).

It is important to note that due to the short incubation period (one hour), the fluorescence in the cell lines (Figure 3-23), was quite minimal and accumulated in the cell membranes but not inside the cytoplasm.

3.3.3.2. DAB-PEG2k-Peptide2

DAB-PEG2k-Pep2 dendriplex cellular uptake inhibition by several inhibitors of different apoptosis pathways was quantitatively measured by flow cytometry to investigate and confirm the mechanism of the dendriplex uptake by the cells.

For the three cell lines examined, pretreating the cells with PLL resulted in more than 80% blockage of DAB-PEG2k-Pep2 dendriplex uptake in the PSMA-negative cell lines PC-3 and DU145, whereas it caused only 45% blockage of the uptake in the PSMA-positive cell line LNCaP. Pretreating cells with 2.5 μ M of Peptide2 resulted in around 50% decrease in the uptake of Pep2 targeted dendriplex in all cell lines examined, with no significant difference among them. Pretreating PSMA-negative cell lines PC-3 and DU145 with phenylarsine oxide (Ph.O) 20 μ M caused around 83% and 28% blockage in the dendriplex uptake respectively. On the other hand, Ph.O caused no reduction in dendriplex uptake after treating PSMA-positive cell line LNCaP. Filipin (10 μ g) caused significant reduction in the cellular uptake of DAB-PEG2k-Pep2 dendriplex with varied extent among cell lines. There was 44% inhibition of uptake in PC-3 cells and 36.4% in LNCaP cells, while inhibition in DU145 cells was 84%. Finally, pre-treating cells with colchicine resulted in around 60% reduction in the uptake of PC-3 and DU145 cells, while it was 37% decrease in dendriplex uptake in LNCaP cells compared with the positive control (DAB-PEG2k-Pep2 dendriplex without pretreatment).

In PC-3 and DU145 cell lines, all of the blockers examined caused significant and varied reductions in the uptake of the dendriplex DAB-PEG2k-Pep2. In PC-3 cells, PLL and Ph.O caused almost complete uptake inhibition, with mean fluorescence intensities of 346.6 ± 14.5 a.u. and 347.6 ± 28.8 a.u. respectively. The other three inhibitors used (Peptide2, filipin and colchicine) reduced fluorescence intensity by 1.7-, 1.8- and 2.5-fold respectively, with values of 1177 ± 39.4 , 1148 ± 85.7 and 816.0 ± 93.2 a.u. respectively, compared with the positive control value of 2047 ± 209 a.u.

In the DU145 cell line, PLL and filipin caused the most significant inhibition of uptake compared with the other blockers used, with mean fluorescence intensity of 222.6 ± 3.75 a.u. and 507.3 ± 47.8 a.u. respectively. Peptide2 and colchicine pretreatment resulted respectively in 3- and 3.5-fold reductions in cellular uptake of the dendriplex, with mean values of 1029 ± 41.5 a.u. and 881.0 ± 123 a.u. Finally, pretreating DU145 with Ph.O caused a 1.3-fold reduction in uptake, with a mean value of 2223 ± 70.3 a.u., compared with 3090 ± 387 a.u. for the unblocked samples.

For the PSMA-positive cell line LNCaP, all of the blockers used resulted in a 40% to 50% reduction in dendriplex uptake, except for Ph.O, which had no blockage effect. There was 2.16- and 1.8-fold reductions in the dendriplex uptake after pre-treating LNCaP cells with Peptide2 and PLL, with mean fluorescence intensity of 839.3 ± 44.4 a.u. and 997.6 ± 80.4 a.u. respectively. The other two blockers, filipin and colchicine, reduced the uptake by 1.57- and 1.58-fold with mean fluorescence intensity of 1154 ± 17.6 a.u. and 1148 ± 45.9 a.u. respectively, compared with 1815 ± 85.4 a.u. for unblocked samples.

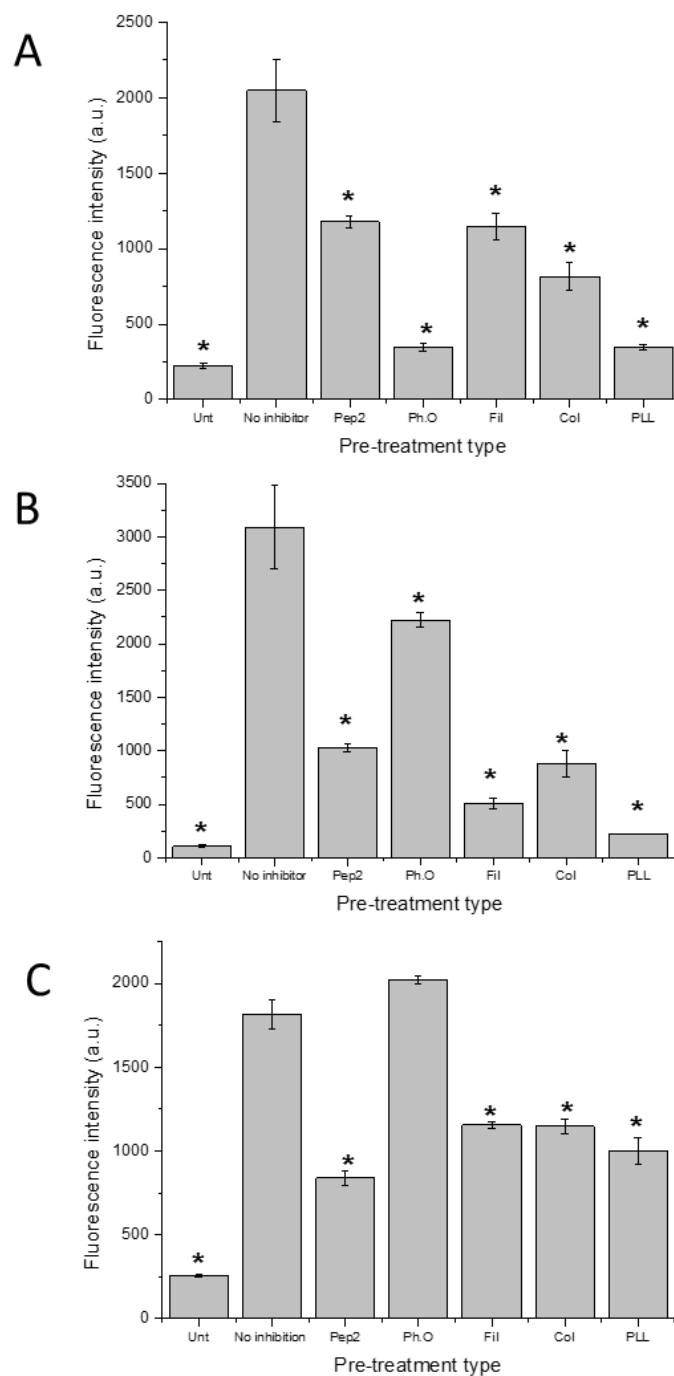


Figure 3-24 Flow cytometry quantification of the cellular uptake of fluorescein-labelled DNA complexed to DAB-PEG2k-Peptide2 dendrimer in prostate cell lines PC-3 (A), DU145 (B) and LNCaP (C) after pretreatment with uptake inhibitors: free Peptide2 (Pep2), phenylarsine oxide (Ph.O), filipin (Fil), colchicine (Col) and poly-L-lysine (PLL) (n = 3), *: p < 0.05 compared with untreated DAB-PEG2k-Pep2 dendriplex.

3.3.4. Peptide2 binding affinity assay

The successful conjugation between FITC and Peptide2 was confirmed using MALDI-TOF (Figure 3-25). The peak at m/z 1921.08 ($z=1$) corresponds to the compound FITC-Pep2 with molar mass 1970. The difference between the actual and detected molar mass of FITC-Pep2 could be due to the loss of COOH group in leucine amino acid (46 m/z), which is a common fragmentation pattern in amino acids and peptides during MALDI analysis (Gogichaeva *et al.*, 2007).

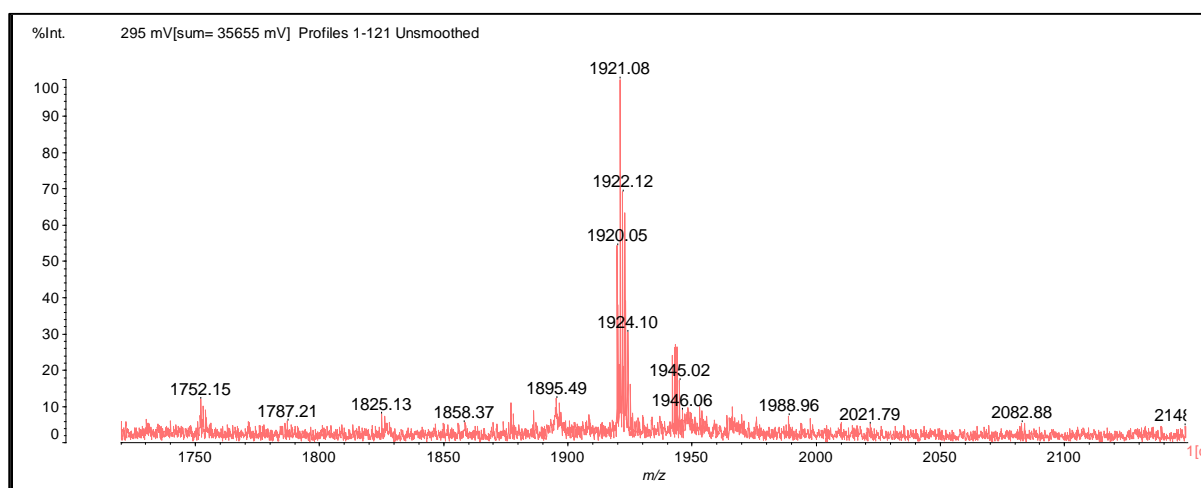


Figure 3-25 MALDI-TOF spectrum of Peptide2 -FITC

All of the cell lines treated with different concentrations of Peptide2 showed different extents of cellular uptake, with higher fluorescence than untreated cells. However, the PSMA-positive LNCaP cells showed significant uptake of FITC-Pep2 compared with PSMA-negative PC-3 and DU145 cells at all concentrations examined, with a mean fluorescence intensity of 4808 ± 545 a.u. for LNCaP cells, compared with 1912 ± 90.3 a.u. and 1074 ± 41.5 a.u. for PC-3 and DU145 cells respectively at the same FITC-Pep2 concentration (100 $\mu\text{g/ml}$). Although PSMA-negative cell lines showed some cellular uptake of FITC-Pep2, the uptake was significantly lower than the one obtained in LNCaP cells.

This assay also investigated the proportion of the cellular population that FITC-Pep2 binds to. Almost half of the LNCaP cells were successfully bound to FITC-Pep2 after 15 minutes incubation, whereas the cellular population percent reduced to 33.9% and 29.4% for the PSMA-negative PC-3 and DU145 cells respectively (

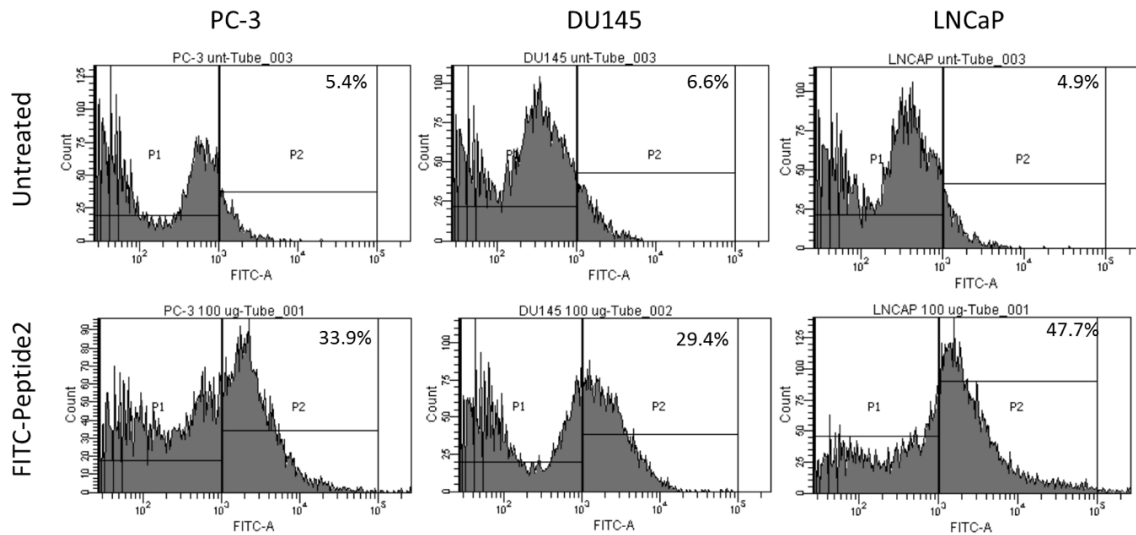


Figure 3-27).

These results provide strong evidence for the successful uptake of Peptide2 by the LNCaP cells compared with PC-3 and DU145 cells, which showed some uptake but not to the same extent as the PSMA-positive cells (Figure 3-26).

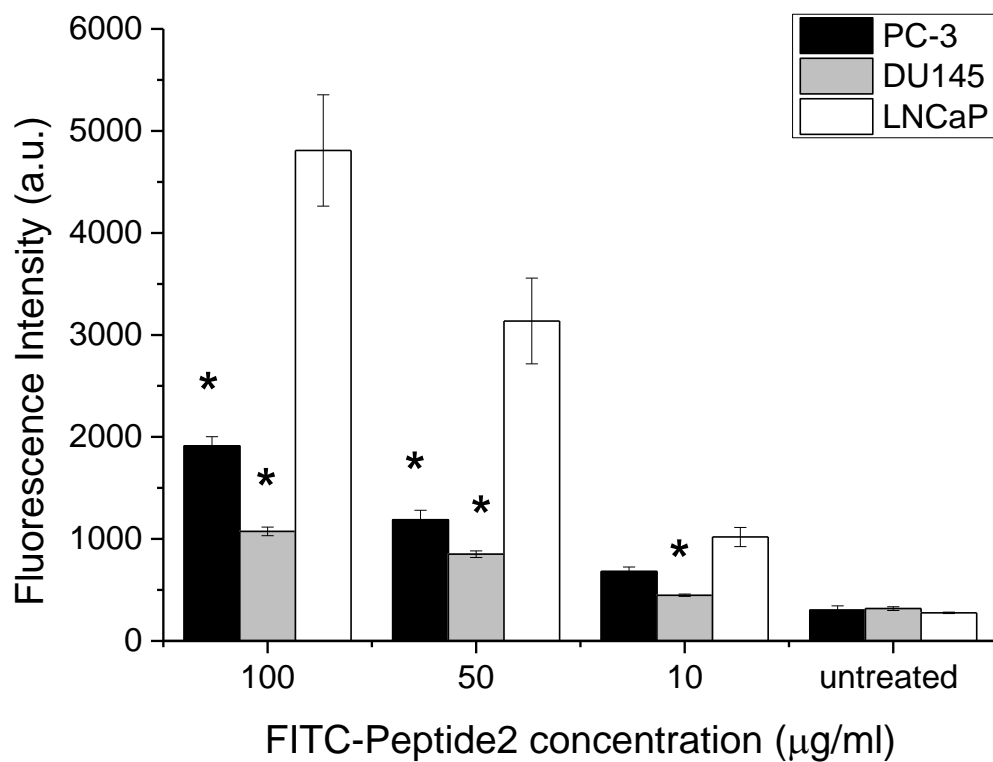


Figure 3-26 Cellular uptake intensity of Peptide2 labelled with FITC in PC-3 (black), DU145 (grey) and LNCaP (white) cell lines (n=3) *: $P \leq 0.05$ compared with the fluorescence intensity of the highest binding at the same concentration.

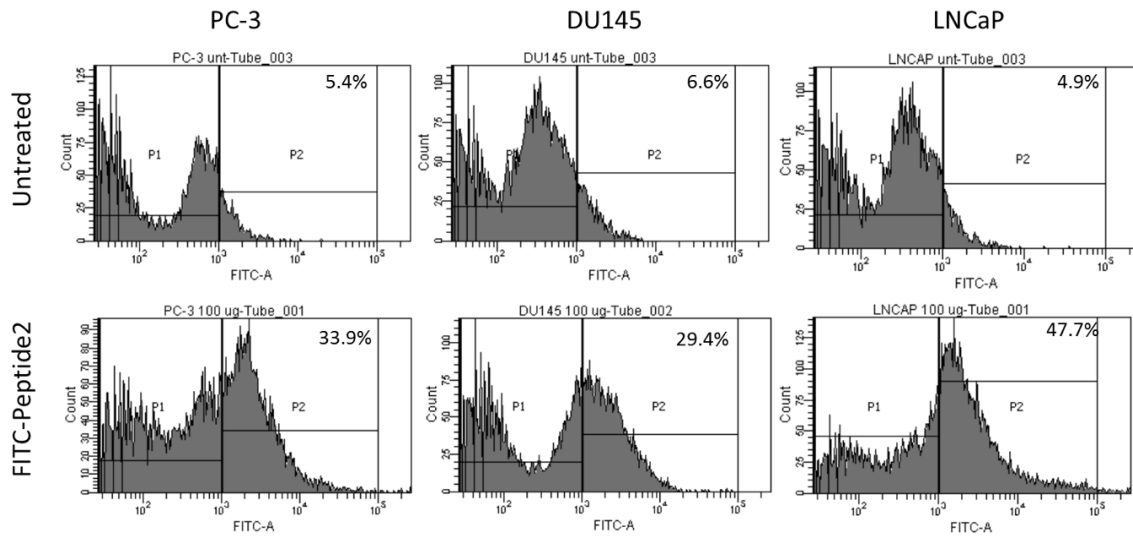


Figure 3-27 Cellular uptake intensity histograms of Peptide2 labelled with FITC in PC-3, DU145 and LNCaP cell lines. The P2 gate represents the percentage of cells with positive FITC-Pep2 binding.

3.3.5. Enzyme-linked immunosorbent assay

All the three cell lines examined successfully produced the cytokine of interest, mTNF α but with various amounts following treatment with DAB-PEG2k-Pep2 dendrimer complexed with DNA encoding mTNF α . After 12 hours of treating cells, the assay detected no TNF α protein in any of the cell lines. PC-3 cells successfully produced some mTNF α cytokine after 24 hours of treatment, whereas the amounts produced by LNCaP and DU145 cells were still undetectable.

In the PSMA-positive LNCaP cell line, the cytokine began to be detectable after two days of incubation and the quantity produced gradually increased until, after seven days of incubation, there was a mean TNF α concentration of 162.6 ± 15.4 pg/ml. Similarly, in DU145 cells, a detectable amount of TNF α was measured after 48 h of incubation and this gradually increased until Day 7, but at a mean concentration of 59.38 ± 5.78 pg/ml, less than half of the LNCaP value. Figure 3-28(A) shows that PC-3 cells started to transfect TNF α earlier than the other cell lines, as noted above, and that the concentration was considerably higher than in the other two lines throughout the period of incubation. It increased sharply until 48 h, when it plateaued at a mean value of around 3.5 ng/ml for a further four days, before decreasing to roughly half this value at Day 7.

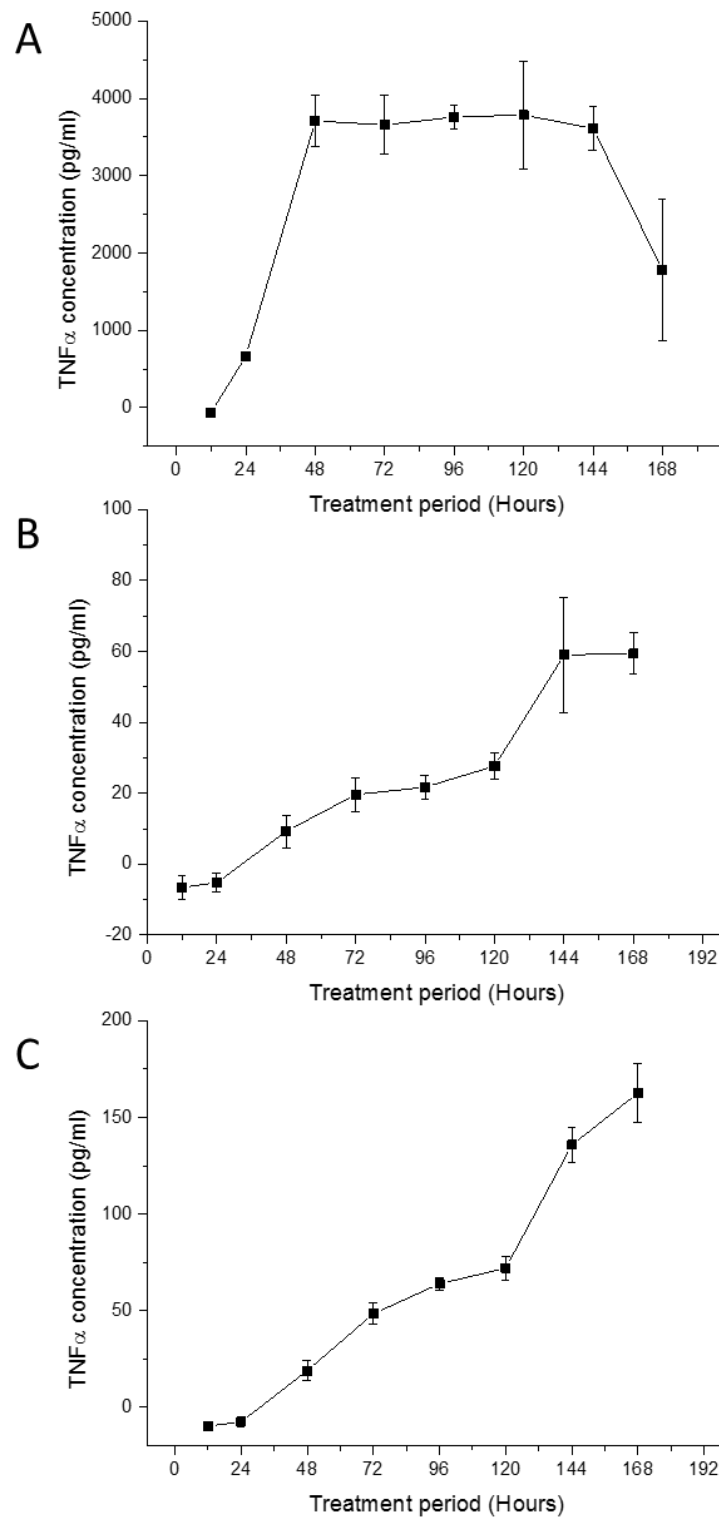


Figure 3-28 DAB-PEG2k-Peptide2 dendriplex-mediated transfection of TNF α after different treatment periods in A) PC-3, B) DU145 and C) LNCaP cell lines, using ELISA as detection method (n = 3).

3.3.6. Tetrazolium reduction assay (MTT)

3.3.6.1. DAB-Lf

Lactoferrin-bearing DAB dendriplex significantly increased the *in vitro* anti-proliferation effect of the therapeutic DNA (TNF α , TRAIL, or IL-12) in PC-3 and DU145 cells. In PC-3 cells, there was a 1.95-fold increase in the anti-proliferative effect in DAB-Lf dendriplex compared with the unconjugated DAB, with an IC₅₀ of 9.97 ± 1.38 $\mu\text{g/ml}$ and 19.5 ± 3.43 $\mu\text{g/ml}$ for DNA encoding TNF α respectively (Figure 3-29). For DNA encoding TRAIL, there was a 3.6-fold increase in the anti-proliferation effect of DAB-Lf upon DAB dendriplexes, at 15.6 ± 3.61 $\mu\text{g/ml}$ and 55.74 ± 22.3 $\mu\text{g/ml}$ respectively. The highest increase in the ratio between DAB-Lf and unmodified DAB dendriplexes in the PC-3 cell line was for DNA encoding IL-12, with an IC₅₀ of 10.8 ± 2.71 $\mu\text{g/ml}$ and 63.3 ± 37.8 $\mu\text{g/ml}$ for DAB-Lf and DAB dendriplexes respectively, recording a 5.86-fold increase in therapeutic effect.

In the DU 145 cells, the treatment of DAB-Lf: TNF α resulted in a 13.2-fold stronger anti-proliferation effect of the DAB-Lf to DAB dendriplexes, with an IC₅₀ of 4.34 ± 0.681 $\mu\text{g/ml}$ and 57.38 ± 95.4 $\mu\text{g/ml}$ respectively. The DNA encoding TRAIL showed a 5.6-fold increase in its anti-proliferation activity after being complexed with DAB-Lf compared with DAB with an IC₅₀ of 3.03 ± 0.69 $\mu\text{g/ml}$ and 17.13 ± 3.77 $\mu\text{g/ml}$ respectively for DAB-Lf and DAB dendriplexes. For the DNA encoding IL-12, 1.6-fold increase in the anti-proliferation between DAB-Lf and DAB was detected with 3.79 ± 0.97 $\mu\text{g/ml}$ for DAB-Lf and 5.92 ± 0.95 $\mu\text{g/ml}$ for unmodified DAB. LNCaP cell line data are still under analysis (Figure 3-30).

In LNCaP cells, the response of cells significantly fluctuated, making the initiation of dose response curve complicated and the data obtained from these curves end to be inaccurate. This is actually due to the nature of LNCaP cells that can easily become detached following the

addition of the MTT solution. Therefore, some of the formazan may have disappeared during medium removal.

Cytotoxicity tests were also performed on the DAB-Lf and DAB nano-carriers without complexing the therapeutic DNA to determine whether the source of the anti-proliferation effect was either the DNA or simply the toxicity of the designed nano-carrier. In all of the cell lines examined, the modified dendrimer DAB-Lf and DAB were found to have 100% survival rate and higher IC_{50} values compared with their dendriplexes, indicating that any therapeutic effect detected in DAB-Lf: DNA and DAB: DNA was from the internalization of the therapeutic DNA inside the cells (

Table 3-2). These findings support our hypothesis that lactoferrin protein improves the transfection of the gene inside the cells, and therefore improve the anti-proliferation effect of the therapeutic gene. Thus, conjugation DAB dendrimer with Lf initiated a prominent gene carrier to target prostate cancer.

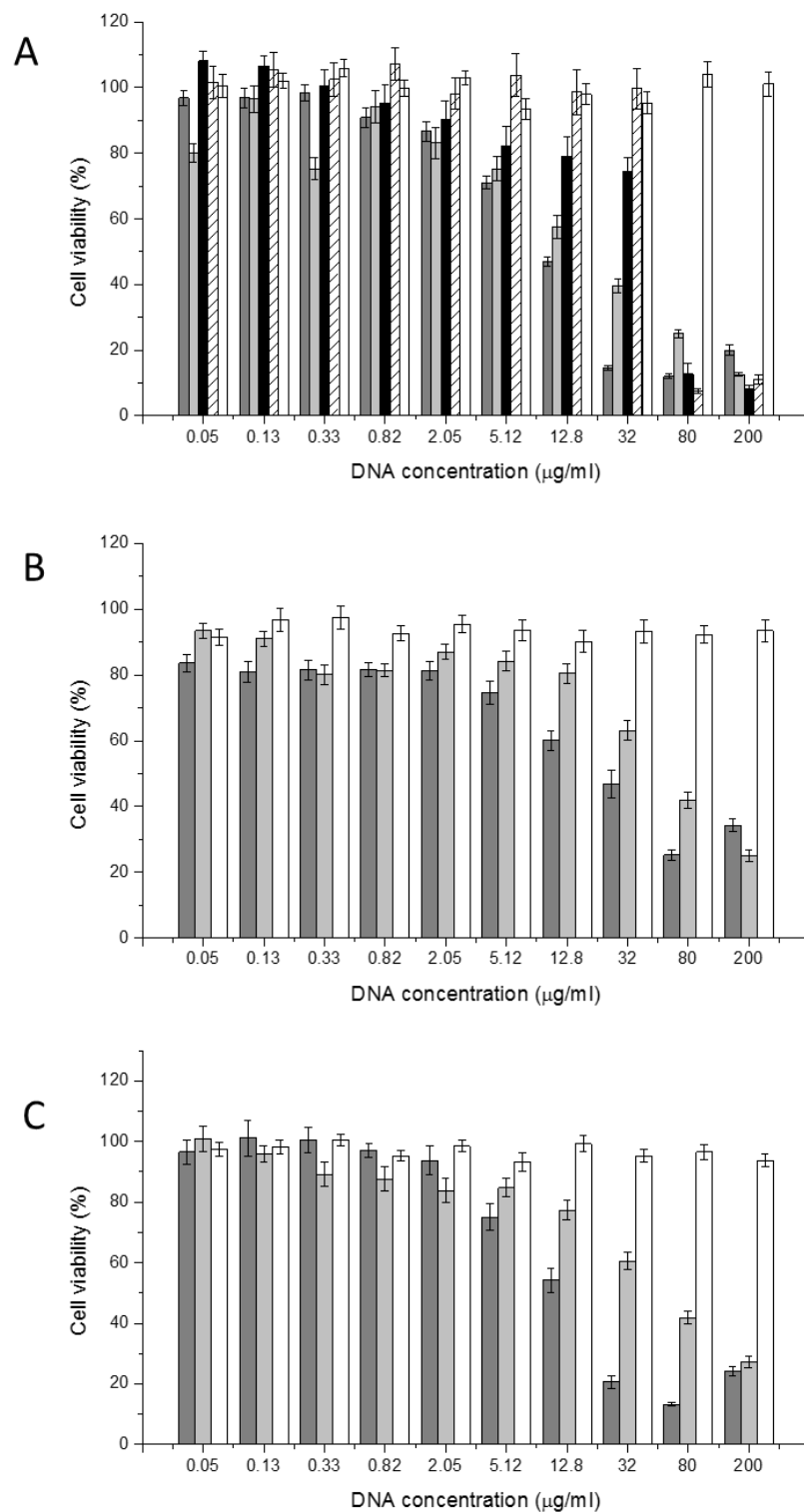


Figure 3-29 Anti-proliferative effect of DAB-Lf: DNA, DAB:DNA, DNA, DAB-Lf and DAB in PC-3 cell line at different concentrations (0.05 to 200 µg/ml), using various therapeutic DNA encoding A) TNF, B) TRAIL, C) IL-12. (Dark grey: DAB-Lf: DNA, grey: DAB: DNA, black: DAB-Lf only, striped white: DAB only, white: DNA only) (n = 15).

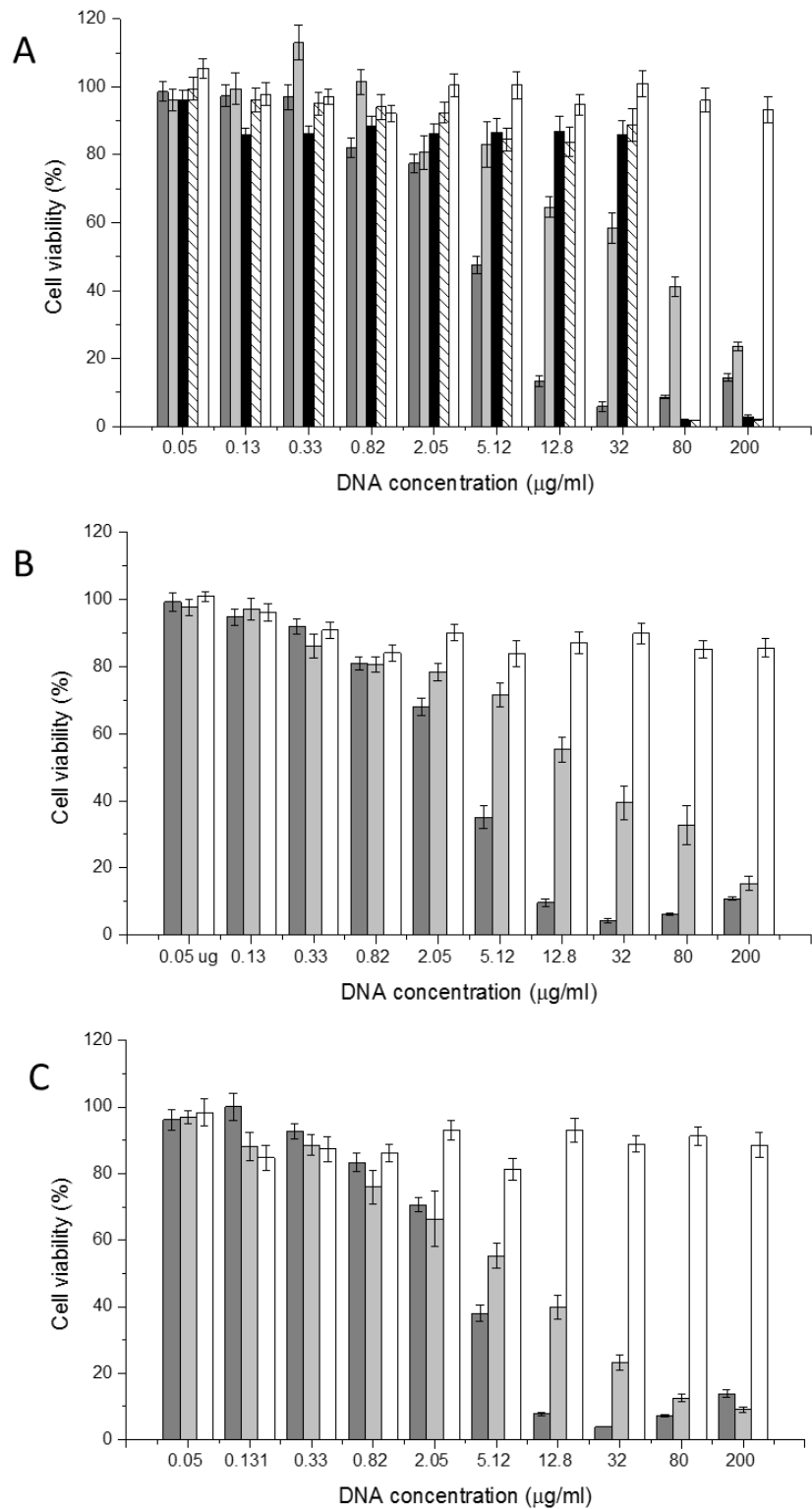


Figure 3-30 Anti-proliferative effect of DAB-Lf: DNA, DAB:DNA, DNA, DAB-Lf and DAB in DU145 cell line at different concentrations (0.05 to 200 µg/ml), using various therapeutic DNA encoding A) TNF, B) TRAIL, C) IL-12. (Dark grey: DAB-Lf: DNA, grey: DAB: DNA, black: DAB-Lf only, striped white: DAB only, white: DNA only) (n = 15).

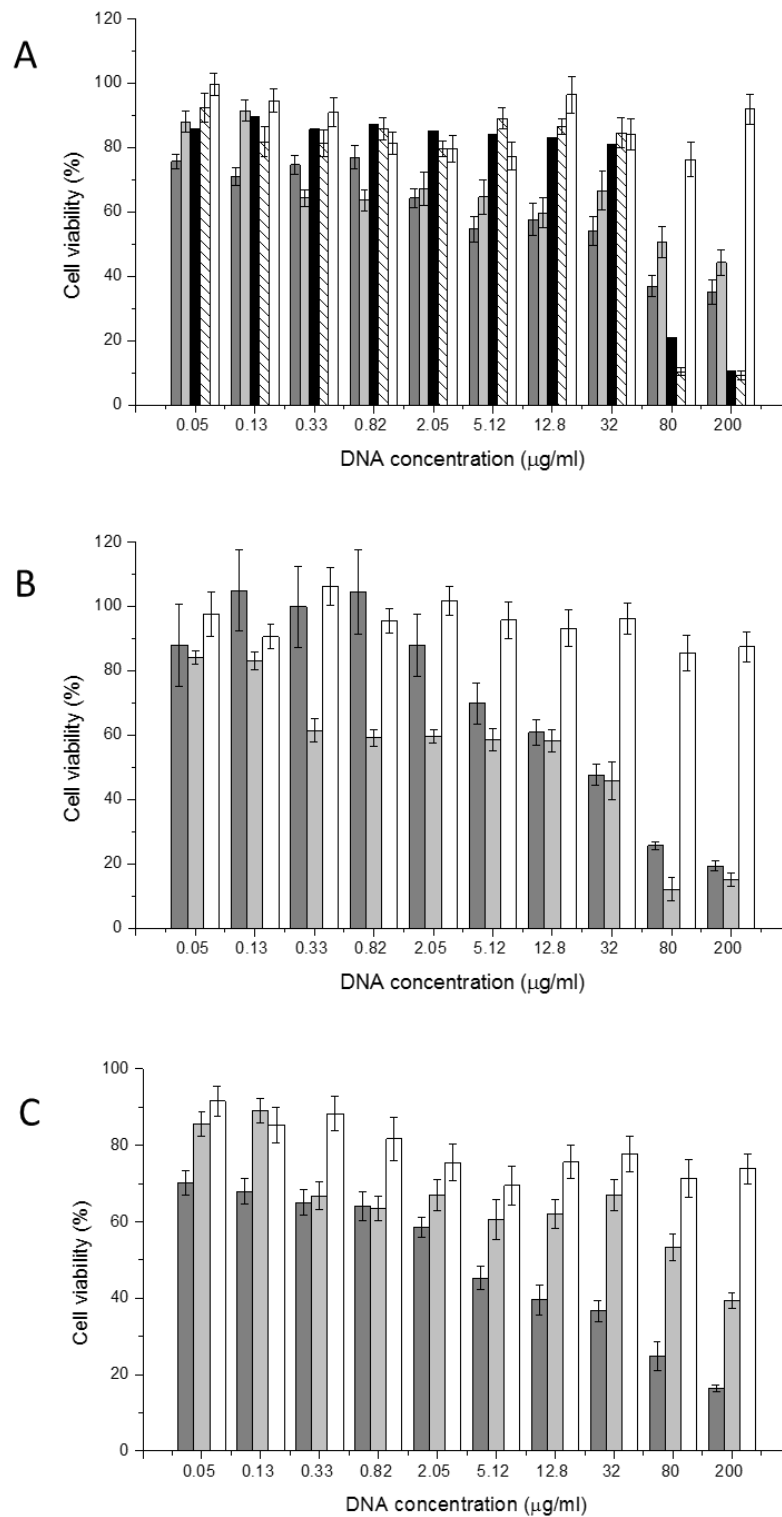


Figure 3-31. Anti-proliferative effect of DAB-Lf: DNA, DAB: DNA, DNA, DAB-Lf and DAB in LNCaP cell line at different concentrations (0.05 to 200 µg/ml), using various therapeutic DNA encoding A) TNF, B) TRAIL, C) IL-12. (Dark grey: DAB-Lf: DNA, grey: DAB: DNA, black: DAB-Lf only, striped white: DAB only, white: DNA only) (n = 15).

Table 3-2 Anti-proliferative activity of DAB-Lf and DAB complexed with various therapeutic DNA (TNF α , TRAIL or IL-12) and the cytotoxic effect of the dendrimers on PC-3, DU145 and LNCaP prostate cancer cell lines.

Cell line	DNA	IC ₅₀ (μ g/ml)				
		DAB-Lf: DNA	DAB:DNA	DAB-Lf	DAB	DNA
PC-3	TNF α	9.97 \pm 1.38	19.5 \pm 8.82	> 50	> 50	n.d.
	TRAIL	15.6 \pm 3.61	55.7 \pm 22.4	> 50	> 50	n.d.
	IL-12	10.8 \pm 2.71	63.3 \pm 37.8	> 50	> 50	n.d.
DU145	TNF α	4.34 \pm 0.68	57.4 \pm 9.51	> 50	> 50	n.d.
	TRAIL	3.03 \pm 0.69	17.1 \pm 3.77	> 50	> 50	n.d.
	IL-12	3.79 \pm 0.97	5.92 \pm 0.95	> 50	> 50	n.d.
LNCaP	TNF α	31.8 \pm 71.5	40.8 \pm 2.64	> 50	> 50	n.d.
	TRAIL	9.85 \pm 5.79	28.2 \pm 46.6	> 50	> 50	n.d.
	IL-12	7.04 \pm 2.68	-	> 50	> 50	n.d.

- n.d. not determined

3.3.6.2. DAB-Peptide2

A preliminary screening for the cytotoxicity of DAB-Pep2 dendrimer was examined in DU145 cell line, to test the safety of this dendrimer. The antiproliferative effect of DAB-Pep2 only and of DAB-Pep2 complexed with DNA encoding TNF α was examined. The data showed that the uncomplexed DAB-Pep2 dendrimer was 100% toxic at a concentration of 64 $\mu\text{g/ml}$, whereas when it was complexed with DNA encoding TNF α (32 $\mu\text{g/ml}$), the toxicity of the formulation decreased at the same concentration (Figure 3-32). As the formulation is toxic, we cannot estimate the improvement in the antiproliferative effect of TNF α and any therapeutic effect would be due to the toxicity of the formulation, rather than to the improvement in delivering the therapeutic DNA to induce apoptosis.

From the above data we can conclude that this formulation needs to be modified. The aim of the modification would be to reduce its cytotoxic effect by lowering the zeta potential of the formulation.

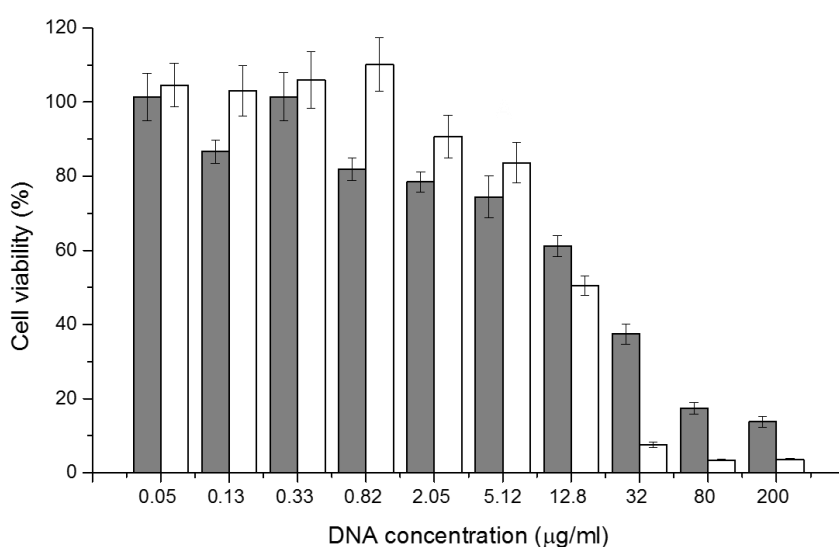


Figure 3-32 Anti-proliferative effect of DAB-Peptide2: DNA (dark grey), and DAB-Peptide2 (white) in DU145 cell line at different concentrations (200 to 0.05 $\mu\text{g/ml}$), using therapeutic DNA encoding TNF α (n = 15).

3.3.6.3. DAB-PEG2k-Peptide2

The antiproliferative effect of DAB-PEG2k-Pep2 dendriplex was examined in the PSMA-negative cell lines PC-3 and DU145 and in the PSMA-positive cell line LNCaP after complexing it with DNA encoding TNF α or TRAIL as apoptosis-inducing cytokines.

Treating PC-3 cells with DAB-PEG2k-Pep2: DNA encoding TNF α dendriplex resulted in an IC₅₀ of 36.04 ± 1.52 μ g/ml, whereas the untargeted dendriplex DAB-PEG: TNF α had a more effective anti-proliferative effect, with a lower IC₅₀ of 25.4 ± 6.93 μ g/ml. However, uncomplexed polymers were found to have almost the same cytotoxic effect as the dendriplexes. Thus, the therapeutic effect of DNA encoding TNF α is uncertain and cannot be determined. This issue did not arise with the other therapeutic DNA, encoding TRAIL, as lower IC₅₀ values were recorded: the IC₅₀ values of DAB-PEG2k-Pep2 and DAB-PEG complexed with DNA encoding TRAIL were 17.1 ± 5.79 μ g/ml and 13.4 ± 3.95 μ g/ml respectively.

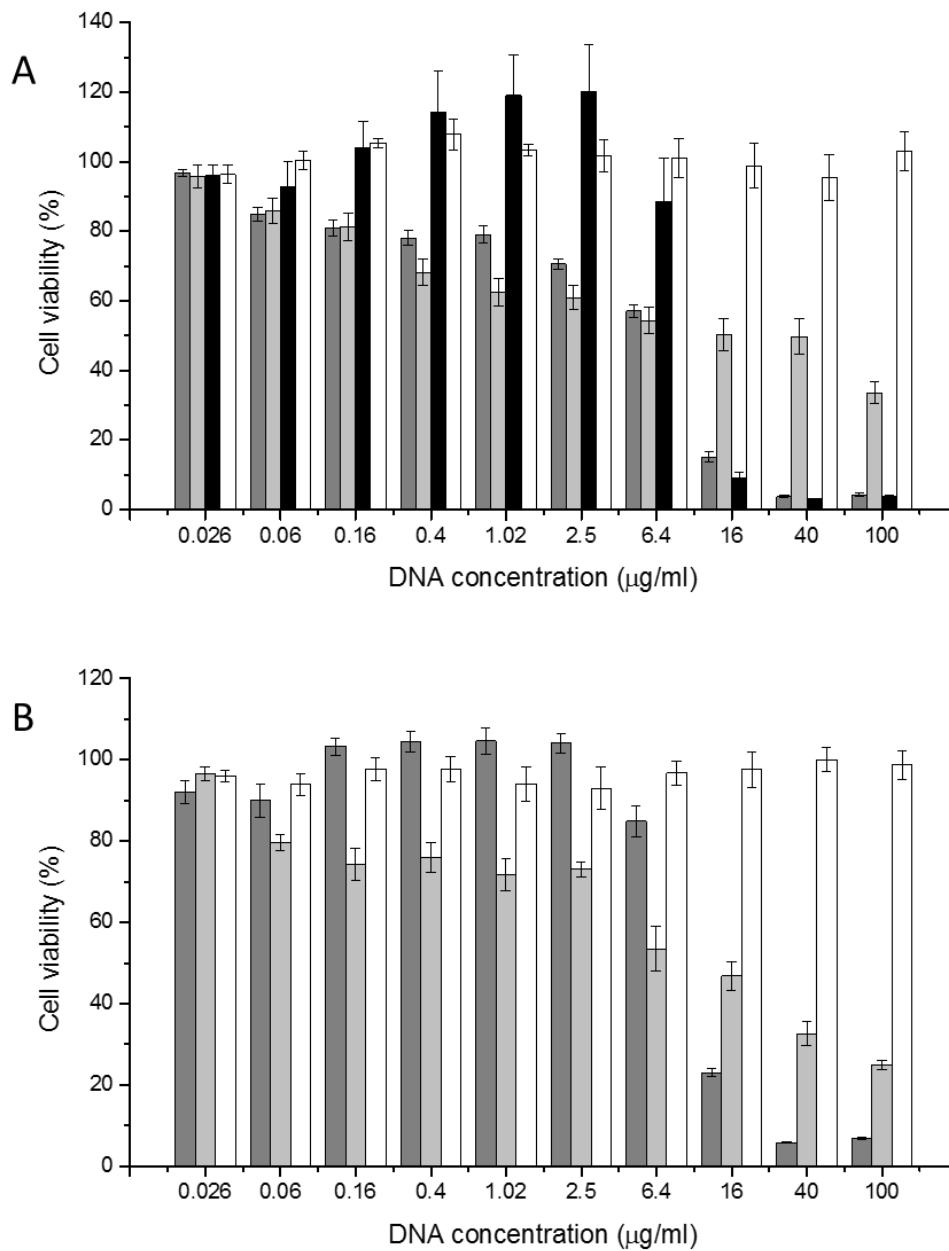


Figure 3-33 Anti-proliferative effect of DAB-PEG2k-Peptide2: DNA, DAB-PEG: DNA, DAB-PEG2k-Peptide2 only, and DNA in PC-3 cells at different concentrations (0.026 to 100 µg/ml), using various therapeutic DNAs encoding A) TNF and B) TRAIL. (Dark grey: DAB-PEG2k-Pep2: DNA, grey: DAB-PEG: DNA, black: DAB-PEG2k-Pep2 only and white: DNA only) (n = 15).

Treating DU145 cells with DAB-PEG2k-Pep2: DNA encoding TNF α dendriplex resulted in an IC₅₀ of 10.58 ± 10.37 $\mu\text{g/ml}$ whereas the untargeted DAB-PEG dendrimer complexed with DNA encoding TNF α showed IC₅₀ value of 6.79 ± 4.22 $\mu\text{g/ml}$. Uncomplexed polymer was toxic at the very high concentrations from 2 to 0.32 mg/ml then the toxicity of the polymer diminished completely. Thus, the therapeutic impact of the dendriplex at the DNA concentrations from 6.4 $\mu\text{g/ml}$ and lower is due to the impact of the DNA used. In both examined DNA, non-targeted dendriplex (DAB-PEG: DNA) showed superior anti-proliferative effect compared with the targeted formulation (DAB-PEG2k-Pep2: DNA) in both DNA encoding TNF α and TRAIL (Table 3-3, Figure 3-34).

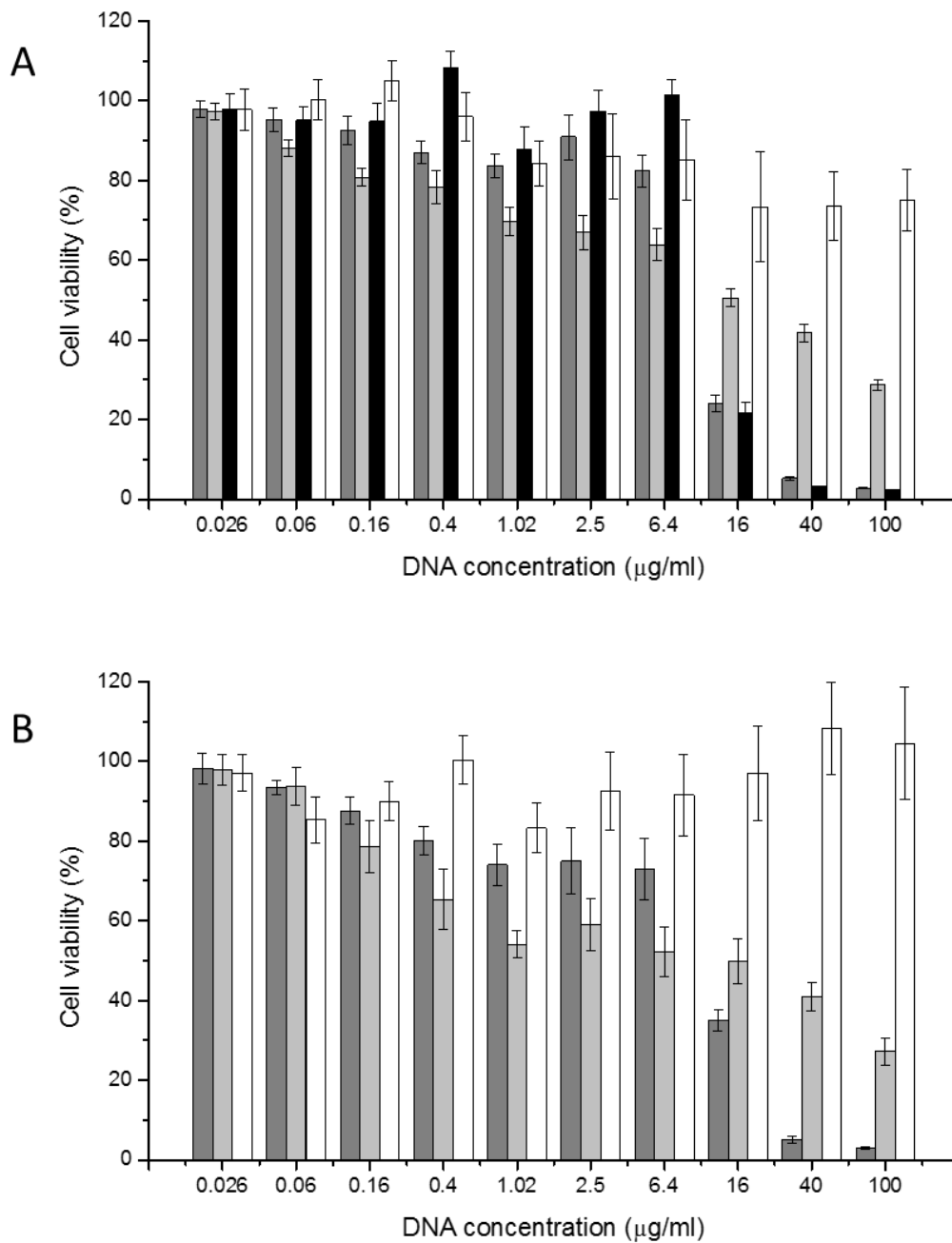


Figure 3-34 Anti-proliferative effect of DAB-PEG2k-Peptide2: DNA, DAB-PEG: DNA, DAB-PEG2k-Peptide2 only, and DNA in DU145 cells at different concentrations (0.026 to 100 µg/ml), using various therapeutic DNAs encoding A) TNF and B) TRAIL. (Dark grey: DAB-PEG2k-Pep2: DNA, grey: DAB-PEG: DNA, black: DAB-PEG2k-Pep2 only and white: DNA only) (n = 15).

Treating the positive control LNCaP cells with DAB-PEG2k-Pep2 dendrimer complexed with DNA encoding TNF α dendriplex resulted in an IC₅₀ of 4.76 \pm 2.66 μ g/ml, whereas the untargeted dendriplex DAB-PEG: TNF α had a significantly higher IC₅₀ value of 14.03 \pm 25.96 μ g/ml. DAB-PEG2k-Pep2 dendrimer alone was not toxic at the same concentration. Treating LNCaP cells with DNA encoding TRAIL complexed with DAB-PEG2k-Pep2 resulted in an improvement in the anti-proliferation compared with non-targeted dendriplex. However, at higher DNA concentrations, DAB-PEG2k-Pep2: DNA encoding TRAIL dendriplex recorded a significantly stronger antiproliferative effect than the non-targeted dendriplex and the dendrimer only (Figure 3-35) at concentrations from 100 to 6.4 μ g/ml.

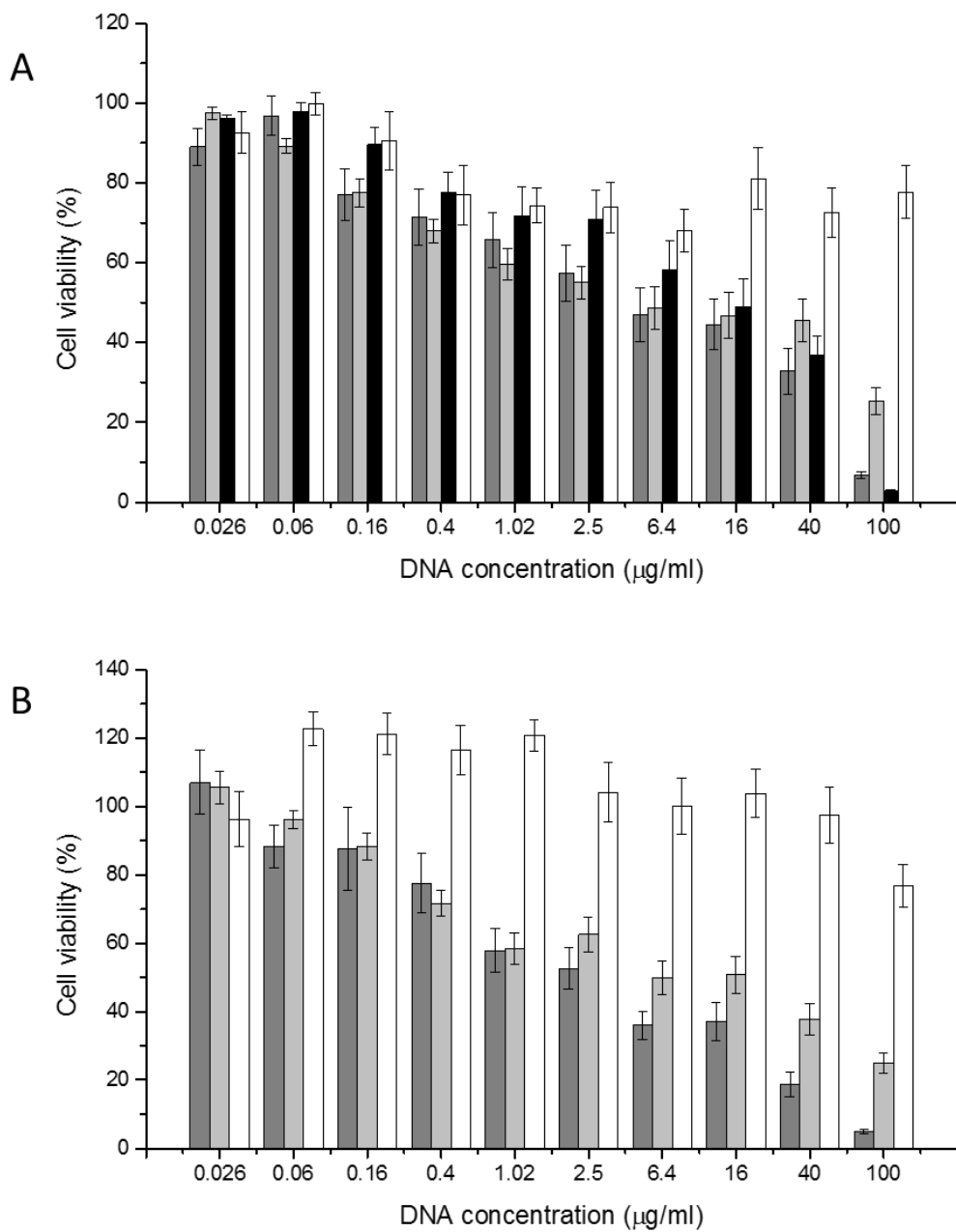


Figure 3-35 Anti-proliferative effect of DAB-PEG2k-Peptide2: DNA, DAB-PEG: DNA, DAB-PEG2k-Peptide2 only and DNA in LNCaP cells at different concentrations (0.026 to 100 µg/ml), using various therapeutic DNAs encoding A) TNF and B) TRAIL. (Dark grey: DAB-PEG2k-Pep2: DNA, grey: DAB-PEG: DNA, black: DAB-PEG2k-Pep2 only and white: DNA only) (n = 15).

Table 3-3 Anti-proliferative activity of DAB-PEG2k-Pep2 and DAB-PEG complexed with various therapeutic DNA (TNF α or TRAIL) and the cytotoxic effect of DAB-PEG2k-Pep2 dendrimer on PC-3, DU145 and LNCaP prostate cancer cell lines.

Cell line	DNA	IC ₅₀ (μ g/ml)			
		DAB-PEG2k-Pep2: DNA	DAB-PEG:DNA	DAB-PEG2k-Pep2	DNA
PC-3	TNF α	6.905 \pm 1.36	n.d.	> 12	n.d.
	TRAIL	9.93 \pm 13.6	3.87 \pm 1.39	> 12	n.d.
DU145	TNF α	10.58 \pm 10.37	6.79 \pm 4.22	> 12	n.d.
	TRAIL	10.97 \pm 8.36	n.d.	> 12	n.d.
LNCaP	TNF α	4.76 \pm 2.66	14.03 \pm 25.96	> 30	n.d.
	TRAIL	1.42 \pm 0.854	1.48 \pm 0.929	> 30	n.d.

- n.d. not determined

3.4. Discussion

Prostate cancer is one of the most common cancer types in men and causes hundreds of thousands of deaths annually worldwide. The high mortality rate of this disease could be due to the scarcity of efficient treatment options, as most of the common treatments are either inefficient in the late stages of the disease and/or associated with undesirable side effects. Gene therapy is one of the rising treatment approaches that is expected to show prominent therapeutic benefits (Lu, 2009). However, the success of this approach relies on the safe delivery of therapeutic genes to the cancer site. Genes usually undergo degradation by serum nuclease enzymes immediately after intravenous administration, reducing the extent of delivery to the target site. The essential purpose of using gene carriers is to protect the plasmid from such degradation.

The previous chapter discussed the different types of gene carrier that might be used; the one selected for this study was diaminobutyric polypropylenimine hexadecaamine (DAB-Am16), modified with three alternative targeting ligands: lactoferrin, PSMA-binding peptide (Peptide2), and integrin-binding peptide (Peptide4). We successfully synthesised DAB-Lf, DAB-Pep2, DAB-PEG2k-Pep2 and DAB-PEG2k-Pep4 as novel non-viral gene carriers having a strong tendency to condense the DNA with persistent stability. Thereafter, testing these carriers for their capability and efficiency in targeting prostate cancer cells is vital to demonstrate the improvement in targeting of these dendrimers after modification.

Examining the efficacy of these carriers *in vitro* will result in various benefits in understanding the extent of prostate cancer targeting and the level of gene transfection improvement before moving forward to *in vivo* studies. In a tumour microenvironment, genes are expected to be hindered by assorted barriers that reduce transfection efficiency. The gene internalization process could be one of the main factors reducing the probability of gene therapy success. The similarity in the negative charge between the cell membrane and the DNA molecule generates

a repulsive force which prevents the DNA from diffusing through the cell membrane. Using the cationic dendrimer DAB as gene carrier has previously been found to improve the uptake of DNA by the cells (Dufès *et al.*, 2005); however, its transfection efficacy is still lower than that obtained by using viral carriers (Thomas *et al.*, 2003).

After successful internalization, dendriplexes tend to cluster inside the cytoplasm, as they will be trapped in an endosome where they are exposed to a mildly acidic (pH 6), enzyme-rich environment with low calcium concentration. Most ligands usually dissociate at that stage and the DNA carried is expected to be hydrolysed as well (Mellman and Yarden, 2013; Blanco *et al.*, 2015). Using the cationic dendrimer polypropylenimine (DAB) as gene carrier in this study has a very important impact in overcoming this endosomal degradation. Most of the amine groups in the dendrimer have pKa values around 10, so they become ionized inside the endosome because of its pH. Thus, the high density of amine groups in these molecules causes a sharp increase in the demand for protons inside the endosome, leading to its expansion and hydrolysis, and the escape of dendriplex (proton sponge effect) (Pérez-Martínez *et al.*, 2011; McCrudden and McCarthy, 2013). However, even after the successful endosomal escape, the surviving DNA molecules are subjected to hydrolysis by the cytoplasmic nucleases unless they pass through the nuclear envelope. The most common processes by which DNA successfully reaches the nucleus are either pore permeabilization, which is applicable to particles smaller than 70 kDa, or during cell division, where the nuclear membrane lyses, allowing the genetic materials to fuse inside the newly generated nucleus, which is the process most commonly expected to occur with cancer cells (Pérez-Martínez *et al.*, 2011; McCrudden and McCarthy, 2013).

Using lactoferrin, Peptide2 and Peptide4 as targeting ligands in the synthesis of the novel gene carriers DAB-Lf, DAB-PEG2k-Pep2 and DAB-PEG2k-Pep4 is expected to have a positive impact in ameliorating the *in vitro* efficacy of the delivered gene of interest. The positive

impact should involve improvement in cellular uptake as well as transfection efficiency. Cellular uptake is expected to occur through receptor-mediated endocytosis that arises due to the use of the targeting ligands lactoferrin, Peptide2 and Peptide4, whose receptors are overexpressed in various prostate cancer cells. Furthermore, the enhancement in the transfection capability of the formulated dendriplex is an indication of a successful cellular uptake, followed by efficient endosomal escape of the dendriplex and finally the effective passage of the plasmid inside the nucleus. Transfection efficiency assay is a good technique to evaluate the improvement associated with the ligands used, since the dendriplex will pass the three most common cellular obstacles mentioned above before expressing the protein encoded by the carried gene. Therefore, efficient transfection data indicate the success of the designed dendrimers in overcoming these cellular barriers.

For the first formulation DAB-Lf, the *in vitro* treatment with DAB-Lf dendriplexes resulted in increased DNA transfection compared with unconjugated DAB in all examined cell lines. The DAB-Lf: DNA weight ratio which resulted in optimum uptake were both 10:1 and 5:1 for the cell lines PC-3 and DU145 while it was 20:1 for LNCaP cells. However, the dendriplex with a weight ratio of 5:1 was chosen for further *in vitro* and *in vivo* experiments. The two weight ratios 10:1 and 5:1 had nearly identical positive potential and particle sizes. The similarity in particle size is due to the fact that both ratios were completely able to condense 80% of the DNA as being fined in PicoGreen[®] assay. Therefore, the lower ratio was selected for the upcoming experiments to overcome any possible toxicity that could arise in the future from using higher ratios.

The use of lactoferrin as a targeting ligand for various organs of the body has been examined in previous publications; however, none has reported the use of Lf to target prostate cancer tissues until recently when Shankaranarayanan (2016) published an article discussing the improvement in the doxorubicin therapeutic effect after conjugating it with lactoferrin to treat

metastatic prostate cancer. The LC_{50} of doxorubicin was decreased four-fold after conjugating it with Lf in DU145 cell line. This article demonstrated the efficacy of Lf as a targeting ligand to prostate cancer cells which supports the original hypothesis of our study. Similarly, DAB-Lf: DNA dendriplex at the weight ratio of 2:1 was examined with different cancer cell lines to test its effect in gene expression. At best, expression was 1.4 times higher than for unconjugated DAB (Lim *et al.*, 2015). This is less than the value obtained in this study with prostate cancer cells, especially PC-3 cells. In a comparison between our results with previous study obtained by the group, the iron binding protein transferrin was used as ligand conjugated to DAB to target prostate cancer (Al Robaian *et al.*, 2014). DNA transfection showed 1.3-fold higher in transfection efficacy compared with DAB dendriplex in PC-3 cells which is much less than the data obtained in this study with an improvement in the transfection by 2.7-fold for the same cell line compared with the unconjugated DAB dendriplex.

Cellular uptake experiments demonstrated the capability of DAB-Lf in increasing the cellular uptake of the DNA qualitatively and quantitatively using confocal microscopy and flow cytometry. The data obtained demonstrated the superiority of DAB-Lf in improving the uptake of the condensed DNA over untargeted DAB in PC-3 and DU 145 cell lines with minimum effect on LNCaP cells. These data are in line with the flow cytometer finding of Wei and colleagues (2012) who found that the uptake of liposomes modified with Lf significantly enhanced by more than double compared with unmodified liposomes in hepatocellular carcinoma. The findings are also compatible with the results obtained by Lim and colleagues (2015), demonstrating the ability of lactoferrin to improve the targeting capability of the dendriplex to different cancer cell lines (A431, B16-F10 and T98G), However, this report is the only one of its kind so far to demonstrate the effect of lactoferrin on targeting different prostate cancer cell lines, as the *in vitro* results show.

Investigating the cellular uptake mechanism of DAB-Lf dendriplex is an important manifesting step to prove that conjugating the targeting ligand lactoferrin is the reason for the improvement in the cellular uptake of this dendriplex through detecting the main uptake pathway. It should also shed light on the potential uptake mechanisms beside LfRs.

In DAB-Lf dendriplex, free lactoferrin was used to block Lf receptors, it resulted in approximately 70% blockage in the uptake of the dendriplex in all cell lines examined. This effect could be due to the competitive tendency between the free Lf and DAB-Lf dendriplex towards LfRs, supporting the original hypothesis that Lf conjugation could improve the uptake of the therapeutic DNA complexed with it. This result is in line with previous publications examining the effect of free Lf on the uptake of modified nanomedicines in various cancer cell lines (Huang *et al.*, 2009; Chen *et al.*, 2010; Lim *et al.*, 2015). Building over these previous studies, 80 μM of free Lf was selected in this study which is lower than the highest concentration used in Chen study.

Phenylarsine oxide and filipin are common inhibitors of clathrin- mediated endocytosis (CME) and clathrin- independent endocytosis (CIE) respectively. Two different doses were selected for each blocker (10 and 20 μM for Ph.O) and (5 and 10 $\mu\text{g/ml}$ for Fil). The low doses of Ph.O and Fil were used before to block these pathways in normal cell lines (Huang *et al.*, 2008). Therefore, the reduction in the cellular uptake obtained from using these low doses might not be sufficient to induce clear blockage effect in case of cancer cells because most of the receptors become overexpressed in cancer cells for up to 200-fold, which is the case with transferrin receptors (TfRs). Therefore, Ph.O and Fil doses have been increased up to the double based on previous studies using these doses with cancer cell lines (Ivanov *et al.*, 2004; Yumoto *et al.*, 2006; Chen *et al.*, 2010). It has been found that blocking these pathways resulted in a significant decrease in the uptake of DAB-Lf dendriplex in all the examined cell lines. Clathrin- mediated endocytosis is the pathway responsible for the uptake of most protein

ligands (Grant and Sato, 2006). Therefore, it was expected that some reduction in the uptake of Lf-bearing DAB dendriplex would be detected after the blocking of this pathway. Previous study by Jiang and colleagues (2011) demonstrated that Lf internalized colorectal cancer cells via clathrin- mediated endocytosis. Caveolae- dependent endocytosis pathway blockage by filipin resulted as well in significant reduction in the DAB-Lf dendriplex uptake indicating the diversity in the cellular uptake of the dendriplex designed.

All cell lines examined showed almost complete blockage in the cellular uptake after pretreatment with poly-L-lysine as an inhibitor of ionic uptake. The presence in excess of lysine in this polymer (zeta potential 50 mV) makes its cellular uptake superior to that of other types of cationic polymer due to the electrostatic interaction between PLL and cell membranes (Chen *et al.*, 2010). As DAB-Lf dendriplex is cationic as well (zeta potential 20 mV), poly-L-lysine pretreatment could hinder the DAB-Lf dendriplex from approaching the cell membrane due to the charge repulsive force between PLL and DAB-Lf dendriplex. This finding highlights the possible contribution of the positive charges on DAB-Lf dendriplex in its uptake by prostate cancer cells.

Several published studies have examined the mechanisms of lactoferrin uptake in various normal and cancerous cell lines (Huang *et al.*, 2009; Chen *et al.*, 2010; Jiang *et al.*, 2011; Lim *et al.*, 2015; Somani *et al.*, 2015). However, no previous work has discussed lactoferrin uptake mechanisms in prostate cancer cells. Jiang and colleagues (2011) examined the different endocytosis pathways for lactoferrin protein and the results of the present experiment are consistent with their findings, except in the case of filipin, where they report no sign of uptake inhibition, in contrast to the present finding of an approximately 2-fold reduction in uptake which could be due to the size of DAB-Lf dendriplex as it is lower than 100 nm.

One of the major techniques used in gene therapy is the induction of controlled cell death (apoptosis) by aiding the cancerous cells to express the cytokines required for this normal

physiological process. Cytokine expression occurs after the successful delivery and transfection of the plasmid DNA encoding these cytokines to the cells and nucleus respectively. Three different cytokines (TNF α , TRAIL and IL-12) were selected in this study for their well-known effect in inducing apoptosis (Chopra *et al.*, 2004; Aldawsari *et al.*, 2011).

Lactoferrin-bearing DAB dendriplex encoding a therapeutic DNA was found to increase the *in vitro* anti-proliferative activity of the dendriplex in the three cell lines tested; significantly lower IC₅₀ values were recorded compared with unmodified DAB. From a comparison of the IC₅₀ values of DNA complexed by DAB-Lf and DAB dendriplexes, we can deduce that these findings are correlated with the improvement in DNA transfection provided by the modified carrier DAB-Lf. More importantly, the cytotoxicity data of DAB-Lf and DAB dendriplex demonstrate that the therapeutic effect obtained is due to the successful delivery of the therapeutic genes, as the dendrimers showed minimum cytotoxic effect. A previous study by the same group also found Lf-bearing DAB dendriplex encoding TNF α to improve the anti-proliferation activity in different cancer cell lines (A431, B16-F10 and T98G) compared with unmodified DAB dendriplex (Lim *et al.*, 2015).

A recent study by Shankaranarayanan and colleagues (2016) investigated the efficacy of lactoferrin in improving the targeting capability of the drug doxorubicin after conjugating it with lactoferrin. Use of this formulation in prostate cancer cells was found to lead to 4-fold reduction in the anti-proliferative efficacy of Lf- doxorubicin compared with free doxorubicin in DU145 cell line. This article is the only one so far reporting an investigation of the efficiency of Lf as a targeting ligand to prostate cancer cells. Its data are in line with the data obtained in our laboratory, as we recorded a reduction in the IC₅₀ value by up to 13-fold in the same cell line after conjugating Lf with DAB.

PSMA has been found to be extensively expressed in prostate cancer tissues compared with normal ones, with a remarkable increase in its expression as the disease progresses (Wright *et*

al., 1995; Silver *et al.*, 1997; Kinoshita *et al.*, 2006). This makes PSMA a possible substantial element in targeting prostate cancer. Peptide2 with the amino acid sequence WQPDTAHHWATL was first identified by Aggarwal *et al.* (2006) as a targeting ligand for the extracellular domain of PSMA. The use of Peptide2 as a targeting ligand for PSMA *in vitro* is expected to cause some improvement in the targeting capability of the dendriplex.

The optimum transfection efficacy of the DAB-Pep2 dendriplex was found to be at the weight ratios 5:1 and 2:1 in the PC-3 and DU145 cell lines respectively, whereas it was 10:1 in the PSMA-positive cell line LNCaP. The 2:1 ratio was selected for use in further *in vitro* and *in vivo* studies, resulting in a 1.3- and 1.8-fold improvement in β -galactosidase expression for PC-3 and DU145 cells respectively, compared with unmodified DAB. There is no previous report of the use of Peptide2 as targeting ligand for a gene carrier to compare the data with.

The LNCaP cell line did not respond very well to the previously mentioned transfection protocol, although it responded normally in the other cellular uptake experiments. This could be due to the nature of LNCaP cells. They are adherent cells, but with weak attachment to the surface of tissue culture plates and a tendency to grow in aggregates. This would negatively affect the accuracy of the transfection and anti-proliferation assays in particular, as these were performed in this study using 96-well plates, which resulted in the process of changing the medium during the treatment and analysis steps being associated with some loss of cells, thus introducing some inaccuracy in the data obtained. In order to overcome this obstacle, we pre-coated the plates with poly-L-lysine before seeding the cells, following the procedure described in Liberio *et al* (2014). 96-well plates were pre-coated with 50 μ l per well of PLL solution at a concentration of 6.4 μ g/ml diluted in distilled water. The plates were incubated overnight at 37 $^{\circ}$ C, then washed once with 200 μ l per well of PBS and used directly for LNCaP cell seeding. This procedure was adopted in all transfection and MTT experiments conducted on the PEGylated forms of DAB-Pep2 dendriplexes and DAB-PEG2k-Pep4 on LNCaP cells only.

The qualitative images obtained with 2:1 DAB-Pep2 dendriplex demonstrated significant improvement in DNA uptake in the PC-3 and DU145 cell lines. This was supported quantitatively by flow cytometry, which showed up to a 2.5-fold increase in dendriplex uptake in DU145. This therapeutic effect could be due to the improvement in the endocytosis of the modified DAB-Pep2.

The PC-3 and DU145 cell lines are well known in the literature to be PSMA-negative (Ghosh *et al.*, 2005), questioning the source of such an improvement in transfection and cellular uptake after treating them with DAB-Pep2 dendriplex. There are two possible explanations. Firstly, some papers have noted some non-specificity in the targeting tendency of Peptide2 monomer (WQPDTAHHWATL) toward PSMA compared with its dimer and trimer (Kim *et al.*, 2013; Pu *et al.*, 2016), which could have some impact in this formulation. The other factor expected to cause the strong impact on cellular uptake is the high zeta potential of the DAB-Pep2 dendriplex, with a mean of 35 mV. Because this study measures the improvement in targeting tendency of the DAB-Pep2 dendriplex by comparing it with the non-targeted dendriplex DAB (5:1) as a positive control and because DAB (5:1) dendriplex has a lower zeta potential (25 mV), some improvement in uptake and transfection with DAB-Pep2 dendriplex is to be expected in all cell lines, even the PSMA-negative one, making the comparison inapplicable in these tests, since the higher potential will result in better uptake regardless of the impact of the targeting ligand.

Furthermore, PSMA expression has been found to be directly proportional to the progression of prostate cancer and the development of androgen-independent cell lines, yet some androgen-independent metastatic cell lines such as PC-3 and DU145 cells have not been described yet to express PSMA in their cell membrane. Numerous researchers have used these cells as models of PSMA-negative and their experiments have yielded reasonable data showing the inability of their PSMA targeted formulations to bind significantly to these cells (Chang *et al.*, 1999;

Ghosh *et al.*, 2005), whereas other studies have proven the existence of PSMA mRNA and protein forms in these cells by using stimulants such as growth factors and estradiol (Laidler *et al.*, 2005). Another study actually elucidates the existence of PSMA in these cells but with low expression in comparison with LNCaP cells (Regino *et al.*, 2009). PSMA expression has also been detected in metastasised tumours in bone, indicating the existence of PSMA in these cells originally (Wright *et al.*, 1995; Silver *et al.*, 1997). Therefore, the reduction in the expression of PSMA in PC-3 and DU145 may be caused by changes in the cells' environment, such as the disappearance of hormones, whereas the metastasised form of the tumours still contains PSMA, as mentioned in several studies (Wright *et al.*, 1995; Silver *et al.*, 1997; Kinoshita *et al.*, 2006).

It has been demonstrated previously that a high zeta potential is associated with high cytotoxicity of nanoparticles (Shao *et al.*, 2015). Therefore, the therapeutic effect of the DAB-Pep2 dendriplex is believed to be associated with some level of toxicity. A preliminary cytotoxicity experiment was conducted to examine the safety of using DAB-Pep2 dendrimer and its dendriplex in high doses in the PSMA-negative DU145 cell line. The dendrimer was found to be cytotoxic even at low concentrations, which would block any therapeutic effect to be obtained from the therapeutic DNA (TNF α).

At that stage of the research, it was important to investigate the efficacy of Peptide2 as targeting ligand to PSMA especially after the significant improvement in DAB-Pep2 uptake the PSMA-negative PC-3 and DU145 cell lines. Therefore, binding affinity assay of Peptide2 to all prostate cancer cell lines was performed using flow cytometry as the quantitative method. There was a significant difference in the binding affinity of FITC-Pep2 between LNCaP, PC-3 and DU145 cells, whereby Peptide2 was shown to have a superiority in binding to LNCaP cells by more than two-fold over PC-3 cells and 4.4-fold over DU145 cells. This finding demonstrates the binding favorability of Peptide2 to PSMA-positive cell line. PSMA-negative cells also showed some level of uptake for Peptide2, which could be due to its chemical

composition as basic peptide, which might facilitate its direct penetration in the cell membrane regardless of the existence of PSMA in its cell membrane (Madani *et al.*, 2011). Pu *et al* (2016) had highlighted the possible non-specificity of WQPDTAHHWATL as a monomeric peptide compared with its trimeric version. However, the finding in his assay demonstrate significant binding of this peptide to PSMA-positive cells.

For the purpose of reducing the cytotoxic effect of DAB-Pep2 dendrimer and improving the physical and chemical properties of its dendriplex, various PEG molecules were conjugated with DAB-Pep2. Several studies have conjugated PEG molecules with dendrimers to obtain improved formulations with lower cytotoxicity, especially with the highest generations of dendrimers (Hashemi *et al.*, 2015).

The measurement of the physical characteristics of these dendriplexes is reported in Chapter 2. Generally, PEGylating DAB-Pep2 resulted in the formation of almost similar sized dendriplexes with lower but efficient DNA condensation capability and significantly lower zeta potential. Introducing PEG molecules to DAB-Pep2 is believed to reduce the cytotoxicity of this polymer. However, this is not the only factor needed to be monitored in gene carriers; the optimal factor in judging the effectiveness of any gene carrier is its ability in efficiently carry the DNA of interest inside the cells, then improve its endosomal escape and release of the DNA inside the nucleus. For this purpose, all the PEGylated polymers targeted with Peptide2 (PEG-DA-Pep2, DAB-PEG3.5k-Pep2 and DAB-PEG2k-PEG3.5k-Pep2) were first screened for their transfection ability. Based on the results obtained, one of the formulations was selected for further *in vitro* investigation.

The transfection results did not follow the same pattern for all three PEGylated polymers of DAB-Pep2, highlighting the effect of PEG size and ratio on the properties of the dendriplex formed. DAB-PEG2k-Pep2 showed significant improvement in the transfection efficacy of LNCaP cells only, whereas the other cell lines showed no significant change in transfection

ability compared with the positive control of PEGylated DAB with no targeting ligand. DAB-PEG2000 (20:1) was selected as positive control at this stage of the study for the purpose of creating a similarity between the control and the polymer of interest, both being conjugated with an equivalent quantity of PEG molecules. Thus, comparing the DAB-PEG2k-Pep2 and DAB-PEG transfection results could specifically elucidate any impact of Peptide2 on transfection.

In light of the findings reported in Chapter two and the transfection results, DAB-PEG2k-Pep2 was selected as the optimal modified polymer for targeting PSMA in this study. Further *in vitro* assays were conducted with this polymer at 20:1 as the optimal weight ratio obtained from the transfection results.

The transfection efficacy of DAB-PEG2k-Pep2 dendriplex was also examined by enzyme-linked immunosorbent assay. The successful transfection of plasmid DNA encoding mTNF α as therapeutic DNA was assessed by ELISA for the three cell lines, which expressed variable amounts of mTNF α cytokine. PC-3 cells were found to produce a much higher concentration of TNF α than the other two cell lines, while the value for LNCaP cells was almost double that of DU145 cells. The results of this assay are in line with the findings of the β -galactosidase transfection assay, that PC-3 cells tended to produce significantly larger amounts of β -galactosidase than did the other cell lines. The variation in expression between the cell lines might not be linked to the binding favourability of the dendriplex to a specific cell line, but instead to the metabolic states of the cell lines. Each of the three lines of cells selected for this study represents a different metastatic region of prostate cancer, with differences in their receptors expression, invasive aggressiveness and growth rates. PC-3 cells are rapidly proliferating and fast growing (they duplicate *in vitro* after 33 h) with a strong invasive tendency compared with DU145 and LNCaP cells, explaining the high transfection abilities of this cell line, since actively growing cells facilitate the passage of the DNA to the nucleus

which lead to more production of the protein encoded by this DNA (Tai *et al.*, 2011; Cunningham and You, 2015).

Although the standard ONPG transfection assay confirmed the successful transfection of plasmid encoding β -galactosidase and the production of β -galactosidase enzyme, which converts the colourless ONPG to the yellow *o*-nitrophenol, it remains an indirect way of measuring transfection. On the other hand, ELISA method was used to directly assess the production of the cytokine of interest through its direct binding to the antibody, giving an accurate evaluation of the amount produced. Furthermore, TNF α transfection assay helped in estimating the time required for the dendriplex to be taken up by the cells and to produce the cytokine of interest. This was achieved by subjecting the cells to various incubation periods after treatment. Overall, 48 to 72 hours of treatment seem ideal for the DAB-PEG2k-Pep2 dendriplex to produce TNF α cytokine.

Qualitative and quantitative studies of the cellular uptake abilities of the dendriplex formed by complexing FITC-labelled DNA with DAB-PEG2k-Pep2 were conducted using LNCaP cells as PSMA-positive cells and PC-3 and DU145 cells as PSMA-negative cell lines. Both assays revealed a binding favourability of DAB-PEG2k-Pep2 to LNCaP cells over the other cells. This was supported by Peptide2 binding affinity studies. PC-3 cells were found to respond significantly to the untargeted DAB-PEG over DAB-PEG2k-Pep2 at the same weight ratio (20:1). This may be a demonstration of the ability of the DAB-PEG2k-Pep2 dendriplex to actively target PSMA-positive cells but not PSMA-negative ones. However, DU145 cells did not follow the same pattern, showing a superiority for the uptake of DAB-PEG2k-Pep2 dendriplex despite being PSMA-negative.

Although cellular uptake experiments would show the preference of the nanoparticle to bind to a specific cell line, this may not be exactly reflected by the transfection results. Cellular uptake experiments reflect only the first *in vitro* stage, which is the extent of uptake of the

targeted dendriplex by a specific cell line, whereas the extent of transfection in each cell line depends partly on cellular uptake as well as on other factors such as lysosomal escape and metabolic activity, which will vary among cell lines (Singh *et al.*, 2012; Cunningham and You, 2015). This variation complicates any comparison between prostate cancer cell lines. For example, in the case of the DAB-PEG2k-Pep2 dendriplex, LNCaP cells were proven to have superior binding affinity to the dendriplex compared with PC-3 cells, yet the cytokine concentration produced after TNF α transfection was significantly higher in the PC-3 cells because they are more strongly proliferating than LNCaP cells (Cunningham and You, 2015). Establishing the cellular uptake mechanism of DAB-PEG2k-Pep2 dendriplex is an important step towards confirming that conjugating Peptide2 would result in an improvement in the cellular uptake in PSMA-positive cells. PSMA has been reported to undergo uptake via receptor-mediated endocytosis through clathrin-mediated endocytosis (Goodman *et al.*, 2007). In addition, this assay would highlight the potential and multiple possible uptake mechanisms of the PEGylated dendriplexes beside the PSMA endocytosis pathway. Blocking different cellular endocytosis pathways in the cells before treating them with DAB-PEG2k-Pep2 dendriplex, followed by quantitatively measuring the extent of dendriplex uptake, would provide insight into the uptake pathways.

Free Peptide2 was used in this study as a blocker for the receptors PSMA. It was used earlier by Aggarwal *et al.* (2006) to inhibit the enzymatic activity of PSMA, which occurs as a result of the binding of this peptide to PSMA. The binding favourability of this peptide to LNCaP cells was confirmed earlier in the present work, by means of a binding affinity study. It was found that pretreating the cells with Peptide2 resulted in around 50% reduction in the uptake of DAB-PEG2k-Pep2 in both PSMA-positive and PSMA-negative cell lines. This finding does not support the original hypothesis that Peptide2 would show some superiority in blocking

LNCaP compared with the other cell lines; there are a number of possible reasons for this effect.

Aggarwal *et al.* (2006) examined the inhibitory effect of Peptide2 on the enzymatic activity of PSMA by incubating different concentrations of Peptide2 with PSMA for 30 minutes, followed by the addition of *N*-acetyl-aspartyl-glutamate and incubation for 15 minutes. When the tendency of the Peptide2 to inhibit the formation of glutamate carboxypeptidase II was quantified, it was found to have an IC₅₀ of 23 μM, which is much higher than the concentration used in our study (2.5 μM). A concentration of 2.5 μM had a limited inhibitory effect in the Aggarwal study, but we were unable to test higher concentrations because we had limited access to Peptide2. Therefore, one explanation for the insignificance of the differences detected between the cells lines after pretreatment with Peptide2 is that we may not have approached a sufficient concentration to show a difference in the blocking effect.

Nevertheless, the PSMA-negative cells PC-3 and DU145 showed around 50% blockage in uptake, similar to the result for the positive cell line LNCaP. Thus, this low concentration had a significant inhibitory effect in all cell lines examined. One possible explanation is that Peptide2 is a basic peptide with an overall zeta potential around 7 mV. Its hydrophilic, basic nature may have facilitated its penetration in the cell membrane, limiting the likelihood of the dendriplex being taken up via alternative mechanisms. It is unknown, however, how this may have disrupted the uptake of DAB-PEG2k-Pep2 in the current state. One possible way to improve the investigation of whether this dendriplex was taken up by PSMA would be to pretreat the cells with a specific antibody known to block PSMA such as PSMA mAbs J591, J415 and J533 (IgG1) antibodies developed by Liu *et al* (1998).

Phenylarsine oxide is a common blocker of clathrin- mediated endocytosis. It has been found that blocking this pathway results in a significant decrease in the uptake of DAB-PEG2k-Pep2 dendriplex in PSMA-negative PC-3 and DU145 cells, but not in PSMA-positive LNCaP cells.

This pathway is believed to be the one responsible for the uptake of ligands binding to PSMA or protein binding receptors generally (Goodman *et al.*, 2007; Zhang *et al.*, 2016); therefore, it was expected that some reduction in the uptake of Peptide2-bearing DAB dendriplex would be detected after the blocking of this pathway by Ph.O in LNCaP cells, with less effect in PC-3 and DU145 cells. However, the data from this assay showed a minimal inhibitory effect of Ph.O in LNCaP cells. There is no obvious explanation for this result, which contradicts earlier findings in this study.

LNCaP cells are well known to represent a good model of adenocarcinoma, whereas PC-3 and DU145 cells resemble more aggressive forms of prostate cancer such as small cell carcinoma (Dozmorov *et al.*, 2009; Tai *et al.*, 2011; Cunningham and You, 2015). Thus, subjecting these cells to similar conditions when studying the mechanism of cellular uptake would be expected to result in a smaller effect being detected in LNCaP cells. Some studies subjected PSMA-positive LNCaP and C4-2 cells to different conditions when investigating the mechanism of cellular uptake of nanoparticles: either a longer incubation period of up to one hour (Nagesh *et al.*, 2016) or significantly higher concentrations of the blockers used (Wu *et al.*, 2014) compared with the conditions used in our study. Nagesh *et al.* (2016) synthesised nanoparticles to treat prostate cancer by targeting PSMA using antibodies; blocking the clathrin-mediated endocytosis pathway using chlorpromazine for one hour led to a 30% reduction in uptake only in PSMA-positive cells (C4-2).

Pretreating cells with filipin resulted in a significant and varied reduction in uptake in all cell lines examined. The dendriplex uptake was strongly blocked in DU145 cells, indicating that the uptake of this dendriplex was highly reliant on caveolae-mediated endocytosis compared with the other pathways in this cell line. The uptake in PC-3 and LNCaP cells was blocked by around half compared with DU145 cells, giving an indication of the major role of caveolae-mediated endocytosis in the uptake of DAB-PEG2k-Pep2 dendriplex.

The use of colchicine, a common blocker of macropinocytosis, resulted in around 50% blockage in all cell lines examined. Macropinocytosis is the usual uptake pathway for particles ≥ 100 nm, yet DAB-PEG2k-Pep2, with an average size of 65 nm, was found to be taken up significantly through macropinocytosis. Colchicine mechanism of action based on inhibiting cellular microtubule polymerisation which affects the cells mitosis and migration abilities. The author demonstrated that colchicine has significant inhibitory role in high generation of PAMAM dendrimers conjugates even if their size is less than 100 nm (Mohammadpour *et al.*, 2017), similarly to the finding obtained here.

In the PSMA-positive LNCaP cells, none of the blockers used caused more than a 50% reduction in the uptake of the DAB-PEG2k-Pep2 dendriplex, due to the nature of this cell line, as mentioned earlier. Wu *et al.* (2014) used the same blockers as this study at significantly higher doses, yet the optimal blockage obtained was 60% at best. This raises the question of whether studying the effect of the designed dendriplex by comparing LNCaP cells as positive control with PC-3 and DU145 cell lines as negative controls would result in comparable data, not mentioning the differences in proliferation rate between these cell lines (Cunningham & You, 2015). One way to overcome this issue is by transfecting PSMA to a cell line known to be PSMA-negative; thus, Chen *et al.* (2016) examined the PSMA targeting tendency of their nanomedicine using the PSMA-negative PC-3 cell line and transfected it to express PSMA, then compared the data between PSMA- positive (PC3-PIP) and PSMA- negative cells (PC3-Flu). The results obtained should be comparable because only one criterion is variable between the cells (PSMA expression). In Chen study (2016), PSMA-targeted nanoplex encoding pTRAIL significantly improved the anti-proliferation effect in PC3-PIP compared with PC3-Flu.

The anti-proliferation of DAB-PEG2k-Pep2 dendriplex using a therapeutic gene (TNF α and TRAIL) was conducted to investigate the therapeutic effect of the complexed DNA.

In MTT experiments, DAB-PEG2k-Pep2 dendrimer complexed with pORF9-mTNF α and pORF9-mTRAIL showed significant improvement in the antiproliferative effect of the targeted dendriplex compared with DAB-PEG dendriplex for the positive control cell line LNCaP, with a more significant difference at higher DNA concentrations. Furthermore, because the weight dendrimer: DNA ratio used in these MTT experiments was 20:1, DAB-PEG2k-Pep2 was found to have relatively low cytotoxicity at high doses compared with the cytotoxic effect of DAB-Pep2 demonstrating the impact of PEG chain in reducing the cytotoxic effect of the polymers (Lee and Larson, 2011).

Generally, these dendriplexes had a weak anti-proliferative effect compared with the modified dendrimers used previously by the group, such as DAB-Lf and DAB-Tf (Al Robaian *et al.*, 2014; Lim *et al.*, 2015). This could be due to the failure of this formulation to successfully transfect the DNA of interest to produce the encoding cytokine and induce cellular apoptosis in low doses. However, this suggestion is contradicted by the ELISA findings, which confirmed the successful formation of mTNF α after 48 h of treatment in all cell lines examined, with variation in the amount of mTNF α formed, based mainly on the metabolic tendency of the cell line, as demonstrated above. Nevertheless, the produced cytokine was found to have a limited anti-proliferative effect at low doses, as an indication for the weak apoptosis effect which could be due to the low concentration of the cytokine, making DAB-PEG2k-Pep2 dendriplex successfully transfect the DNA of interest but not in a manner comparable with DAB-Lf and DAB dendriplexes. In order to confirm this hypothesis, an ELISA assay would need to be performed on DAB-Lf and DAB dendriplexes encoding TNF α to compare the findings.

The third targeting ligand selected for this study was Peptide4 (PRPRGDNPLT), the active binding site of the cyclic peptide EETI-II 2.5F, which has been examined before and found to bind efficiently with favourability to the integrin receptors $\alpha v \beta 5$, $\alpha v \beta 3$, $\alpha_{III} \beta 3$ and $\alpha 5 \beta 1$ (Kimura *et al.*, 2009; Moore *et al.*, 2013). Compared with normal prostate tissues, prostate cancer

showed a considerably increased presence of some of these integrin heterodimers, such as $\alpha_V\beta_3$, $\alpha_{IIb}\beta_3$, and $\alpha_5\beta_1$, as reported in various papers (Zheng *et al.*, 1999; Fornaro *et al.*, 2001; Suyin *et al.*, 2013). Therefore, we hypothesised that using the active site of EETI-II 2.5F as targeting ligand would improve the cellular uptake of the dendriplex DAB-PEG2k-Pep4 by prostate cancer cells *in vitro*.

A DNA transfection assay was performed, but the cell lines showed no improvement in β -galactosidase expression compared with the positive control DAB-PEG (20:1) at any of the ratios examined, so this formulation may require some modifications to obtain better outcomes. Two possibilities are assumed to be linked to this unpromising outcome. Firstly, this study was the first to examine the active binding site (PRPRGDNPPLT) of the cyclic peptide EETI-II 2.5F instead of the full peptide, which may have reduced the targeting capability of the peptide. Alternatively, the ratio of Peptide4 used may have been sub-optimal, so increasing the ratio of Peptide4 might increase its exposure to integrin receptors in the cell membrane, thus improving the targeting tendency.

Chapter 4 : *In vivo* evaluation of lactoferrin-bearing polypropylenimine dendriplex

4.1. Introduction

Although *in vitro* experiments assist in understanding the biological response of various prostate cancer cells to the novel gene carrier DAB-Lf, they are insufficient to gain a full understanding of the therapeutic efficacy and associated toxicity of systemic administration of DAB-Lf dendriplexes. *In vitro* assays cannot reproduce the tumour microenvironment and the cellular interactions that the drug would encounter after intravenous administration (Ittmann *et al.*, 2013).

An intravenously administered nanomedicine is expected to face obstacles to its efficacy during its circulation in the bloodstream, before reaching the target site. Understanding these systemic barriers and their relation to the physical and chemical properties of the nanoparticle is important for the design of the treatment, as they could reduce its efficacy.

The original difficulty in gene therapy is the degradation of DNA after intravenous administration, caused by the direct contact of the naked DNA molecules with serum nuclease enzymes. Using gene carriers has been found to mitigate this direct effect, allowing enough time for the DNA to circulate in the bloodstream and accumulate at the target site.

However, according to the nature of the gene carrier used, different kind of impediments may arise. As nanoparticles enter the bloodstream, they come into contact with a complex mixture of substrates such as plasma proteins, blood cells, enzymes and components of the immune system (Alex and Sharma, 2013). These molecules interact with the nanoparticles in different ways according to their charge, size and composition. They are generally found to be deleterious to the nanoparticles, either by causing their non-specific binding to different cell types or by facilitating their elimination by the reticuloendothelial system after their opsonisation, thus reducing the likelihood of the nanomedicine reaching the target site (Santander-Ortega *et al.*, 2016).

Cationic dendrimers tend to have a positive potential due to the high density of amine groups in their molecules, which allows them to undergo electrostatic interactions with DNA molecules (Dufès *et al.*, 2005). This high zeta potential tends to diminish after the condensation of the DNA molecules, leaving the dendriplexes with a slight positive to neutral potential. A relatively positive zeta potential will tend to improve the cellular uptake of the dendriplex by forming an attraction between the oppositely charged cell membrane and dendriplex, but at the same time it will increase the chance of the non-specific binding of these dendriplexes with any anionic molecules in the bloodstream, including different proteins and non-targeted cells. This may lead to dramatic changes in the biodistribution and biological effect of the dendriplex. For example, the interaction between the dendriplex and serum proteins after IV administration can lead to a partial or complete coating of the dendriplex surface by these serum proteins. A partial coating may cause heterogeneity in the surface charge and therefore aggregation of the nanoparticles, while complete coating could have either a positive impact, by improving the colloidal stability of the nanoparticles, or a negative one, by masking the targeting ligand in the dendriplex and thus lowering the targeting tendency of the formulation or assisting the clearance of the dendriplex by macrophages.

There is no clear prediction of how the zeta potential of the dendriplex would interact with the *in vivo* environment. It has been suggested that the zeta potential should preferably not exceed 25 to 30 mV (Durymanov *et al.*, 2015; Bhattacharjee, 2016). The only way to attain a better understanding of the impact of these systemic interactions is to perform *in vivo* experiments (Alex and Sharma, 2013).

Dendriplexes that successfully travel through the systemic circulation and safely reach the cancer site will face another barrier, in the form of the extracellular matrix (ECM) generated by cancer tissues; the ECM is generally composed of proteins such as collagen and laminin,

glycoproteins and polysaccharides, connected together and has been found to be responsible for various biochemical properties of tumours (Lu *et al.*, 2012). This dynamic niche creates a partition that limits the ability of nanoparticles to approach the cancer cells.

Each of these systemic barriers will affect the therapeutic efficacy of the nanomedicine and *in vivo* studies are essential in order to better understand the extent of these effects and their overall impact.

This chapter reports an investigation of the *in vivo* therapeutic efficacy and toxicity of the gene carrier lactoferrin-bearing DAB dendrimer, before and after complexing it with different therapeutic DNA molecules, by measuring the tumoricidal activity of these dendriplexes when injected intravenously into nude mice carrying subcutaneous xenograft prostate tumours. Tumour growth rate, tumour regression, animals weight changes and survival are the parameters considered in this study as indicators of the efficacy and possible toxicity of these dendriplexes.

4.1.1. Animal models

Animal models are often used to provide preclinical predictions of the efficacy and cytotoxicity of any drug. There are two common ways of generating malignant tumours in animal models: either grafting tumour cells into immunocompromised animals (syngeneic or xenogeneic) or using genetically engineered animals with a cancer genotype. The tumours thus generated are believed to provide the fundamental knowledge about human tumours. In xenograft models, human prostate cancer cells are implanted into animals (usually mice) subcutaneously or orthotopically. Orthotopic cancer models have been found to be superior to subcutaneous ones because they reflect the prostate microenvironment, with a strong tendency to generate metastatic tumours. However, establishing orthotopic models is associated with some difficulties such as the inability to follow up the tumour growth except by using MRI.

Additionally, the creation of orthotopic models requires surgery to inject the cells into the mouse prostate, which carries a high risk of causing certain infections that nude mice may not be able to withstand (Richmond and Su, 2008; Pavese *et al.*, 2013).

The discovery of nude mice (BALB/c) in 1980 made tumour xenografting possible as these animals lack a thymus, thus lack of thymus-dependent immune function because of their inability to produce T-lymphocytes to generate an immune response to extraneous tissues or cells. Nevertheless, BALB/c nude mice still have functioning B-lymphocytes and NK cells (Morton and Houghton, 2007; Valkenburg and Williams, 2011).

Several benefits are associated with the use of human tumour xenograft models. They represent the actual biology and microenvironment of human tumours, including all of the changes in genetic features. Time is also saved, as xenograft tumours are usually ready for treatment trials to start within weeks of cell implantation, whereas with other models such as genetic engineering it may be months before the animals are ready for treatment (Richmond and Su, 2008). Although xenografting has proven to be a good method of predicting the therapeutic and cytotoxic effects of various anti-cancer drugs, there is a strong debate as to its efficacy in representing an accurate tumour model. The main reason for this is that such *in vivo* tumours are generated by injecting cancer cell lines that have first been subcultured for a long time; therefore, they no longer precisely represent the physiology of the original tumours from which they were extracted. They usually lose the ability to generate a tissue architecture that resembles the original tumour because of changes in the expression of some genes, leading to changes in the pattern of interaction with the environment and treatment response (Morton and Houghton, 2007; Yee *et al.*, 2015; Rea *et al.*, 2016).

During *in vivo* studies and for the purpose of estimating the therapeutic effects of any intravenously injected therapeutic agent, three types of tumour response are usually measured:

the growth rate of the tumours, their size and the survival rate of the animals (Richmond and Su, 2008).

4.1.2. Bioluminescence imaging

Bioluminescence is a phenomenon which occurs naturally in species including *Photinus pyralis*, a beetle which emits visible light from a substrate containing luciferase, a light-producing enzyme. This process is exploited in bioluminescence imaging (BLI), a technique for the optical imaging of tissues or structures in living laboratory animals by detecting light emitted from them. BLI is a fundamental method in most laboratories dealing with animals because of several advantages over alternative imaging techniques, such as its low cost, its ease of use and its various *in vivo* applications. Of particular value is the ability to acquire data without the need for animal sacrifice, plus the possibility of continuous observation of a single animal, which reduces the risk of error arising from inter-animal variation (Sato *et al.*, 2004; Close *et al.*, 2011).

The mechanism of BLI is based on measuring the visible light emitted after injecting the subject animal with a reporter enzyme. This is usually luciferase, which mediates the oxidation of luciferin, causing it to emit light in the visible region at 560 nm; this bioluminescence has a half-life of 2 hours. The reaction occurs when luciferase catalyses luciferin with the assistance of ATP to form luciferyl adenylate, which is oxidised to form oxyluciferin, a bioluminescent substance. This technique of *in vivo* imaging, using a reporter enzyme to track biological processes in a living organism, is possible in mammals because mammalian tissues do not naturally undergo any bioluminescence reactions, which eliminates any background noise and improves image resolution.

Bioluminescence can be detected even when emitted from deep tissues a few centimetres inside the body. Generating bioluminescence is depending on several factors including: the depth of

the imaged tissue, the amount of luciferase expression, and the sensitivity of the detector used (Sadikot and Blackwell, 2005). Luciferase expression is correlated with the number of reporter cells carrying the luciferase gene.

The quality of data obtained by BLI is affected by certain factors that should be considered to obtain valuable images. Firstly, the luciferase reaction is affected by the quantities of oxygen, ATP and luciferin; if any of these elements is insufficient, the emitted light which is detected will not reflect the true activity of luciferase (Sadikot and Blackwell, 2005).

The imaging equipment is basically composed of a light-tight chamber in which the animal is placed, a high quantum efficiency charged couple device (CCD) camera kept at a temperature between -80 and -90 °C to reduce thermal noise and gas anaesthesia tubes to immobilise the animal. It is usual to take two images of each animal, a photographic image followed by a bioluminescent one; these are then superimposed so that the location of the bioluminescence is mapped (Figure 4-1). The time required to obtain such images varies from a few seconds to several minutes, depending on signal strength. Various software packages can be used to display the images acquired (Close *et al.*, 2010).

There are several applications for BLI, mainly depending on the aim of the *in vivo* study. Using luciferase-tagged cell lines or tissues is a common method of tracking the study target to measure the therapeutic effect of drugs and is also useful in studying various aspects of cancer such as tumour progression. There are a variety of cell lines commercially available that are bioengineered with the luc gene to produce luciferase protein (Close *et al.*, 2010).

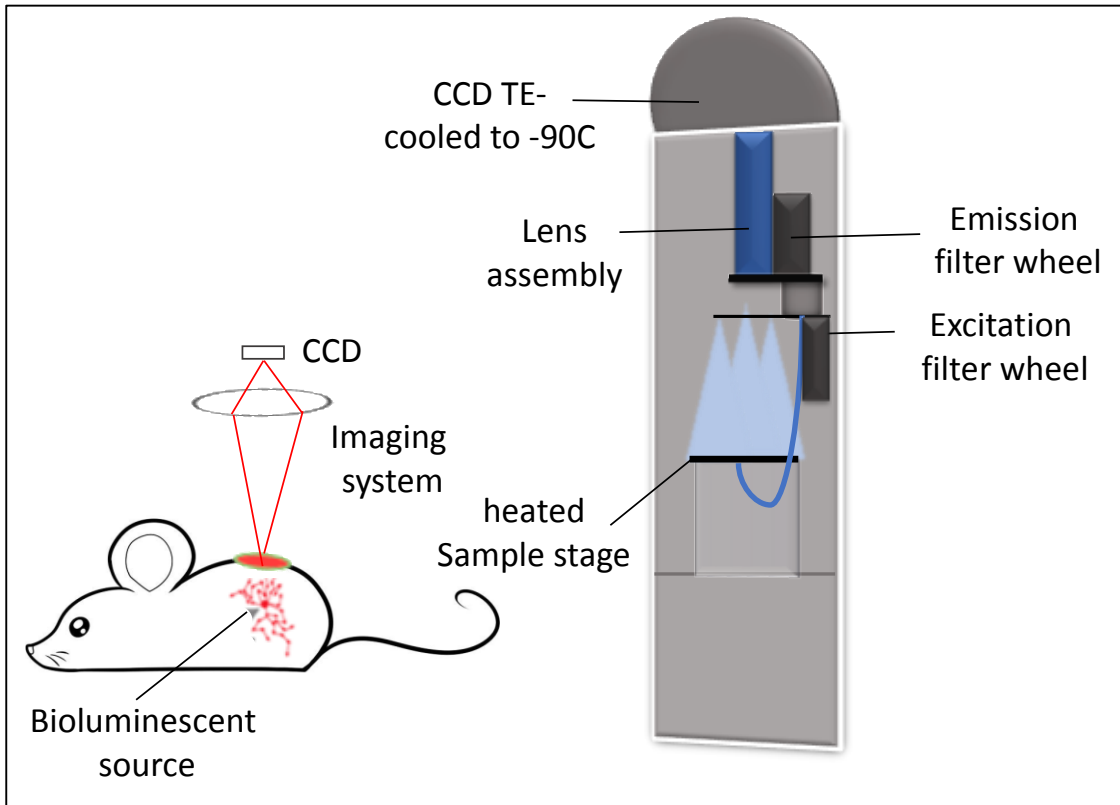


Figure 4-1 Bioluminescent imaging instrumentation (adapted from Behrooz *et al.*, 2013)

4.2 Materials and methods

4.2.1 Materials

Table 4-1 List of materials used in chapter 4.

Materials	Supplier
Lactoferrin- bearing polypropyleneimine (DAB) dendriplex	Prepared as described in Chapter 2
Phosphate buffered saline tablet	Sigma-Aldrich, UK
MEM	Invitrogen, UK
Foetal Bovine Serum (FBS)	Invitrogen, UK
L-Glutamine	Invitrogen, UK
Penicillin-Streptomycin	Invitrogen, UK
Trypsin	Invitrogen, UK
Ampicillin	Sigma-Aldrich, UK
PC-3 cells	The European Collection of Cell Cultures (Salisbury, UK)
Luciferase Assay Reagent	Promega, UK.
Passive Lysis Buffer (5x)	Promega, UK.
DU145 cells	The European Collection of Cell Cultures (Salisbury, UK)

4.2.2. Methods

4.2.2.1. Cell culture

Prostate cancer cell lines (PC-3 and DU145) were purchased frozen from European and American collections of cell cultures. They were cultured and passaged several times before being used in the experiments.

PC-3 and DU145 cells were grown in Minimum Essential Medium (MEM) as monolayers in a T75 flask. The media was supplemented with 10% (v/v) foetal bovine serum, 1% (v/v) L-glutamine and 0.5% (v/v) penicillin-streptomycin. The cell culture flasks were kept in the incubator at 37 °C and 5% carbon dioxide in a humid atmosphere.

4.2.2.2. Laboratory animals

The animals selected for the *in vivo* experiments were immunocompromised BALB/c male mice. They were randomly separated into groups of five and kept at 19 to 23 °C and 12-hour light-dark cycle. The animals were fed classic mice diet and water. The *in vivo* experiments were approved by the local ethics committee and carried out with conformity of UK Home Office regulations.

4.2.2.3. Therapeutic efficacy

PC-3M-Luc-C6 and DU145 cancer cells were injected subcutaneously into both flanks of immunodeficient BALB/c male mice at 1×10^6 cells per flank. Once the tumours become palpable and vascularized at a diameter of 5 mm. the mice were randomly separated into groups of five, each of which was given a different intravenous treatment as follows: Lf-bearing DAB dendrimer complexed with DNA encoding TNF α , TRAIL or IL-12; the targeting dendrimer (DAB-Lf) alone; and naked DNA (50 μ g of DNA). Treatment was repeated every other day until five doses had been given, ending on Day 10. The mice were weighed daily after tumour development as a measurement for any treatment toxicity. Tumour diameters were also

measured daily using calliper measurements to obtain the tumour volume using the following equation:

$$\text{Volume} = d^3 \times \pi/6. \quad (4)$$

4.2.2.4. Bioluminescence imaging

Tumour regression was observed by bioluminescence imaging using an IVIS Spectrum (Calliper Life Sciences, Hopkinton, MA). Mice with PC-3M-luc-C6 tumours were treated with DAB-Lf: DNA encoding TNF α as described above. The mice were injected intraperitoneally with D-luciferin in a dose of 150 mg/kg, ten minutes before imaging. The animals were anaesthetized with isoflurane inhalation on the 1st, 3rd, 5th, 7th and 9th days of treatment. Living Image[®] software was used to detect the light emitted from the bioluminescent tumours for two minutes and the images were displayed as a pseudo-colour overlay onto a grey scale image.

4.2.3. Statistical analysis

One-way ANOVA and Tukey multiple comparisons tests (OriginPro software) were used to determine the statistical significance of differences. A p-value of 0.05 or less was considered significant.

4.3. Results

4.3.1. Therapeutic efficacy

4.3.1.1. PC-3 xenograft tumours

Intravenous administration of lactoferrin-bearing DAB dendrimer complexed with DNA encoding TNF α , TRAIL or IL-12 resulted in tumour regression within 24 h of the first injection in PC-3 tumours (Figure 4-2, A). Mice injected with DAB-Lf: DNA encoding TNF α showed immediate and continuous regression in tumour size until the ninth day, when the tumours stopped regressing and showed some signs of slow growth for six days. After the final dose, 70% of tumours continued to shrink while the remaining were not responding to the treatment until they have been eliminated from the study. The remaining tumours continued in regression until the end of the study. At the end of the treatment, 70% of tumours showed significant regression and the remaining 30% had slower grown rate compared with the control group. There was no weight loss in the animals treated with DAB-Lf: DNA encoding TNF α , demonstrating the good tolerability of the treatment.

A different response pattern was observed in the group treated with DNA encoding TRAIL complexed with DAB-Lf. Generally, the response to treatment was lower than in the DAB-Lf: TNF α group; some tumours immediately responded to the treatment and started regressing, while the others maintained their original size for a week. After the fifth dose, some of the tumours showed slow growth, while others maintained their size until Day 14, when one of the animals was removed from the study for approaching the allowed tumour size. The remaining tumours were going through slow tumour growth or tumour regression. 40% of the tumours were completely eradicated at the end of the trial.

In the group treated with DAB-Lf: IL-12, some of the tumours start to respond to the treatment by regressing, while the remaining showed a reduction in tumour growth compared with the

control group treated with DNA only. Two weeks after starting the therapy, two of the animals had been sacrificed because of enlarged tumours, while the remaining animals in the group maintained a slow rate of tumour growth until the end of the treatment, while one mouse showed complete regression in the tumours. Thus, 60% of the treatment group survived until the end of the experiment.

For DU145 xenograft tumours, the intravenous administration of lactoferrin-bearing DAB dendrimer complexed with DNA encoding TNF α , TRAIL or IL-12 resulted in tumour regression within 24 h of the first injection (Figure 4-3, A). The DAB-Lf: DNA encoding TNF α treatment group showed immediate tumour regression after the first dose, followed by continuous regression in 70% of the tumours, while the remaining 30% showed some constant slow growth until they reached the maximum size allowed, when the animals were sacrificed. Half of the tumours had completely disappeared at the end of the treatment. The animals tolerated the treatment very well and showed no sign of toxicity or weight loss during the treatment period. Animals were sacrificed during the treatment period because of their tumours reaching maximum allowed size by the Home Office, but not because of weight loss.

Animals treated with DAB-Lf: DNA dendriplex encoding TRAIL showed some signs of tumour regression after the first dose, followed by continuous regression in 40% of the tumours; the remaining 60% maintained their size until day five, when they started to show some signs of slow growth before reaching maximum size and being sacrificed. There was no sign of weight loss during the treatment period.

Similarly, in the group treated with DAB-Lf: IL-12, some of the tumours started to respond to treatment by regressing after the first dose, while in others there was either a reduction in tumour growth rate or an increase in overall growth, but at a lower rate than in the group treated with DNA only. By Day 22, three animals had been sacrificed due to tumour enlargement and

at the end of the treatment 20% of the tumours had completely disappeared, while 20% had slow growth compared with the DNA-only control group.

The average survival rate was significantly improved in all DAB-Lf: DNA dendriplexes, by around 14 days in animals carrying PC-3 tumours and ten days in animals with DU145 xenograft tumours. This was due to the reduction in tumour growth rate in these groups compared with DNA only or DAB-Lf complexed with nontherapeutic DNA.

By contrast, PC-3 and DU145 tumours treated with DNA only (TNF α , TRAIL or IL-12) or with DAB-Lf dendrimer only showed continues growth of the tumours in a similar manner to the untreated group. These animals were sacrificed after significant tumour growth, i.e. when the diameter reached 10 mm.

The treated animals showed no sign of toxicity or significant weight loss during the treatment period, indicating that the treatments were all well tolerated by the animals (Figure 4-2, B and Figure 4-3, B). All the sacrifice of animals during the study was due to their tumour enlargement reaching the maximum allowed size.

At the end of the experiment, 70% of PC-3 tumours treated with DAB-Lf complexing DNA encoding TNF α had completely disappeared, while the remaining 30% showed no sign of response to the treatment (Figure 4.2 C). Similarly, 40% of mice treated with DAB-Lf: TRAIL underwent complete disappearance of their tumours, while 20% showed partial response to the treatment. Finally, 20% of mice treated with DAB-Lf: IL-12 showed complete disappearance of the tumours and 10% had a partial response, while the remaining 70% had continuously growing tumours but at a slower rate than in the group treated with naked DNA and in the untreated group.

Half of the DU145 tumours treated with DAB-Lf complexing DNA encoding TNF α had completely disappeared by the end of treatment, while 20% showed some signs of tumour regression (Figure 4-3, C). 20% of tumours had completely disappeared in animals treated with DAB-Lf: DNA encoding TRAIL and IL-12 with significant tumour regression in 30% and 10% of the tumours respectively.

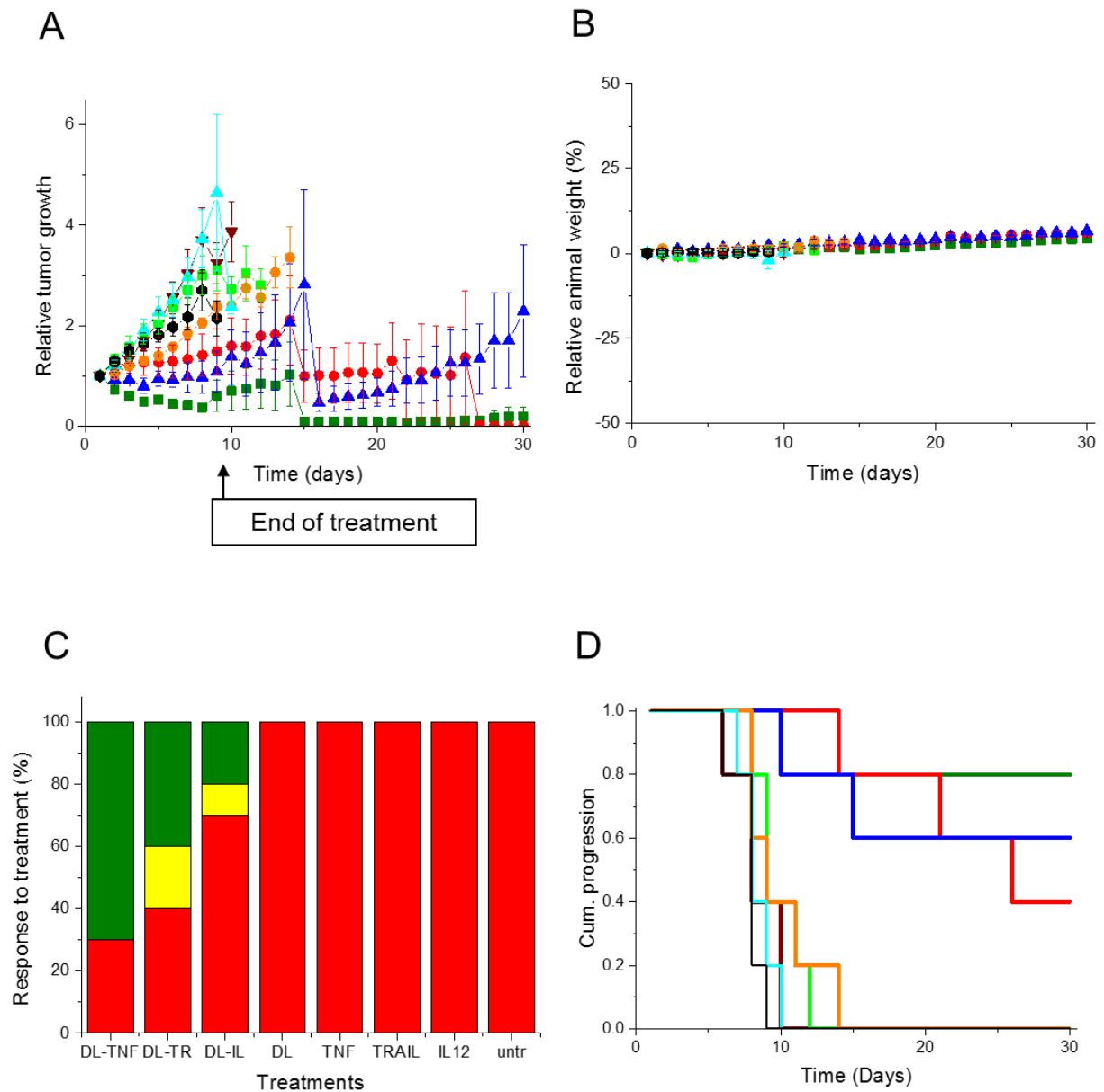


Figure 4-2 (A) Tumour growth studies in PC-3 xenograft tumour model after intravenous injection of lactoferrin-bearing DAB dendrimer complexed with DNA encoding TNF α (green), TRAIL (red), IL-12 (blue), or DAB-Lf only (brown), uncomplexed DNA encoding TNF α (pale green), TRAIL (orange) and IL-12 (cyan) (DNA dose 50 μ g/ml), and an untreated group (black). Tumour size was measured using a caliper. (B) Percentage change in animal body weight during treatment period (colour code as A). (C) Overall tumour response to treatments at the end of the study (Green: complete eradication, Yellow: tumour regression, and Red: tumour growth compared with the original size).(D) Time to disease progression where animals were removed from the study once their tumour reached 10 mm diameter.

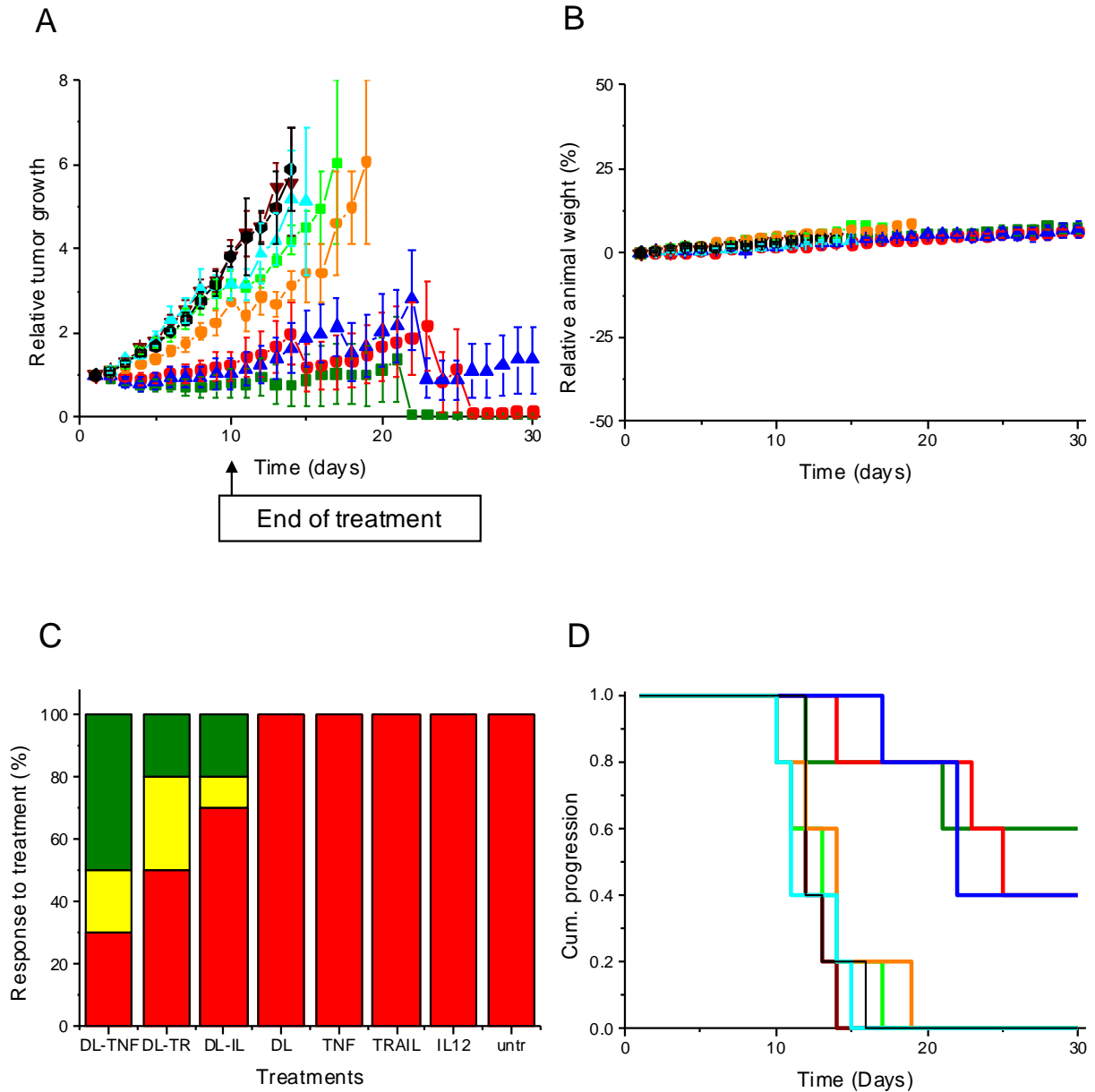


Figure 4-3 (A) Tumour growth studies in DU145 xenograft tumour model after intravenous injection of lactoferrin-bearing DAB dendrimer complexed with DNA encoding TNF α (green), TRAIL (red), IL-12 (blue), or DAB-Lf only (brown), uncomplexed DNA encoding TNF α (pale green), TRAIL (orange) and IL-12 (cyan) (pale blue) (DNA dose 50 μ g/ml), and an untreated group (black). Tumour size was measured using a caliper. (B) Percentage change in animal body weight during treatment period (colour code as A). (C) Overall tumour response to treatments at the end of the study (Green: complete eradication, Yellow: tumour regression, and Red: tumour growth compared with the original size). (D) Time to disease progression where animals were removed from the study once their tumour reached 10 mm diameter.

4.3.2. Bioluminescence imaging

Images obtained by IVIS spectrum showed continuous regression in tumour size for the animal groups treated with lactoferrin-bearing DAB dendriplex complexed with DNA encoding TNF α , TRAIL or IL-12 from the first treatment injection (Figure 4-4). No sign of tumour regression was detected in either the animals treated with uncomplexed DNA or the untreated group, with proportional growth of their tumours.

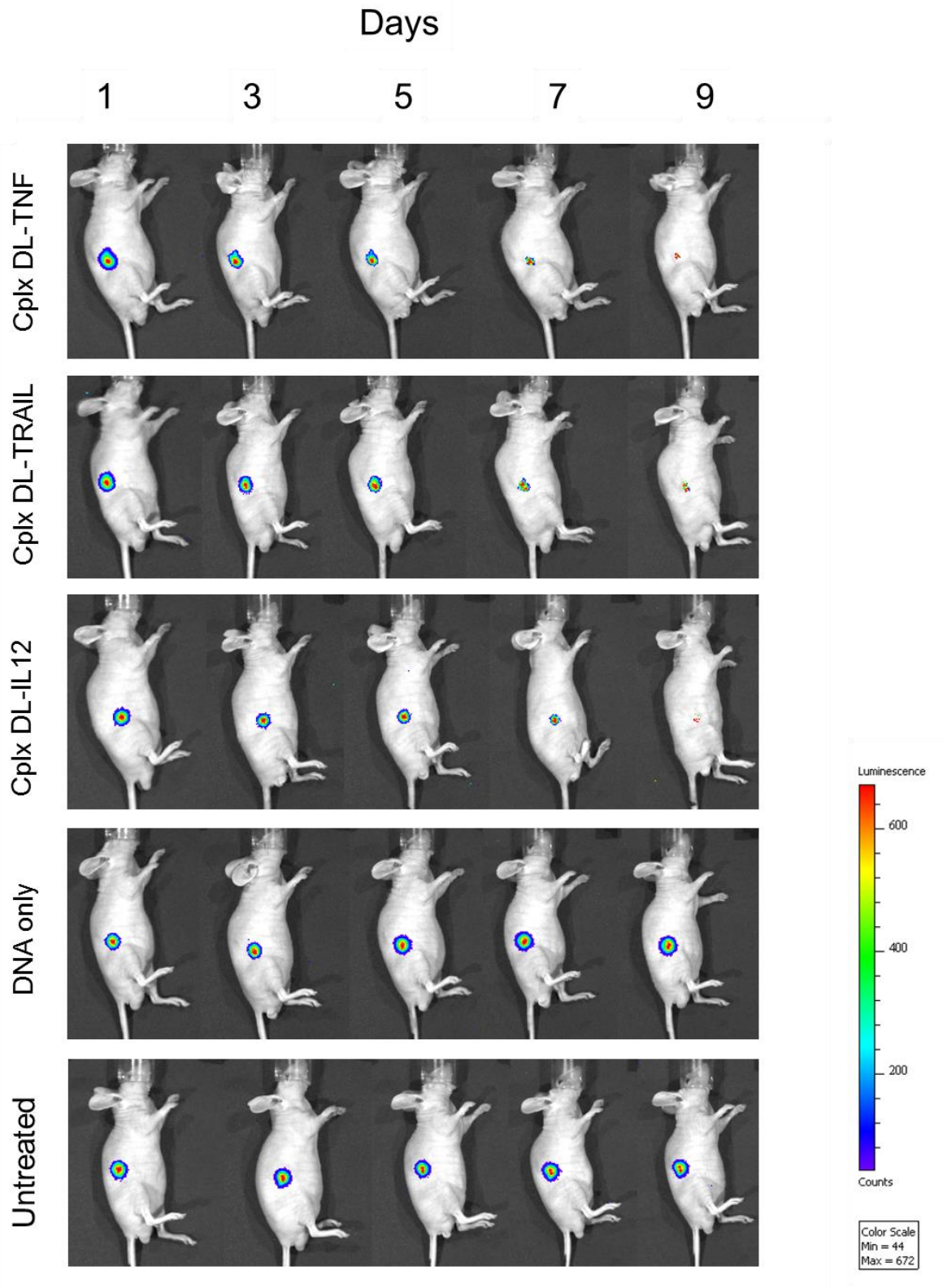


Figure 4-4 Bioluminescence imaging of the tumours after treatment with lactoferrin-bearing DAB dendriplex complexed with DNA encoding TNF α (cplx DL-TNF), TRAIL (cplx DL-TRAIL) and IL-12 (cplx DL-IL12) in a PC-3M-Luc-C6 tumour model.

4.4. Discussion

Earlier chapters have reported how the non-viral gene carrier diaminobutyric polypropylenimine hexadecaamine (DAB), which is well-known for its DNA condensation capability, was modified with the iron binding protein lactoferrin to improve the ability of the gene carrier to target prostate cancer cells, both *in vitro* and *in vivo*. Chapter three confirmed that the transfection efficacy and anti-proliferation effect of the DNA molecules condensed by the modified dendrimer DAB-Lf were significantly improved over unmodified DAB, providing considerable evidence for the success of the designed DAB-Lf dendrimer in transfecting the genetic material and overcoming all of the common cellular obstacles.

In this chapter, we have examined the ability of DAB-Lf dendriplexes to overcome systemic barriers to transfection and have reported the tumoricidal effect of different DNA molecules complexed with this carrier. The use of lactoferrin-bearing DAB dendrimer as carrier for different therapeutic genes encoding TNF α , TRAIL and IL-12 for *in vivo* experiments resulted in significant tumour regression, growth rate reduction and survival rate improvement in nude mice bearing xenograft tumours generated from the human cell lines PC-3 and DU145. Complete tumour regression was also detected in 70% and 40% of the PC-3 tumours after intravenous administration of DAB-Lf encoding TNF α and TRAIL respectively at the end of the treatment cycle (day 30). Similarly, in DU145 tumours, there was 50% complete disappearance in the tumours treated with DAB-Lf: DNA encoding TNF α . In a previous study carried out by the group, Al Robaian *et al.* (2014) obtained around 60% regression in prostate cancer PC-3 xenograft tumours and 50% regression in DU145 tumours after intravenously injecting the mice with DNA encoding TNF α carried by transferrin-bearing DAB dendrimer. Similarly, Kircheis *et al.* (2002) reported an inhibition in tumour growth with complete tumour regression for up to 60% of animals after IV injection of DNA encoding TNF α carried by transferrin-bearing PEI in fibrosarcoma xenograft animal models.

Conjugating lactoferrin to the gene carrier DAB successfully improved the therapeutic efficacy of the gene encoding TNF α compared with unmodified DAB dendriplexes carrying the same therapeutic gene, whereas 30% tumour regression was detected after injecting the mice with DAB: TNF α dendriplex (Lim *et al.*, 2015). This improvement in therapeutic effect demonstrates the significant positive impact of the modified carrier DAB-Lf in assisting the passage of the condensed DNA through both systemic and cellular barriers, producing a significant tumoricidal effect. It also supports the original hypothesis that lactoferrin conjugation would ameliorate the targeting of the nanoparticles to prostate cancer cells. Moreover, this study demonstrates the effectiveness of using apoptosis gene therapy to treat prostate cancer even as a single therapy.

The failure to show any therapeutic effect in the other animal groups, injected with DAB-Lf or DNA only, also supports the original hypothesis that the therapeutic effect of the gene would be seen upon its successful complexation with the modified dendrimer. No therapeutic effect was expected in animals treated with uncomplexed DNA, because the DNA molecules would fail to reach the tumour site. The group injected with DAB-Lf dendrimer alone was included in the study to reveal any toxic effect of the carrier as well as any possible anticancer effect that might arise from the use of lactoferrin as ligand in this formulation.

This study is not the first to demonstrate the advantages of using the iron-binding protein lactoferrin as targeting ligand for prostate cancer. Suryanarayanan Shankaranarayanan *et al.* (2016) also used Lf to improve the targeting of doxorubicin to prostate cancer. Their *in vivo* experiments showed significant inhibition in tumour development in transgenic mice exhibiting adenocarcinoma of the prostate (TRAMP) after treating them with Lf-DOX, whereas most of the animals in the untreated and doxorubicin groups were sacrificed due to tumour enlargement or significant weight loss.

This study used DNA encoding the TNF α and TRAIL cytokines because of their well-known apoptotic action against cancer cells (Norian *et al.*, 2011; Tse *et al.*, 2012). DNA encoding TNF α and TRAIL have been used before in various studies to treat different cancerous tumours, either alone or in combination with therapies such as radio- or chemotherapy, using various types of gene carrier, mostly viral ones. Delivering TNF α gene using viral vectors to target different cancer models by intratumoural (Mauceri *et al.*, 1996) or intravenous injection (Tandle *et al.*, 2009) resulted in significant inhibition in tumour growth, but with no sign of tumour suppression. Chung *et al.* (1998) treated nude mice with xenograft prostate tumours, using a combination of radiotherapy together with TNF α gene carried by adenovirus injected intravenously, resulting in tumour volume regression in comparison with each treatment alone. However, these studies are not comparable to our findings, because the nature of the carrier was different.

TRAIL has been examined previously for its potential apoptotic effect on cancer cells (Kim *et al.*, 2006; Norian *et al.*, 2011). The first study to investigate the TRAIL gene for its therapeutic anticancer apoptotic effect was by Griffith *et al.* (2000), who used adenovirus to deliver the gene to cells *in vitro* before moving to *in vivo* trials of the treatment of many different cancer types. Growth inhibition and tumour regression were detected when TRAIL DNA was delivered using an adeno-associated virus *in vivo* in colorectal tumour models (Mohr *et al.*, 2004). A 50% regression of breast cancer xenograft tumours was also detected after combination therapy with doxorubicin by intratumoural injection (Lin *et al.*, 2002). DNA encoding TRAIL failed to show any sign of tumour regression after being complexed with a prostate cancer targeted nanoplex *in vivo*, while combination therapy with the prodrug 5-fluorocytosine (5-FC) resulted in significant reduction in tumour growth (Chen *et al.* 2016).

There is no previous work comparing the effectiveness of TNF α and TRAIL in inducing apoptosis in cancer cells. Previous papers have reported the effectiveness of both genes in suppressing tumour growth and some studies have reported a tumour regression effect. However, in this study, TNF α showed a tumoricidal effect up to 30% greater than that of TRAIL *in vivo*; in contrast to the *in vitro* finding which showed the superiority of both TRAIL and IL-12 in inducing anti-proliferation effect in all examined cell lines (PC-3, DU145 and LNCaP) showing significantly lower IC₅₀ values compared with TNF α .

IL-12 is an interleukin that is usually generated in response to antigen stimulation, initiating an immune reaction against it through the activation of T-lymphocytes, which stimulates the production of interferon gamma (INF γ). Therefore, using the IL-12 gene in cancer therapy is expected to generate an immunomodulatory response against cancer cells (Lasek *et al.*, 2014). Intratumoural injection of virally carried IL-12 gene in an orthotopic prostate cancer mouse model resulted in more than 50% reduction in tumour size (Nasu *et al.*, 1999). Other studies reported significant tumour regression, depending mainly on the site of injection. Intratumoural injection of plasmid IL-12 together with electroporation to increase the permeability of the cell membrane resulted in 47% tumour regression in C57BL/6 mice but not BALB/c nude mice, whereas applying the same therapy using intramuscular injections resulted in slowing the tumours growth compared with the control group (Lucas *et al.*, 2002). In our study, the dendriplex with DNA encoding IL-12 resulted in less tumour regression than the other two cytokines examined. One possible explanation is that the nude mice were unable to mount an efficacious immune reaction by activating T-lymphocytes in response to IL-12 injections, because they lacked a thymus (Kelland *et al.*, 2004).

In conclusion, lactoferrin-bearing DAB dendrimer was successful in improving the anti-cancer effect of condensed genes encoding various cytokines. It improved the survival rate of the

animals to around 20 days compared with uncomplexed DNA. We observed 70% and 40% of complete tumour regression at the end of the study without any sign of weight loss. DAB-Lf has therefore been demonstrated to be a promising carrier in targeting prostate cancer tumours *in vivo*.

Chapter 5 : General Discussion

In the late 1980s, the concept of active targeting in nanomedicine started to prevail worldwide. It was based mainly on conjugating an antibody, proteins, peptides, or small molecular ligands that are well known to bind to specific cell membrane receptors to a nanocarrier for the purpose of increasing the concentration and accumulation of nanoparticles in the targeted cells or organs (Hoffman, 2008). Selecting a suitable ligand for targeting prostate cancer is the first key step towards synthesising targeted nanoparticles successfully. In this study, three targeting ligands were selected to target different receptors found to be overexpressed in prostate cancer cells. Lactoferrin receptors, PSMA and integrin are all proven to be overexpressed in various cancerous tissues compared with normal tissues including prostate.

Lactoferrin was the first targeting ligand selected in this study as it was found to show strong ability to bind to lactoferrin as well as transferrin receptors which are overexpressed in cancerous tissues (VanSande and VanCamp, 1981; Elfinger *et al.*, 2007; Adlerova *et al.*, 2008; Tuccari and Barresi, 2011), in addition to its multifunctional properties as an antimicrobial, antioxidant and, more importantly, intrinsic anticancer effects. Therefore, lactoferrin seemed to be one possible ligand choice that could be expected to increase the targeting capability of DAB to prostate cancer cells.

Lactoferrin generated its anticancer effect by causing cancer cells apoptosis through the activation of caspase 8 and caspase 3. It increases the release of the transmembrane protein Fas, which has the ability to induce cell apoptosis when bound to its death receptors (Gibbons *et al.*, 2011). Fujita *et al.* (2004) tested the effect of Lf on colon cancer *in vivo* and found that Lf increase the mRNA level of Fas, and the Fas protein by more than a double compared to the control group. There was also a significant increase in the expression of caspases 8 and 3 (Fujita *et al.*, 2004). In addition, Lf was also found to decrease tumours angiogenesis, a possible mechanism of action is the significant reduction in endothelial cell proliferation and the

increases in the production of the anti-angiogenic cytokine IL-18 (Shimamura *et al.*, 2004; Legrand *et al.*, 2008). However, in our study we did not directly investigate the anticancer activity of Lf but instead, we assessed the anti-cancer effect of the formulation DAB-Lf both *in vitro* and *in vivo*. *In vitro*, there were no significant differences in the cytotoxicity between DAB-Lf and DAB dendrimer without DNA, as both were fully non-toxic at a concentration 160 µg/ml in all cell lines examined. *In vivo*, intravenously injecting the mice with DAB-Lf only (250 µg) in an amount equivalent to the one used to complex the DNA as a screening for the cytotoxic effect of the carrier, resulted in no therapeutic effect. Thus, Lf did not appear to contribute in the therapeutic effect obtained from using DAB-Lf dendriplex, in our experiments.

On the use of Lf as targeting ligand, several studies have evaluated its use in targeting different cancer tumours such as brain, liver and lung (Elfinger *et al.*, 2007; Huang *et al.*, 2008; Kurmi *et al.*, 2011; Lim *et al.*, 2015; Wei *et al.*, 2012), while one recently published study discussed the use of Lf as targeting ligand for prostate cancer (Shankaranarayanan *et al.*, 2016).

Kurmi *et al.* (2011) tested the ability of Lf to target lung tissues after conjugating it with DAB dendrimer (5G) to deliver methotrexate (MTX). The result was compared with the targeting ability of DAB-MTX and MTX alone. There was a significant increase in the half-life of the drug after its binding to Lf, plus a significant targeting ability of almost twofold superiority compared to DAB-MTX, and a 2.5-fold superiority over free MTX. Similarly, Wei *et al.* (2012) used Lf to target hepatocellular carcinoma by conjugating it with PEGylated liposome. The targeted liposome showed 2.2-fold improvement in the targeting compared with non-targeted liposome after being examined *in vitro*. *In vivo*, Lf improved the accumulation of the liposome 12h post injection. In our study, DAB-Lf successfully improved the uptake of the dendriplex by 2.1- folds compared with the untargeted dendriplex in PC-3 cells in a similar rate to the data obtained in the studies discussed above.

The second targeted receptor, selected in this study, is PSMA which is expressed primarily on all forms of prostate tissues with some low expression in the nervous system, liver, kidney and small intestine. More importantly, it has been found to be expressed in solid tumours such as prostate, lung, breast and colon cancer (Shen *et al.*, 2013; Dassie *et al.*, 2014). Although PSMA has been detected in several tumour types, it is uniquely overexpressed in prostate cancerous tissues (epithelium cells), which makes it a suitable biomarker to be investigated in therapeutic and diagnostic applications. It is strongly expressed in both primary and metastatic cancer cells, an expression that increases with the malignancy of the disease (Goodman *et al.*, 2007).

PSMA expression in prostate cancer cells has been found to be correlated with androgen sensitivity. LNCaP is an androgen-sensitive epithelial cancer cell express PSMA in its cell membrane. Conversely, PC-3 and DU145 metastatic cancer cells in the bone and brain respectively were found not to express PSMA, although its DNA and mRNA have been detected in these cells (Laidler *et al.*, 2005). These findings would seem to contradict the claim that PSMA expression increases as prostate cancer progresses (Goodman *et al.*, 2007; Yao *et al.*, 2010), as both PC-3 and DU145 cells represent late stages of the disease. There is no clear mechanism behind the loss of PSMA protein expression in these cells.

Using PSMA as a target for treating prostate cancer has several benefits. PSMA has been found to be particularly overexpressed in prostate epithelial cells. Although there is still no known natural ligand that can bind to PSMA, several researchers have succeeded in preparing synthetic binding antibodies and peptides with a good tendency to couple with the extracellular domain of PSMA (Aggarwal *et al.*, 2006; Kinoshita *et al.*, 2006). Furthermore, PSMA ensures the uptake of bound molecules by receptor-mediated endocytosis through clathrin-coated pits, in a manner similar to transferrin receptors (Goodman *et al.*, 2007). This property facilitates the uptake of encapsulated drugs or genes inside the cells. The expression of PSMA in prostate cancer tissues has been found to be correlated with the progress of the disease (Yao *et al.*, 2009;

Liu *et al.*, 2012; Tse *et al.*, 2015). Therefore, targeting PSMA would be very beneficial for treating primary and metastasised cancer tumours.

Various studies have targeted prostate cancer through PSMA by conjugating the nanoparticles with specific antibodies, PSMA inhibitors or peptides (Bouchelouche *et al.*, 2010; Wu *et al.*, 2010; Kasten *et al.*, 2013; Shen *et al.*, 2013). Peptide2 (WQPDTAHHWATL), in particular, was first highlighted in 2006 by Aggarwal as a selective peptide for the extracellular domain of PSMA identified through random phage library. Later, Wu *et al.* (2010) introduced three amino acids to each side of the peptide for the purpose of improving its targeting. Therefore, conjugating this core peptide with the gene carrier DAB is expected to improve the targeting capability of the dendriplex, as well as the cellular uptake of the therapeutic gene through receptor-mediated endocytosis. However, to date, no studies have examined this peptide as a targeting ligand after conjugating it with nanoparticles.

The third and final targeted receptor in this study is integrin. Several integrin receptors have been found to be overexpressed in prostate cancer cells, with differentiation in their expression as the cancer progresses, whereas other receptors have been detected only in cancer tissues, not in normal ones. The following integrin heterodimer receptors have been demonstrated in different studies to be overexpressed in prostate cancer: $\alpha v\beta_6$, $\alpha v\beta_3$, $\alpha_{IIb}\beta_3$, $\alpha_6\beta_1$, $\alpha_5\beta_1$, and $\alpha_6\beta_4$ (Fornaro *et al.*, 2001; Suyin *et al.*, 2013). Among these, $\alpha v\beta_3$ has been found to be expressed in prostate cancer cells at an intensity that varies with the metastatic and invasion tendency of the cells. PC-3 cells extensively express $\alpha v\beta_3$, while LNCaP cells do not, explaining the greater invasion capability of PC-3 over LNCaP cells, as $\alpha v\beta_3$ tends to adhere to vitronectin in the ECM (Zheng *et al.*, 1999). In addition, $\alpha_5\beta_1$ is shown to be expressed in PC-3 as it has a role in their adhesion and invasion behaviour (Stachurska *et al.*, 2012).

RGD is a peptide motif that is responsible for cell adhesion in ECM. Different RGD binding

integrins are overexpressed in prostate cancer cells, making an RGD peptide a possible ligand for prostate cancer. EETI-II 2.5F is an RGD peptide designed by Kimura and colleagues (2009) to target integrin receptors overexpressed in cancer: $\alpha v\beta_5$, $\alpha v\beta_3$, $\alpha_{IIb}\beta_3$ and $\alpha_5\beta_1$. This peptide has been used before as an imaging probe to target brain tumours and particularly $\alpha_5\beta_1$ receptors (Moore *et al.*, 2013). In this study, we selected the active binding site of the EETI-II 2.5F peptide PRPRGDNPPPLT (Peptide4) to be conjugated with DAB dendrimer as the targeting ligand for prostate cancer.

After a successful synthesis and characterisation of the physiochemical characteristics of the targeted dendrimers (DAB-Lf, DAB-Pep2, DAB-PEG2k-Pep2 and DAB-PEG2k-Pep4) and their dendriplexes, each of the conjugated targeting ligands (Lf, Peptide2, and Peptide4) resulted in a different impact on the final physiochemical properties of the synthesised nanoparticles because these ligands exhibit various differences in their nature, size and charge. Firstly, Lf is a protein with a molar size of 82 kDa, whereas the size of Peptide2 and Peptide4 is 1.5 and 2 kDa, respectively. This huge difference in size is believed to have a major impact on the overall size and zeta potential generated in DAB-Lf, DAB-Pep2, and DAB-Pep4 dendriplexes. DAB-Lf resulted in a mean zeta of 19.6 mV, while both DAB-Pep2 and DAB-Pep4 showed very high charged dendriplexes with zeta potential of over 30 mV which could be explained by the fact that more dendrimers are required to obtain full condensation of the DNA in the case of DAB-Pep2 and DAB-Pep4, i.e. higher overall zeta potential. This variation in zeta potential essentially affects the safety of the designed dendriplexes, as demonstrated later using MTT assay. In all three dendriplexes, we used the same generation of DAB dendrimer (generation 3), and the same amount of DNA was condensed, making the conjugated targeting ligand the only changing factor between these dendriplexes. All three targeting ligands are generally soluble in aqueous solutions, however, the core difference between them is that Lf is actually a natural protein that is normally synthesised inside the body

and is well-known to be non-toxic, whereas the used peptides were both synthetic and their safety profile was not assessed beforehand. Thus, the used synthetic peptides contributed to the overall cytotoxicity as well as the high zeta potential initiated in DAB-Pep2 and DAB-Pep4 dendriplexes. The high zeta potential of DAB-Pep2 and DAB-Pep4 dendriplexes was then reduced by introducing different molar ratios of PEG polymer to the dendrimer.

The size of the dendriplexes formulated is directly correlated with the zeta potential generated. By comparing the size of the highest dendrimer, DNA weight ratio used (20:1) of the different dendriplexes formed, we concluded that DAB-Lf had the largest size with a mean size of 66.37 ± 0.96 nm, whereas DAB-Pep2 and DAB-Pep4 had a lower mean size of 59.87 ± 0.67 nm and 58.25 ± 0.24 nm, respectively. The reduction in the size of the dendriplex is also correlated with an increase in the zeta potential. One possible explanation is that in DAB-pep2 and DAB-Pep4, more dendrimers are required to form a stable spherically shaped dendriplex than in the case with DAB-Lf, resulting in highly charged dendriplex but with better complexing property for the DNA and therefore the formation of smaller compacted nanoparticles. This suggestion was actually supported by the PicoGreen[®] assay findings where at a weight ratio of 20:1 DAB-Lf was able to condense 80% of the DNA, whereas it was 90 to 100% in the case of DAB-Pep2. In general, it seems that the size and zeta of the dendriplexes are in reverse relation, wherein a higher zeta is associated with better complexation and therefore a smaller particle size (Aldawsari *et al.*, 2011; Li *et al.*, 2015).

For the purpose of improving the physiochemical properties of DAB-Pep2 and DAB-Pep4, different ratios of the PEG chain were introduced to the DAB-Pep2 dendrimer. The introduction of PEG molecules resulted in a significant reduction of the zeta potential of DAB-Pep2 and DAB-Pep4 to 23.28 ± 0.96 mV and 19.5 ± 5.43 mV respectively, while increasing the size for up to 64.86 ± 1.7 nm in the case of DAB-Pep2. However, this was not the case with

DAB-Pep4, where the introduction of the PEG chain reduced the zeta potential but did not result in a detectable change in size.

The AFM finding showed that all three dendriplexes (DAB-Lf, DAB-PEG2k-Pep2 and DAB-PEG2k-Pep4) were spherical in shape with size that was almost similar to the one obtained by DLS. DAB-PEG2k-Pep4 showed a larger size with a mean value of 81.83 ± 21.9 nm, which could be due to the agglomeration of more than one particle.

In vitro studies were carried out for DAB-Lf, DAB-Pep2 and DAB-PEG2k-Pep2, with preliminary screening of DAB-PEG2k-PEG3.5k-Pep2, DAB-PEG3.5k-Pep2 and DAB-PEG2k-Pep4. We started the *in vitro* experiments with DNA transfection assay. The aim was to investigate the capability of the various dendriplexes at different weight ratios between the polymer and DNA in successfully bringing about improvement in DNA transfection over the control. From the finding obtained, we can determine whether or not the modified dendrimer will lead to an improvement in gene transfection, as well as being able to select the optimal weight ratio for carrying out further *in vitro* studies. Both DAB-Lf and DAB-Pep2 showed an improvement in the transfection finding over the positive control DAB in low weight ratios 5:1 and 2:1 respectively in all cell lines. Introducing PEG, however, significantly reduces the transfection tendency in the low weight ratios, keeping the two possible ratios that would have a positive impact as 20:1 and 10:1. This is actually in line with the DNA complexation findings. Based on transfection studies, we decided to stop working with integrin targeted dendrimer DAB-PEG2k-Pep4, as it did not show any improvement compared with the controls. Further improvement of this formulation is thus required. Some suggestions include increasing the molar ratio of the targeting ligand, using a larger DAB generation, and different PEG chain length and ratio.

The quantitative cellular uptake finding demonstrates the superiority of Lf in improving the

uptake in all examined cells. However, this was not the case with Peptide2 formulation, as its measuring was affected by other characteristics such as DAB-Pep2 dendriplex high zeta potential. The PEGylated DAB-Pep2 showed a superiority in the uptake by LNCaP and DU145 but not PC3 cells. Therefore, for a better understanding of the exact uptake pathway of the dendriplex, the mechanism of cellular uptake studies was performed. In both DAB-Lf and DAB-PEG2k-Pep2, the uptake of the dendriplex was actually the sum of diverse pathways including a significant inhibition of the ionic uptake, as all the dendriplexes examined in this study were cationic. The other blocked pathways showed various levels of inhibition including clathrin-mediated endocytosis and caveolae-mediated endocytosis. The main difference between DAB-Lf and DAB-PEG2k-Pep2 is the impact of blocking the macropinocytosis pathway through pre-treating the cells with colchicine. Pretreating the cells with colchicine showed no inhibition in the DAB-Lf uptake but a significant inhibition for the DAB-PEG2k-Pep2 uptake in all examined cells. Although both DAB-Lf and DAB-PEG2k-Pep2 dendriplexes have an average size smaller than 100 nm, this pathway is expected to have no impact in the uptake of these dendriplexes. There is noticeable different in the zeta potential between DAB-Lf and DAB-PEG2k-Pep2 dendriplexes, which would be related to the positive uptake of DAB-PEG2k-Pep2 dendriplex through macropinocytosis, because DAB-PEG2k-Pep2 has a higher zeta potential than DAB-Lf. Thus, this zeta potential attracts other particles in the cell culture medium such as proteins through electrostatic interactions causing an enlargement in the overall size of the dendriplex (Mahmoudi *et al.*, 2011), explaining the uptake of DAB-PEG2k-Pep2 dendriplex via macropinocytosis. Therefore, studying the size and zeta of the synthesised dendriplex using culture medium instead of glucose 5% would seem to be more useful to improve the understanding of the impact of protein binding on the circulation in the physiochemical characteristics of the dendriplex.

Anti-proliferation examination using therapeutic DNA encoding TNF α , TRAIL and IL-12 was

carried out to examine the capability of these modified dendrimers (DAB-Lf, DAB-Pep2 and DAB-PEG2k-Pep2) in improving the apoptotic effect produced by these cytokines through improving the active targeting and comparing the data with non-targeted formulation. In the case of DAB-Lf, all complexed DNA showed significant improvement in IC_{50} compared with DAB dendrimer complexing the same DNA, thereby expressing the impact of Lf in improving the uptake of the dendriplex and thereafter the endosomal escape and transfection.

On the other hand, using Peptide2 as targeting ligand did not result in such effective data, as with Lf. The preliminary screening for DAB-Pep2 showed that the dendrimer had high cytotoxicity. It also demonstrated that complexing the DNA with the dendrimer would result in reducing its cytotoxicity. This effect would be expected, as complexing the dendrimer with DNA will likely neutralise the vast majority of the cationic groups in the dendrimer (primary amine groups) by forming electrostatic interaction with the DNA (Dufès *et al.*, 2005).

The anti-proliferation effect of the DAB-PEG2k-Pep2 dendriplex was examined after complexing plasmid encoding TNF α and TRAIL. For both PSMA-negative PC-3 and DU145 cell lines, the non-targeted dendriplex showed preferable therapeutic effect with lower IC_{50} values, whereas LNCaP cells were found to respond better to the targeted formulation, thus supporting the original hypothesis that Peptide2 is a PSMA-specific ligand. Owing to the fact that we used a high ratio of DAB-PEG2k-Pep2 to DNA (20:1), the first three concentrations in the MTT curve were associated with high toxicity that seemed similar to that between the DAB-PEG2k-Pep2 dendrimer and its dendriplex. At DNA concentration of 6.4 $\mu\text{g/ml}$, the DAB-PEG2k-Pep2 dendrimer found to be non-toxic, making this concentration ideal for comparing between different dendriplexes. In PC-3 and DU145 cells, the non-targeted dendriplex DAB-PEG resulted in superior anti-proliferation effect over DAB-PEG2k-Pep2, whereas this was not the case with LNCaP cells that either showed no significant difference in the case of TNF α

or superiority of the targeted formulation in the case of TRAIL treatment.

By comparing the anti-proliferation effect obtained from DAB-Lf and DAB-PEG2k-Pep2, we can conclude that Lf had resulted in better targeting impact than Peptide2. DAB-Lf dendriplexes were non-toxic and seemed to dramatically result in better cellular uptake and more importantly better transfection for the DNA inside the cells, which can be highlighted from the finding of the MTT assay. In contrast, Peptide2 was shown to have toxic effect on the cells and in our effort to reduce this toxicity, it was found that introducing PEG molecules successfully reduced the toxicity but it also affected the DNA condensation efficiency of the third generation DAB. Furthermore, using the weight ratio 20:1 in the case of DAB-PEG2k-Pep2 dendriplex could be one of the reasons behind the low efficiency in the MTT finding. Which means that this ratio might be efficient for cellular uptake but inside the cytoplasm, the transfection of DNA is affected. Although it might be early to draw any conclusion from the finding obtained so far but using a high weight ratio of DAB-PEG2k-Pep2 (20:1) would result in efficient DNA complexation even though it would negatively affect the release of DNA into the endosome. This would be supported by comparing the transfection finding of DAB-Lf at the same weight ratio (20:1).

Having successfully demonstrated that the TNF α cytokine was produced in the cells after treating them with DAB-PEG2k-Pep2 dendrimer complexed with DNA encoding TNF α , the anti-proliferation findings were expected to be more efficient. A possible explanation for this result is that the cytokine produced after delivering the DNA using DAB-PEG2k-Pep2 is not high enough to produce the therapeutic effect expected compared to DAB-Lf. Using TNF α cytokine as apoptosis inducer has been examined in several studies by means of the usual concentration of 20 ng/ml of TNF α to record its apoptosis effect (Guo *et al.*, 2014; Zheng *et al.*, 2017). This concentration is significantly higher than the amount detected in the ELISA

test in our study in all cell lines examined. However, to confirm this hypothesis, a transfection study using ELISA assay should be carried for DAB-Lf to compare the concentration of TNF α cytokine formed.

In the literature, DAB PEGylation was usually carried out for large generations (DAB-Am32 and DAB-Am64) with the purpose of diminishing the charge and reducing the cytotoxicity usually associated with such a high charge (Taratula *et al.*, 2009; Thakur *et al.*, 2015). However, we could not find any study that used the PEG chain to conjugate the third generation DAB dendrimer. Therefore, the impact of PEG chains on DAB-PEG and DAB-PEG2k-Pep2 required more investigation. Although it was found to improve transfection in the high weight ratio of 20:1, thereby suggesting the overcoming of the cellular barriers and successful production of β -galactosidase, the MTT findings were lower than expected. This discrepancy in the results leads to the outcome that PEGylating the third generation DAB dendrimer might successfully reduce its cytotoxicity, but it might have also negatively affected the endosomal escape of the formulated dendriplex. Further investigation is thus needed if we are to confirm this hypothesis.

In this study, the DNA encoding TNF α and TRAIL were chosen as the therapeutic genes to be complexed with the modified dendrimers due to their well-known cellular apoptosis effect (Norian *et al.*, 2011; Tse *et al.*, 2012). In the literature, TNF α and TRAIL have been used to treat different cancer tumours using mainly viral vectors (Lin *et al.*, 2003; Seol *et al.*, 2003; Mohr *et al.*, 2004; Jiménez *et al.*, 2010) and some non-viral vectors (Su *et al.*, 2013; Wang *et al.*, 2015; Gao *et al.*, 2016).

In vivo studies on the apoptotic effect of TNF α have yielded promising data either by using TNF α in combination with other therapies such as chemo or radiotherapy (Chung *et al.*, 1998; Su *et al.*, 2013) or as a single therapy (Al Robaian *et al.*, 2014). Su *et al.* (2013) injected the

TNF α gene carried by modified DAB dendrimers intravenously alone (or in combination with Doxil[®]) into neuroblastoma xenograft models so as to study the possibility of improving TNF α expression in targeted tumour site. *In vivo* findings demonstrate the synergistic effect associated with intravenously injecting the animals with the polyplex followed by Doxil[®] in the next day for four doses, resulting in a significant reduction in tumour growth rate compared with each therapy alone. Furthermore, TNF α have been used before as a single therapy approach to treat cancer using non-viral gene carriers. Kircheis *et al.* (2002) intravenously injected transferrin-targeted polymer PEI as a carrier of TNF α to target three different cancer tissue origins (neuroblastoma, fibrosarcoma and melanoma), which resulted in tumour growth inhibition as well as complete tumour regression for up to 60% of animals in fibrosarcoma xenograft animal models. This was also demonstrated in our laboratory: intravenously injecting mice with transferrin-bearing dendriplexes carrying DNA encoding TNF α was found to cause significant tumour volume regression with an overall tumour disappearance in up to 90% and 50% of tumours in epidermoid carcinoma and prostate carcinoma xenograft models, respectively (Koppu *et al.*, 2010; Al Robaian *et al.*, 2014). By comparing these findings with the results obtained in this study, intravenously injecting DAB-Lf dendrimer complexed with DNA encoding TNF α has resulted in complete tumour regression in 70% and 50% of tumours in the PC-3 and DU145 xenograft tumour models, respectively. These studies demonstrate the effectiveness of using protein- targeted cationic dendrimers to improve the therapeutic efficacy of DNA encoding TNF α as a single therapy for treating different cancer tumours including prostate.

DNA encoding TRAIL was also used as apoptotic agent. Some studies highlight that certain types of cancer cells could develop resistance to TRAIL's apoptotic effect, including prostate cancer cells: LNCaP cells were found to have full resistance to TRAIL-induced apoptosis, while DU145 was semi-sensitive, and PC-3 was fully sensitive to its apoptotic effect (Shankar

et al., 2005). However, this was not demonstrated in the *in vitro* findings, as DU145 responded very efficiently to TRAIL treatment with IC₅₀ value 3.56 +/- 0.69 µg/ml, which was significantly lower than the one detected with PC-3 15.6 +/- 3.61 µg/ml after complexing TRAIL with DAB-Lf. This was not the case with *in vivo* studies as TRAIL treatment resulted in better therapeutic effect for treating PC-3 xenograft tumours compared to DU145, with 40% and 20% tumour regression, respectively.

Complexing DNA encoding TRAIL with targeted carriers and injecting it intravenously to treat various xenograft tumours has been carried out before with variable findings. Gao *et al.* (2016) used transferrin as a cancer targeting ligand and injected mice intravenously with PAMAM-Tf: TRAIL complex in a dose of 200 µg DNA every two days for five doses. The results showed significant improvement in the survival rate with reduction in tumour growth. In comparison with the finding obtained in this study, treating mice with 50 µg dendriplex every other day for five doses resulted in significant improvement in the survival rate, reduction in tumour growth, together with 40% complete tumour regression.

Chapter 6 : Conclusion and future plans

6.1. Conclusion

Prostate cancer is estimated to cause 1.1 million diagnosed cases with around 307,000 deaths worldwide on an annual basis (GLOBOCAN, 2012). There has been great progress with regard to prostate cancer treatments in the last two decades including an approval of some novel treatments such as immunotherapy (sipuleucel-T) and hormonal therapy (abiraterone acetate and enzalutamide) which have improved survival in men with the late stages and recurrent cancer, not to mention improvement in their lifestyle (Pawlita and Brennan, 2013; Attard *et al.*, 2016). However, with the remarkable progress in prostate cancer treatments in recent years, the choices are still limited and the improvement in the survival rate did not approach six months at best in all the mentioned drugs.

One possible new approach to treating cancer is gene therapy, which is currently hindered by the lack of a safe and effective gene carrier. Therefore, gene delivery methods must be developed to ensure the successful transfer and transfection of the gene of interest to the targeted cells. The main challenge in gene delivery is how to synthesize an efficacious delivery system capable of targeting the required tissue without side effects (Wang *et al.*, 2013).

Cationic dendrimers such as diaminobutyric polypropylenimine (DAB) are found to be very efficient in gene complexation through the generation of electrostatic interactions between phosphate groups in the DNA and amine groups in the dendrimer (Dufès *et al.*, 2005). This complexation protects the gene from the surrounding environment and prevents the degradation of DNA by the nuclease enzymes in the circulation (Wang *et al.*, 2013). It also reduces the repulsion between the DNA and cell membrane that arises from their charges, which in turn improves the ability of the gene to penetrate these cells (McCrudden and McCarthy, 2013).

In this study, we have demonstrated that apoptosis gene therapy could result in tumours eradication even as a single therapy approach, using lactoferrin- bearing DAB dendrimer as a targeted gene carrier.

In vitro, the cellular uptake of fluorescein-labelled DNA was significantly improved after being complexed with DAB-Lf in PC-3, DU145 and LNCaP prostate cancer cells, as quantitatively confirmed by the flow cytometer. The anti-proliferative efficacy of DAB-Lf complexed with therapeutic plasmid DNA encoding TNF α , TRAIL or IL-12 was significantly improved compared to the unmodified DAB dendriplex by up to 13.2-folds when treating DU145 cells with DAB-Lf dendriplex encoding TNF α . *In vivo*, there were 70% and 50% complete disappearances of the PC-3 and DU145 tumours respectively after intravenously injecting the mice with DAB-Lf dendriplexes encoding TNF α .

We have also demonstrated that PEGylating peptide- bearing DAB dendrimers resulted in improving the physiochemical properties of the dendriplex as well as reducing its toxicity. DAB-PEG2k-Pep2 dendrimer was found to have efficiently condensed the DNA for the weight ratios 20:1 and 10:1 by more than 70%. The DNA condensation tendency was reduced compared with DAB-Pep2. The zeta potential was reduced after PEGylation, whereas the size of the dendriplex increased. *In vitro*, DAB-PEG2k-Pep2 was found to improve gene transfection for the PSMA-positive cell line by a 2.7-fold improvement compared to the positive control. Cellular uptake finding also supports this result with a 1.36-fold improvement in the uptake for LNCaP cells. The anti-proliferation results showed significant improvement in the IC₅₀ compared with the unmodified DAB-PEG dendriplex by up to 2.94-fold when treating LNCaP cells with DAB-PEG2k-Pep2 dendriplex encoding TNF α ; whereas, as expected, the other cell lines revealed the superiority of the non-targeted formulation.

In summary, Lactoferrin-bearing DAB dendrimer has been demonstrated to be a promising carrier in targeting prostate cancer tumours, reflecting the efficacy of using Lf as a targeting

ligand. This study is one of only a few that show such tumour regression after intravenous administration of gene therapy using non-viral vectors as a single therapy approach. Peptide2 appeared to be a promising targeting ligand for PSMA, as DAB-PEG2k-Pep2 dendriplex showed significant improvement in transfection and cellular uptake for LNCaP cells as the PSMA-positive cell line. However, further improvement in formulation is required so as to obtain the optimal anti-proliferation impact after complexing DNA encoding therapeutic cytokines.

6.2. Future work

In this study, various targeting ligands were used to synthesise three novel delivery systems for targeting prostate cancer. These novel delivery systems were synthesised, characterised and subjected to a preliminary *in vitro* screening. Based on the findings obtained, some of the formulations were subjected to further *in vitro* studies, and only DAB-Lf succeeded to *in vivo* experiments. The formulations resulted in variability in the finding due mainly to the targeting ligand conjugated with. The findings of this thesis led to certain proposals that might be applicable to future work.

Intravenously injecting mice with DNA encoding TNF α or TRAIL complexed with DAB-Lf dendrimer has resulted in significant tumoricidal finding and tumour regression after examining their impact on subcutaneous xenograft tumour models. However, a deeper understanding of the designed dendriplex's impact on the prostate microenvironment as well as the effect of the therapy on the metastasized regions is required. Thus, the next suggested step is to carry out *in vivo* studies using more advanced tumour models such as using mice with transgenic adenocarcinoma of the mouse prostate (TRAMP) or -implanting BALB/C mice with prostate cancer cells directly in the prostate to generate an orthotopic tumour model (Pavese *et al.*, 2013).

Furthermore, dual targeting of nanoparticles, based on the introduction of two receptor binding elements instead of only one, could further improve cancer cell recognition and cellular uptake (Saul *et al.*, 2006). This dual-receptor internalization mechanism is expected to result in higher selectivity and transfection efficacy. In both the thesis and literature, it has been demonstrated that conjugating transferrin and lactoferrin proteins with the third generation DAB dendrimer to act as targeting ligands for prostate cancer has led to an outstanding finding in gene therapy (Al Robaian *et al.*, 2014; Lim *et al.*, 2015). In addition, targeting PSMA using Peptide2 was found to have selective binding to PSMA-positive cells. Therefore, preparing a new

nanoparticle with dual-targeting strategy by conjugating DAB with lactoferrin as well as Peptide2 would improve the targeting tendency by doubling the chance of cellular uptake through receptor-mediated endocytosis either through LfR or PSMA.

In addition, a combinational therapy through co-administration of complementary nucleic acids: co-administration of plasmid DNA encoding TNF α with either interferon (IFN- γ) or tumour necrosis factor-related apoptosis-inducing ligand (TRAIL), would improve the therapeutic efficacy of the dendriplex.

Another possible combinational therapy is co-administration of drug and gene therapy. This has been examined before using both viral and non-viral carriers involving DNA encoding TRAIL and TNF α co-administration with doxorubicin (Lin *et al.*, 2002; Su *et al.*, 2013; Chen *et al.*, 2016).

Furthermore, investigating the impact of PEGylation on DAB dendrimer was carried out in this study for the purpose of reducing the cytotoxicity generated by the introduction of peptides (Peptide2 and Peptide4). Although conjugating PEG chains with DAB-Am16 resulted in a significant reduction of the zeta potential and cytotoxicity accordingly, it also reduced DAB-Am16 abilities in condensing the DNA and was suspected to have a negative impact on the endosomal escape and transfection. Owing to the fact that the third generation of DAB dendrimer is known for its high DNA condensation tendency and relative low cytotoxicity (Zinselmeyer *et al.*, 2002), PEGylating it might not result in ideal findings. Therefore, the following suggestions are recommended for improving the synthesis of peptide-targeted dendrimers:

- Using high generations of DAB dendrimer (DAB-Am32 and DAB Am64) to conjugate the peptides instead of generation three, and conjugating them with various ratios of polyethylene glycol polymer (PEG) chains followed by conjugation with Peptide2 or Peptide4. Better outcomes would be expected (compared to generation three) because

PEGylating a larger generation of DAB is expected to diminish the cytotoxicity while maintaining the complete DNA condensation tendency (Zinselmeyer *et al.*, 2002).

- In Chapter two, the targeting peptides amount used was equivalent to one- fold of the molar concentration of DAB-Am16 dendrimer. However, in order to improve the chance of ligands' exposure to the targeted receptors after complexing the DNA, a higher molar ratio should be used. Conjugating the PEGylated DAB-Am32 and DAB-Am64 dendrimers with a higher molar ratio of targeting ligands could therefore lead to improvement in the active targeting of these dendriplexes.

References

- ABBAS, T. & DUTTA, A. 2009. p21 in cancer: intricate networks and multiple activities. *Nature Reviews Cancer*, 9, 400-414.
- ADLEROVA, L., BARTOSKOVA, A. & FALDYNA, M. 2008. Lactoferrin: a review. *Veterinari Medicina*, 53, 457-468.
- AGGARWAL, S., SINGH, P., TOPALOGLU, O., ISAACS, J. T. & DENMEADE, S. R. 2006. A dimeric peptide that binds selectively to prostate-specific membrane antigen and inhibits its enzymatic activity. *Cancer Research*, 66, 9171-9177.
- AGHA-MOHAMMADI, S. & LOTZE, M. T. 2000. Immunomodulation of cancer: potential use of selectively replicating agents. *Journal of Clinical Investigation*, 105, 1173-1176.
- AL ROBAIAN, M., CHIAM, K. Y., BLATCHFORD, D. R. & DUFÈS, C. 2014. Therapeutic efficacy of intravenously administered transferrin-conjugated dendriplexes on prostate carcinomas. *Nanomedicine*, 9, 421-434.
- ALDAWSARI, H., EDRADA-EBEL, R., BLATCHFORD, D. R., TATE, R. J., TETLEY, L. & DUFÈS, C. 2011. Enhanced gene expression in tumors after intravenous administration of arginine-, lysine- and leucine-bearing polypropylenimine polyplex. *Biomaterials*, 32, 5889-99.
- ALEX, S. M. & SHARMA, C. P. 2013. Nanomedicine for gene therapy. *Drug Delivery and Translational Research*, 3, 437-445.
- ALLAY, J. A., STEINER, M. S., ZHANG, Y., REED, C. P., COCKROFT, J. & LU, Y. 2000. Adenovirus p16 gene therapy for prostate cancer. *World Journal of Urology*, 18, 111-20.
- ALLEN, T. M. 1997. Liposomes - Opportunities in drug delivery. *Drugs*, 54, 8-14.
- AN, J., SUN, Y. P., ADAMS, J., FISHER, M., BELLDEGRUN, A. & RETTIG, M. B. 2003. Drug interactions between the proteasome inhibitor bortezomib and cytotoxic chemotherapy, tumor necrosis factor (TNF) alpha, and TNF-related apoptosis-inducing ligand in prostate cancer. *Clinical Cancer Research*, 9, 4537-45.
- ANGIUS, F. & FLORIS, A. 2015. Liposomes and MTT cell viability assay: An incompatible affair. *Toxicology in Vitro*, 29, 314-319.
- ANTUNES, A. A., REIS, S. T., LEITE, K. R., REAL, D. M., SOUSA-CANAVEZ, J. M., CAMARA-LOPES, L. H., DALL'OGLIO, M. F. & SROUGI, M. 2014. Re: PGC and PSMA in prostate cancer diagnosis: tissue analysis from biopsy samples. *International Brazilian Journal of Urology*, 40, 285-285.
- ARAFAT, W., ZHOU, T., NAOUM, G. E. & BUCHSBAUM, D. J. 2015. Targeted radiotherapy potentiates the cytotoxicity of a novel anti-human DR5 monoclonal antibody and the adenovirus encoding soluble TRAIL in prostate cancer. *Journal of the Egyptian National Cancer Institute*, 27, 205-15.
- ARTIBANI, W. 2012. Landmarks in prostate cancer diagnosis: the biomarkers. *British Journal of Urology*, 110 Suppl 1, 8-13.
- ASHKENAZI, A., PAI, R. C., FONG, S., LEUNG, S., LAWRENCE, D. A., MASTERS, S. A., BLACKIE, C., CHANG, L., MCMURTREY, A. E., HEBERT, A., DEFORGE, L., KOUMENIS, I. L., LEWIS, D., HARRIS, L., BUSSIERE, J., KOEPPEN, H., SHAHROKH, Z. & SCHWALL, R. H. 1999. Safety and antitumor activity of recombinant soluble Apo2 ligand. *Journal of Clinical Investigation*, 104, 155-162.

- AZARE, J., LESLIE, K., AL-AHMADIE, H., GERALD, W., WEINREB, P. H., VIOLETTE, S. M. & BROMBERG, J. 2007. Constitutively activated Stat3 induces tumorigenesis and enhances cell motility of prostate epithelial cells through integrin beta 6. *Molecular and Cellular Biology*, 27, 4444-4453.
- AZZI, S., HEBDA, J. K. and GAVARD, J. 2013. Vascular permeability and drug delivery in cancer. *Frontiers in oncology*, 3, 211.
- BAGNALL P. 2014. Diagnosis and treatment of prostate cancer. *Nursing Times*, 110 (9), 12-15.
- BAIG, F. A., HAMID, A., MIRZA, T. & SYED, S. 2015. Ductal and Acinar Adenocarcinoma of Prostate: Morphological and Immunohistochemical Characterization. *Oman Medical Journal*, 30, 162-6.
- BANERJEE, D., BROEREN, M. A. C., VAN GENDEREN, M. H. P., MEIJER, E. W. & RINALDI, P. L. 2004. An NMR study of the supramolecular chemistry of modified poly(propyleneimine) dendrimers. *Macromolecules*, 37, 8313-8318.
- BARCZYK, M., CARRACEDO, S. & GULLBERG, D. 2010. Integrins. *Cell and Tissue Research*, 339, 269-280.
- BARETTON, G. B., KLENK, U., DIEBOLD, J., SCHMELLER, N. & LOHRS, U. 1999. Proliferation- and apoptosis-associated factors in advanced prostatic carcinomas before and after androgen deprivation therapy: prognostic significance of p21/WAF1/CIP1 expression. *British Journal of Cancer*, 80, 546-555.
- BARRESI, G. & TUCCARI, G. 1984. LACTOFERRIN IN BENIGN HYPERTROPHY AND CARCINOMAS OF THE PROSTATIC GLAND. *Virchows Archiv a-Pathological Anatomy and Histopathology*, 403, 59-66.
- BEHROOZ, A., KUO, C., XU, H. & RICE, B. 2013. Adaptive row-action inverse solver for fast noise-robust three-dimensional reconstructions in bioluminescence tomography: theory and dual-modality optical/computed tomography *in vivo* studies. *Journal of Biomedical Optics*, 18, 8216-8227.
- BENDAS, G. 2001. Immunoliposomes - A promising approach to targeting cancer therapy. *Biodrugs*, 15, 215-224.
- BERTRAND, N., WU, J., XU, X. Y., KAMALY, N. & FAROKHZAD, O. C. 2014. Cancer nanotechnology: The impact of passive and active targeting in the era of modern cancer biology. *Advanced Drug Delivery Reviews*, 66, 2-25.
- BHATTACHARJEE, S. 2016. DLS and zeta potential - What they are and what they are not? *Journal of Controlled Release*, 235, 337-351.
- BLAESE, R. M., CULVER, K. W., MILLER, A. D., CARTER, C. S., FLEISHER, T., CLERICI, M., SHEARER, G., CHANG, L., CHIANG, Y., TOLSTOSHEV, P., GREENBLATT, J. J., ROSENBERG, S. A., KLEIN, H., BERGER, M., MULLEN, C. A., RAMSEY, W. J., MUUL, L., MORGAN, R. A. & ANDERSON, W. F. 1995. T lymphocyte-directed gene therapy for ADA- SCID: initial trial results after 4 years. *Science*, 270, 475-80.
- BLANCO, E., SHEN, H. & FERRARI, M. 2015. Principles of nanoparticle design for overcoming biological barriers to drug delivery. *Nature Biotechnology*, 33, 941-51.
- BONKHOFF, H., STEIN, U. & REMBERGER, K. 1993. DIFFERENTIAL EXPRESSION OF ALPHA-6 AND ALPHA-2 VERY LATE ANTIGEN INTEGRINS IN THE NORMAL, HYPERPLASTIC, AND NEOPLASTIC PROSTATE - SIMULTANEOUS DEMONSTRATION OF CELL-SURFACE RECEPTORS AND THEIR EXTRACELLULAR LIGANDS. *Human Pathology*, 24, 243-248.
- BOOKSTEIN, R., RIO, P., MADREPERLA, S. A., HONG, F., ALLRED, C., GRIZZLE, W. E. & LEE, W. H. 1990. Promoter deletion and loss of retinoblastoma gene expression in human prostate carcinoma. *Proceedings of the National Academy of Sciences of the United States of America*, 87, 7762-6.

- BOUCHELOUCHE, K., CHOYKE, P. L. & CAPALA, J. 2010. Prostate Specific Membrane Antigen - A Target for Imaging and Therapy with Radionuclides. *Discovery Medicine*, 44, 55-61.
- BRAWER, M. K. 2005. Prostatic intraepithelial neoplasia: an overview. *Reviews in Urology*, 7 Suppl 3, S11-8.
- BURDELSKI, C., DIECKMANN, T., HEUMANN, A., HUBE-MAGG, C., KLUTH, M., BEYER, B., STEUBER, T., POMPE, R., GRAEFEN, M., SIMON, R., MINNER, S., TSOURLAKIS, M. C., KOOP, C., IZBICKI, J., SAUTER, G., KRECH, T., SCHLOMM, T., WILCZAK, W. & LEBOK, P. 2016. p16 upregulation is linked to poor prognosis in ERG negative prostate cancer. *Tumor Biology*, 37, 12655-12663.
- CALABRO, F. & STERNBERG, C. N. 2007. Current indications for chemotherapy in prostate cancer patients. *European Urology*, 51, 17-26.
- CANCER RESEARCH UK. 2015. *Prostate cancer incidence statistics* [online]. Available at: <http://www.cancerresearchuk.org/cancer-info/cancerstats/types/prostate/incidence/uk-prostate-cancer-incidence-statistics> (19/11/2017).
- CHANG, S. S. 2004. Overview of prostate-specific membrane antigen. *Reviews in Urology*, 6 Suppl 10, S13-8.
- CHANG, S. S., REUTER, V. E., HESTON, W. D. W., BANDER, N. H., GRAUER, L. S. & GAUDIN, P. B. 1999. Five different anti-prostate-specific membrane antigen (PSMA) antibodies confirm PSMA expression in tumor-associated neovasculature. *Cancer Research*, 59, 3192-3198.
- CHATTOPADHYAY, M. K., PARK, M. H. & TABOR, H. 2008. Hypusine modification for growth is the major function of spermidine in *Saccharomyces cerevisiae* polyamine auxotrophs grown in limiting spermidine. *Proceedings of the National Academy of Sciences of the United States of America*, 105, 6554-6559.
- CHAWLA-SARKAR, M., LINDNER, D. J., LIU, Y. F., WILLIAMS, B., SEN, G. C., SILVERMAN, R. H. & BORDEN, E. C. 2003. Apoptosis and interferons: Role of interferon-stimulated genes as mediators of apoptosis. *Apoptosis*, 8, 237-249.
- CHEEVER, M. A. & HIGANO, C. S. 2011. PROVENGE (Sipuleucel-T) in Prostate Cancer: The First FDA-Approved Therapeutic Cancer Vaccine. *Clinical Cancer Research*, 17, 3520-3526.
- CHEN, H. L., LI, X. K., BAI, R. C., WU, Y. B., FAN, Y. F. & CHAO, J. B. 2013. Discrimination of Cys from Hcy by an Iridium(III) Complex Based on Time-Dependent Luminescence. *Organometallics*, 32, 6226-6231.
- CHEN, H. L., TANG, L., QIN, Y., YIN, Y. J., TANG, J., TANG, W. W., SUN, X., ZHANG, Z. R., LIU, J. & HE, Q. 2010. Lactoferrin-modified procationic liposomes as a novel drug carrier for brain delivery. *European Journal of Pharmaceutical Sciences*, 40, 94-102.
- CHEN, Z. H., PENET, M. F., KRISHNAMACHARY, B., BANERJEE, S. R., POMPER, M. G. & BHUJWALLA, Z. M. 2016. PSMA-specific theranostic nanoplex for combination of TRAIL gene and 5-FC prodrug therapy of prostate cancer. *Biomaterials*, 80, 57-67.
- CHINNAIYAN, A. M., PRASAD, U., SHANKAR, S., HAMSTRA, D. A., SHANAIAH, M., CHENEVERT, T. L., ROSS, B. D. & REHEMTULLA, A. 2000. Combined effect of tumor necrosis factor-related apoptosis-inducing ligand and ionizing radiation in breast cancer therapy. *Proceedings of the National Academy of Sciences of the United States of America*, 97, 1754-1759.
- CHOPRA, D. P., MENARD, R. E., JANUSZEWSKI, J. & MATTINGLY, R. R. 2004. TNF-alpha-mediated apoptosis, in normal human prostate epithelial cells and tumor cell lines. *Cancer Letters*, 203, 145-154.

- CHUNG, T. D. K., MAUCERI, H. J., HALLAHAN, D. E., YU, J. Q. J., CHUNG, S. M., GRDINA, W. L., YAJNIK, S., KUFE, D. W. & WEICHSELBAUM, R. R. 1998. Tumor necrosis factor-alpha-based gene therapy enhances radiation cytotoxicity in human prostate cancer. *Cancer Gene Therapy*, 5, 344-349.
- CLOSE, D. M., XU, T. T., SAYLER, G. S. & RIPP, S. 2011. *In vivo* Bioluminescent Imaging (BLI): Noninvasive Visualization and Interrogation of Biological Processes in Living Animals. *Sensors*, 11, 180-206.
- COUTURIER, M., BEX, F., BERGQUIST, P. L. & MAAS, W. K. 1988. Identification and classification of bacterial plasmids. *Microbiology Reviews*, 52, 375-95.
- COWEN, D., SALEM, N., ASHOORI, F., MEYN, R., MEISTRICH, M. L., ROTH, J. A. & POLLACK, A. 2000. Prostate cancer radiosensitization *in vivo* with adenovirus-mediated p53 gene therapy. *Clinical Cancer Research*, 6, 4402-8.
- CUNNINGHAM, D. & YOU, Z. 2015. *In vitro* and *in vivo* model systems used in prostate cancer research. *Journal of Biological Methods*, 2, 17.
- CURIEL D. T., DOUGLAS J. T. 2005. *Cancer Gene Therapy*. Totowa, New Jersey: Humana Press.
- DASSIE, J. P., HERNANDEZ, L. I., THOMAS, G. S., LONG, M. E., ROCKEY, W. M., HOWELL, C. A., CHEN, Y. N., HERNANDEZ, F. J., LIU, X. Y., WILSON, M. E., ALLEN, L. A., VAENA, D. A., MEYERHOLF, D. K. & GIANGRANDE, P. H. 2014. Targeted Inhibition of Prostate Cancer Metastases with an RNA Aptamer to Prostate-specific Membrane Antigen. *Molecular Therapy*, 22, 1910-1922.
- DAMBER, J. E., AUS, G. 2008. Prostate Cancer. *The Lancet*. 371, 1710-1721.
- DAVIS, T. L., CRESS, A. E., DALKIN, B. L. & NAGLE, R. B. 2001. Unique expression pattern of the alpha 6 beta 4 integrin and laminin-5 in human prostate carcinoma. *Prostate*, 46, 240-248.
- DENIS, S. & ERIC, R. W. 2014. Confocal Microscopy. In: WNEK, G and BOWLIN, G. *Encyclopedia of Biomaterials and Biomedical Engineering*, New York: Taylor & Francis.705-714.
- DESGROSELLIER, J. S. & CHERESH, D. A. 2010. Integrins in cancer: biological implications and therapeutic opportunities (vol 10, pg 9, 2010). *Nature Reviews Cancer*, 10, 890-890.
- DI LORENZO, G., AUTORINO, R., FIGG, W. D. & DE PLACIDO, S. 2007. Hormone-refractory prostate cancer - Where are we going? *Drugs*, 67, 1109-1124.
- DIPIPPO, V. A., OLSON, W. C., NGUYEN, H. M., BROWN, L. G., VESSELLA, R. L. & COREY, E. 2015. Efficacy Studies of an Antibody-Drug Conjugate PSMA-ADC in Patient-Derived Prostate Cancer Xenografts. *Prostate*, 75, 303-313.
- DOZMOROV, M. G., HURST, R. E., CULKIN, D. J., KROPP, B. P., FRANK, M. B., OSBAN, J., PENNING, T. M. & LIN, H.-K. 2009. Unique Patterns of Molecular Profiling Between Human Prostate Cancer LNCaP and PC-3 Cells. *Prostate*, 69, 1077-1090.
- DUFES, C., UCHEGBU, I. F. & SCHATZLEIN, A. G. 2005. Dendrimers in gene delivery. *Advanced Drug Delivery Reviews*, 57, 2177-2202.
- DUFÈS, C., KEITH, W. N., BILSLAND, A., PROUTSKI, I., UCHEGBU, I. F. & SCHÄTZLEIN, A. G. 2005. Synthetic anticancer gene medicine exploits intrinsic antitumor activity of cationic vector to cure established tumors. *Cancer Research*, 65, 8079-84.
- DUNEHOO, A. L., ANDERSON, M., MAJUMDAR, S., KOBAYASHI, N., BERKLAND, C. & SIAHAAN, T. J. 2006. Cell adhesion molecules for targeted drug delivery. *Journal of Pharmaceutical Sciences*, 95, 1856-1872.

- DURYMANOV, M. O., ROSENKRANZ, A. A. & SOBOLEV, A. S. 2015. Current Approaches for Improving Intratumoral Accumulation and Distribution of Nanomedicines. *Theranostics*, 5,1007-1020.
- DUTTA, D. & DONALDSON, J. G. 2012. Search for inhibitors of endocytosis: Intended specificity and unintended consequences. *Celularl Logistics*, 2, 203-208.
- EASTHAM, J. A., HALL, S. J., SEHGAL, I., WANG, J. X., TIMME, T. L., YANG, G., CONNELLCROWLEY, L., ELLEDGE, S. J., ZHANG, W. W., HARPER, J. W. & THOMPSON, T. C. 1995. IN-VIVO GENE-THERAPY WITH P53 OR P21 ADENOVIRUS FOR PROSTATE-CANCER. *Cancer Research*, 55, 5151-5155.
- EATON, P. & WEST, P. 2010. *Atomic Force Microscopy*. Oxford: Oxford University Press.
- ELFINGER, M., MAUCKSCH, C. & RUDOLPH, C. 2007. Characterization of lactoferrin as a targeting ligand for nonviral gene delivery to airway epithelial cells. *Biomaterials*, 28, 3448-3455.
- ELOJEIMY, S., MCKILLOP, J. C., EL-ZAWAHRY, A. M., HOLMAN, D. H., LIU, X., SCHWARTZ, D. A., DAY, T. A., DONG, J. Y. & NORRIS, J. S. 2006. FasL gene therapy: a new therapeutic modality for head and neck cancer. *Cancer Gene Therapy*, 13, 739-745.
- FAROOQI, A. A. & DE ROSA, G. 2013. TRAIL and microRNAs in the treatment of prostate cancer: therapeutic potential and role of nanotechnology. *Applied Microbiology and Biotechnology*, 97, 8849-57.
- FASBENDER, A., MARSHALL, J., MONINGER, T. O., GRUNST, T., CHENG, S. & WELSH, M. J. 1997. Effect of co-lipids in enhancing cationic lipid-mediated gene transfer *in vitro* and *in vivo*. *Gene Therapy*, 4, 716-725.
- FEINBAUM, R. 1998. Escherichia coli, Plasmids, and Bacteriophages, in Ausubel, F. M., Brent, R., Kingston, R. E., Moore, D. D., Seidman, J. G., Smith, J. A., Struhl, K. (eds.) *Current Protocols in Molecular Biology*. John Wiley & Sons Inc. 1.5.1-1.5.17.
- FELGNER, P. L., GADEK, T. R., HOLM, M., ROMAN, R., CHAN, H. W., WENZ, M., NORTHROP, J. P., RINGOLD, G. M. & DANIELSEN, M. 1987. Lipofection: a highly efficient, lipid-mediated DNA-transfection procedure. *Proceedings of the National Academy of Sciences of the United States of America*, 84, 7413-7.
- FILELLA, M., ZHANG, J. W., NEWMAN, M. E. & BUFFLE, J. 1997. Analytical applications of photon correlation spectroscopy for size distribution measurements of natural colloidal suspensions: Capabilities and limitations. *Colloids and Surfaces a-Physicochemical and Engineering Aspects*, 120, 27-46.
- FIZAZI, K., MARTINEZ, L. A., SIKES, C. R., JOHNSTON, D. A., STEPHENS, L. C., MCDONNELL, T. J., LOGOTHETIS, C. J., TRAPMAN, J., PISTERS, L. L., ORDONEZ, N. G., TRONCOSO, P. & NAVONE, N. M. 2002. The association of p21((WAF-1/CIP1)) with progression to androgen-independent prostate cancer. *Clinical Cancer Research*, 8, 775-781.
- FORNARO, M., MANES, T. & LANGUINO, L. R. 2001. Integrins and prostate cancer metastases. *Cancer and Metastasis Reviews*, 20, 321-331.
- FRESHNEY, R. I. 2006. Basic Principles of Cell Culture. In: VUNJAK-NOVAKOVIC, G AND FRESHNEY, R. I. *Culture of Cells for Tissue Engineering*. Glasgow: John Wiley & Sons. 4-21.
- FREYTAG, S. O., STRICKER, H., MOVSAS, B. & KIM, J. H. 2007. Prostate cancer gene therapy clinical trials. *Molecular Therapy*, 15, 1042-1052.
- FUJITA, K., MATSUDA, E., SEKINE, K., IIGO, M. & TSUDA, H. 2004. Lactoferrin enhances Fas expression and apoptosis in the colon mucosa of azoxymethane-treated rats. *Carcinogenesis*, 25, 1961-1966.

- FUJIWARA, T., GRIMM, E. A., MUKHOPADHYAY, T., CAI, D. W., OWENSCHAUB, L. B. & ROTH, J. A. 1993. A retroviral wild-type p53 expression vector penetrates human lung-cancer spheroids and inhibits growth by inducing apoptosis. *Cancer Research*, 53, 4129-4133.
- GAO, H. J., SHI, W. D. & FREUND, L. B. 2005. Mechanics of receptor-mediated endocytosis. *Proceedings of the National Academy of Sciences of the United States of America*, 102, 9469-9474.
- GAO, S., LI, J., JIANG, C., HONG, B. & HAO, B. 2016. Plasmid pORF-hTRAIL targeting to glioma using transferrin-modified polyamidoamine dendrimer. *Drug Design Development and Therapy*, 10, 1-11.
- GARNICK, M. 2016. *Hormone therapy for prostate cancer* [online]. Available at: <http://www.harvardprostateknowledge.org/hormone-therapy-for-prostate-cancer> (30/11/2016).
- GAUDIN, P. B., ROSAI, J. & EPSTEIN, J. I. 1998. Sarcomas and related proliferative lesions of specialized prostatic stroma - A clinicopathologic study of 22 cases. *American Journal of Surgical Pathology*, 22, 148-162.
- GENE THERAPY NET (2017). Viral Vectors. [online] Available at: <http://www.genetherapynet.com/viral-vectors.html> (28/11/17).
- GERHARD, R., JOHN, H., AKTORIES, K. & JUST, I. 2003. Thiol-modifying phenylarsine oxide inhibits guanine nucleotide binding of Rho but not of Rac GTPases. *Molecular Pharmacology*, 63, 1349-55.
- GHOSH, A. & HESTON, W. D. W. 2004. Tumor target prostate specific membrane antigen (PSMA) and its regulation in prostate cancer. *Journal of Cellular Biochemistry*, 91, 528-539.
- GHOSH, A., WANG, X., KLEIN, E. & HESTON, W. D. 2005a. Novel role of prostate-specific membrane antigen in suppressing prostate cancer invasiveness. *Cancer Research*, 65, 727-31.
- GHOSH, A., WANG, Y. N., KLEIN, E. & HESTON, W. D. W. 2005b. Novel role of prostate-specific membrane antigen in suppressing prostate cancer invasiveness. *Cancer Research*, 65, 727-731.
- GIBBONS, J. A., KANWAR, R. K. & KANWAR, J. R. 2011. Lactoferrin and cancer in different cancer models. *Frontiers in Bioscience*, 3, 1080-8.
- GIRLING, J. S., WHITAKER, H. C., MILLS, I. G. & NEAL, D. E. 2007. Pathogenesis of prostate cancer and hormone refractory prostate cancer. *Indian Journal of Urology*, 23, 35-42.
- GLOBOCAN. 2012. *Prostate cancer, estimated incidence, mortality and prevalence worldwide in 2012* [online]. Available at: http://globocan.iarc.fr/Pages/fact_sheets_cancer.aspx (30/11/2017).
- GOEL, H. L., LI, J., KOGAN, S. & LANGUINO, L. R. 2008. Integrins in prostate cancer progression. *Endocrine-Related Cancer*, 15, 657-664.
- GOGICHAIEVA, N. V., WILLIAMS, T. & ALTERMAN, M. A. 2007. MALDI TOF/TOF tandem mass spectrometry as a new tool for amino acid analysis. *Journal of the American Society for Mass Spectrometry*, 18, 279-284.
- GOODMAN, O. B., BARWE, S. P., RITTER, B., MCPHERSON, P. S., VASKO, A. J., KEEN, J. H., NANUS, D. M., BANDER, N. H. & RAJASEKARAN, A. K. 2007. Interaction of prostate specific membrane antigen with clathrin and the adaptor protein complex-2. *International Journal of Oncology*, 31, 1199-1203.
- GOTOH, A., KAO, C., KO, S. C., HAMADA, K., LIU, T. J. & CHUNG, L. W. 1997. Cytotoxic effects of recombinant adenovirus p53 and cell cycle regulator genes (p21 WAF1/CIP1 and p16CDKN4) in human prostate cancers. *Journal of Urology*, 158, 636-41.

- GOWDA, G. A. N., GOWDA, Y. N. & RAFTERY, D. 2015. Expanding the Limits of Human Blood Metabolite Quantitation Using NMR Spectroscopy. *Analytical Chemistry*, 87, 706-715.
- GRACA, G., DUARTE, I. F., GOODFELLOW, B. J., CARREIRA, I. M., COUCEIRO, A. B., DOMINGUES, M. D., SPRAUL, M., TSENG, L. H. & GIL, A. M. 2008. Metabolite profiling of human amniotic fluid by hyphenated nuclear magnetic resonance spectroscopy. *Analytical Chemistry*, 80, 6085-6092.
- GRANT, B. D. SATO, M. 2006. *Intracellular trafficking* [online]. Available at: http://www.wormbook.org/chapters/www_intracellulartrafficking/intracellulartrafficking.pdf (15/12/2016).
- GRIFFITH, K. L. & WOLF, R. E., JR. 2002. Measuring beta-galactosidase activity in bacteria: cell growth, permeabilization, and enzyme assays in 96-well arrays. *Biochemical and Biophysical Research Communications*, 290, 397-402.
- GRIFFITH, T. S., ANDERSON, R. D., DAVIDSON, B. L., WILLIAMS, R. D. & RATLIFF, T. L. 2000. Adenoviral-mediated transfer of the TNF-related apoptosis-inducing ligand/apo-2 ligand gene induces tumor cell apoptosis. *Journal of Immunology*, 165, 2886-2894.
- GRIFFITH, T. S. & BROGHAMMER, E. L. 2001. Suppression of tumor growth following intralesional therapy with TRAIL recombinant adenovirus. *Molecular Therapy*, 4, 257-266.
- GRIFFITH, T. S., STOKES, B., KUCABA, T. A., EAREL, J. K., VANOOSTEN, R. L., BRINCKS, E. L. & NORIAN, L. A. 2009. TRAIL Gene Therapy: From Preclinical Development to Clinical Application. *Current Gene Therapy*, 9, 9-19.
- GRONBERG, H. 2003. Prostate cancer epidemiology. *Lancet*, 361, 859-64.
- GROTH, D., KEIL, O., SCHNEIDER, M. & RESZKA, R. 1998. Transfection assay for dual determination of toxicity and gene expression. *Analytical Biochemistry*, 258, 141-3.
- GU, J. L., WANG, B., LIU, Y. A., ZHONG, L. Z., TANG, Y. F., GUO, H., JIANG, T., WANG, L. W., LI, Y. & CAI, L. 2014. Murine Double Minute 2 siRNA and wild-type p53 gene therapy interact positively with zinc on prostate tumours *in vitro* and *in vivo*. *European Journal of Cancer*, 50, 1184-1194.
- GUO, S., MESSMER-BLUST, A. F., WU, J., SONG, X., PHILBRICK, M. J., SHIE, J.-L., RANA, J. S. & LI, J. 2014. Role of A20 in cIAP-2 Protection against Tumor Necrosis Factor alpha (TNF-alpha)-Mediated Apoptosis in Endothelial Cells. *International Journal of Molecular Sciences*, 15, 3816-3833.
- GUPTA, G. P. & MASSAGUE, J. 2006. Cancer metastasis: Building a framework. *Cell*, 127, 679-695.
- HAMMERICH K, H. AYALA, G. E. AND WHEELER, T. M. 2008. Anatomy of the prostate gland and surgical pathology of prostate cancer. In: HRICAK, H and SCARDINO, P. *Prostate cancer*. Cambridge: Cambridge University Press. 1-14.
- HAN, L., ZHAO, J., LIU, J., DUAN, X. L., LI, L. H., WEI, X. F., WEI, Y. & LIANG, X. J. 2014. A universal gene carrier platform for treatment of human prostatic carcinoma by p53 transfection. *Biomaterials*, 35, 3110-3120.
- HANSEN, C. G. & NICHOLS, B. J. 2009. Molecular mechanisms of clathrin-independent endocytosis. *Journal of Cell Science*, 122, 1713-21.
- HASHEMI, M., AYATOLLAHI, S., PARHIZ, H., MOKHTARZADEH, A., JAVIDI, S. & RAMEZANI, M. 2015. PEGylation of Polypropylenimine Dendrimer with Alkylcarboxylate Chain Linkage to Improve DNA Delivery and Cytotoxicity. *Applied Biochemistry and Biotechnology*, 177, 1-17.

- HEDLUND, T. E., MEECH, S. J., SRIKANTH, S., KRAFT, A. S., MILLER, G. J., SCHAACK, J. B. & DUKE, R. C. 1999. Adenovirus-mediated expression of Fas ligand induces apoptosis of human prostate cancer cells. *Cell Death and Differentiation*, 6, 175-182.
- HEGMANS, J. & AERTS, J. 2014. Immunomodulation in cancer. *Current Opinion in Pharmacology*, 17, 17-21.
- HEMANN, M. T. & LOWE, S. W. 2006. The p53-Bcl-2 connection. *Cell Death and Differentiation*, 13, 1256-1259.
- HERAWI, M., MONTGOMERY, E. A. & EPSTEIN, J. I. 2006. Gastrointestinal stromal tumors (GISTs) on prostate needle biopsy - A clinicopathologic study of 8 cases. *American Journal of Surgical Pathology*, 30, 1389-1395.
- HERMANSON, G. T. 2013. *Bioconjugate Techniques*. London: Elsevier Inc.
- HOFFMAN, A. S. 2008. The origins and evolution of "controlled" drug delivery systems. *Journal of Controlled Release*, 132, 153-163.
- HONARY, S. & ZAHIR, F. 2013. Effect of Zeta Potential on the Properties of Nano-Drug Delivery Systems - A Review (Part 2). *Tropical Journal of Pharmaceutical Research*, 12, 265-273.
- HOROSZEWICZ, J. S., KAWINSKI, E. & MURPHY, G. P. 1987. Monoclonal-antibodies to a new antigenic marker in epithelial prostatic cells and serum of prostatic-cancer patients. *Anticancer Research*, 7, 927-936.
- HOROSZEWICZ, J. S., LEONG, S. S., KAWINSKI, E., KARR, J. P., ROSENTHAL, H., CHU, T. M., MIRAND, E. A. & MURPHY, G. P. 1983. LNCaP model of human prostatic carcinoma. *Cancer Research*, 43, 1809-18.
- HU, X. W. & SUN, Y. 2012. Triptolide sensitizes TRAIL-induced apoptosis in prostate cancer cells via p53-mediated DR5 up-regulation. *Molecular Biology Reports*, 39, 8763-8770.
- HUANG, F. Y., CHEN, W. J., LEE, W. Y., LO, S. T., LEE, T. W. & LO, J. M. 2013. *In vitro* and *in vivo* evaluation of lactoferrin-conjugated liposomes as a novel carrier to improve the brain delivery. *International Journal of Molecular Sciences*, 14, 2862-74.
- HUANG, R., KE, W., LIU, Y., JIANG, C. & PEI, Y. 2008. The use of lactoferrin as a ligand for targeting the polyamidoamine-based gene delivery system to the brain. *Biomaterials*, 29, 238-46.
- HUANG, R. Q., KE, W. L., HAN, L., LIU, Y., SHAO, K., YE, L. Y., LOU, J. N., JIANG, C. & PEI, Y. Y. 2009. Brain-targeting mechanisms of lactoferrin-modified DNA-loaded nanoparticles. *Journal of Cerebral Blood Flow and Metabolism*, 29, 1914-1923.
- HULL, G. W., MCCURDY, M. A., NASU, Y., BANGMA, C. H., YUANG, G., SHIMURA, S., LEE, H. M., WANG, J. X., ALBANI, J., EBARA, S., SATO, T., TIMME, T. L. & THOMPSON, T. C. 2000. Prostate cancer gene therapy: Comparison of adenovirus-mediated expression of interleukin 12 with interleukin 12 plus B7-1 for in situ gene therapy and gene-modified, cell-based vaccines. *Clinical Cancer Research*, 6, 4101-4109.
- HUNT, K. K. VORBURGER, S. A. SWISHER, S. G. 2007. *Gene therapy for cancer*. New Jersey: Humana Press.
- HYER, M., SUDARSHAN, S., SCHWARTZ, D., DONG, J. Y. & NORRIS, J. 2003a. Quantification and characterization of the bystander effect in prostate cancer cells following adenovirus-mediated FasL expression. *Journal of Urology*, 169, 216-217.

- HYER, M. L., SUDARSHAN, S., SCHWARTZ, D. A., HANNUN, Y., DONG, J. Y. & NORRIS, J. S. 2003b. Quantification and characterization of the bystander effect in prostate cancer cells following adenovirus-mediated FasL expression. *Cancer Gene Therapy*, 10, 330-339.
- HYER, M. L., VOELKEL-JOHNSON, C., RUBINCHIK, S., DONG, J. & NORRIS, J. S. 2000. Intracellular Fas ligand expression causes Fas-mediated apoptosis in human prostate cancer cells resistant to monoclonal antibody-induced apoptosis. *Molecular Therapy*, 2, 348-358.
- ITTMANN, M., HUANG, J., RADAELLI, E., MARTIN, P., SIGNORETTI, S., SULLIVAN, R., SIMONS, B. W., WARD, J. M., ROBINSON, B. D., CHU, G. C., LODA, M., THOMAS, G., BOROWSKY, A. & CARDIFF, R. D. 2013. Animal Models of Human Prostate Cancer: The Consensus Report of the New York Meeting of the Mouse Models of Human Cancers Consortium Prostate Pathology Committee. *Cancer Research*, 73, 2718-2736.
- IVANOV, A. I., NUSRAT, A. & PARKOS, C. A. 2004. Endocytosis of epithelial apical junctional proteins by a clathrin-mediated pathway into a unique storage compartment. *Molecular Biology of the Cell*, 15, 176-88.
- JEONG, Y.-I., KIM, D.-G., JANG, M.-K. & NAH, J.-W. 2008. Preparation and spectroscopic characterization of methoxy poly(ethylene glycol)-grafted water-soluble chitosan. *Carbohydrate Research*, 343, 282-289.
- JIA, L. T., CHEN, S. Y. & YANG, A. G. 2012. Cancer gene therapy targeting cellular apoptosis machinery. *Cancer Treatment Reviews*, 38, 868-876.
- JIANG, R. L., LOPEZ, V., KELLEHER, S. L. & LONNERDAL, B. 2011. Apo- and holo-lactoferrin are both internalized by lactoferrin receptor via clathrin-mediated endocytosis but differentially affect ERK-signaling and cell proliferation in Caco-2 cells. *Journal of Cellular Physiology*, 226, 3022-3031.
- JIANG, T., ZHOU, C. D., GU, J. L., LIU, Y. N., ZHAO, L. J., LI, W., WANG, G. J., LI, Y. & CAI, L. 2013. Enhanced therapeutic effect of cisplatin on the prostate cancer in tumor-bearing mice by transfecting the attenuated Salmonella carrying a plasmid co-expressing p53 gene and mdm2 siRNA. *Cancer Letters*, 337, 133-142.
- JIANG, Y. Y., LIU, C., HONG, M. H., ZHU, S. J. & PEI, Y. Y. 2007. Tumor cell targeting of transferrin-PEG-TNF-alpha conjugate via a receptor-mediated delivery system: Design, synthesis, and biological evaluation. *Bioconjugate Chemistry*, 18, 41-49.
- JIMENEZ-LARA, A. M., ARANDA, A. & GRONEMEYER, H. 2010. Retinoic acid protects human breast cancer cells against etoposide-induced apoptosis by NF-kappaB-dependent but cIAP2-independent mechanisms. *Molecular Cancer*, 9, 15.
- JIN, J., SUI, B. W., GOU, J. X., LIU, J. S., TANG, X., XU, H., ZHANG, Y. & JIN, X. Q. 2014. PSMA Ligand Conjugated PCL-PEG Polymeric Micelles Targeted to Prostate Cancer Cells. *Plos One*, 9, 11.
- JIN, W., QIN, B., CHEN, Z., LIU, H., BARVE, A. & CHENG, K. 2016. Discovery of PSMA-specific peptide ligands for targeted drug delivery. *International Journal of Pharmaceutics*, 513, 138-147.
- KAKHKI, V. R., ANVARI, K., SADEGHI, R., MAHMOUDIAN, A. S. & TORABIAN-KAKHKI, M. 2013. Pattern and distribution of bone metastases in common malignant tumors. *Nuclear medicine review. Central & Eastern Europe*, 16, 66-9.
- KALIBEROV, S. A., KALIBEROVA, L. N., STOCKARD, C. R., GRIZZLE, W. E. & BUCHSBAUM, D. J. 2004. Adenovirus-mediated FLT1-targeted proapoptotic gene therapy of human prostate cancer. *Molecular Therapy*, 10, 1059-1070.
- KAMIMURA, K. SUDA, T. ZHANG, G. LIU, D. 2011. Advances in gene delivery systems. *Pharmaceutical Medicine*, 25(5): 293-306.

- KASMAN, L., LU, P. & VOELKEL-JOHNSON, C. 2007. The histone deacetylase inhibitors depsipeptide and MS-275, enhance TRAIL gene therapy of LNCaP prostate cancer cells without adverse effects in normal prostate epithelial cells. *Cancer Gene Therapy*, 14, 327-334.
- KASTEN, B. B., LIU, T. C., NEDROW-BYERS, J. R., BENNY, P. D. & BERKMAN, C. E. 2013. Targeting prostate cancer cells with PSMA inhibitor-guided gold nanoparticles. *Bioorganic & Medicinal Chemistry Letters*, 23, 565-568.
- KATO, A., MAKI, K., EBINA, T., KUWAJIMA, K., SODA, K. & KURODA, Y. 2007. Mutational analysis of protein solubility enhancement using short peptide tags. *Biopolymers*, 85, 12-18.
- KELLAND, L. R. 2004. "Of mice and men": values and liabilities of the athymic nude mouse model in anticancer drug development. *European Journal of Cancer*, 40, 827-836.
- KIM, C. Y., JEONG, M., MUSHIAKE, H., KIM, B. M., KIM, W. B., KO, J. P., KIM, M. H., KIM, M., KIM, T. H., ROBBINS, P. D., BILLIAR, T. R. & SEOL, D. W. 2006. Cancer gene therapy using a novel secretable trimeric TRAIL. *Gene Therapy*, 13, 330-338.
- KIM, D., KIM, S. K., VAENCIA, C. A. & LIU, R. 2013. Tribody: Robust Self-Assembled Trimeric Targeting Ligands with High Stability and Significantly Improved Target-Binding Strength. *Biochemistry*, 52, 7283-7294.
- KIM, K. M., WON, Y. W., ADHIKARY, P. P., HWANG, Y. M. & KIM, Y. H. 2011. Suicidal gene therapy against tumor using reducible poly (oligo-d-arginine). *Journal of Controlled Release*, 152, E148-E149.
- KIM, T. I., BAEK, J. U., BAI, C. Z. & PARK, J. S. 2007. Arginine-conjugated polypropylenimine dendrimer as a non-toxic and efficient gene delivery carrier. *Biomaterials*, 28, 2061-2067.
- KIMURA, R. H., LEVIN, A. M., COCHRAN, F. V. & COCHRAN, J. R. 2009. Engineered cystine knot peptides that bind alpha v beta 3, alpha v beta 5, and alpha 5 beta 1 integrins with low-nanomolar affinity. *Proteins-Structure Function and Bioinformatics*, 77, 359-369.
- KINOSHITA, Y., KURATSUKURI, K., LANDAS, S., IMAIDA, K., ROVITO, P. M., WANG, C. Y. & HAAS, G. P. 2006. Expression of prostate-specific membrane antigen in normal and malignant human tissues. *World Journal of Surgery*, 30, 628-636.
- KIRCHEIS, R., OSTERMANN, E., WOLSCHEK, M. F., LICHTENBERGER, C., MAGIN-LACHMANN, C., WIGHTMAN, L., KURSA, M. & WAGNER, E. 2002. Tumor-targeted gene delivery of tumor necrosis factor-alpha induces tumor necrosis and tumor regression without systemic toxicity. *Cancer Gene Therapy*, 9, 673-680.
- KLAJNERT, B. & BRYCZEWSKA, M. 2001. Dendrimers: properties and applications. *Acta Biochimica Polonica*, 48, 199-208.
- KO, S. C., GOTOH, A., THALMANN, G. N., ZHAU, H. E., JOHNSTON, D. A., ZHANG, W. W., KAO, C. H. & CHUNG, L. W. K. 1996. Molecular therapy with recombinant p53 adenovirus in an androgen-independent, metastatic human prostate cancer model. *Human Gene Therapy*, 7, 1683-1691.
- KOPPU, S., OH, Y. J., EDRADA-EBEL, R., BLATCHFORD, D. R., TETLEY, L., TATE, R. J. & DUFES, C. 2010. Tumor regression after systemic administration of a novel tumor-targeted gene delivery system carrying a therapeutic plasmid DNA. *Journal of Controlled Release*, 143, 215-221.
- KUCHENTHAL, C. H. & MAISON, W. 2010. Antibody recruiting small molecules: a new option for prostate tumor therapy by psma targeting. *Chembiochem*, 11, 1052-1054.
- KULIK, A. & DABKOWSKI, M. 2011. Prostate cancer radiotherapy. *Wspolczesna Onkologia-Contemporary Oncology*, 15, 317-322.

- KURMI, B. D., GAJBHIYE, V., KAYAT, J. & JAIN, N. K. 2011. Lactoferrin-Conjugated Dendritic Nanoconstructs for Lung Targeting of Methotrexate. *Journal of Pharmaceutical Sciences*, 100, 2311-2320.
- KWAN, A. H., MOBLI, M., GOOLEY, P. R., KING, G. F. & MACKAY, J. P. 2011. Macromolecular NMR spectroscopy for the non-spectroscopist. *FEBS journal*, 278, 687-703.
- LAIDLER, P., DULIŃSKA, J., LEKKA, M. & LEKKI, J. 2005. Expression of prostate specific membrane antigen in androgen-independent prostate cancer cell line PC-3. *Archives of Biochemistry and Biophysics*, 435, 1-14.
- LAMPMAN, G. M. PAVIA, D. L. KRIZ, G. S. & VYVYAN, J. A. 2008. *Introduction to Spectroscopy, International Edition*. Cengage Learning.
- LAOUINI, A. JAAFAR-MAALEJ, C. LIMAYEM-BLOUZA, I. STAR, S. CHARCOSSET, C. FESSI H. 2012. Preparation, Characterization and Applications of Liposomes: State of the Art. *Journal of Colloid Science and Biotechnology*, 1, 147-168.
- LASEK, W., ZAGOŹDŹON, R. & JAKOBISIAK, M. 2014. Interleukin 12: still a promising candidate for tumor immunotherapy? *Cancer Immunology Immunotherapy*, 63, 419-35.
- LEE, H. & LARSON, R. G. 2011. Effects of PEGylation on the Size and Internal Structure of Dendrimers: Self-Penetration of Long PEG Chains into the Dendrimer Core. *Macromolecules*, 44, 2291-2298.
- LEGRAND, D., PIERCE, A., ELASS, E., CARPENTIER, M., MARILLER, C. & MAZURIER, J. 2008. Lactoferrin structure and functions. *Bioactive Components of Milk*, 606, 163-194.
- LEMARIE, F., CROFT, D. R., TATE, R. J., RYAN, K. M. & DUFES, C. 2012. Tumor regression following intravenous administration of a tumor-targeted p73 gene delivery system. *Biomaterials*, 33, 2701-2709.
- LEMBO, D., SWAMINATHAN, S., DONALISIO, M., CIVRA, A., PASTERO, L., AQUILANO, D., VAVIA, P., TROTTA, F. & CAVALLI, R. 2013. Encapsulation of Acyclovir in new carboxylated cyclodextrin-based nanosponges improves the agent's antiviral efficacy. *International Journal of Pharmaceutics*, 443, 262-272.
- LEVAY, P. F. & VILJOEN, M. 1995. LACTOFERRIN - A GENERAL-REVIEW. *Haematologica*, 80, 252-267.
- LEWIS, J. K. WEI, J. & SIUZDAK, G. 2000. Matrix-assisted laser desorption/ionization mass spectrometry in peptide and protein analysis [online]. *Encyclopedia of Analytical Chemistry*. Available at: https://masspec.scripps.edu/publications/public_pdf/64_art.pdf (30/11/2016)
- LI, J., LI, S., XIA, S., FENG, J., ZHANG, X., HAO, Y., CHEN, L. & ZHANG, X. 2015. Enhanced transfection efficiency and targeted delivery of self-assembling h-R3-dendriplexes in EGFR-overexpressing tumor cells. *Oncotarget*, 6, 26177-26191.
- LI, J., PIEHLER, L. T., QIN, D., BAKER, J. R., TOMALIA, D. A. & MEIER, D. J. 2000. Visualization and characterization of poly(amidoamine) dendrimers by atomic force microscopy. *Langmuir*, 16, 5613-5616.
- LI, Y. M., XU, B., BAI, T. & LIU, W. G. 2015. Co-delivery of doxorubicin and tumor-suppressing p53 gene using a PUSS-based star-shaped polymer for cancer therapy. *Biomaterials*, 55, 12-23.
- LIBERIO, M. S., SADOWSKI, M. C., SOEKMADJI, C., DAVIS, R. A. & NELSON, C. C. 2014. Differential Effects of Tissue Culture Coating Substrates on Prostate Cancer Cell Adherence, Morphology and Behavior. *PLOS One*, 9, 112122.

- LIM, L. Y., KOH, P. Y., SOMANI, S., AL ROBAIAN, M., KARIM, R., YEAN, Y. L., MITCHELL, J., TATE, R. J., EDRADE-EBEL, R., BLATCHFORD, D. R., MULLIN, M. & DUFÈS, C. 2015. Tumor regression following intravenous administration of lactoferrin- and lactoferricin-bearing dendriplexes. *Nanomedicine*, 11, 1445-54.
- LIN, T. Y., HUANG, X. F., GU, J., ZHANG, L. D., ROTH, J. A., XIONG, M. M., CURLEY, S. A., YU, Y. H., HUNT, K. K. & FANG, B. L. 2002. Long-term tumor-free survival from treatment with the GFP-TRAIL fusion gene expressed from the hTERT promoter in breast cancer cells. *Oncogene*, 21, 8020-8028.
- LIN, T. Y., ZHANG, L. D., DAVIS, J., GU, J., NISHIZAKI, M., JI, L., ROTH, J. A., XIONG, M. M. & FANG, B. L. 2003. Combination of TRAIL gene therapy and chemotherapy enhances antitumor and antimetastasis effects in chemosensitive and chemoresistant breast cancers. *Molecular Therapy*, 8, 441-448.
- LIU, A. Y., BRUBAKER, K. D., GOO, Y. A., QUINN, J. E., KRAL, S., SORENSEN, C. M., VESSELLA, R. L., BELLDEGRUN, A. S. & HOOD, L. E. 2004. Lineage relationship between LNCaP and LNCaP-derived prostate cancer cell lines. *Prostate*, 60, 98-108.
- LIU, H., RAJASEKARAN, A. K., MOY, P., XIA, Y., KIM, S., NAVARRO, V., RAHMATI, R. & BANDER, N. H. 1998. Constitutive and antibody-induced internalization of prostate-specific membrane antigen. *Cancer Research*, 58, 4055-4060.
- LIU, J. & SHAPIRO, J. I. 2003. Endocytosis and signal transduction: basic science update. *Biological Research for Nursing*, 5, 117-28.
- LIU, T. C., NEDROW-BYERS, J. R., HOPKINS, M. R., WU, L. S. Y., LEE, J., REILLY, P. T. A. & BERKMAN, C. E. 2012. Targeting prostate cancer cells with a multivalent PSMA inhibitor-guided streptavidin conjugate. *Bioorganic & Medicinal Chemistry Letters*, 22, 3931-3934.
- LIU, Y. B., PETERSON, D. A., KIMURA, H. & SCHUBERT, D. 1997. Mechanism of cellular 3-(4,5-dimethylthiazol-2-yl)-2,5-diphenyltetrazolium bromide (MTT) reduction. *Journal of Neurochemistry*, 69, 581-593.
- LIU, Z., WANG, F. & CHEN, X. 2008. Integrin alpha(v)beta (3)-Targeted Cancer Therapy. *Drug Development Research*, 69, 329-339.
- LONGMIRE, M., CHOYKE, P. L. & KOBAYASHI, H. 2008. Clearance properties of nano-sized particles and molecules as imaging agents: considerations and caveats. *Nanomedicine (Lond)*, 3, 703-717.
- LU, P. F., WEAVER, V. M. & WERB, Z. 2012. The extracellular matrix: A dynamic niche in cancer progression. *Journal of Cell Biology*, 196, 395-406.
- LU, W. J., AMATRUDA, J. F. & ABRAMS, J. M. 2009. p53 ancestry: gazing through an evolutionary lens. *Nature Reviews Cancer*, 9, 758-62.
- LU, Y. 2009. Transcriptionally regulated, prostate-targeted gene therapy for prostate cancer. *Advanced Drug Delivery Reviews*, 61, 572-588.
- LUCAS, M. L., HELLER, L., COPPOLA, D. & HELLER, R. 2002. IL-12 plasmid delivery by *in vivo* electroporation for the successful treatment of established subcutaneous B16.F10 melanoma. *Molecular Therapy*, 5, 668-675.
- MA, G., SHIMADA, H., HIROSHIMA, K., TADA, Y., SUZUKI, N. & TAGAWA, M. 2009. Gene medicine for cancer treatment: commercially available medicine and accumulated clinical data in China. *Drug Design, Development and Therapy*, 2, 115-22.

- MABJEESH, N. J., ZHONG, H. & SIMONS, J. W. 2002. Gene therapy of prostate cancer: current and future directions. *Endocrine-Related Cancer*, 9, 115-139.
- MADANI, F., LINDBERG, S., LANGEL, U., FUTAKI, S. & GRASLUND, A. 2011. Mechanisms of cellular uptake of cell-penetrating peptides. *Journal of biophysics (Hindawi Publishing Corporation: Online)*, 2011, 414729-414729.
- MAHMOUDI, M., LYNCH, I., EJTEHADI, M. R., MONOPOLI, M. P., BOMBELLI, F. B. & LAURENT, S. 2011. Protein-Nanoparticle Interactions: Opportunities and Challenges. *Chemical Reviews*, 111, 5610-5637.
- MALIK, R. D. DAKWAR, G. HARDEE, M. E. SANFILIPPO, N. J. ROSENKRANTZ, A. B. & TANEJA, S. S. 2011. Squamous Cell Carcinoma of the Prostate. *Reviews in Urology*, 13, 56-60.
- MARBERGER, M., BARENTSZ, J., EMBERTON, M., HUGOSSON, J., LOEB, S., KLOTZ, L., KOCH, M., SHARIAT, S. F. & VICKERS, A. 2012. Novel approaches to improve prostate cancer diagnosis and management in early-stage disease. *Bju International*, 109, 1-7.
- MARELLI, U. K., RECHENMACHER, F., SOBAHI, T. R., MAS-MORUNO, C. & KESSLER, H. 2013. Tumor Targeting via Integrin Ligands. *Frontiers in Oncology*, 3, 222.
- MARKOWICZ, M., SZYMANSKI, P., CISZEWSKI, M., KLYS, A. & MIKICIUK-OLASIK, E. 2012. Evaluation of poly(amidoamine) dendrimers as potential carriers of iminodiacetic derivatives using solubility studies and 2D-NOESY NMR spectroscopy. *Journal of Biological Physics*, 38, 637-656.
- MASTROBATTISTA, E. & HENNINK, W. E. 2012. Polymers for gene delivery: Charged for success. *Nature Materials*, 11, 10-2.
- MAUCERI, H. J., HANNA, N. N., WAYNE, J. D., HALLAHAN, D. E., HELLMAN, S. & WEICHSELBAUM, R. R. 1996. Tumor necrosis factor alpha (TNF-alpha) gene therapy targeted by ionizing radiation selectively damages tumor vasculature. *Cancer Research*, 56, 4311-4314.
- MAURER, T., POURNARAS, C., AGUILAR-PIMENTEL, J. A., THALGOTT, M., HORN, T., HECK, M., HEIT, A., KUEBLER, H., GSCHWEND, J. E. & NAWROTH, R. 2013. Immunostimulatory CpG-DNA and PSA-peptide vaccination elicits profound cytotoxic T cell responses. *Urologic Oncology*, 31, 1395-401.
- MAZHAR, D. & WAXMAN, J. 2004. Gene therapy for prostate cancer. *British Journal of Urology International*, 93, 465-469.
- MCCAIN, J. 2014. Drugs that offer a survival advantage for men with bone metastases resulting from castration-resistant prostate cancer: new and emerging treatment options. *P & T: a peer-reviewed journal for formulary management*, 39, 130-43.
- MCCRUDEN, C. M. & MCCARTHY, H. O. 2013. Cancer gene therapy- key biological concepts in the design of multifunctional non-viral delivery systems. In: MOLINA, F. *Gene therapy- Tools and potentials applications* Croatia; InTech. 213-248.
- MCCOY, J. P. 2002. Basic principles of flow cytometry. *Hematology-Oncology Clinics of North America*, 16, 229-243.
- MCCMAHON, H. T. & BOUCROT, E. 2011. Molecular mechanism and physiological functions of clathrin-mediated endocytosis. *Nature Reviews Molecular Cell Biology*, 12, 517-533.
- MCNEAL, J. E. 1968. Regional morphology and pathology of prostate. *American Journal of Clinical Pathology*, 49, 347-357.

- MCTAGGART, S. & AL-RUBEAI, M. 2002. Retroviral vectors for human gene delivery. *Biotechnology Advances*, 20, 1-31.
- MELLMAN, I. & YARDEN, Y. 2013. Endocytosis and Cancer. *Cold Spring Harbor Perspectives in Biology*, 5, 016949.
- MESTERS, J. R., BARINKA, C., LI, W. X., TSUKAMOTO, T., MAJER, P., SLUSHER, B. S., KONVALINKA, J. & HILGENFELD, R. 2006. Structure of glutamate carboxypeptidase II, a drug target in neuronal damage and prostate cancer. *The European Molecular Biology Organization Journal*, 25, 1375-1384.
- MILECKI, P., ANTCZAK, A., MARTENKA, P. & KWIAS, Z. 2011. What is the possible role of PSA doubling time (PSADT) and PSA velocity (PSAV) in the decision-making process to initiate salvage radiotherapy following radical prostatectomy in patients with prostate cancer. *Central European Journal of Urology*, 64, 67-70.
- MILLER, J. H. 1972. *Experiments in molecular genetics*. New York: Cold Spring Harbor Laboratory.
- MILJKOVIC-SELIMOVIC, B. BABIC, T. KOCIC, B. STOJANOVIC, P. RISTIC, L. & DINIC, M. 2007. Bacterial Plasmids, *Acta Medica Medianae*, 46 (4) 61-65.
- MOFFATT, S., PAPASAKELARIOU, C., WIEHLE, S. & CRISTIANO, R. 2006. Successful *in vivo* tumor targeting of prostate-specific membrane antigen with a highly efficient J591/PEI/DNA molecular conjugate. *Gene Therapy*, 13, 761-772.
- MOHAMMADPOUR, R., SAFARIAN, S., BUCKWAY, B. & GHANDEHARI, H. 2017. Comparative Endocytosis Mechanisms and Anticancer Effect of HPMA Copolymer- and PAMAM Dendrimer-MTCP Conjugates for Photodynamic Therapy. *Macromolecular Bioscience*, 17, 1600333.
- MOHR, A., HENDERSON, G., DUDUS, L., HERR, I., KUERSCHNER, T., DEBATIN, K. M., WEIHER, H., FISHER, K. J. & ZWACKA, R. M. 2004. AAV-encoded expression of TRAIL in experimental human colorectal cancer leads to tumor regression. *Gene Therapy*, 11, 534-543.
- MONTAUDO, G., SAMPERI, F. & MONTAUDO, M. S. 2006. Characterization of synthetic polymers by MALDI-MS. *Progress in Polymer Science*, 31, 277-357.
- MOORE, S. J., GEPHART, M. G. H., BERGEN, J. M., SU, Y. R. S., RAYBURN, H., SCOTT, M. P. & COCHRAN, J. R. 2013. Engineered knottin peptide enables noninvasive optical imaging of intracranial medulloblastoma. *Proceedings of the National Academy of Sciences of the United States of America*, 110, 14598-14603.
- MORGAN, K. 2014. Plasmid 101: *Origin of Replication* [online]. Available at: <http://blog.addgene.org/plasmid-101-origin-of-replication> (09/10/2015)
- MORRIS, J. C., RAMLOGAN-STEEL, C. A., YU, P., BLACK, B. A., MANNAN, P., ALLISON, J. P., WALDMANN, T. A. & STEEL, J. C. 2014. Vaccination with tumor cells expressing IL-15 and IL-15R alpha inhibits murine breast and prostate cancer. *Gene Therapy*, 21, 393-401.
- MORTON, C. L. & HOUGHTON, P. J. 2007. Establishment of human tumor xenografts in immunodeficient mice. *Nature Protocols*, 2, 247-50.
- MOSMANN, T. 1983. Rapid colorimetric assay for cellular growth and survival - application to proliferation and cyto-toxicity assays. *Journal of Immunological Methods*, 65, 55-63.
- MOUSAVIZADEH, A., JABBARI, A., AKRAMI, M. & BARDANIA, H. 2017. Cell targeting peptides as smart ligands for targeting of therapeutic or diagnostic agents: a systematic review. *Colloids and surfaces. B, Biointerfaces*, 158, 507-517.

- MUENCHEN, H. J., LIN, D. L., WALSH, M. A., KELLER, E. T. & PIENTA, K. J. 2002. Tumor necrosis factor-alpha-induced apoptosis in prostate cancer cells through inhibition of nuclear factor-kappa B by an I kappa B alpha "super-repressor" (Retraction of vol 6, pg 1969, 2000). *Clinical Cancer Research*, 8, 3961-3961.
- MUNOZ, F., FRANCO, P., CIAMMELLA, P., CLERICO, M., GIUDICI, M., FILIPPI, A. R. & RICARDI, U. 2007. Squamous cell carcinoma of the prostate: long-term survival after combined chemoradiation. *Radiation Oncology*, 2, 15.
- MURUVE, N. A. 2013. *Prostate Anatomy* [online]. Available at: <http://emedicine.medscape.com/article/1923122-overview#aw2aab6b4> (12/11/2016).
- MÄNNISTÖ, M., RÖNKKÖ, S., MÄTTÖ, M., HONKAKOSKI, P., HYTTINEN, M., PELKONEN, J. & URTTI, A. 2005. The role of cell cycle on polyplex-mediated gene transfer into a retinal pigment epithelial cell line. *Journal of Gene Medicine*, 7, 466-76.
- NABI, I. R. & LE, P. U. 2003. Caveolae/raft-dependent endocytosis. *Journal of Cell Biology*, 161, 673-677.
- NAGESH, P. K. B., JOHNSON, N. R., BOYA, V. K. N., CHOWDHURY, P., OTHMAN, S. F., KHALILZAD-SHARGHI, V., HAFEEZ, B. B., GANJU, A., KHAN, S., BEHRMAN, S. W., ZAFAR, N., CHAUHAN, S. C., JAGGI, M. & YALLAPU, M. M. 2016. PSMA targeted docetaxel-loaded superparamagnetic iron oxide nanoparticles for prostate cancer. *Colloids and Surfaces B: Biointerfaces*, 144, 8-20.
- NAKANISHI, H., MAZDA, O., SATOH, E., ASADA, H., MORIOKA, H., KISHIDA, T., NAKAO, M., MIZUTANI, Y., KAWAUCHI, A., KITA, M., IMANISHI, J. & MIKI, T. 2003. Nonviral genetic transfer of Fas ligand induced significant growth suppression and apoptotic tumor cell death in prostate cancer *in vivo*. *Gene Therapy*, 10, 434-442.
- NANDE, R., GRECO, A., GOSSMAN, M. S., LOPEZ, J. P., CLAUDIO, L., SALVATORE, M., BRUNETTI, A., DENVIR, J., HOWARD, C. M. & CLAUDIO, P. P. 2013. Microbubble-assisted p53, RB, and p130 gene transfer in combination with radiation therapy in prostate cancer. *Current Gene Therapy*, 13, 163-74.
- NASU, Y., BANGMA, C. H., HULL, G. W., LEE, H. M., WANG, J., MCCURDY, M. A., SHIMURA, S., YANG, G., TIMME, T. L. & THOMPSON, T. C. 1999. Adenovirus-mediated interleukin-12 gene therapy for prostate cancer: suppression of orthotopic tumor growth and pre-established lung metastases in an orthotopic model. *Gene Therapy*, 6, 338-349.
- NATALI, S. & MIJOVIC, J. 2009. Molecular Dynamics of PEG-Dendrimer Blends and PEGylated Dendrimers. *Macromolecules*, 42, 6799-6807.
- NELSON, W. G. DE MARZO, A. & M. ISAACS, W. B. 2003. Prostate Cancer. *The New England Journal of Medicine*, 349, 366-381.
- NORIAN, L. A., JAMES, B. R. & GRIFFITH, T. S. 2011. Advances in Viral Vector-Based TRAIL Gene Therapy for Cancer. *Cancers (Basel)*, 3, 603-20.
- NOVARA, G., FICARRA, V., MOCELLIN, S., AHLERING, T. E., CARROLL, P. R., GRAEFEN, M., GUAZZONI, G., MENON, M., PATEL, V. R., SHARIAT, S. F., TEWARI, A. K., VAN POPPEL, H., ZATTONI, F., MONTORSI, F., MOTTRIE, A., ROSEN, R. C. & WILSON, T. G. 2012. Systematic Review and Meta-analysis of Studies Reporting Oncologic Outcome After Robot-assisted Radical Prostatectomy. *European Urology*, 62, 382-404.

- NWANESHIUDU, A. KUSCHAL, C. SAKAMOTO, F. H. ANDERSON, R. R. SCHWARZENBERGER, K. & YOUNG, R. C. 2012. Introduction to Confocal Microscopy. *Journal of Investigative Dermatology*, 132,1-5.
- OGRIS, M. & WAGNER, E. 2002. Targeting tumors with non-viral gene delivery systems. *Drug Discovery Today*, 7, 479-485.
- PANARITI, A., MISEROCCHI, G. & RIVOLTA, I. 2012. The effect of nanoparticle uptake on cellular behavior: disrupting or enabling functions? *Nanotechnology, science and applications*, 5, 87-100.
- PANG, Z. Q., GAO, H. L., CHEN, J., SHEN, S., ZHANG, B., REN, J. F., GUO, L. R., QIAN, Y., JIANG, X. G. & MEI, H. 2012. Intracellular delivery mechanism and brain delivery kinetics of biodegradable cationic bovine serum albumin-conjugated polymersomes. *International Journal of Nanomedicine*, 7, 3421-3432.
- PAVESE, J., OGDEN, I. M. & BERGAN, R. C. 2013. An Orthotopic Murine Model of Human Prostate Cancer Metastasis. *Journal of Visualized Experiments*, 79, 50873.
- PEPE, P. & ARAGONA, F. 2013. Prostate cancer detection rate at repeat saturation biopsy: PCPT risk calculator versus PCA3 score versus case-finding protocol. *Canadian Journal of Urology*, 20, 6620-4.
- PEREZ-MARTINEZ, F. C., GUERRA, J., POSADAS, I. & CENA, V. 2011. Barriers to Non-Viral Vector-Mediated Gene Delivery in the Nervous System. *Pharmaceutical Research*, 28, 1843-1858.
- PETERSON, J., ALLIKMAA, V., SUBBI, J., PEHK, T. & LOPP, M. 2003. Structural deviations in poly(amidoamine) dendrimers: a MALDI-TOF MS analysis. *European Polymer Journal*, 39,33-42.
- PHILIPPOU, Y. DEV, H. & SOORIAKUMARAN, P. 2014. Diagnosis and Screening. In: TEWARI, A. K. WHELAN, P. and GRAHAM, J. D. *Prostate Cancer Diagnosis and Clinical Management*. Chichester, UK: John Wiley & Sons. 16-33.
- POZZOLINI, M., SCARFI, S., BENATTI, U. & GIOVINE, M. 2003. Interference in MTT cell viability assay in activated macrophage cell line. *Analytical Biochemistry*, 313, 338-341.
- PU, F., SALARIAN, M., XUE, S., QIAO, J., FENG, J., TAN, S., PATEL, A., LI, X., MAMOUNI, K., HEKMATYAR, K., ZOU, J., WU, D. & YANG, J. J. 2016. Prostate-specific membrane antigen targeted protein contrast agents for molecular imaging of prostate cancer by MRI. *Nanoscale*, 8, 12668-12682.
- RADER, H. J., NGUYEN, T. T. T. & MULLEN, K. 2014. MALDI-TOF Mass Spectrometry of Polyphenylene Dendrimers up to the Megadalton Range. Elucidating Structural Integrity of Macromolecules at Unrivaled High Molecular Weights. *Macromolecules*, 47, 1240-1248.
- RAHMAN, M. LANE, A. SWINDELL, A. BARTRAM, S. 2006. *Introduction to flow cytometry* [online]. Available at: <http://www.ufjf.br/imunologia/files/2010/03/Flow-Cytometry-introduction.pdf> (09/12/2016).
- RAI, V. & DEY, N. 2011. The Basics of Confocal Microscopy. In: WANG, C. C. *Laser Scanning, Theory and Applications*. Rijeka, Croatia: In Tech. 75-96.
- RAMON, J. DENIS, L. J. 2007. *Prostate Cancer*. New York: Springer Berlin Heidelberg
- RAVI, M., PARAMESH, V., KAVIYA, S. R., ANURADHA, E. & SOLOMON, F. D. 2015. 3D cell culture systems: advantages and applications. *Journal of Cellular Physiology*, 230, 16-26.
- RAWLINGS, N. D. & BARRETT, A. J. 1997. Structure of membrane glutamate carboxypeptidase. *Biochimica Et Biophysica Acta-Protein Structure and Molecular Enzymology*, 1339, 247-252.

- REA, D., DEL VECCHIO, V., PALMA, G., BARBIERI, A., FALCO, M., LUCIANO, A., DE BIASE, D., PERDONA, S., FACCHINI, G. & ARRA, C. 2016. Mouse Models in Prostate Cancer Translational Research: From Xenograft to PDX. *Biomed Research International*. 2016, 9750795.
- REDDY, P. R. & RAJU, N. 2012. Gel-Electrophoresis and Its Applications. In: MAGDELDIN, S. *Gel Electrophoresis- Principles and Basics*. Croatia: In Tech. 15-32.
- REGINO, C. A., WONG, K. J., MILENIC, D. E., HOLMES, E. H., GARMESTANI, K., CHOYKE, P. L. & BRECHBIEL, M. W. 2009. Preclinical evaluation of a monoclonal antibody (3C6) specific for prostate-specific membrane antigen. *Current Radiopharmaceuticals*, 2, 9-17.
- REYNOLDS, A. R. & KYPRIANOU, N. 2006. Growth factor signalling in prostatic growth: significance in tumour development and therapeutic targeting. *British Journal of Pharmacology*, 147, S144-S152.
- RICHMOND, A. & SU, Y. J. 2008. Mouse xenograft models vs GEM models for human cancer therapeutics. *Disease Models & Mechanisms*, 1, 78-82.
- RISS, T.L. MORAVEC, R. A. NILES, A. L. DUELLMAN, S. BENINK, H. A. WORZELLA, T. J. & MINOR, L. 2013. Cell Viability Assays. In: SITTAMPALAM GS, COUSSENS NP, NELSON H, *et al. Assay Guidance Manual* [online]. Bethesda (MD): Eli Lilly & Company and the National Center for Advancing Translational Sciences.
- ROCERS, K. 2011. *The Reproductive System*. New York: Britannica Educational Publishing.
- RODRÍGUEZ-HERNÁNDEZ, C. O. TORRES-GARCÍA, S. E. OLVERA-SANDOVAL, C. RAMÍREZ-CASTILLO, F. Y. MURO, A. L. AVELAR-GONZALEZ, F. J. AND GUERRERO-BARRERA, A. L. 2014. Cell culture: history, development, and prospects. *International journal of current research and academic review*, 2(12): 188-200.
- ROYUELA, M., DE MIGUEL, M. P., RUIZ, A., FRAILE, B., ARENAS, M. I., ROMO, E. & PANIAGUA, R. 2000. Interferon-gamma and its functional receptors overexpression in benign prostatic hyperplasia and prostatic carcinoma: parallelism with c-myc and p53 expression. *European Cytokine Network*, 11, 119-127.
- RUSSELL, P. J. & KINGSLEY, E. A. 2003. Human Prostate Cancer Cell Lines In: RUSSELL, P. J., JACKSON, P. AND KINGSLEY, E. A. *Prostate Cancer Methods and Protocols*. Totowa, NJ: Humana Press Inc. 21-39.
- RYAN, C. J., SMITH, M. R., DE BONO, J. S., MOLINA, A., LOGOTHETIS, C. J., DE SOUZA, P., FIZAZI, K., MAINWARING, P., PIULATS, J. M., NG, S., CARLES, J., MULDER, P. F., BASCH, E., SMALL, E. J., SAAD, F., SCHRIJVERS, D., VAN POPPEL, H., MUKHERJEE, S. D., SUTTMANN, H., GERRITSEN, W. R., FLAIG, T. W., GEORGE, D. J., YU, E. Y., EFSTATHIOU, E., PANTUCK, A., WINQUIST, E., HIGANO, C. S., TAPLIN, M. E., PARK, Y., KHEOH, T., GRIFFIN, T., SCHER, H. I., RATHKOPF, D. E. & INVESTIGATORS, C.-A.-. 2013. Abiraterone in metastatic prostate cancer without previous chemotherapy. *New England Journal of Medicine*, 368, 138-48.
- SADIKOT, R. T. B. & LACKWELL, T. S. 2005. Bioluminescence Imaging. *Proceedings of the American Thoracic Society*, 2(6):537-540.
- SAMAN, D. M., LEMIEUX, A. M., LUTFIYYA, M. N. & LIPSKY, M. S. 2014. A review of the current epidemiology and treatment options for prostate cancer. *Dm Disease-a-Month*, 60, 150-154.
- SANLIOGLU, A. D., KOKSAL, I. T., KARACAY, B., BAYKARA, M., LULECI, G. & SANLIOGLU, S. 2006. Adenovirus-mediated IKKbetaKA expression sensitizes prostate carcinoma cells to TRAIL-induced apoptosis. *Cancer Gene Therapy*, 13, 21-31.

- SANTANDER-ORTEGA, M. J. LOZANO, M. V. UCHEGBU, I. F. & SCHATZLEIN, A. G. 2016. Dendrimers for gene therapy. In: NARAIN, R. *Polymers and Nanomaterials for Gene Therapy*. Cambridge: Elsevier. 113-146.
- SASAKI, R., SHIRAKAWA, T., ZHANG, Z. J., TAMEKANE, A., MATSUMOTO, A., SUGIMURA, K., MATSUO, M., KAMIDONO, S. & GOTOH, A. 2001. Additional gene therapy with Ad5CMV-p53 enhanced the efficacy of radiotherapy in human prostate cancer cells. *International Journal of Radiation Oncology*, 51, 1336-45.
- SATO, A., KLAUNBERG, B. & TOLWANI, R. 2004. *In vivo* bioluminescence imaging. *Comparative Medicine*, 54, 631-634.
- SATO, T., NESCHADIM, A., LAVIE, A., YANAGISAWA, T. & MEDIN, J. A. 2013. The Engineered Thymidylate Kinase (TMPK)/AZT Enzyme-Prodrug Axis Offers Efficient Bystander Cell Killing for Suicide Gene Therapy of Cancer. *PLOS One*, 8, 78711.
- SCHALLY, A. V. BLOCK, N. L. 2010. Luteinizing Hormone-Releasing Hormone and Its Agonistic, Antagonistic, and Targeted Cytotoxic Analogs in Prostate Cancer. In: FIGG, W. D. CHAU, C. H. and SMALL, E. J. *Drug Management of Prostate Cancer*. New York: Springer. 27-39.
- SCHATZLEIN, A. G., ZINSELMAYER, B. H., ELOUZI, A., DUFES, C., CHIM, Y. T., ROBERTS, C. J., DAVIES, M. C., MUNRO, A., GRAY, A. I. & UCHEGBU, I. F. 2005. Preferential liver gene expression with polypropylenimine dendrimers. *Journal of Controlled Release*, 101, 247-58.
- SCHNITZER, J. E., OH, P., PINNEY, E. & ALLARD, J. 1994. Filipin-sensitive caveolae-mediated transport in endothelium - reduced transcytosis, scavenger endocytosis, and capillary-permeability of select macromolecules. *Journal of Cell Biology*, 127, 1217-1232.
- SCHUMACHER, G., BRUCKHEIMER, E. M., BEHAM, A. W., HONDA, T., BRISBAY, S., ROTH, J. A., LOGOTHETIS, C. & MCDONNELL, T. J. 2001. Molecular determinants of cell death induction following adenovirus-mediated gene transfer of wild-type p53 in prostate cancer cells. *International Journal of Cancer*, 91, 159-166.
- SEKI, M., IWAKAWA, J., CHENG, H. & CHENG, P. W. 2002. p53 and PTEN/MMAC1/TEP1 gene therapy of human prostate PC-3 carcinoma xenograft, using transferrin-facilitated lipofection gene delivery strategy. *Human Gene Therapy*, 13, 761-773.
- SELLECK, W. A., CANFIELD, S. E., HASSEN, W. A., MESECK, M., KUZMIN, A. I., EISENSMITH, R. C., CHEN, S. H. & HALL, S. J. 2003. IFN-gamma sensitization of prostate cancer cells to Fas-mediated death: A gene therapy approach. *Molecular Therapy*, 7, 185-192.
- SELMAN, S. H. 2011. The McNeal Prostate: A Review. *Urology*, 78, 1224-1228.
- SEMWOGERERE, D. & WEEKS, E. R. 2005. Confocal Microscopy. *Encyclopedia of Biomaterials and Biomedical Engineering*, 10.1, 1-10.
- SEOL, J. Y., PARK, K. H., HWANG, C. I., PARK, W. Y., YOO, C. G., KIM, Y. W., HAN, S. K., SHIM, Y. S. & LEE, C. T. 2003. Adenovirus-TRAIL can overcome TRAIL resistance and induce a bystander effect. *Cancer Gene Therapy*, 10, 540-548.
- SHAFI, F. & SALTON, M. R. J. 1960. DISAGGREGATION OF BACTERIAL CELL WALLS BY ANIONIC DETERGENTS. *Journal of General Microbiology*, 23, 137-141.
- SHAH, R. B. ZHOU, M. 2012. *Prostate Biopsy Interpretation: an illustrated guide*. Berlin: Springer.
- SHALEV, M., THOMPSON, T. C., KADMON, D., AYALA, G., KERNEN, K. & MILES, B. J. 2001. Gene therapy for prostate cancer. *Urology*, 57, 8-16.

- SHAN, Y. B., LUO, T., PENG, C., SHENG, R. L., CAO, A. M., CAO, X. Y., SHEN, M. W., GUO, R., TOMAS, H. & SHI, X. Y. 2012. Gene delivery using dendrimer-entrapped gold nanoparticles as nonviral vectors. *Biomaterials*, 33, 3025-3035.
- SHAN, Y. P. & WANG, H. D. 2015. The structure and function of cell membranes examined by atomic force microscopy and single-molecule force spectroscopy. *Chemical Society Reviews*, 44,3617-3638.
- SHANKAR, S., CHEN, X. & SRIVASTAVA, R. K. 2005. Effects of sequential treatments with chemotherapeutic drugs followed by TRAIL on prostate cancer *in vitro* and *in vivo*. *Prostate*, 62,165-86.
- SHANKAR, S., SINGH, T. R. & SRIVASTAVA, R. K. 2004. Ionizing radiation enhances the therapeutic potential of TRAIL in prostate cancer *in vitro* and *in vivo*: Intracellular mechanisms. *Prostate*, 61, 35-49.
- SHANKARANARAYANAN, J. S., KANWAR, J. R., AL-JUHAISHI, A. J. & KANWAR, R. K. 2016. Doxorubicin Conjugated to Immunomodulatory Anticancer Lactoferrin Displays Improved Cytotoxicity Overcoming Prostate Cancer Chemo resistance and Inhibits Tumour Development in TRAMP Mice. *Scientific Reports*, 6, 32062.
- SHAO, N. M., SU, Y. Z., HU, J. J., ZHANG, J. H., ZHANG, H. F. & CHENG, Y. Y. 2011. Comparison of generation 3 polyamidoamine dendrimer and generation 4 polypropylenimine dendrimer on drug loading, complex structure, release behavior, and cytotoxicity. *International Journal of Nanomedicine*, 6, 3361-3372.
- SHAO, X.-R., WEI, X.-Q., SONG, X., HAO, L.-Y., CAI, X.-X., ZHANG, Z.-R., PENG, Q. & LIN, Y.-F. 2015. Independent effect of polymeric nanoparticle zeta potential/surface charge, on their cytotoxicity and affinity to cells. *Cell Proliferation*, 48, 465-474.
- SHARMA, B., MA, W. X., ADJEI, I. M., PANYAM, J., DIMITRIJEVIC, S. & LABHASETWAR, V. 2011. Nanoparticle-mediated p53 gene therapy for tumor inhibition. *Drug Delivery and Translational Research*, 1, 43-52.
- SHEN, D. W., XIE, F. & EDWARDS, W. B. 2013. Evaluation of Phage Display Discovered Peptides as Ligands for Prostate-Specific Membrane Antigen (PSMA). *PLOS One*, 8, 68339.
- SHI, J., CHEN, J., SERRADJI, N., XU, X. M., ZHOU, H., MA, Y. X., SUN, Z. H., JIANG, P., DU, Y. P., YANG, J. B., DONG, C. Z. & WANG, Q. 2013. PMS1077 Sensitizes TNF-alpha Induced Apoptosis in Human Prostate Cancer Cells by Blocking NF-kappa B Signaling Pathway. *PLOS One*, 8, 61132.
- SHIMAMURA, M., YAMAMOTO, Y., ASHINO, H., OIKAWA, T., HAZATO, T., TSUDA, H. & IIGO, M. 2004. Bovine lactoferrin inhibits tumor-induced angiogenesis. *International Journal of Cancer*, 111, 111-116.
- SHIMKO, A. POVOLOTCKAIA, A. & MIKHAYLOVA, A. 2012. Zeta potential measurement principle (Laser Doppler Electrophoresis) [online]. Available at: <http://laser.spbu.ru/en/research-eng/dzeta-eng.html> (30/11/2016).
- SHUKLA, S. & GUPTA, S. 2004. Suppression of constitutive and tumor necrosis factor alpha-induced nuclear factor (NF)-kappaB activation and induction of apoptosis by apigenin in human prostate carcinoma PC-3 cells: correlation with down-regulation of NF-kappaB-responsive genes. *Clinical Cancer Research*, 10, 3169-78.
- SILVER, D. A., PELLICER, I., FAIR, W. R., HESTON, W. D. W. & CORDONCARDO, C. 1997. Prostate-specific membrane antigen expression in normal and malignant human tissues. *Clinical Cancer Research*, 3, 81-85.

- SINGER, V. L., JONES, L. J., YUE, S. T. & HAUGLAND, R. P. 1997. Characterization of PicoGreen reagent and development of a fluorescence-based solution assay for double-stranded DNA quantitation. *Analytical Biochemistry*, 249, 228-238.
- SINGH, J., MICHEL, D., CHITANDA, J. M., VERRALL, R. E. & BADEA, I. 2012. Evaluation of cellular uptake and intracellular trafficking as determining factors of gene expression for amino acid-substituted gemini surfactant-based DNA nanoparticles. *Journal of Nanobiotechnology*, 10, 1186.
- SOMANI, S., ROBB, G., PICKARD, B. S. & DUFÈS, C. 2015. Enhanced gene expression in the brain following intravenous administration of lactoferrin-bearing polypropylenimine dendriplex. *Journal of Controlled Release*, 217, 235-42.
- SUTHERLAND, M. GORDON, A. SHNYDER, S. D. PATTERSON, L. H. and SHELDRAKE, H. M. 2012. RGD-Binding Integrins in Prostate Cancer: Expression Patterns and Therapeutic Prospects against Bone Metastasis. *Cancers*, 4, 1106-1145.
- SPURGERS, K. B., COOMBES, K. R., MEYN, R. E., GOLD, D. L., LOGOTHETIS, C. J., JOHNSON, T. J. & MCDONNELL, T. J. 2004. A comprehensive assessment of p53-responsive genes following adenoviral-p53 gene transfer in Bcl-2-expressing prostate cancer cells. *Oncogene*, 23, 1712-1723.
- STACHURSKA, A., ELBANOWSKI, J. & KOWALCZYNSKA, H. M. 2012. Role of alpha 5 beta 1 and alpha v beta 3 integrins in relation to adhesion and spreading dynamics of prostate cancer cells interacting with fibronectin under *in vitro* conditions. *Cell Biology International*, 36, 883-892.
- STANIZZI, M. A. & HALL, S. J. 2007. Clinical experience with gene therapy for the treatment of prostate cancer. *Reviews in Urology*, 9 Suppl 1, S20-8.
- STASKO, N. A., JOHNSON, C. B., SCHOENFISCH, M. H., JOHNSON, T. A. & HOLMUHAMEDOV, E. L. 2007. Cytotoxicity of polypropylenimine dendrimer conjugates on cultured endothelial cells. *Biomacromolecules*, 8, 3853-3859.
- STEPHEN, J. J. 2012. *Prostate Cancer Diagnosis: PSA, Biopsy and Beyond*. New York: Springer Berlin Heidelberg.
- STEVENSON, M., HALE, A. B. H., HALE, S. J., GREEN, N. K., BLACK, G., FISHER, K. D., ULBRICH, K., FABRA, A. & SEYMOUR, L. W. 2007. Incorporation of a laminin-derived peptide (SIKVAV) on polymer-modified adenovirus permits tumor-specific targeting via alpha 6-integrins. *Cancer Gene Therapy*, 14, 335-345.
- STOLBERG, S. G. 1999. The biotech death of Jesse Gelsinger. *The New York Times Magazine*, 136-140, 149-150.
- STONE, K. R., MICKEY, D. D., WUNDERLI, H., MICKEY, G. H. & PAULSON, D. F. 1978. ISOLATION OF A HUMAN PROSTATE CARCINOMA CELL LINE (DU 145). *International Journal of Cancer*, 21, 274-281.
- SU, B. W., CENGIZEROGLU, A., FARKASOVA, K., VIOLA, J. R., ANTON, M., ELLWART, J. W., HAASE, R., WAGNER, E. & OGRIS, M. 2013. Systemic TNF alpha Gene Therapy Synergizes with Liposomal Doxorubicine in the Treatment of Metastatic Cancer. *Molecular Therapy*, 21, 300-308.
- SUBBI, J., AGURAIUJA, R., TANNER, R., ALLIKMAA, V. & LOPP, M. 2005. Fragmentation of poly(amidoamine) dendrimers in matrix-assisted laser desorption. *European Polymer Journal*, 41, 2552-2558.
- SUYIN, P. C. DICKINSON, J. L. HOLLOWAY, A. F. 2013. Integrins in Prostate Cancer Invasion and Metastasis. In: G. HAMILTON, ed., *Advances in Prostate Cancer*, 1st ed. Rijeka: InTech, 621-639.

- TAI, S., SUN, Y., SQUIRES, J. M., ZHANG, H., OH, W. K., LIANG, C.-Z. & HUANG, J. 2011a. PC3 Is a Cell Line Characteristic of Prostatic Small Cell Carcinoma. *Prostate*, 71, 1668-1679.
- TAI, S., SUN, Y., SQUIRES, J. M., ZHANG, H., OH, W. K., LIANG, C. Z. & HUANG, J. T. 2011b. PC3 Is a Cell Line Characteristic of Prostatic Small Cell Carcinoma. *Prostate*, 71, 1668-1679.
- TAIRA, K. KATAOKA, K. & NIIDOME, T. 2005. *Non-viral gene therapy: Gene design and delivery*. New York: Springer Berlin Heidelberg.
- TAKAHASHI, T., HOSHI, S., SATOH, M., KANEDA, T., SUZUKI, K. I., NAKAGAWARA, K. I. & ORIKASA, S. 1999. The study of PSA gene expression on urogenital cell lines. *International Journal of Urology*, 6, 526-31.
- TANDLE, A., HANNA, E., LORANG, D., HAJITOU, A., MOYA, C. A., PASQUALINI, R., ARAP, W., ADEM, A., STARKER, E., HEWITT, S. & LIBUTTI, S. K. 2009. Tumor Vasculature-targeted Delivery of Tumor Necrosis Factor-alpha. *Cancer*, 115, 128-139.
- TANG, L., YANG, X. J., YIN, Q., CAI, K. M., WANG, H., CHAUDHURY, I., YAO, C., ZHOU, Q., KWON, M., HARTMAN, J. A., DOBRUCKI, I. T., DOBRUCKI, L. W., BORST, L. B., LEZMIG, S., HELFERICH, W. G., FERGUSON, A. L., FAN, T. M. & CHENG, J. J. 2014. Investigating the optimal size of anticancer nanomedicine. *Proceedings of the National Academy of Sciences of the United States of America*, 111, 15344-15349.
- TARATULA, O., GARBUZENKO, O. B., KIRKPATRICK, P., PANDYA, I., SAVLA, R., POZHAROV, V. P., HE, H. & MINKO, T. 2009. Surface-engineered targeted PPI dendrimer for efficient intracellular and intratumoral siRNA delivery. *Journal of Controlled Release*, 140, 284-293.
- TAVORA, F., KRYVENKO, O. N. & EPSTEIN, J. I. 2013. Mesenchymal tumours of the bladder and prostate: an update. *Pathology*, 45, 104-115.
- THAKUR, S., KESHARWANI, P., TEKADE, R. K. & JAIN, N. K. 2015. Impact of pegylation on biopharmaceutical properties of dendrimers. *Polymer*, 59, 67-92.
- THOMAS, C. E., EHRHARDT, A. & KAY, M. A. 2003. Progress and problems with the use of viral vectors for gene therapy. *Nature Reviews Genetics*, 4, 346-358.
- TORTORELLA, S. & KARAGIANNIS, T. C. 2014. Transferrin Receptor-Mediated Endocytosis: A Useful Target for Cancer Therapy. *Journal of Membrane Biology*, 247, 291-307.
- TOY, R., PEIRIS, P. M., GHAGHADA, K. B. & KARATHANASIS, E. 2014. Shaping cancer nanomedicine: the effect of particle shape on the *in vivo* journey of nanoparticles. *Nanomedicine*, 9, 121-134.
- TRAUGER, S. A., WEBB, W. & SIUZDAK, G. 2002. Peptide and protein analysis with mass spectrometry. *Spectroscopy-an International Journal*, 16, 15-28.
- TSCHARNUTER, W. 2000. Photon Correlation Spectroscopy in Particle Sizing. *Encyclopedia of Analytical Chemistry* [online]. Available at: http://chenglongresearch.weebly.com/uploads/1/9/9/4/19942735/pcs_in_particle_sizing.pdf (30/11/2016).
- TSE, B. W., SCOTT, K. F. & RUSSELL, P. J. 2012. Paradoxical roles of tumour necrosis factor-alpha in prostate cancer biology. *Prostate Cancer*, 2012, 128965.
- TSE, B. W. C., COWIN, G. J., SOEKMADJI, C., JOVANOVIĆ, L., VASIREDDY, R. S., LING, M. T., KHATRI, A., LIU, T. Q., THIERRY, B. & RUSSELL, P. J. 2015. PSMA-targeting iron oxide magnetic nanoparticles enhance MRI of preclinical prostate cancer. *Nanomedicine*, 10, 375-386.

- TSUGAMA, D., LIU, S. K. & TAKANO, T. 2011. A rapid chemical method for lysing Arabidopsis cells for protein analysis. *Plant Methods*, 7, 22.
- TUCCARI, G. & BARRESI, G. 2011. Lactoferrin in human tumours: immunohistochemical investigations during more than 25 years. *Biometals*, 24, 775-784.
- TUCKER, I. M., CORBETT, J. C. W., FATKIN, J., JACK, R. O., KASZUBA, M., MACCREATH, B. & MCNEIL-WATSON, F. 2015. Laser Doppler Electrophoresis applied to colloids and surfaces. *Current Opinion in Colloid & Interface Science*, 20, 215-226.
- TUGUES, S., BURKHARD, S. H., OHS, I., VROHLINGS, M., NUSSBAUM, K., VOM BERG, J., KULIG, P. & BECHER, B. 2015. New insights into IL-12-mediated tumor suppression. *Cell Death and Differentiation*, 22, 237-46.
- TUTING, T., GAMBOTTO, A., BAAR, J., DAVIS, I. D., STORKUS, W. J., ZAVODNY, P. J., NARULA, S., TAHARA, H., ROBBINS, P. D. & LOTZE, M. T. 1997. Interferon-alpha gene therapy for cancer: retroviral transduction of fibroblasts and particle-mediated transfection of tumor cells are both effective strategies for gene delivery in murine tumor models. *Gene Therapy*, 4, 1053-1060.
- TZENG, S. Y., WILSON, D. R., HANSEN, S. K., QUIÑONES-HINOJOSA, A. & GREEN, J. J. 2016. Polymeric nanoparticle-based delivery of TRAIL DNA for cancer-specific killing. *Bioengineering & Translational Medicine*, 1, 149-159.
- VALKENBURG, K. C. & WILLIAMS, B. O. 2011. Mouse models of prostate cancer. *Prostate cancer*, 895238.
- VAN HORSSSEN, R., TEN HAGEN, T. L. M. & EGGERMONT, A. M. M. 2006. TNF-alpha in cancer treatment: Molecular insights, antitumor effects, and clinical utility. *Oncologist*, 11, 397-408.
- VANSANDE, M. & VANCAMP, K. 1981. LACTOFERRIN IN HUMAN-PROSTATE TISSUE. *Urological Research*, 9, 241-244.
- VOELKEL-JOHNSON, C., KING, D. L. & NORRIS, J. S. 2002. Resistance of prostate cancer cells to soluble TNF-related apoptosis-inducing ligand (TRAIL/Apo2L) can be overcome by doxorubicin or adenoviral delivery of full-length TRAIL. *Cancer Gene Therapy*, 9, 164-172.
- WAGNER, D. G. 2016. Pathology of Small Cell Prostate Carcinoma. Medscape [online]. Available at: <http://emedicine.medscape.com/article/1611899-overview> (12/7/2016).
- WAGNER, E., CUIEL, D. & COTTEN, M. 1994. DELIVERY OF DRUGS, PROTEINS AND GENES INTO CELLS USING TRANSFERRIN AS A LIGAND FOR RECEPTOR-MEDIATED ENDOCYTOSIS. *Advanced Drug Delivery Reviews*, 14, 113-135.
- WALCZAK, H. 2013. Death Receptor-Ligand Systems in Cancer, Cell Death, and Inflammation. *Cold Spring Harbor Perspectives in Biology*, 5, 8698.
- WALLY, J. & BUCHANAN, S. K. 2007. A structural comparison of human serum transferrin and human lactoferrin. *Biometals*, 20, 249-262.
- WANG, C. Y., MAYO, M. W. & BALDWIN, A. S. 1996. TNF- and cancer therapy-induced apoptosis: Potentiation by inhibition of NF-kappa B. *Science*, 274, 784-787.
- WANG, F. F., CHEN, L., ZHANG, R., CHEN, Z. P. & ZHU, L. 2014. RGD peptide conjugated liposomal drug delivery system for enhance therapeutic efficacy in treating bone metastasis from prostate cancer. *Journal of Controlled Release*, 196, 222-233.

- WANG, H. Y., MCKNIGHT, N. C., ZHANG, T., LU, M. L., BALK, S. P. & YUAN, X. 2007. SOX9 is expressed in normal prostate basal cells and regulates androgen receptor expression in prostate cancer cells. *Cancer Research*, 67, 528-536.
- WANG, W. W., LI, W. Z., MA, N. & STEINHOFF, G. 2013. Non-Viral Gene Delivery Methods. *Current Pharmaceutical Biotechnology*, 14, 46-60.
- WANG, Y., LI, L., SHAO, N. M., HU, Z. Q., CHEN, H., XU, L. Q., WANG, C. P., CHENG, Y. Y. & XIAO, J. R. 2015. Triazine-modified dendrimer for efficient TRAIL gene therapy in osteosarcoma. *Acta Biomaterialia*, 17, 115-124.
- WANG, Y. T., WANG, M. M., CHEN, H., LIU, H. M., ZHANG, Q. & CHENG, Y. Y. 2016. Fluorinated dendrimer for TRAIL gene therapy in cancer treatment. *Journal of Materials Chemistry B*, 4, 1354-1360.
- WARING, P. & MULLBACHER, A. 1999. Cell death induced by the Fas/Fas ligand pathway and its role in pathology. *Immunology and Cell Biology*, 77, 312-317.
- WATANABE, M., NASU, Y., KASHIWAKURA, Y., KUSUMI, N., TAMAYOSE, K., NAGAI, A., SASANO, T., SHIMADA, T., DAIDA, H. & KUMON, H. 2005. Adeno-associated virus 2-mediated intratumoral prostate cancer gene therapy: long-term maspin expression efficiently suppresses tumor growth. *Human Gene Therapy*, 16, 699-710.
- WATSON, D. G. 2012. *Pharmaceutical Analysis: A Textbook for Pharmacy Students and Pharmaceutical Chemists*. Churchill Livingstone: Elsevier.
- WEE, Z. N., LI, Z. M., LEE, P. L., LEE, S. T., LIM, Y. P. & YU, Q. 2014. EZH2-Mediated Inactivation of IFN-gamma-JAK-STAT1 Signaling Is an Effective Therapeutic Target in MYC-Driven Prostate Cancer. *Cell Reports*, 8, 204-216.
- WEENER, J. W., VAN DONGEN, J. L. J. & MEIJER, E. W. 1999. Electrospray mass spectrometry studies of poly(propylene imine) dendrimers: Probing reactivity in the gas phase. *Journal of the American Chemical Society*, 121, 10346-10355.
- WEI, M. Y., XU, Y. H., ZOU, Q., TU, L. X., TANG, C. Y., XU, T., DENG, L. H. & WU, C. B. 2012. Hepatocellular carcinoma targeting effect of PEGylated liposomes modified with lactoferrin. *European Journal of Pharmaceutical Sciences*, 46, 131-141.
- Westermeier, R. (2005) Gel Electrophoresis, *Encyclopedia of Life Science*, 10, 1-6.
- WILEY, S. R., SCHOOLEY, K., SMOLAK, P. J., DIN, W. S., HUANG, C. P., NICHOLL, J. K., SUTHERLAND, G. R., SMITH, T. D., RAUCH, C., SMITH, C. A. & GOODWIN, R. G. 1995. Identification and characterization of a new member of the TNF family that induces apoptosis. *Immunity*, 3, 673-682.
- WILSON, J. M. 1996. Adenoviruses as gene-delivery vehicles. *New England Journal of Medicine*, 334, 1185-1187.
- WIRTH, T., PARKER, N. & YLA-HERTTUALA, S. 2013. History of gene therapy. *Gene*, 525, 162-169.
- WISHART, D. S., FEUNANG, Y. D., MARCU, A., GUO, A. C., LIANG, K., VÁZQUEZ-FRESNO, R., SAJED, T., JOHNSON, D., LI, C., KARU, N., SAYEEDA, Z., LO, E., ASSEMPOUR, N., BERJANSKII, M., SINGHAL, S., ARNDT, D., LIANG, Y., BADRAN, H., GRANT, J., SERRA-CAYUELA, A., LIU, Y., MANDAL, R., NEVEU, V., PON, A., KNOX, C., WILSON, M., MANACH, C. & SCALBERT, A. 2018. HMDB 4.0: the human metabolome database for 2018. *Nucleic Acids Research*, 46, D608-D617.

- WOENCKHAUS, J. & FENIC, I. 2008. Proliferative inflammatory atrophy: a background lesion of prostate cancer? *Andrologia*, 40, 134-7.
- WON, Y. W., YOON, S. M., LIM, K. S. & KIM, Y. H. 2012. Self-Assembled Nanoparticles with Dual Effects of Passive Tumor Targeting and Cancer-Selective Anticancer Effects. *Advanced Functional Materials*, 22, 1199-1208.
- WONG, R. S. Y. 2011. Apoptosis in cancer: from pathogenesis to treatment. *Journal of Experimental & Clinical Cancer Research*, 30, 87.
- WRIGHT, G. L., HALEY, C., BECKETT, M. L. & SCHELLHAMMER, P. F. 1995. Expression of prostate-specific membrane antigen in normal, benign, and malignant prostate tissues. *Urologic Oncology*, 1, 18-28.
- WU, P., KUDROLLI, T. A., CHOWDHURY, W. H., LIU, M. M., RODRIGUEZ, R. & LUPOLD, S. E. 2010. Adenovirus targeting to prostate-specific membrane antigen through virus-displayed, semirandom peptide library screening. *Cancer Research*, 70, 9549-53.
- WU, X., TAI, Z., ZHU, Q., FAN, W., DING, B., ZHANG, W., ZHANG, L., YAO, C., WANG, X., DING, X., LI, Q., LI, X., LIU, G., LIU, J. & GAO, S. 2014. Study on the prostate cancer-targeting mechanism of aptamer-modified nanoparticles and their potential anticancer effect *in vivo*. *International Journal of Nanomedicine*, 9, 5431-5440.
- XIANG, B., DONG, D.-W., SHI, N.-Q., GAO, W., YANG, Z.-Z., CUI, Y., CAO, D.-Y. & QI, X.-R. 2013. PSA-responsive and PSMA-mediated multifunctional liposomes for targeted therapy of prostate cancer. *Biomaterials*, 34, 6976-6991.
- XIAO, L., JOO, K. I., LIM, M. & WANG, P. 2012. Dendritic cell-directed vaccination with a lentivector encoding PSCA for prostate cancer in mice. *PLOS One*, 7, e48866.
- XIONG, L., LIU, Y. H., ZHANG, Y. P., ZHANG, S. B., PU, X. Z., GARDNER, T. A., JENG, M. H. & KAO, C. H. 2007. Fas ligand delivery by a prostate-restricted replicative adenovirus enhances safety and antitumor efficacy. *Clinical Cancer Research*, 13, 5463-5473.
- XU, W., NEILL, T., YANG, Y., HU, Z., CLEVELAND, E., WU, Y., HUTTEN, R., XIAO, X., STOCK, S. R., SHEVRIN, D., KAUL, K., BRENDLER, C., IOZZO RENATO, V. & SETH, P. 2015. The systemic delivery of an oncolytic adenovirus expressing decorin inhibits bone metastasis in a mouse model of human prostate cancer. *Gene Therapy*, 22, 247-256.
- YAO, V., BERKMAN, C. E., CHOI, J. K., O'KEEFE, D. S. & BACICH, D. J. 2010. Expression of Prostate-Specific Membrane Antigen (PSMA), Increases Cell Folate Uptake and Proliferation and Suggests a Novel Role for PSMA in the Uptake of the Non-Polyglutamated Folate, Folic Acid. *Prostate*, 70, 305-316.
- YE, Y. J., SUN, Y., ZHAO, H. L., LAN, M. B., GAO, F., SONG, C., LOU, K. Y., LI, H. & WANG, W. 2013. A novel lactoferrin-modified beta-cyclodextrin nanocarrier for brain-targeting drug delivery. *International Journal of Pharmaceutics*, 458, 110-117.
- YEE, N. S., IGNATENKO, N., FINNBERG, N., LEE, N. & STAIRS, D. 2015. Animal models of cancer biology. *Cancer Growth and Metastasis*, 8(1), 115-118.
- YELLEPEDDI, V. K., VANGARA, K. K. & PALAKURTHI, S. 2013. Poly(amido)amine (PAMAM) dendrimer-cisplatin complexes for chemotherapy of cisplatin-resistant ovarian cancer cells. *Journal of Nanoparticle Research*, 15.

- YOSHIMURA, I., IKEGAMI, S., SUZUKI, S., TADAKUMA, T. & HAYAKAWA, M. 2002. Adenovirus mediated prostate specific enzyme prodrug gene therapy using prostate specific antigen promoter enhanced by the Cre-loxP system. *Journal of Urology*, 168, 2659-64.
- YU, R., MANDLEKAR, S., RUBEN, S., NI, J. & KONG, A. N. 2000. Tumor necrosis factor-related apoptosis-inducing ligand-mediated apoptosis in androgen-independent prostate cancer cells. *Cancer Research*, 60, 2384-9.
- YUAN, F., DELLIAN, M., FUKUMURA, D., LEUNIG, M., BERK, D. A., TORCHILIN, V. P. & JAIN, R. K. 1995. VASCULAR-PERMEABILITY IN A HUMAN TUMOR XENOGRAFT - MOLECULAR-SIZE DEPENDENCE AND CUTOFF SIZE. *Cancer Research*, 55, 3752-3756.
- YUE, Q. H., HU, X. B., YIN, Y., SU, M. Q., CHENG, X. D., YANG, L., ZHOU, T. C. & HAO, X. K. 2009. Inhibition of prostate cancer by suicide gene targeting the FCY1 and HSV-TK genes. *Oncology Reports*, 22, 1341-1347.
- YUMOTO, R., NISHIKAWA, H., OKAMOTO, M., KATAYAMA, H., NAGAI, J. & TAKANO, M. 2006. Clathrin-mediated endocytosis of FITC-albumin in alveolar type II epithelial cell line RLE-6TN. *American Journal of Physiology-Lung Cellular and Molecular Physiology*, 290, L946-55.
- ZAROGULIDIS, P., DARWICHE, K., SAKKAS, A., YARMUS, L., HUANG, H., LI, Q., FREITAG, L., ZAROGULIDIS, K. & MALECKI, M. 2013. Suicide Gene Therapy for Cancer - Current Strategies. *Journal of Genetic Syndromes and Gene Therapy*, 4, 16849.
- ZHANG, H. L., LIU, X. G., WU, F. B., QIN, F. F., FENG, P., XU, T., LI, X. & YANG, L. 2016. A Novel Prostate-Specific Membrane-Antigen (PSMA) Targeted Micelle-Encapsulating Wogonin Inhibits Prostate Cancer Cell Proliferation via Inducing Intrinsic Apoptotic Pathway. *International Journal of Molecular Sciences*, 17, 676.
- ZHANG, X., HU, H. M., LIU, T. B., YANG, Y. Y., PENG, Y. F., CAI, Q. Q. & FANG, L. J. 2014. Multi-armed poly(L-glutamic acid)-graft-polypropyleneimine as effective and serum resistant gene delivery vectors. *International Journal of Pharmaceutics*, 465, 444-454.
- ZHAO, Y., YANG, J. L., SHI, J. J., GONG, Y. N., LU, Q. H., XU, H., LIU, L. P. & SHAO, F. 2011. The NLRC4 inflammasome receptors for bacterial flagellin and type III secretion apparatus. *Nature*, 477, 596-U257.
- ZHENG, D. Q., WOODARD, A. S., FORNARO, M., TALLINI, G. & LANGUINO, L. R. 1999. Prostatic carcinoma cell migration via alpha(v)beta(3) integrin is modulated by a focal adhesion kinase pathway. *Cancer Research*, 59, 1655-1664.
- ZHENG, L., WANG, W., NI, J., MAO, X., SONG, D., LIU, T., WEI, J. & ZHOU, H. 2017. Role of autophagy in tumor necrosis factor-alpha-induced apoptosis of osteoblast cells. *Journal of investigative medicine : the official publication of the American Federation for Clinical Research*, 65, 1014-1020.
- ZHENG, Y., JI, S., CZERWINSKI, A., VALENZUELA, F., PENNINGTON, M. & LIU, S. 2014. FITC-Conjugated Cyclic RGD Peptides as Fluorescent Probes for Staining Integrin alpha(v)beta(3)/alpha(v)beta(5) in Tumor Tissues. *Bioconjugate Chemistry*, 25, 1925-1941.
- ZIAEE, S., CHU, G. C., HUANG, J. M., SIEH, S. & CHUNG, L. W. 2015. Prostate cancer metastasis: roles of recruitment and reprogramming, cell signal network and three-dimensional growth characteristics. *Translational Andrology and Urology*, 4, 438-54.
- ZINSELMAYER, B. H., MACKAY, S. P., SCHATZLEIN, A. G. & UCHEGBU, I. F. 2002. The lower-generation polypropyleneimine dendrimers are effective gene-transfer agents. *Pharmaceutical Research*, 19, 960-967.

Appendix I: List of Publications

1. Altwaijry, N., Somani, S., Parkinson, J., Tale, R. J., Keating, P., Warzecha, M., Mackenzie, G., Leung, H. Y., and Dufès, C. 2018. Regression of prostate tumors after intravenous administration of lactoferrin-bearing polypropylenimine dendriplexes encoding TNF- α , TRAIL and interleukin-12. *Drug Delivery*, 25, 679-689. (<https://www.tandfonline.com/doi/full/10.1080/10717544.2018.1440666>)
2. Somani, S., Laskar, P., Altwaijry, N., Kewcharoenpong, P., Robb, G., Pickard, B. S., Dufès, C. 2018. PEGylation of polypropylenimine dendrimers: effects on cytotoxicity, DNA condensation, gene delivery and expression in cancer cells. (submitted).
3. Altwaijry, N., Somani, S., and Dufès, C. 2018. Targeted non-viral gene therapy for prostate cancer. (in preparation)

Appendix II : Conference Abstracts

1. Altwaijry, N., Somani, S., and Dufès, C. Synthesis, characterization and *in vitro* evaluation of a novel tumour-targeted dendrimer as a non-viral gene delivery vector for prostate cancer therapy. 9th Saudi Students Conference, University of Birmingham, Birmingham, UK (13 – 14 February 2016), Poster presentation.
2. Altwaijry, N., Somani, S., and Dufès, Prostate tumour regression following intravenous administration of lactoferrin-bearing polypropylenimine dendriplex. SIPBS research day, University of Strathclyde. Glasgow, UK (November 2016), Oral presentation.
3. Altwaijry, N., Somani, S., Parkinson, J., Tale, R. J., and Dufès, C. Lactoferrin-bearing polypropylenimine dendriplex and its therapeutic efficacy in targeting prostate cancer tumours. European Nanomedicine Meeting 2017, King's College London, London, UK (3-4 April 2017), Poster presentation.
4. Altwaijry, N., Somani, S., Parkinson, J., Tale, R. J., and Dufès, C. Therapeutic efficacy of lactoferrin-bearing polypropylenimine dendriplex in targeting prostate cancer tumours. UKICRS 2017, University of Strathclyde. Glasgow, UK (30-31 May 2017), Oral presentation and poster presentation.
5. Altwaijry, N., Somani, S., Parkinson, J., Tale, R. J., and Dufès, Prostate tumour regression following intravenous administration of lactoferrin-bearing polypropylenimine dendriplex. CRS 2017, Boston, USA (16-19 July 2017), Poster presentation.

Others

1. Best poster in medical and biomedical science award (First), 9th Saudi Student conference, University of Birmingham, UK, February 2016
2. University of Strathclyde postgraduate travel award for poster presentation to attend Controlled Release Society annual meeting and exposition 2017, Boston, USA.